

# Important Notice

This copy may be used only for the purposes of research and private study, and any use of the copy for a purpose other than research or private study may require the authorization of the copyright owner of the work in question. Responsibility regarding questions of copyright that may arise in the use of this copy is assumed by the recipient.

UNIVERSITY OF CALGARY

Using multicomponent seismic data to delineate hydrocarbon reservoirs: 2D-3C Willesden  
Green, Alberta and 3D-3C Manitou Lake, Saskatchewan

by

Roxana Maria Varga

A THESIS

SUBMITTED TO THE FACULTY OF GRADUATE STUDIES  
IN PARTIAL FULFILMENT OF THE REQUIREMENTS FOR THE  
DEGREE OF MASTER OF SCIENCE

DEPARTMENT OF GEOSCIENCE

CALGARY, ALBERTA

MAY, 2009

© Roxana Maria Varga, 2009

UNIVERSITY OF CALGARY  
FACULTY OF GRADUATE STUDIES

The undersigned certify that they have read, and recommend to the Faculty of Graduate Studies for acceptance, a thesis entitled “Using multicomponent seismic data to delineate hydrocarbon reservoirs: 2D-3C Willesden Green, Alberta and 3D-3C Manitou Lake, Saskatchewan” submitted by ROXANA MARIA VARGA in partial fulfillment of the requirements for the degree of MASTER OF SCIENCE.

---

Supervisor, Dr. Robert R. Stewart, Department of Geoscience

---

Co-supervisor, Dr. John Bancroft, Department of Geoscience

---

Dr. Larry Lines, Department of Geoscience

---

Dr. Ian D. Gates, Department of Chemical and  
Petroleum Engineering

---

Date

## ABSTRACT

Multicomponent seismic analysis can be a powerful tool for reservoir delineation. Analyzing both compressional (PP) and converted (PS) wavefields can provide detailed information about lithologies, fluid saturation and subsurface structures. Two projects are considered in this thesis: a 2D-3C (two dimensional seismic survey recorded on three component geophones) project from Willesden Green, Alberta and the 3D-3C (three dimensional seismic survey recorded on three component geophones) project from Manitou Lake, Saskatchewan.

The Upper Cretaceous (Turonian) Second White Speckled Shale (2WS) is the zone of interest at Willesden Green. PP and PS synthetic seismograms generated from borehole logs correlate well with the surface seismic data. Post-stack PP and PS inversion was applied to the vertical and radial components to yield P and S impedances.

V<sub>p</sub>/V<sub>s</sub> estimates (from horizon correlations after registration) show anomalous values around 1.6 to 1.8 in zones of interest around the producing wells. This result was helpful for sand/shale discrimination, considering that shale's V<sub>p</sub>/V<sub>s</sub> values are usually higher than 1.9.

Lower Cretaceous fluvial sand channels with high porosity and permeability in the Manitou Lake area of Saskatchewan contain important oil and gas reserves. The goal here is to use 3C-3D seismic data to differentiate sand versus shale and find hydrocarbon-filled porosity. Well logs and synthetic seismograms are used to correlate the PP and PS seismic sections from the 3C-3D seismic survey, to better delineate the Colony and Sparky reservoir sands. Detailed registration of multicomponent seismic data aims to

reduce the uncertainty of traditional channel interpretation and improve well targeting. Mode-converted (PS) seismic amplitudes complement traditional PP channel interpretations. PP and PS amplitude maps show different aspects of the Sparky and Colony sand channels. Curvature co-rendered with the PP/PS amplitude envelope or curvature co-rendered with coherence can better delineate the edges of the channels, providing information about the top and bottom of the reservoir. Seismic attributes such as AVO, fluid factor, LMR ( $\lambda$ - $\mu$ - $\rho$ ), and joint inversion methods provide additional information. The simultaneous inversion method followed by Vp/Vs maps can complement the information for drilled wells and give confidence in identifying new drilling locations. Vp/Vs values less than 2.15, from PP and PS maps (registered in PP time), correlate with productive zones.

## ACKNOWLEDGEMENTS

I would like to thank everyone who made this project possible. Especially to Dr. Robert Stewart for supervising my efforts, providing his constant encouragement, knowledge, experience and support.

Thanks to Dr. John Bancroft, Dr. Larry Lines and Dr. Joe Wong for helpful advice and discussions.

I give my special thanks to Brian Russell for help with Hampson-Russell software.

I give also my special thanks to Murray Roth for help with Transform Software.

Thanks to Graham Pye (Response Seismic Survey Ltd) for donating the Willesden Green seismic data, and Brian Szatkowsky (Calroc Energy Ltd.) for donating the 3C-3D Manitou Lake seismic data and logs.

Thanks to Peter Cary (Sensor Geophysical Ltd) for processing the Willesden Green data.

Thanks to Hanxing Lu and Kevin Hall for processing the Manitou Lake data.

Thanks to John Prutzman (Transform Software), Carmen Dumitrescu (Sensor Geophysical Ltd) and Ianusz Peron (Hampson-Russell) for their time, advices and help with the software.

Thanks to David Feuchtwanger (formerly of Aguila Explorations Consultants Ltd) and Maria Quijada for help and collaboration.

I would like to show my appreciation to Kevin Hall, Rolf Maier, Kayla Bonham and Joan Embleton for their time and sharing of knowledge.

I acknowledge CREWES (Consortium for Research in Elastic Wave Exploration Seismology) for financial and technical support. Thanks to sponsors, staff and students for discussions suggestions, and help.

Finally I would like to thank to my family, without whom this project would not have been completed.

## **DEDICATION**

To my son, Adrian Alexander

## TABLE OF CONTENTS

APPROVAL PAGE.....	ii
ABSTRACT.....	iii
ACKNOWLEDGEMENTS .....	v
DEDICATION.....	vi
TABLE OF CONTENTS.....	vii
LIST OF FIGURES.....	x
LIST OF TABLES.....	xviii
GLOSSARY OF TERMS.....	xix

### **Chapter 1: Introduction**

1.1 Background.....	1
1.2 Thesis objective, structure and datasets used.....	5
1.3 Software used.....	6

### **Chapter 2: Willesden Green oilfield, Alberta, 2D-3C Project**

2.1 Introduction.....	8
2.2 Study location and data.....	9
2.3 Previous work.....	10
2.4 Geology and stratigraphy.....	12
2.5 Geologic model of the reservoir.....	20
2.6 Acquisition and processing for 3-C surface seismic and VSP.....	24
2.7 PP Interpretation.....	24
2.8 PP Inversion.....	30
2.9 PS Interpretation.....	34
2.10 PP and PS interpretation.....	37
2.11 PS Inversion.....	40
2.12 Anomalous zones for line WG1.....	43
2.13 Anomalous zones for line WG2.....	47
2.14 Joint inversion of Willesden Green data.....	50
2.14 A Joint inversion of line WG1.....	50

2.14B Joint inversion of line WG2.....	54
2.14C Anomalous zones for Willesden Green.....	57
2.15 Conclusions.....	58
<b>Chapter 3: Manitou Lake, Saskatchewan, 3D-3C Project</b>	
3.1 Introduction.....	61
3.2 Location.....	62
3.3 Geology and stratigraphy.....	63
3.4 Geologic model of the reservoir.....	66
3.5 Acquisition and processing for 3-C 3-D surface seismic.....	68
3.6 Lithology differentiation.....	71
3.7 PP Interpretation.....	74
3.8 PP and PS interpretation.....	80
<b>Chapter 4: Attributes at Manitou Lake</b>	
4.1 PP and PS Amplitude Maps.....	93
4.2 Amplitude Envelope and Curvature.....	95
4.3 Curvature, Coherence and Recursive Inversion.....	102
4.4 PP and PS Amplitude Maps and Vp/Vs Maps.....	110
<b>Chapter 5: AVO Analysis at Manitou Lake</b>	
5.1 AVO Simultaneous inversion.....	112
5.2 AVO Attributes.....	117
5.21 AVO Product A*B.....	118
5.22 AVO Scaled Poisson's ratio A+B.....	121
5.23 AVO Elastic Constants.....	122
5.24 AVO Fluid Factor.....	123
5.25 AVO LMR.....	125

<b>Chapter 6: Joint Inversion at Manitou Lake</b>	
6.1 Joint Inversion Method.....	128
6.2 Joint Inversion Results.....	130
6.3 Conclusions.....	136
<b>Chapter 7: Summary and recommendations</b> .....	139
REFERENCES.....	141

## LIST OF FIGURES

<b>Figure 1.1:</b> Multicomponent seismic workflow including PP and PS wave interpretation plus joint analysis.....	2
<b>Figure 1.2:</b> Map of Alberta and Saskatchewan showing the location of Willesden Green and Manitou Lake.....	5
<b>Figure 2.1:</b> Location of Willesden Green, Alberta.....	9
<b>Figure 2.2:</b> Location of the study area with the two 2D-3C seismic lines.....	11
<b>Figure 2.3:</b> Simplified stratigraphic nomenclature of Cretaceous successions in the central plains of Alberta (modified).....	15
<b>Figure 2.4:</b> Generalized stratigraphy of the Colorado Group in the Western Canada sedimentary basin (modified).....	16
<b>Figure 2.5:</b> Gamma ray and P wave sonic logs and cross-plot for well 1-35-41-6.....	19
<b>Figure 2.6:</b> P-wave sonic, S-wave sonic (from Castagna’s equation), Computed Poisson and Density logs for the well 1-35-41-6.....	20
<b>Figure 2.7:</b> Vp/Vs, P wave, S wave sonic logs for well 6-15-41-6 in PP time.....	22
<b>Figure 2.8:</b> Schematic geologic model of 2WS.....	22
<b>Figure 2.9:</b> a) S-wave sonic (from Castagna’s equation), Gamma Ray, Density and P wave logs for the well 6-15-41-6 in PP time. b) P wave sonic, S wave sonic, Gamma Ray, Vp/Vs for well 6-15-41-6 in PS time.....	23
<b>Figure 2.10:</b> WG2 seismic line correlated with the corridor stack (VET) from well 8-13-41-6. Red arrows show the first and second white speckled shale.....	25
<b>Figure 2.11:</b> WG2 seismic line correlated with the zero offset VSP stretched to two way time at the well 8-13-41-6 location.....	25
<b>Figure 2.12:</b> Sonic log at well log 1-35-41-6 and synthetic seismogram correlated with seismic line WG2, the vertical stack, PP zero offset synthetic and the radial stack in PP time.....	26
<b>Figure 2.13:</b> Well 1-35-41-6: P-wave sonic (red) zero offset synthetic (blue), PP-vertical stack, the Zoeppritz synthetic and the cross-correlation coefficient.....	28

<b>Figure 2.14:</b> 35 Hz Ricker wavelet for the synthetic PP trace, frequency band: 8-75 Hz.....	28
<b>Figure 2.15:</b> a) Well log correlations on line WG2: a) 8-26-41-6, b) 1-35-41-6, c) 8-13-41-6.....	29
<b>Figure 2.16:</b> Tie line between lines WG1 and WG2 on PP data.....	30
<b>Figure 2.17:</b> PP Model-based inversion- algorithm.....	32
<b>Figure 2.18:</b> Model-P impedance used for inversion on line WG2.....	32
<b>Figure 2.19:</b> PP Model based inversion (zoomed) at well 8-26-41-6W5 on line WG2....	33
<b>Figure 2.20:</b> PP Model-based inversions at well 1-35-41-6 on line WG2.....	33
<b>Figure 2.21:</b> 25 Hz Ricker wavelet for the synthetic PS trace, frequency band: 5-50 Hz.....	35
<b>Figure 2.22:</b> PS correlation on line WG2 with well 8-26-41-6 in PS time.....	36
<b>Figure 2.23:</b> PS correlation on line WG1 with well 16-15-41-6 in PS time .....	36
<b>Figure 2.24:</b> PP and PS horizons after registration (in PP time) and horizon match: line WG2, well 1-35-41-6.....	39
<b>Figure 2.25:</b> PS model-S impedance for inversion in PP time on line WG1, at well 6-15-41-6.....	40
<b>Figure 2.26:</b> Model-based PS Inversion in PP time on line WG2 at well 8-26-41-6W5.....	41
<b>Figure 2.27:</b> PS model-based inversion result for line WG2 at well location 8-13 at the 2WS formation.....	42
<b>Figure 2.28:</b> The ratio of the PP to PS inversion in PP time on line WG2.....	43
<b>Figure 2.29:</b> Wells on Line WG1: cumulative oil and gas production of the 2WS horizon up to year 2007.....	44
<b>Figure 2.30:</b> The ratio of PP to PS impedance inversion for line WG1.....	45-46
<b>Figure 2.31:</b> Wells from on Line WG2: cumulative oil and gas production of the 2WS horizon up to year 2007.....	47-48
<b>Figure 2.32:</b> The impedance ratio of PP inversion to PS inversion for Line WG2....	48-49
<b>Figure 2.33:</b> PP and PS data in ProMC after registration and horizon match;line WG1.50	

<b>Figure 2.34:</b> Models built in ProMC for line WG1 at well 6-15-41-6 l; a) P-wave model and b) S-wave model.....	51
<b>Figure 2.35:</b> Statistically extracted wavelets for joint inversion of line WG1 data.....	52
<b>Figure 2.36:</b> Joint inversion results for line WG1: a) Vp/Vs values, b) Zp or P-wave inversion and c) Zs or S-wave inversion.....	53
<b>Figure 2.37:</b> Statistically extracted wavelets for joint inversion of line WG2 data.....	55
<b>Figure 2.38:</b> PP and PS data in ProMC after registration and horizon match: line WG2.55	
<b>Figure 2.39:</b> Joint inversion results for line WG2.....	56
<b>Figure 2.40:</b> Wells from Accumap on Line WG1 and WG2: cumulative oil and gas production from 2WS, up until 2007.....	58
<b>Figure 3.1:</b> Left: Map of major heavy-oil deposits of Alberta and Saskatchewan, and location of the study area .....	63
<b>Figure 3.2:</b> Paleogeographic reconstruction of the Upper Mannville deposition.....	64
<b>Figure 3.3:</b> Stratigraphic columns for west central Saskatchewan.....	65
<b>Figure 3.4:</b> Depositional model for the Colony sand member after Putnam and Oliver..	67
<b>Figure 3.5:</b> Acquisition geometry of the Manitou Lake survey.....	69
<b>Figure 3.6:</b> Well 11-17 location: Comparison of migrated PP in PP time to migrated PS in PS time.....	71
<b>Figure 3.7:</b> a) Log plots showing Gamma Ray and Vp/Vs for well A11-17; b) Crossplot: Vp/Vs versus GR.....	72
<b>Figure 3.8:</b> a) Suite of logs for well a) A11-17 and b) C07-16.....	73
<b>Figure 3.9:</b> Well log correlation with seismic, well A11-17.....	76
<b>Figure 3.10:</b> PP section showing the Colony (blue) and Sparky (red) horizons at the C7-16 well locations. Green arrows show the Colony (above) and Sparky (below) channels. The inserted logs are GR in red and the S-wave sonic in blue.....	78
<b>Figure 3.11:</b> Well C7-16:(1) S (in blue) and P (in red) sonic logs; (2) porosity (blue) and Gamma ray;( 3) density (red) and resistivity (blue);(4)Vp/Vs and the migrated PP section showing an amplitude increase at the Colony sand channel.....	78

<b>Figure 3.12:</b> Amplitude map showing PP RMS amplitudes at the Colony horizon, with a 20 ms window below the horizon.....	79
<b>Figure 3.13:</b> Amplitude map showing PP RMS amplitudes at the Colony sand channel, produced by Calroc Energy.....	79
<b>Figure 3.14:</b> Amplitude map showing PP RMS amplitudes at the Sparky, with a centered 10 ms window. Below comparing with the previous amplitude map processed by Calroc Energy Inc.....	80
<b>Figure 3.15:</b> Synthetic, seismic and well log correlation in PS time at well A11-17. The used wavelet (below) was extracted from the PS seismic data. From left to right: the Gamma ray log, the P-wave (blue), the S-wave (red) and the density.....	83
<b>Figure 3.16:</b> Seismic and well log correlation in PS time at well A11-17.....	84
<b>Figure 3.17:</b> Inline 100: PS migrated and filtered 15-20-30-45 (left) and PP section high cut filtered 10-15-50-60 (right) stretched in PP time at well A11-17.....	85
<b>Figure 3.18:</b> Well A11-17: Registration and horizon matching.....	86
<b>Figure 3.19:</b> Well A11-17: Zoomed image of the PP migrated stack after the registration using horizon match.....	87
<b>Figure 3.20:</b> Well C10-17: Zoomed image of the PP migrated stack after the registration using horizon match.....	88
<b>Figure 3.21:</b> Time structure maps on the registered horizons in PP time: a) Colony and b) Sparky.....	89
<b>Figure 3.22:</b> Isochron map between Colony and Sparky, on PP migration in PP time...	90
<b>Figure 3.23:</b> Unregistered PP-PS display in Transform software.....	91
<b>Figure 3.24:</b> Registration using amplitude envelope in Transform software.....	92
<b>Figure 3.25:</b> Registered PP and PS data showing the gamma adjustment (residual), in Transform software.....	92
<b>Figure 4.1:</b> PP Colony (left) and Sparky (right) time slices.....	93
<b>Figure 4.2:</b> Left: PS Colony and right: Sparky amplitude envelope.....	94
<b>Figure 4.3:</b> PP (left) and PS (right) amplitudes on the Sparky horizon.....	94
<b>Figure 4.4:</b> Attribute response to channel features preserved in the geologic record....	95
<b>Figure 4.5:</b> The sensitivity of curvature attributes to channels.....	96

<b>Figure 4.6:</b> Sign convention for 3D curvature attributes.....	96
<b>Figure 4.7:</b> a) PP (top) and PS (bottom) amplitude envelope at the Colony, co-rendered with the PP minimum negative curvature (bump-map).....	97
<b>Figure 4.7:</b> b) PP (top) and PS (bottom) amplitude envelope at the Sparky, co-rendered with the PP minimum negative curvature (bump-map).....	99
<b>Figure 4.8:</b> a) PP (top) and PS (bottom) amplitude envelope at the Colony, co-rendered with the PP maximum positive curvature (bump-map).....	98
<b>Figure 4.8:</b> b) PP (top) and PS (bottom) amplitude envelope at the Sparky, co-rendered with the PP maximum positive curvature (bump-map).....	100
<b>Figure 4.9:</b> Left: the Colony and right: Sparky horizons in Transform software. a) PP+ PS Curvature is corendered for PP and PS data at the Colony (left) and Sparky (right) interpreted horizons. b) PP+PS Recursive Inversions corendered for PP and PS data in Transform software after applying a zero phase decon and a median filter for spectral enhancement: Colony is on the left side and Sparky on the right.....	104
<b>Figure 4.10:</b> Left: PP, data at the Colony horizon showing the maximum Curvature co-rendered with the recursive Inversion; Right: PS data at the Colony horizon showing the amplitude envelope co-rendered with the recursive inversion.....	105
<b>Figure 4.11:</b> Top: Colony horizon on PP data; bottom: incoherence on recursive inversion at the Colony horizon co-rendered with the maximum curvature (bump-map shadows) and illumination applied.....	106
<b>Figure 4.12:</b> Top: Sparky horizon on PP data; bottom: incoherence on recursive inversion at the Sparky horizon co-rendered with the maximum curvature (bump-map shadows) and illumination applied.....	107
<b>Figure 4.13:</b> Top: Colony horizon on PP data: PP maximum positive curvature co-rendered with PP recursive inversion; below: PP and PS recursive inversions co-rendered at the Colony horizon.....	108
<b>Figure 4.14:</b> PP and PS amplitude maps (left) for the Colony channels are compared with the previous (center) PP interpretation. Vp/Vs maps of the registered PP and PS data are on the left side of the picture.....	110
<b>Figure 4.15:</b> PP and PS amplitude maps (left) for the Sparky sand channels are compared with the previous (center) PP interpretation. Vp/Vs maps of the registered PP and PS data are on the left side of the picture.....	111

<b>Figure 5.1:</b> Summary of AVO Methodology, 2007.....	114
<b>Figure 5.2:</b> PP-gathers used in the prestack AVO inversion.The incident angles are in colours.....	115
<b>Figure 5.3:</b> The ratio of $Z_p/Z_s$ for the Colony sand channel (left) and Sparky (right) after AVO prestack inversion.....	116
<b>Figure 5.4:</b> After the simultaneous inversion a $Z_p$ (P impedance) versus $V_p/V_s$ crossplot for the Colony sand channel (above), and the Colony map showing RMS amplitudes with the crossplot (below).....	116
<b>Figure 5.5:</b> Lithology differentiation for $Z_p/Z_s$ after the simultaneous inversion for well C7-16 location.....	117
<b>Figure 5.6:</b> Left: traces in a seismic gather reflect from the subsurface at increasing angles of incidence $\theta$ ; right: plot of two terms of Aki-Richards' equation.....	118
<b>Figure 5.7:</b> The offset synthetic at well A11-17: the Colony horizon (red) and Sparky horizon (pink). The Colony shows a class III AVO anomaly and the Sparky class II...	119
<b>Figure 5.8:</b> Gradient versus intercept crossplot (upper left) showing class II and III anomaly at the top of the reservoirs, circled in red (upper right).....	119
<b>Figure 5.9:</b> Gradient versus intercept shows class II and III anomaly at the base of the reservoirs, according to the gradient versus intercept chart.....	120
<b>Figure 5.10:</b> The AVO classification (left) after Rutherford/Williams and AVO classification after A. Brown.....	120
<b>Figure 5.11:</b> The sum $A+B$ is proportional to the change in Poisson's Ratio. Above: the scaled Poisson's ratio at the well 2A-11(left) and C7-16(right). Below: the Colony and Sparky horizons showing the Poisson's ratio.....	121
<b>Figure 5.12:</b> The elastic contrasts derived from the three term AVO: Above Colony and below Sparky time slices.....	123
<b>Figure 5.13:</b> Fluid factor for well A-11-17 (top); bottom the fluid factor for a Colony time slice (left) and Sparky (right).....	124
<b>Figure 5.14:</b> Above: MR versus LR from the LMR crossplot: $\lambda\rho$ versus $\mu\rho$ shows the anomalous gas sand in orange. Below, are the results at the Sparky (right) and Colony (left) time slices.....	126

<b>Figure 6.1:</b> The extracted statistical wavelets (in time above and phase below) from the PP data (left) and from the PS data transformed in PP time (right) used for the joint inversion in ProMC.....	128
<b>Figure 6.2:</b> Joint PP-PS inversion procedures.....	129
<b>Figure 6.3:</b> Joint PP-PS inversion: density at well A11-17: inserted curves: Gamma ray P-wave, S-wave and porosity.....	130
<b>Figure 6.4:</b> Above:Vp/Vs values after joint inversion at the Colony horizon. Values less than 2.15 show the productive sands, in yellow. Below: previous Colony PP amplitude map from Calroc Energy.....	132
<b>Figure 6.5:</b> Above:Vp/Vs values after joint inversion at the Sparky horizon. Values less than 2.15 show the productive sands, in yellow. Below: previous Sparky PP amplitude map from Calroc Energy.....	133
<b>Figure 6.6:</b> Cumulative oil production up to 2008 from Accumap, at the Manitou Lake area. All three wells are producing since at least June, 2006.....	134-135

## **LIST OF TABLES**

Table 3.1.Acquisition Parameters (Kinetex Inc.)

Table 5.1.Petrophysical analysis for LMR (Goodway et al, 1997)

## GLOSSARY OF SCIENTIFIC TERMS

This glossary of technical terms provides context and meaning to many expressions and words used in this thesis (after Miller, 1984, Watson, 2004, Sheriff, 2006).

**1-WS:** First White Speckled Shale.

**2-WS:** Second White Speckled Shale.

**3-C seismic survey:** A three-component (3-C) seismic survey which uses a conventional energy source and is recorded with geophones that respond to ground motions in three orthogonal directions (3-C geophones).

**3-C Geophone:** Seismic recording device with three orthogonal coils which respond to ground motion in three orthogonal directions.

**3C-2D seismic survey:** Two-dimensional seismic survey recorded on 3-C geophones.

**3C-3D seismic survey:** Three-dimensional seismic survey recorded on 3-C geophones.

**Acoustic Impedance:** The product of density and seismic velocity. Reflectivity depends on changes in acoustic impedance.

**Amplitude:** The excursion of a seismic trace from its null value.

**Amplitude spectrum:** The Amplitude versus frequency-relationship such as computed in a Fourier analysis.

**Attribute, seismic:** A measurement derived from seismic data, usually based on measurements of time, amplitude, frequency; generally time-based measurements relate to structure, amplitude-based ones to stratigraphy and reservoir characterization, and frequency-based ones to stratigraphy and reservoir characterization.

**ACP: Asymptotic binning:** This concept was introduced by Garotta et al. (1985) for PS-wave processing: the reflected S-wave returns to the surface more vertically than the incident P-wave, thus the reflection or conversion point is not midway between the source and receiver ; furthermore, this conversion point location moves toward the receiver for shallower reflections and larger  $V_p/V_s$  values; the whole trace is put at the location defined by a reflector depth at the location that is large compared with the source receiver offset. For a single layer case, this would be  $X_a = X / (1 + V_p/V_s)$ , where  $X_a$  is the conversion point offset from the receiver position and  $X$  is the source receiver offset.

**API Gravity:** A standard adopted by the American Petroleum Institute for expressing the specific weight of oils: ° API gravity =  $-131.5 + 141.5 / (\text{specific gravity})$ . API 5 to 22 is considered heavy oil, 22 to 31 medium, and greater than 31, light condensate.

**API Units:** A unit of counting rate for the gamma-ray log. The difference between the high and low radioactivity sections in the American Petroleum Institute calibration pit is defined as 200 API units.

**AVO, Amplitude variation with offset:** The variation in the amplitude of a seismic reflection with source-geophone distance; depends on the velocity, density and Poisson ratio contrasts at the reflecting boundary. Used as hydrocarbon indicator for gas.

**Bandpass filter:** A filter which allows the passage of a specified frequency range and attenuate others.

**Bright spot:** An increase of amplitude assumed to be caused by hydrocarbon accumulation.

**CDP:** Common depth point representing the midpoint between a source and receiver.

**Converted wave:** Seismic energy that has traveled partly as a P-wave and partly as an S-wave, being converted from one to the other upon reflection or refraction at oblique incidence on an interface.

**Crosscorrelation function:** A measure of the similarity of two waveforms, of the degree of linear relationship between them; normalized crosscorrelation is also called **correlation coefficient**.

**Dipole sonic log:** Sonic logging tool with dipole source that records P- and S-wave transit times.

**Gamma-ray log (GR):** A well log that records natural radioactivity; in sediments, the log mainly reflects shale content because minerals containing radioactive isotopes.

**Heavy oil:** A type of crude petroleum characterized by high viscosity (less than 10 000 mPa.s) and API gravity between 10 and 20°API. The crude oil at Manitou Lake is considered heavy oil, according to its gravity 12 °API).

**Inversion:** Determining the cause from observation of effects. Inversion has to satisfy constraints that are imposed. The manufacture of a **seismic log** from seismic data is an example of one-dimensional inversion.

**Isochron:** the time thickness or interval travelttime between two interpreted seismic horizons.

**Mode:** Refers to type of wave propagation, e.g. compressional mode or shear mode.

**Multicomponent seismic:** Seismic data acquired with more than one source and/or receiver mode.

**Poisson's ratio:** The ratio of the fractional transverse contraction to the fractional longitudinal extension when a rod is stretched; if density is known, specifying Poisson's ratio is equivalent to specifying the ratio of  $V_s/V_p$ , where  $V_s$  and  $V_p$  are S- and P-wave velocities. Values ordinarily range from 0.5 (no shear strength, e.g., fluid) to 0.

**P-wave:** Pressure, compressional, or longitudinal elastic body wave; direction of propagation is parallel to particle motion.

**PP-seismic:** Seismic waves traveling down as P-waves, reflecting from an interface, and traveling up as P-waves. In this thesis, waves recorded on the vertical component of the geophone are assumed to be largely PP mode.

**PS-seismic:** Seismic waves traveling down as P-waves, reflecting and converting at an interface, and traveling up as S-waves. In this thesis, waves recorded on the radial component of the geophone are assumed to be largely PS mode.

**Radial component:** Horizontal geophone coil which responds to horizontal ground motion in line with the source-receiver azimuth.

**Ricker wavelet:** A zero-phase wavelet, the second derivative of the Gaussian function; it is often used as a zero-phase embedded wavelet in modeling and synthetic seismogram manufacture.

**Seismic:** Having to do with elastic waves; energy may be transmitted through the body of an elastic solid by body waves of two kinds: P-waves (compressional waves) or S-waves (shear waves).

**SP:** Shot point, i.e. station number for seismic source location.

**SP log:** known also as "Spontaneous Potential", a well log of the difference between the potential of a movable electrode in the borehole and a fixed reference electrode at the surface.

**Static correction, statics:** Corrections applied to seismic data to compensate for the effects of variations in elevation, near-surface low-velocity-layer (weathering) thickness, weathering velocity and/or reference to a datum.

**S-wave:** Shear, converted or transverse elastic body wave; direction of propagation is perpendicular to particle motion.

**Synthetic seismogram:** An artificial seismic reflection record manufactured by assuming that a particular waveform travels through an assumed model;(1) in the zero-offset

case, convolving a wavelet with a reflectivity series;(2) in the offset case, a layered model is ray-traced using a chosen geometry and an artificial shot gather is computed, which can also be stacked.

**TOC:** total organic content; percent by weight of the total organic carbon.

**Transverse component:** Horizontal geophone coil which responds to horizontal ground motion orthogonal to the source-receiver azimuth.

**Tuning:** Constructive or destructive interference resulting from two or more reflectors spaced closer than a quarter of the dominant wavelength. The composite wavelet exhibits amplitude and phase effects that depend on the time delays between the successive reflection events and the magnitude and polarity of their associated reflection coefficients, and also on the shape of the embedded wavelet.

**Vertical component:** Vertical geophone coil which responds to vertical ground motion.

**Vibroseis:** A seismic method in which a vibrator is used as an energy source to generate a controlled wavetrain. The vibrator generates waves of continuously varying frequency content.

**V<sub>p</sub>:** P-wave velocity.

**V<sub>p</sub>/V<sub>s</sub>:** Ratio of P-wave velocity to S-wave velocity; it is sensitive to lithology or interstitial fluid.

**V<sub>s</sub>:** S-wave velocity.

**VSP or Vertical seismic profiling:** Measurements of the response of a geophone at various depths in a borehole to sources on the surface.

**Well log:** A record of one or more physical measurements as a function of depth in a borehole.

**Zoeppritz equations:** Equations which express the partition of energy when a plane wave impinges on an interface at an arbitrary angle; the directions of the reflected or transmitted waves obey Snell's law.

## CHAPTER 1 INTRODUCTION

### 1.1 BACKGROUND

Geophysical exploration in the oil and gas industry requires ever more detailed information about the subsurface (Stewart, 2007). In the attempt to determine the actual rock type (e.g., sand versus shale), find sand channels, or to determine the presence of fluids, the interpretation of S-wave properties coupled with P-wave imaging can assist in understanding the subsurface (Stewart et al., 1993).

Compressional (P) waves on an interface at non-normal incidence partition into transmitted and reflected P and shear (S) waves. Reflected P wave energy is largely recorded on the vertical component (PP) of the receiver, whereas the reflected S wave acts on the radial (horizontal) component (PS) of the motion sensors. Due to the difference in wavelength, reflectivity, and travel path, processed PS seismic sections may show significant changes in both amplitude and character when compared with the PP section (Miller, 1996).

A multicomponent interpretation workflow (Figure 1.1) is suggested by Xu and Stewart (2006) and Stewart (2007):

- Interpret the P-wave data to the fullest extent possible, including: geological review of the area, log analysis and editing, PP synthetic seismogram generation, and correlation of the synthetic seismograms with the surface seismic sections or volumes. VSP (vertical seismic profiling) data can help with a more confident interpretation.

- Pick PP horizons to create time structure maps, determine time-thicknesses between horizons, search for amplitude features and undertake AVO analysis and inversions.
- Take the logs and construct PS synthetic seismograms (possibly use a  $V_p$  to  $V_s$  relationship to generate an S-wave log), create a geological model or a gross PP to PS section mapping function, correlate the PS synthetic seismogram to the PS section in PS time.
- PP and PS data “registration” (shrink the PS sections in time to find a correlation with PP time), and extract  $V_p/V_s$  values varying in depth and with each surface location. PS data can be assessed in both PS and PP time.

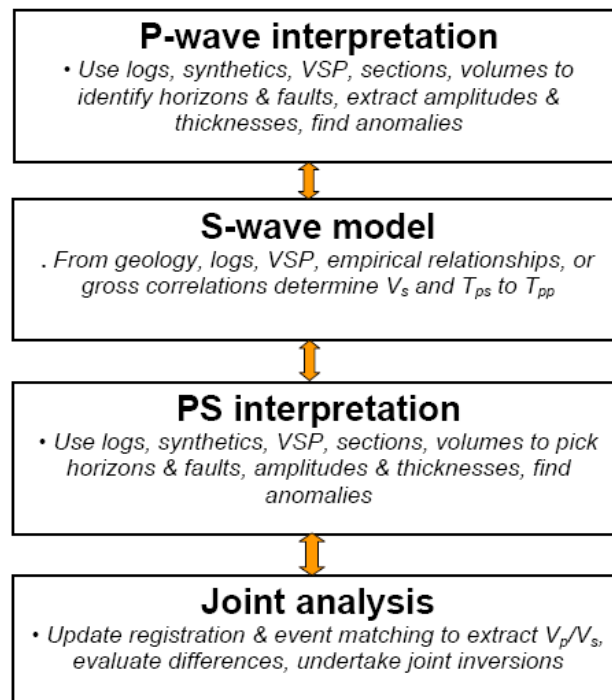


Figure 1.1: Multicomponent seismic workflow including PP and PS wave interpretation plus joint analysis, from Xu and Stewart (2006) and Stewart (2007).

Larson (1996) and Margrave et al. (1998) developed an interpretation technique for the analysis of 3-D multicomponent volumes, showing that time slices, horizon and isochron

maps, coupled with the PP and PS results, can all be useful. PS data can be interpreted on their own, but generally will be analyzed in conjunction with P-wave sections or volumes. Thus, a primary aspect of interpretation is correlating the PP and PS events (Stewart et al., 2002).

Seismic attributes at a given reflection time or horizon can be collected for either PP or PS data (Garotta, 2002).

Shear (S)-waves are insensitive to fluids, slower than pressure (P)-waves, and polarized. These three properties suggest that shear-wave exploration has potential for: imaging structure through gas clouds, increased resolution (the difference in velocity between P and S waves), fluid and lithology discrimination, imaging low acoustic impedance, and fracture detection by analysis of shear wave splitting (Garotta, 2002).

Seismic velocities are affected by numerous geologic factors including rock matrix mineralogy, porosity, pore geometry, pore fluid, bulk density, effective stress, depth of burial, type and degree of cementation, and the degree and orientation of fracturing (Miller, 1996). Domenico (1984) used Pickett's (1963) data to demonstrate that  $V_s$  in sandstones is 2 to 5 times more sensitive to variations in porosity than  $V_p$  in sandstones.

Kuster et al. (1974) indicate that pore aspect ratio has a strong influence on  $V_p$  and  $V_s$ . Anstey's (1991) conclusions of the factors that control S-wave velocity were: first the cementation, then the grain shape and the number and angularity of the grain contacts, intrinsic rigidity of the grain material or cement, clay content and grain size. Porosity, as such, is not a major control on S-wave velocity; the number of grain contacts affects the rigidity of the rock. For fine-grained rocks, cement is likely to form preferentially in small pores and thus the rocks will have a higher rigidity than do the coarse-grained

rocks. Coarse-grained rocks that are well rounded and well-sorted have fairly good porosity and have many rigid contacts and thus, a high S-wave velocity for that porosity (Hilterman, 2001).

Knowing that  $V_s$  can be more sensitive than  $V_p$  to porosity (Domenico, 1984) and to clay content (Minear, 1982), an increase in clay content (decrease in porosity) should result in an increase in  $V_p/V_s$ . This result has been observed in sand/shale sequences (Garrotta et al., 1985). The increase in  $V_p/V_s$  with “shaliness” (the proportion of shale to sand in the rock) has been used in seismic field studies to outline sandstone channels encased in shales (Garrota et al., 1985).

$V_p/V_s$  values are sensitive to gas in most clastics and will often show a marked decrease in its presence (McCormack et al., 1985). P-wave energy is delayed, scattered, and attenuated when passing through gas-bearing sediment (Stewart et al., 2003). As “bright spots” or amplitude anomalies were supposed to originate from gas on P wave data, they should not show up in the S wave mode because shear propagation is not disturbed by gas (Garotta, 2000). We expect P and S modes to behave differently in saturated rocks (Garotta, 2002).

Rock properties such as  $V_p/V_s$  or Poisson’s ratio can be extracted from multicomponent seismic data, and important information about fluid type, porosity, or mineralogy can be revealed (Miller and Stewart, 1990). Compressional seismic velocity alone is not a good lithology indicator, as  $V_p$  can have the same value for various rock types.  $V_s$  can bring additional information and reduce the interpretational ambiguity.

## 1.2 THESIS OBJECTIVE, STRUCTURE AND DATASETS USED

This thesis discusses two cases in which multicomponent seismic data were used to help in the search for hydrocarbons: in one, a 2D-3C project from Alberta at Willesden Green, the hydrocarbon reservoir is a fractured shale with occurrences of sands, while in the other, a 3D-3C project from Saskatchewan at Manitou Lake, the zone of interest consists of sand channels (Figure 1.2). Analysis of both datasets shows how PS data can bring additional information to geophysical exploration.

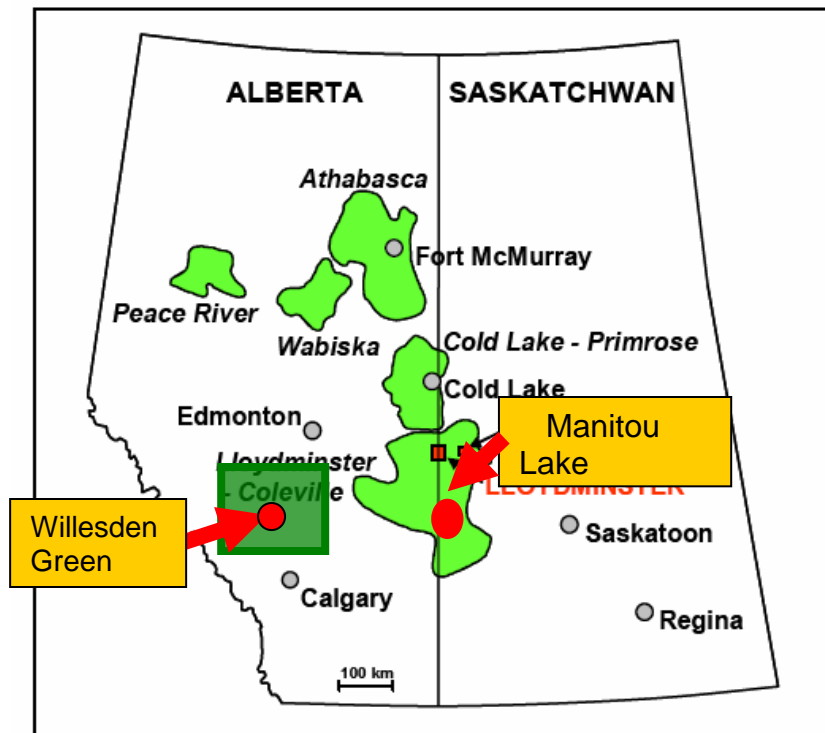


Figure 1.2: Map of Alberta and Saskatchewan (modified after Watson, 2004) showing the location of Willesden Green and Manitou Lake. The green areas hosts heavy oil deposits.

The objectives of this thesis are as follows: (1) to develop an interpretation techniques using PP and PS seismic data, (using multiple attributes and two different software

packages), (2) investigate which attributes correlate with well production information for two study areas (3) use a combination of attributes to suggest future drilling locations.

The Upper Cretaceous (Turonian) Second White Speckled Shale (2WS) shale at Willesden Green, and the lower Cretaceous fluvial sand channels at the Manitou Lake of Saskatchewan, contain important oil and gas reserves. The Alberta case study is described in Chapter 2, and the Manitou Lake case from Saskatchewan is described in Chapter 3.

### **1.3 SOFTWARE USED**

Different software was used with the steps of multicomponent interpretation. For Chapter 2, where 2D interpretation was performed, the following packages have been used to process and interpret the data:

- The two 2D seismic lines at Willesden Green were reprocessed in 2004 by Peter Cary at Sensor Geophysical, Calgary. The vertical and radial migrated stacks were generated using the ProMAX seismic processing package.
- The correlation of well logs to the seismic data was manually done by using the Hampson-Russell eLog package. The ProMC software package was used to analyze PP and PS datasets simultaneously with one scale, and to create the  $V_p/V_s$  sections.
- Inversion was performed using Hampson-Russell's Strata package, where both PP and PS impedance sections were constructed and analyzed.

- The Accumap System was used to retrieve well logs, and to get information on well production and operation.

For Chapter 3, concerning the Manitou Lake 3C-3D seismic study, the following packages have been used to process and interpret the data:

- The data have been processed to a final migrated volume by Hanxing Lu and Kevin Hall at the CREWES project, by using ProMAX software.
- Log correlations with the seismic, and the registration between PP and PS data, were performed by using Hampson-Russell's ProMC from the Geoview package.
- Post-stack inversions were performed with Hampson-Russell's Strata, and the software analysis package from Transform.
- The AVO program under Geoview was used to analyze the pre-stack seismic data: the Amplitude Versus Offset (AVO) anomalies were evaluated to determine the fluid content of the rocks; simultaneous inversions were performed and the LMR method was used.
- The joint PP-PS inversion was performed in the ProMC package (Hampson-Russell).
- The registration was performed in ProMC and Transform software.
- Transform Software was used for more attributes and a detailed 3D interpretation, to delineate the channel edges. Amplitude envelope, coherency, curvature, and recursive inversion were co-rendered in this work.

## **CHAPTER 2 WILLESDEN GREEN OILFIELD, ALBERTA, 2D-3C PROJECT**

### **2.1 INTRODUCTION**

In this chapter, 2D multicomponent seismic data and well logs from Willesden Green, Alberta, are used to investigate an oil reservoir interval. The Upper Cretaceous (Turonian) Second White Speckled Shale (2WS) represents the zone of interest.

In the attempt to understand subsurface lithologies, it is useful to use not just P wave properties, but those of the S wave as well. Recent interest in the use of PS waves to help characterizing reservoirs has lead to the acquisition of multicomponent surveys in the industry. The combination of pure P wave measurements with the converted waves can provide more information about the rock structure, state of fracturing, pore fluids, lithologic type, and stratigraphy (Stewart, 1990; Stewart et al., 1993).

The Second White Speckled Shale (2WS) is picked on geophysical logs by its high gamma response (Travis, 2002). As calcite percentage in the source rock increases toward pure limestone, the hydrocarbon potential decreases. A number of wells in the area have produced, and still produce oil and gas from the 2WS. However, because a number of penetrations of the 2WS shale have not produced oil, existing exploration techniques (e.g., conventional P-wave prospecting) are not considered adequate. In an attempt to better delineate productive zones, 2D multicomponent seismic surveys were undertaken by Response Seismic Survey, and converted-waves (PS) were analyzed along with the P-wave data (Stewart et al., 1993).

## 2.2 STUDY LOCATION AND DATA

The Willesden Green oilfield, located in south-central Alberta (Figure 2.1), covers 50,827 hectares, and is the second largest Cardium field after Pembina (both in area and initial oil in place). The associated oil in place of this pool is 929 MMBbls, and the cumulative production to date is 140 MMBbls. Several productive horizons in this area, including the Second White Speckled Shale (2WS), Cardium, Viking and Glauconitic sands, continue to produce significant quantities of oil and gas.

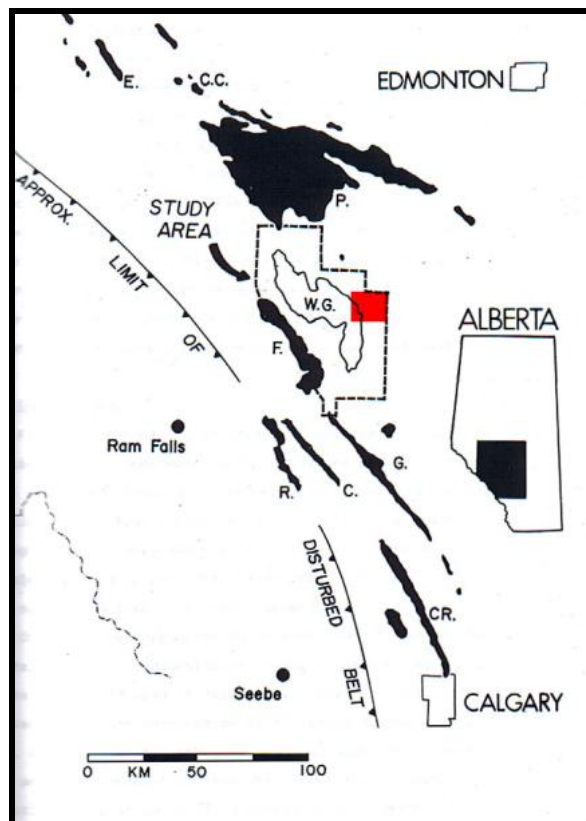


Figure 2.1: Location of Willesden Green (W.G.), Alberta (map from Keith, 1985). The red rectangle indicates the area of interest and the two crossing 2D-3C lines.

Data from the Willesden Green area include well logs, VSP, and 2D-3C seismic lines. The red square in Figure 2.1 shows the location of the 2D-3C lines in south-central Alberta. Figure 2.2 provides a zoomed image of the area of interest, with the Response Seismic Surveys map (T41, R5-6) showing the 2 crossing lines (WG1 and WG2). WG1, an east-northeast line with CDPs from 1 to 729 (blue rectangles) is crossed by line WG2, a north-northwest line with CDPs from 1 to 599 (green rectangles), Varga et al.,( 2007).

Three wells were used for line WG1: 6-15-41-6W5, 16-15-41-6W5, and 8-13-41-6W5. Two more wells are used with line WG2: 1-35-41-6W5 and 8-26-41-6W5, as shown in Figure 2.2. The well ties with the seismic are represented by black circles.

## **2.3 PREVIOUS WORK**

Stewart et al. (1993) undertook a preliminary interpretation of Willesden Green data. Their overall goal was to assess the data quality, correlate the information, and seek anomalies that could be connected with the oil production in the Second White Speckled Shale (2WS).

The three Willesden Green VSP surveys (two offset surveys and one zero-offset) were conducted in 1990 at the 8-13-41-6W5 location by Schlumberger of Canada. Response Seismic Surveys Ltd. acquired the two 3-C surface seismic lines in 1992. The surface data was first processed by Pulsonic Geophysical Ltd. (Cary et al., 1993).

There were reasonable ties (Figure 2.11) among the synthetic seismogram, VSP sections, and PP and PS surface seismic sections (Stewart et al., 1993) for both lines. A compelling

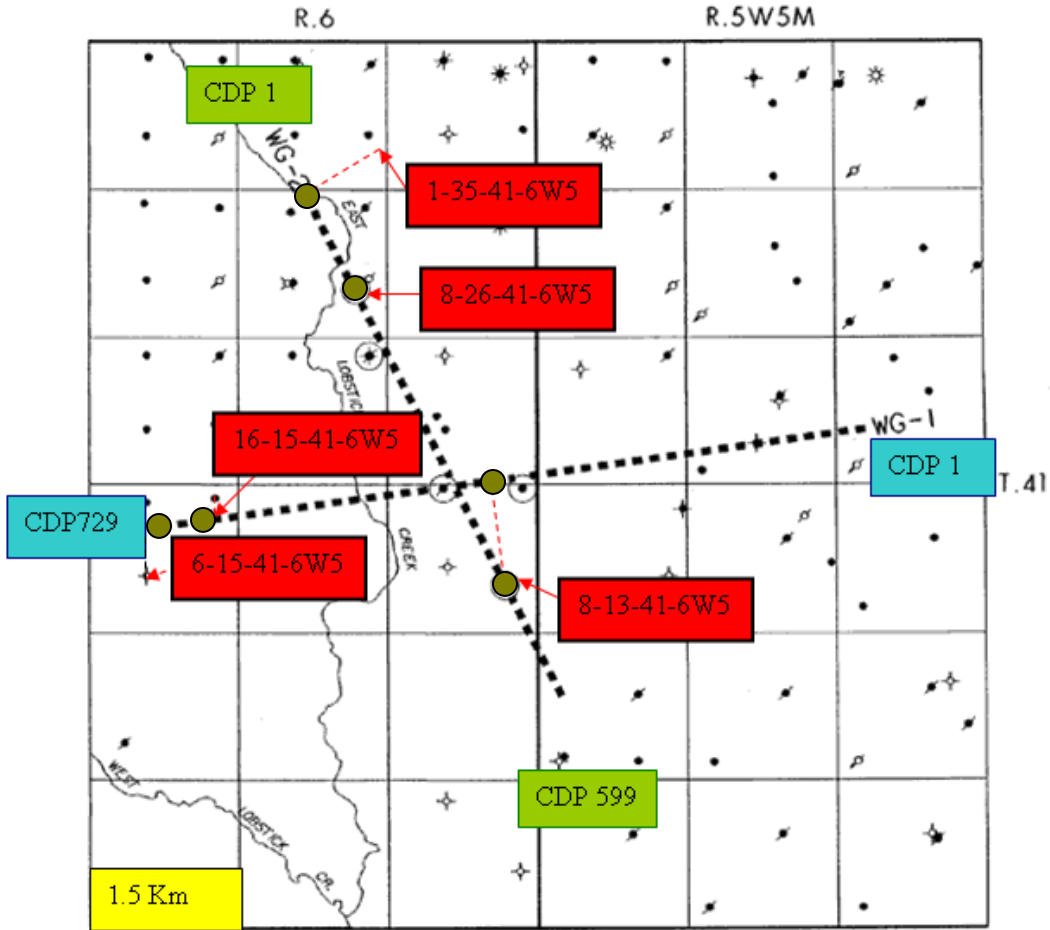


Figure 2.2: Location of the study area with the two 2D-3C seismic lines (modified from Response Seismic Surveys Ltd.). Olive circles indicate the seismic tie points with the wells (Varga et al., 2007)

preliminary interpretation was made of the seismic signature of the geology. There was not found an obvious evidence of velocity change with azimuth or shear wave-splitting, to indicate fracturing of the 2WS. The two lines were reprocessed in 2004 by Peter Cary at Sensor Geophysical Ltd. Vertical and radial migrated stacks were generated. The processing flow for the PP section was conventional and included surface-consistent deconvolution, time-variant spectral whitening, refraction statics, trim statics, CDP stack and migration. The processing flow for the PS section included asymptotic CDP binning,

surface consistent deconvolution, refraction statics, trim statics, CDP stack and migration. The goal of this thesis is to refine the previous interpretation and improve the previous results by registering the radial and vertical sections in PP time, invert the PP and PS data and predict drilling locations.

## **2.4 GEOLOGY AND STRATIGRAPHY**

The geologic framework of the Willesden Green area is discussed in this section. The reservoir is situated in the upper Cretaceous interval of the Colorado Group.

The Colorado Group is of significant economic importance in that it contains about 14% of the total Western Canada hydrocarbon reserves and about 80% of the reserves within the Middle Jurassic to Cretaceous foreland basin succession (Podruski et al., 1988; Porter, 1992). It was deposited during a period of global sea level high stand, which, with the downflexing of the North American craton, led to increased accommodation and thick, geographically continuous shale deposition (Leckie et al., 1994). Relative sea level fluctuations resulted in condensed sections and regressive siltstone and sandstone packages (Bloch et al., 1999). The Colorado group contains several sandstone and conglomerate units, some of which are prolific hydrocarbon producers. These include the Basal Colorado Sandstone, Spinney Hill Sandstone, Viking formation, St. Walburg Sandstone, Barons Sandstone, the Dunvegan Formation, sandstones of the lower Kaskapau Formation, sandstones of the Second White Speckled Shale, the Cardium formation, Medicine Hat Sandstone, and the Alderson member of the Lea Park Formation; within the Colorado Group, the First and Second White Speckled Shales, the

Fish Scales Zone, and shale at the base of the Shaftesbury Formation, which are more radioactive than overlying and underlying shales, have high total organic carbon contents, and contain considerable hydrocarbon generating potential. An interval such as the Second White Speckled Shale is potentially both a source and a reservoir rock. The Colorado Group thins eastward from about 700 m in southwestern Alberta to 200 m in the Manitoba Escarpment.

Most studies of the Colorado Group have focused on investigations of the coarser-grained reservoir units like the Cardium formation. However, the shale-dominated sequences within the Colorado Group provide a much more complete record of deposition and a more comprehensive picture of Cretaceous paleogeography (Bloch et al. 1994) as outlined in Figure 2.3.

The Second White Speckled Shale (Colorado Group) is an Upper Cretaceous, fine-grained, laminated clay sediment, deposited in a shallow to open marine environment. It is a mainly calcareous shale and mudstone with intercalated chalk, calcarenite, bentonite, calcite, and phosphorite and localized occurrences of sandstone and siltstone (Lexicon of Canadian Stratigraphy, Western Canada). The shale is characterized by a high total organic carbon content, high hydrogen indices, and high radioactivity on well logs. On gamma-ray logs, the Second White Speckled Shale interval is typically radioactive as a result of elevated uranium content associated with abundant kerogen (buried organic matter, broken down and converted into petroleum by combined effects of heat and time) in the shale. Discrete radioactive spikes also occur as a result of bentonites deposited in the shales (Travis, 2002).

The 2WS is a good stratigraphic marker and has a thickness of between 45m and 70m. It is overlain by the Colorado shale and underlain by the Belle Fourche shale. It is both a source and a reservoir rock (in shales the hydrocarbon may remain trapped within the source rock), containing type II kerogen. The kerogen type will influence the chemistry of the generated hydrocarbons, and the amount of organic matter (TOC) which exerts a strong influence on the adsorption capacity of the shale (Travis, 2002). Adsorption is the adhesion of a single layer of gas molecules to the internal surfaces of the coal or shale matrix (Hill, 2000). 2WS percent by weight of the total organic carbon (TOC) values range from 1-5 % (Travis, 2002).

It is suggested by Travis (2002) that the 2WS may retain significant amounts of generated liquid hydrocarbons due to its fine-grained nature. At greater burial depths, these hydrocarbons would be transformed (cracked) to gas. For the production of shale gas, a fracture system must be developed within the source rock to contribute storage capacity (porosity) and migration pathways (permeability) for the gas (Fig. 2.4.).

Sand lenses within the shale sequences are also common and could represent local zones of enhanced porosity and permeability within the overall shale reservoir (McKinstry, 2001). The 2WS formation represents a yet undeveloped unconventional gas play within the Western Canada Sedimentary Basin (Travis, 2002)

The Cardium Formation was deposited along the western margin of the Cretaceous Interior Seaway within the Alberta Foreland basin of the Canadian Cordillera. It is the main sandstone unit within the Alberta (Colorado) group and contains about 100 m of interbedded sandstones and shales, as in Figure 2.3. It is overlain by the Wapiabi

Formation which is about 600 m thick, which consists mostly of shales. The top of the Cardium formation is recognized by the first appearance of a thin chert pebble bed, the main sandstone unit within the Alberta (Colorado) group, and contains about 100 m of

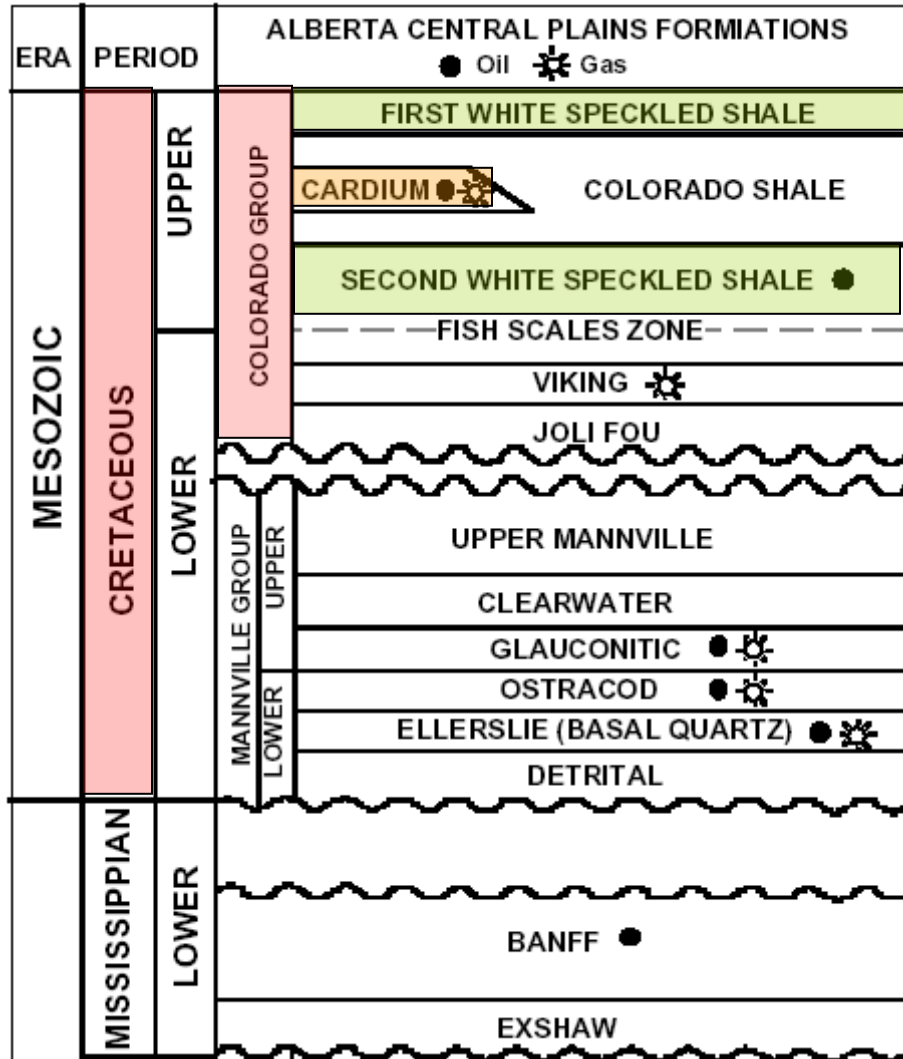


Figure 2.3: Modified from the simplified stratigraphic nomenclature of Cretaceous successions in the central plains of Alberta (after Kohrs and Norman, 1988).

interbedded sandstones and shales, as shown in Figure 2.3. It is overlain by the Wapiabi Formation which is about 600 m thick, and which consists mostly of shales. The Cardium formation occurs below the First White Specks (the 1WS, is a regionally recognizable

well log marker), but above the main Cardium sandstones and conglomerates. The thickest Cardium conglomerates are preferentially accumulated in the East and Northeast of the Willesden Green area (Keith, 1985). Some scouring of the Cardium sandstone by the conglomerates is probable within Willesden Green. Storm-generated geostrophic flow may have been responsible for the offshore transport of the Cardium sands and conglomerates into this area (Keith, 1985).

The Cardium zone is sometimes difficult to pick and, as shown by Griffith, (1981), has frequently been incorrectly positioned. The markers with possible high resistivity kicks which are identifiable on gamma logs are the 1WS shale and the 2WS shale.

Seals are generally formed by interbedded mudstones, but may result from juxtaposition of low permeability rocks over reservoir rocks by thrusting.

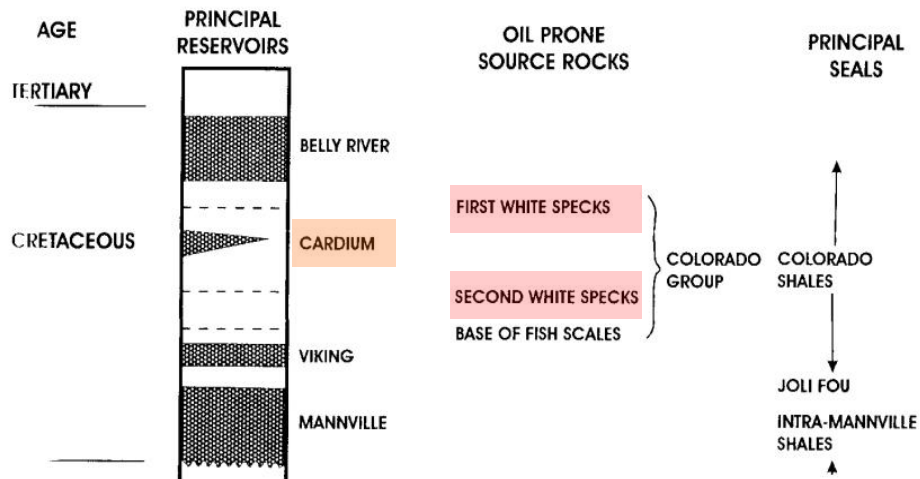


Figure 2.4: Modified from Generalized Stratigraphy of the Colorado Group in the Western Canada Sedimentary Basin (after Creaney and Allen, 1992).

A crossplot of gamma ray versus Vp for well 1-35-41-6 (Figure 2.5) differentiates the lithologies. Three major types of lithology were selected: sands (yellow), shales (olive),

and silts combined with sands and shales (orange). Low values in gamma ray log (less than 75 API) and low P wave velocity (less than 4000m/s) indicates permeable sand interval with high porosities. Higher values on gamma ray log and higher velocities delineate the silts mixed with sands and shales. The highest values on gamma ray logs (higher than 125 API) were defined as shales (olive). The lowest value in gamma ray in Figure 2.5 a) shows the Cardium formation at depth 1900m-2000m and indicates sands (yellow). The Cardium is the main sandstone unit, showing a decrease on P-wave and S-wave logs, a decrease in density and an obvious decrease on gamma ray. The 2WS shows vertical sequences of shales (olive) alternating with silts and sands and occurs at depths between 2080m-2120m.

In this thesis, I will mainly analyze the productive Second White Speckled Shale. Summarizing information about the 2WS (Figure 2.4 and 2.5), we note that it:

- is deposited in the latest Cenomanian to Middle Turonian in an open-marine environment, represented by a time of maximum sea level. The fine, laminated character suggests deep-water deposition with low sedimentation rates; the lack of bioturbation and preservation of abundant organic matter supports water bottom anoxia (absence of oxygen) theory. The quiet, deep marine deposition of the 2WS formation allows for the potential preservation of total organic carbon (TOC) with a type II marine/algal kerogen (Travis, 2002).
- is mainly a calcareous shale and mudstone with intercalated chalk, calcarenite, calcite, and localized occurrences of sandstones and siltstones.

It can incorporate a sequence of shaly sandstones and siltstones (about 6m below the 2WS shale) termed the Second White Specs Sandstone (monotonously repeated light fine and very fine grained sandstones and coarse grained siltstones) which is correlative with Phillips sandstone in southern Alberta (Lexicon of Canadian Stratigraphy, 1997).

- has occurrences of sand lenses that could represent local zones of enhanced porosity and permeability within the overall shale reservoir. The permeability and porosity can be achieved through localized natural fractures developed from structural influences (McKinstry, 2001).
- is a good stratigraphic marker showing an increase on P-wave logs and a bigger increase on the S-wave logs, a decrease in density, and a jump (kick) in gamma ray log response followed by a decrease (Figures 2.5 and 2.6). , its thickness varying between 20m to 40m.
- is a source rock of light crude oil and gas within Alberta (Figure 2.4)- contains kerogen II (which generates oil and gas).
- is a reservoir rock (in shale the hydrocarbon may remain trapped within the source rock). This is possible due to associated coarser grained silts and sand beds within the shales that may act as local reservoirs (McKinstry, 2001). The 2WS hold large volumes of potential hydrocarbon; its expulsion of the generated hydrocarbon is considered to be poor, and hence the generated oil is held within the system and upon continued heating is cracked to gas (Travis, 2002).

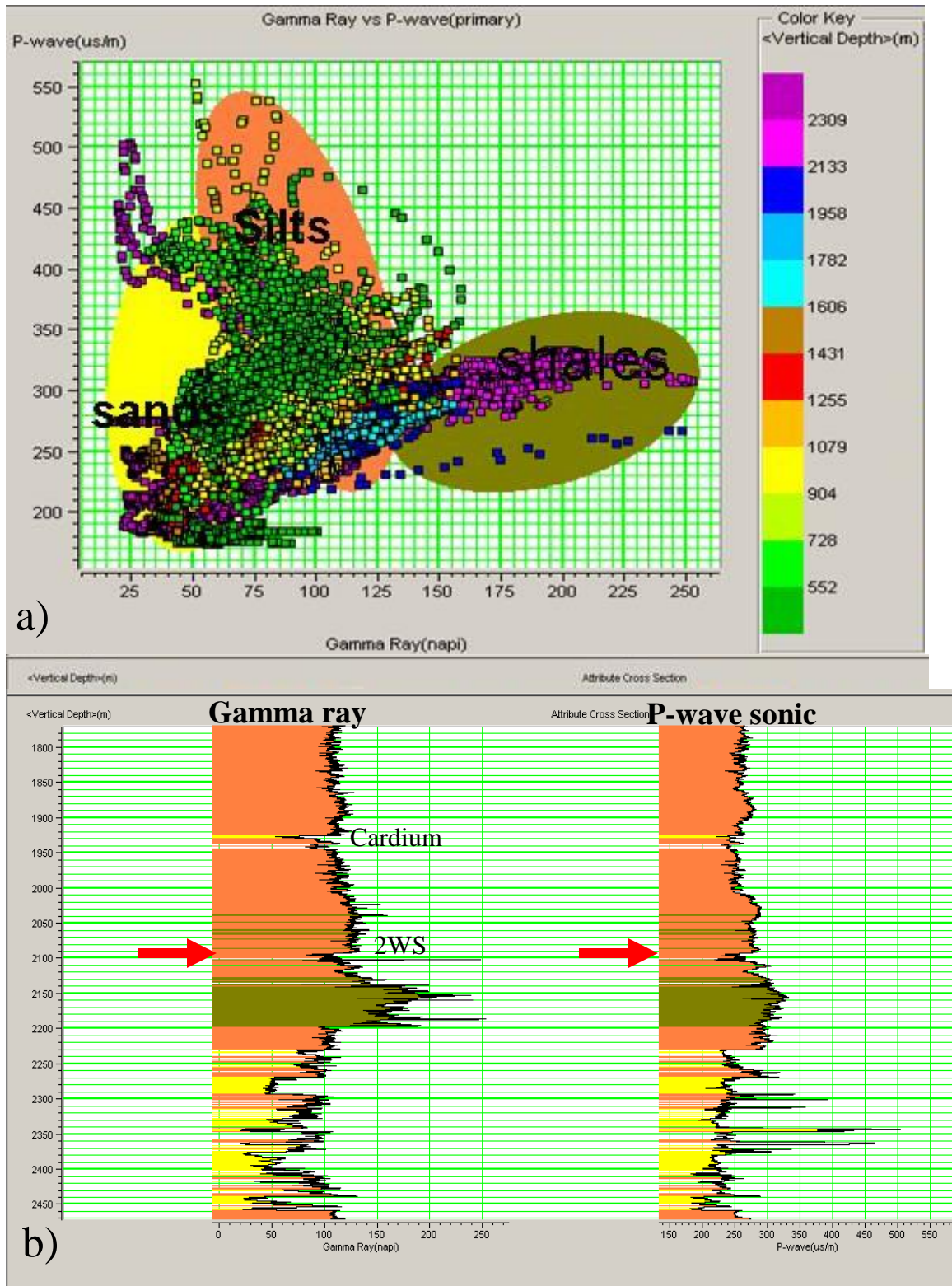


Figure 2.5: a) Gamma ray and P-wave sonic logs for well 1-35-41-6. a) A cross-plot for well 1-35-41-6 delineates the zones with different lithology. b) Three major types of lithology were selected: sands (yellow), shales (olive) and silts (orange) on the gamma ray (left) and the P-wave sonic (right) logs.

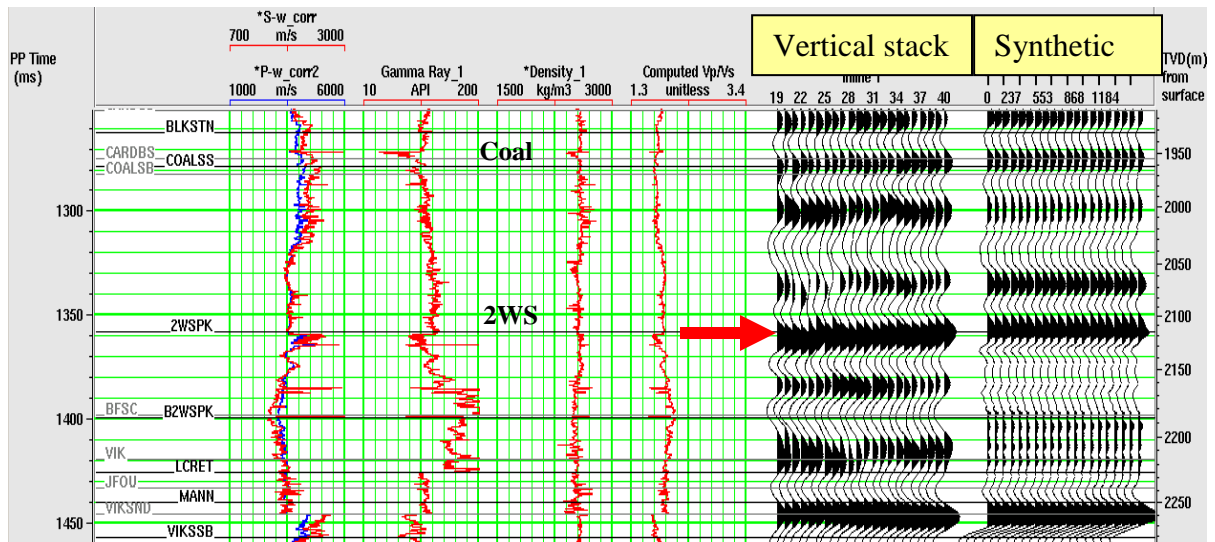


Figure 2.6: Left to right: P-wave sonic (blue), S-wave sonic in red (from Castagna's equation), gamma-ray, density and the computed Vp/Vs logs, the migrated PP section and the PP Zoeppriz synthetic at the well 1-35-41-6 location.

Figure 2.6 shows a strong pick at the 2WS horizon, indicated with red arrow; it shows a jump (kick) on the P-wave sonic and the computed S-wave sonic (with Castagna's equation 2.2). The top of the formation is picked as a half meter low spike in gamma ray response, followed by relatively high gamma readings (Travis, 2002), as seen in Figures 2.6, 2.7 and 2.9.

## 2.5 GEOLOGIC MODEL OF THE RESERVOIR

A geologic model was created to understand the 2WS reservoir and its Vp/Vs anomalies from the PP and PS sections. This model helped to identify the oil-saturated Second white speckled shale. A good correlation between Vp/Vs (from amplitude inversions and time thickness ratio) and oil production is found. 2WS is a source and a reservoir rock: oil and gas form from the preserved soft parts of ancient organisms that were buried, and then broken down and converted into petroleum by the combined effects of heat and

time. Buried organic matter is called kerogen, and a petroleum source is any rock that contains enough kerogen to generate oil or gas. Most source rocks are shales with a total organic content (TOC) of at least 3 % (McGeary and Plummer, 2006). Considerations of the 2WS reservoir for a schematic geologic model can be seen in Figure 2.8:

- 2WS is a mainly calcareous shale formation with occurrences of sandstones and siltstones (enhanced porosity and permeability).
- Increasing sand in the reservoir yields porosity (good reservoir) – lower  $V_p$  and gives higher  $V_s$  (Figures 2.6 and 2.9), so we suggest that increasing sand versus shale or limestone could lower the  $V_p/V_s$  value.
- Increasing calcite / limestone cementation in the reservoir yields higher  $V_p$  value (Figures 2.6, 2.7 and 2.8) as in the schematic geologic model from Figure 2.8.
- The presence of hydrocarbons lowers  $V_p$ , and  $V_p/V_s$  (Figure 2.7 and 2.9).
- The 2WS represent a yet undeveloped unconventional oil/gas play within the Western Canada Sedimentary basin, with the potential to generate large volumes of hydrocarbon (Travis, 2002).
- For production of shale gas, a fracture system may be developed within the source rock to contribute storage capacity (porosity) and migration pathways (permeability) for the gas (Travis, 2002).

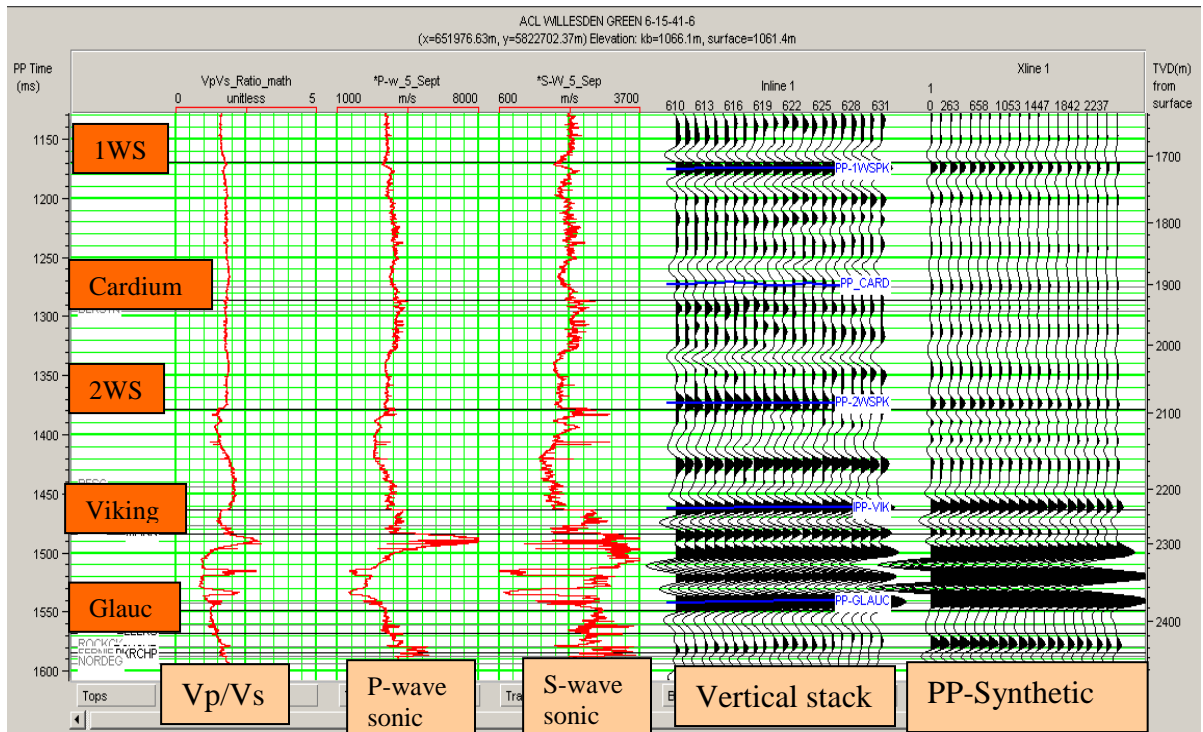


Figure 2.7: From left to right: Vp/Vs, P wave, S wave sonic logs followed by the PP migrated section and the Zoeppritz offset synthetic at well 6-15-41-6 location in PP time. The picked horizons on the vertical migrated stack are in blue.

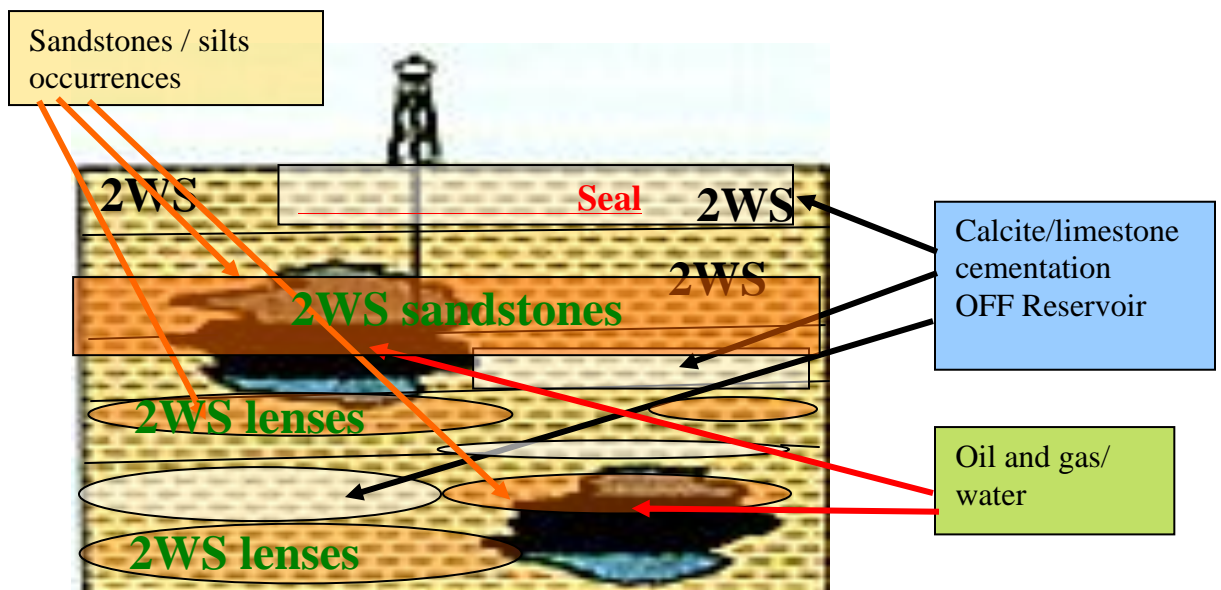


Figure 2.8: Schematic geologic model of 2WS (modified from McGeary and Plummer, 2006).

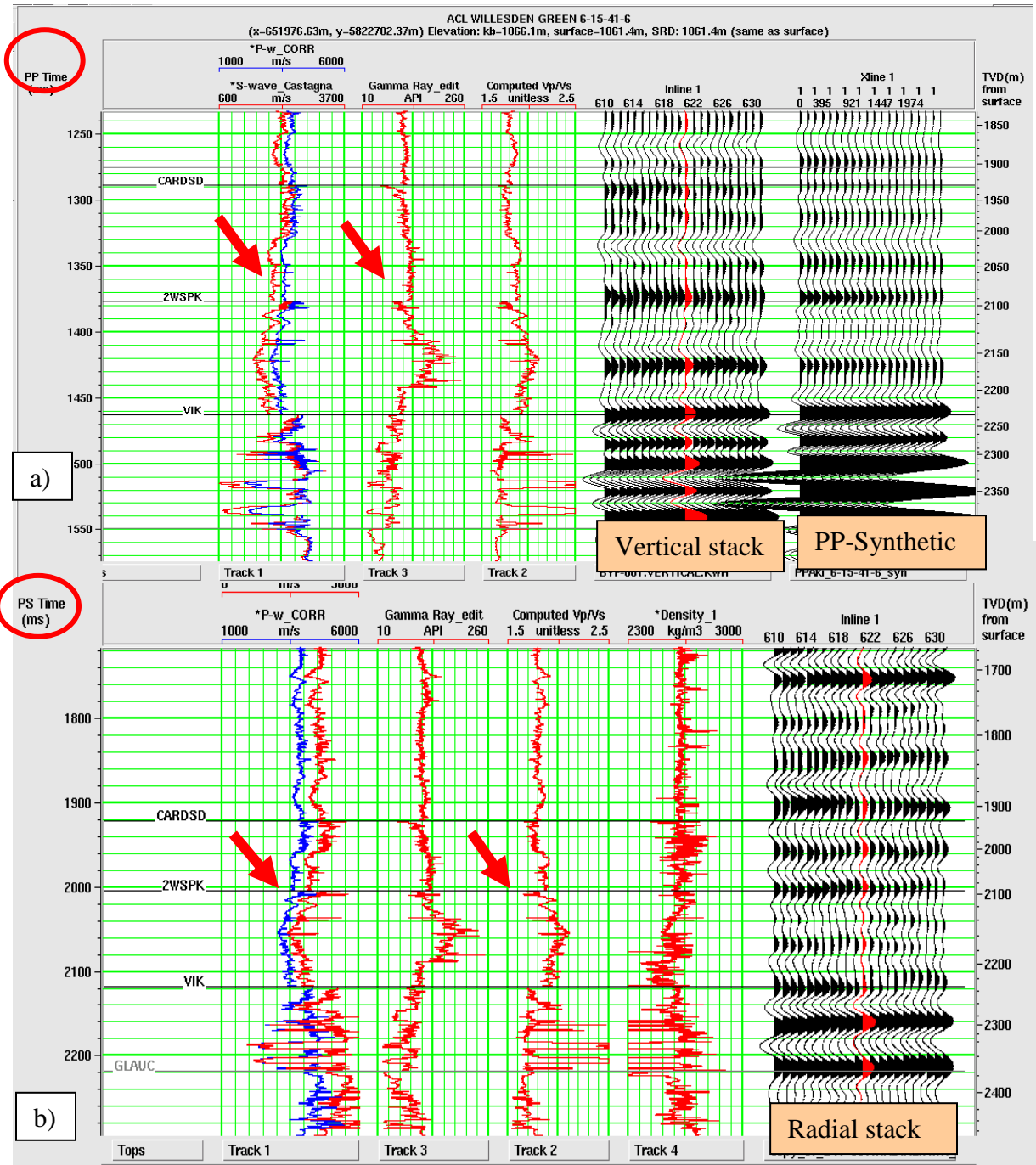


Figure 2.9: a) From left to right: S-wave sonic (from Castagna's equation) in red and P-wave sonic in blue, Gamma Ray, Vp/Vs, vertical migrated stack and PP Aki-Richards offset synthetic for well 6-15-41-6 in PP time, on line WG1. b) P wave sonic (blue), S-wave sonic (red), gamma ray, Vp/Vs, density and radial migrated stack for well 6-15-41-6 in PS time. Red arrows indicate the 2WS formation.

## **2.6 ACQUISITION AND PROCESSING FOR 3-C SURFACE SEISMIC AND VSP**

The surface seismic surveys used vertical vibrators, and three component (3-C) geophones and receivers with offset up to 2520 m. The two surface lines were shot at 70 degrees to one another, with a 60 m source interval and 20 m receiver interval. The source consisted of four Mertz M18 vibrators sweeping for 12 s over an 8-70 Hz range. Records were vertically stacked twelve times. The geophones used were 3-C HGS 10 Hz receivers, planted in a 45 cm augured hole. There were 252 live stations in a split-spread configuration, providing far offsets of 2520 m. The VSP data were acquired at well 8-13-41-6 with vertical vibrator sources and 3-C downhole receivers over a depth interval of 400 m and 2175 m (Stewart et al., 1993).

The 3-C surface seismic data were reprocessed in 2004 by Peter Cary at Sensor Geophysical. Vertical and radial migrations were generated. The processing flow for the PP section was conventional and included surface-consistent deconvolution, time-variant spectral whitening, refraction statics, trim statics, CDP stack, and migration. The processing flow for the PS section included asymptotic (ACP) binning, surface consistent deconvolution, refraction statics, trim statics, CDP stacking, and migration.

## **2.7 PP INTERPRETATION**

As a first step in providing a more confident interpretation, VSP data and the corridor stack (VET) from well 8-13-41-6 were stretched to tie the PP seismic data on line WG2 (Figures 2.10 and 2.11). Available log suites for most wells include P-wave sonic, density, gamma ray, resistivity, and SP logs. The next step was to correlate the PP

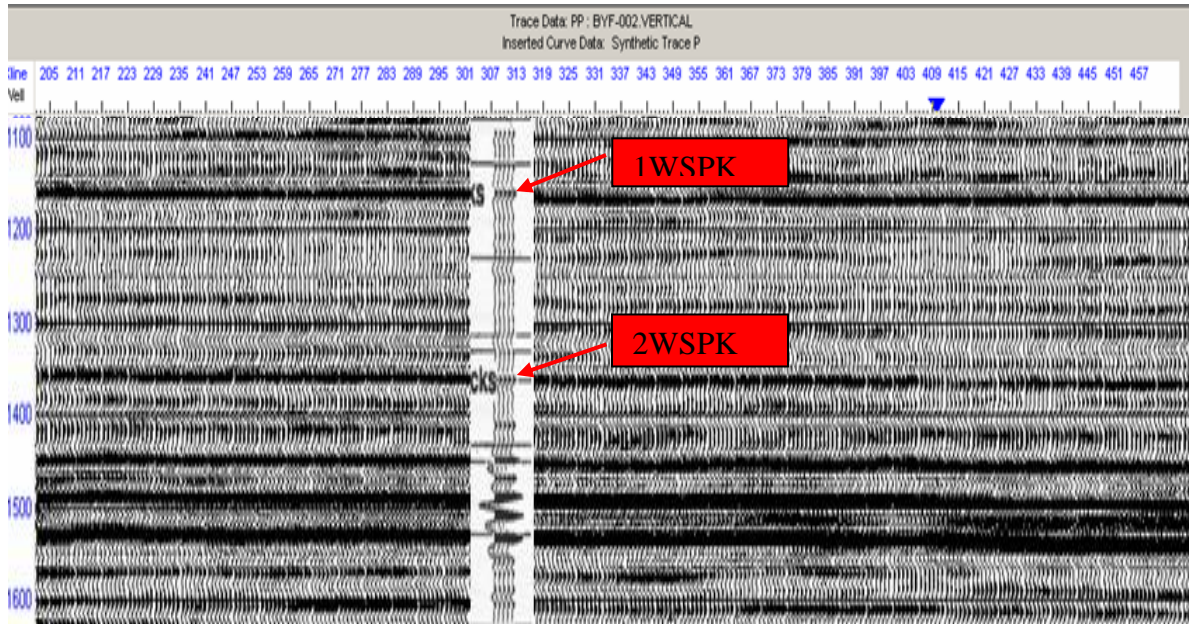


Figure 2.10: WG2 seismic line correlated with the corridor stack (VET - from Stewart et al., 2003), at the well 8-13-41-6 location. Red arrows show the first and second white speckled shale.

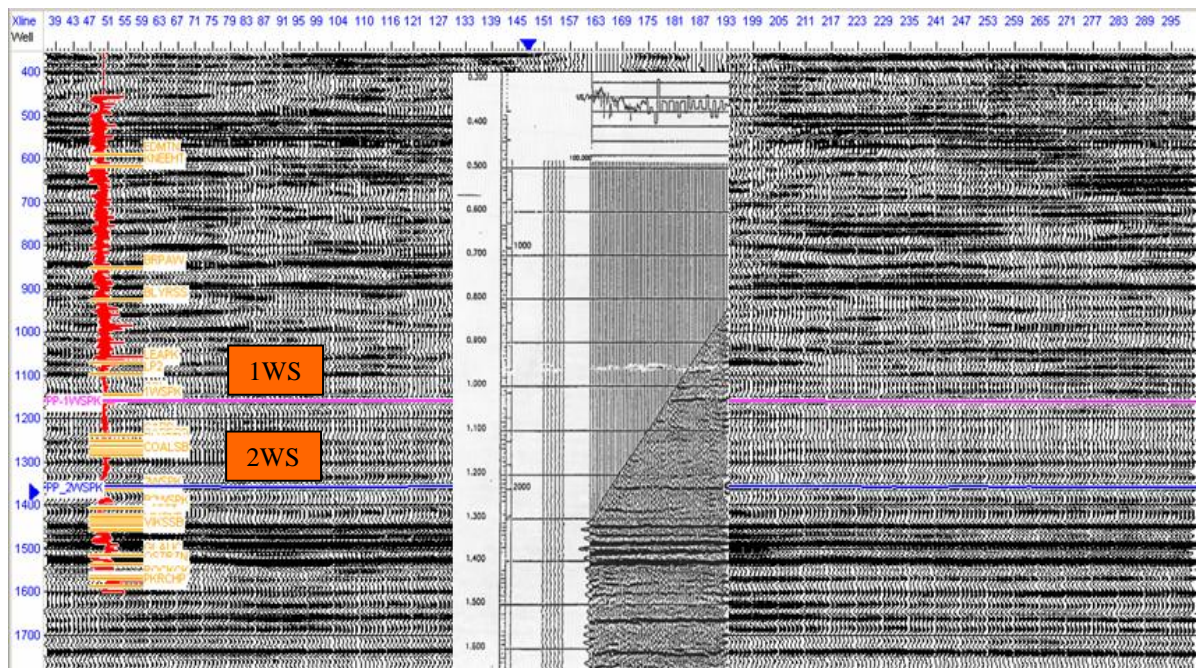


Figure 2.11: WG2 seismic line correlated with the zero offset VSP stretched to two way time at the well 8-13-41-6 location (Stewart et al., 2003). The pink horizon shows the First White Speckled Shale (1WS), the blue one shows the Second White Speckled Shale (2WS). Both horizons are nicely seen on the VSP.

seismic data with the well logs, using the Hampson-Russell software packages eLog and ProMC, as in Figure 2.12. By convolving the reflectivity with a wavelet, the synthetic

traces (in blue) were generated. Then, each pick from the seismic data (in red) was correlated with a pick from the synthetic trace. The well log was stretched according to this correspondence, as in Figures 2.19, 2.12 and 2.13.

In Fig. 2.12, note from left to right the P wave sonic, the zero offset synthetic seismogram (blue), the vertical surface seismic, the PP offset prestack synthetic and the

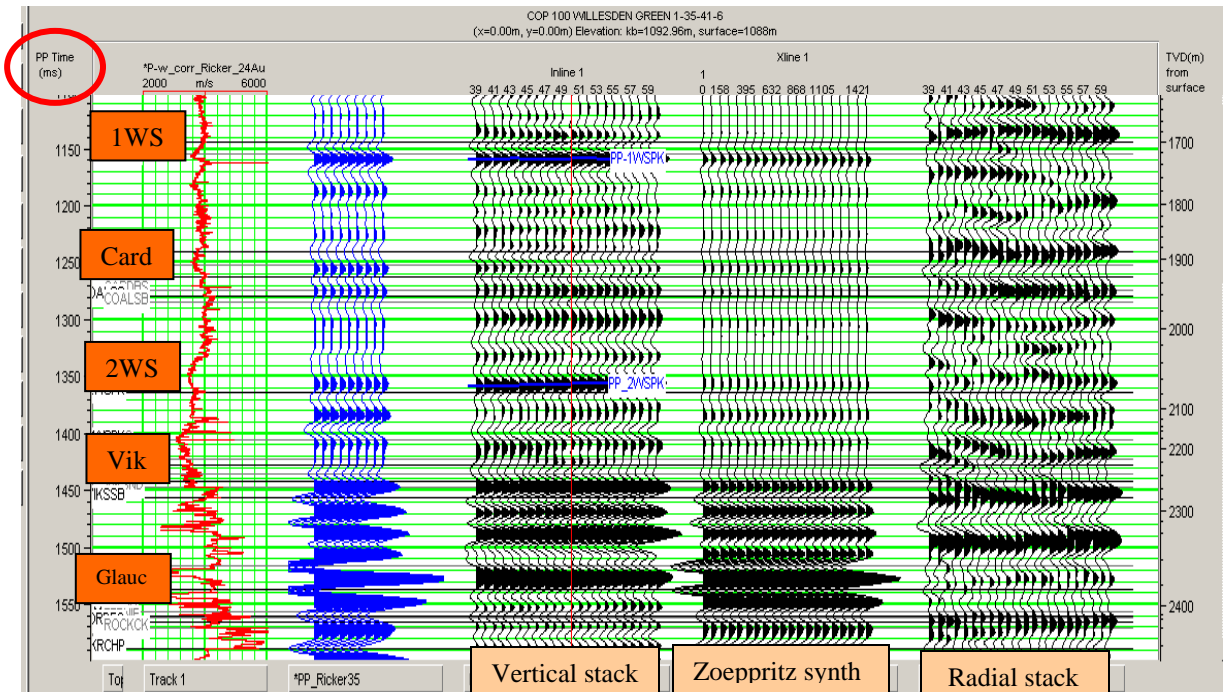


Figure 2.12: From left to right: Sonic log (red) at well log 1-35-41-6 and synthetic seismogram created with a 35Hz Ricker wavelet (blue) correlated with seismic line WG2, the vertical stack; PP Zoeppritz offset synthetic and the radial stack in PP time.

radial surface seismic, all in PP time. In the ProMC package the PS data were squeezed to match the PP time. A 35 Hz Ricker wavelet was created to match the PP seismic data (the vertical seismic data were bandpass filtered at 8-12-60-75 Hz after the processing). The wavelet parameters (Figure 2.14) are: dominant frequency = 35 Hz, sample rate = 2 ms, wavelet length = 100 ms, phase type = constant phase.

In Fig. 2.13, note that the correlation coefficient is almost zero phase, with a correlation of 80%. The interpreted horizon for 1WS is about 1160 ms, and about 1360 ms for the 2WS. The Zoeppritz application from the ProMC package was used to create the prestack synthetics (Figure.2.12) with the number of offsets being 20 and a maximum offset of 1500 m. The Zoeppritz equations give the reflection and transmission coefficients for plane waves as a function of angle of incidence and six independent elastic parameters, three for each side of the reflecting interface (Shuey, 1985). In Figures 2.9, 2.12 and 2.13 note the kicks (jumps) in velocities on the sonic logs at the markers: 1WS and 2WS. According to the correlation, we can describe the following depth of tops: 1SW around 1710 m, Cardium around 1890 m and 2WS at 2070 m. Well 1-35-41-6 (Figure 2.15 b) has a gamma ray log which is a good indicator of the natural radioactivity of the rocks. Radioactive minerals are components of clays and shales. The same steps were used in the PP correlation on line WG1 with well 6-15-41-6 (Figure 2.15 c and 2.9). The correlation coefficient was around 81%. A 35 Hz Ricker wavelet (Figure 2.14) was created for the zero offset synthetic (in blue). The Zoeppritz offset prestack synthetic was created with a number of offsets of 20 m and a maximum offset of 2500 m. The interpreted horizon for 1WS is around 1160 ms and for 2WS 1370 ms, which ties well with line WG2. On line WG1, three wells were correlated with the seismic: 6-15, 16-15 and 8-13. On line WG2, also three wells were correlated with the seismic: 1-35, 8-26 and 8-13. Coal beds were identified on the geophysical logs; coal has several unique physical properties including low natural radioactivity, low density, and high resistance to electrical currents; these properties contrast with those of most other rocks in the coal-bearing sequence.

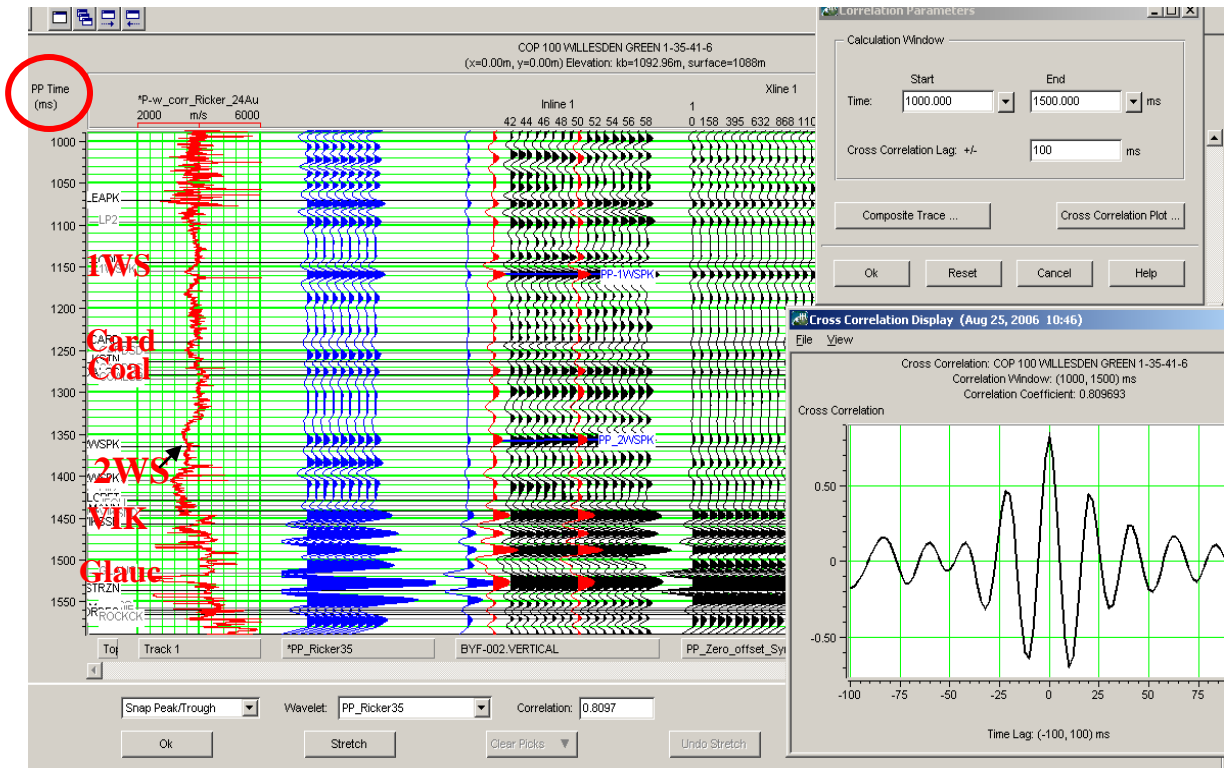


Figure 2.13: From left to right, at Well 1-35-41-6: P-wave sonic (red) zero offset synthetic (blue), PP-vertical stack, the Zoeppritz synthetic, and the cross-correlation coefficient; correlation with seismic data was around 80%.

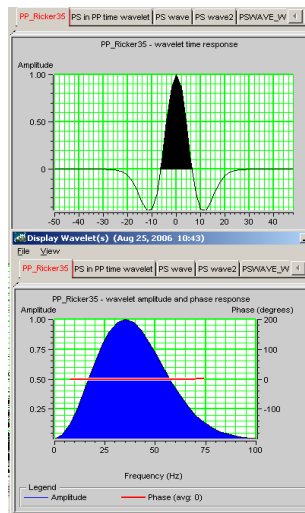


Figure 2.14: 35 Hz Ricker wavelet for the synthetic PP trace - with frequency band 10-65 Hz.

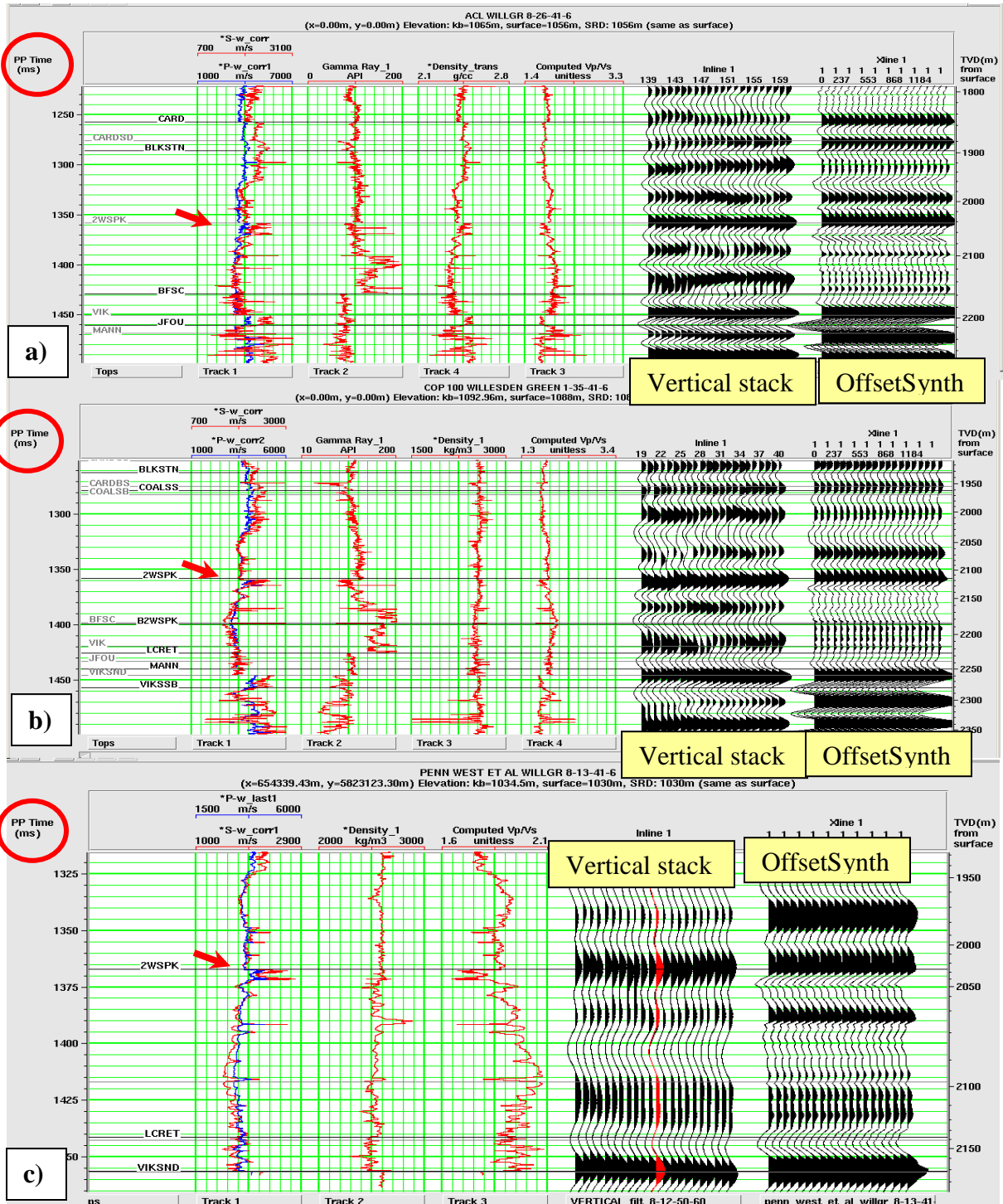


Figure 2.15: Well log correlations on line WG2; from left to right: a) 8-26-41-6: P (blue) and S-wave sonic (red), gamma ray, density, Vp/Vs in PP time, vertical stack and the Zoeppritz offset synthetic; b) 1-35-41-6: P (blue) and S-wave sonic (red), gamma ray, density, Vp/Vs in PP time, vertical stack and the Zoeppritz offset synthetic; c) 8-13-41-6: P (blue) and S-wave sonic (red), density, Vp/Vs in PP time, vertical stack and the Zoeppritz offset synthetic. Red arrows indicate the 2WS horizon. The synthetic modeling was created by convolving the wavelet with the reflectivity series.

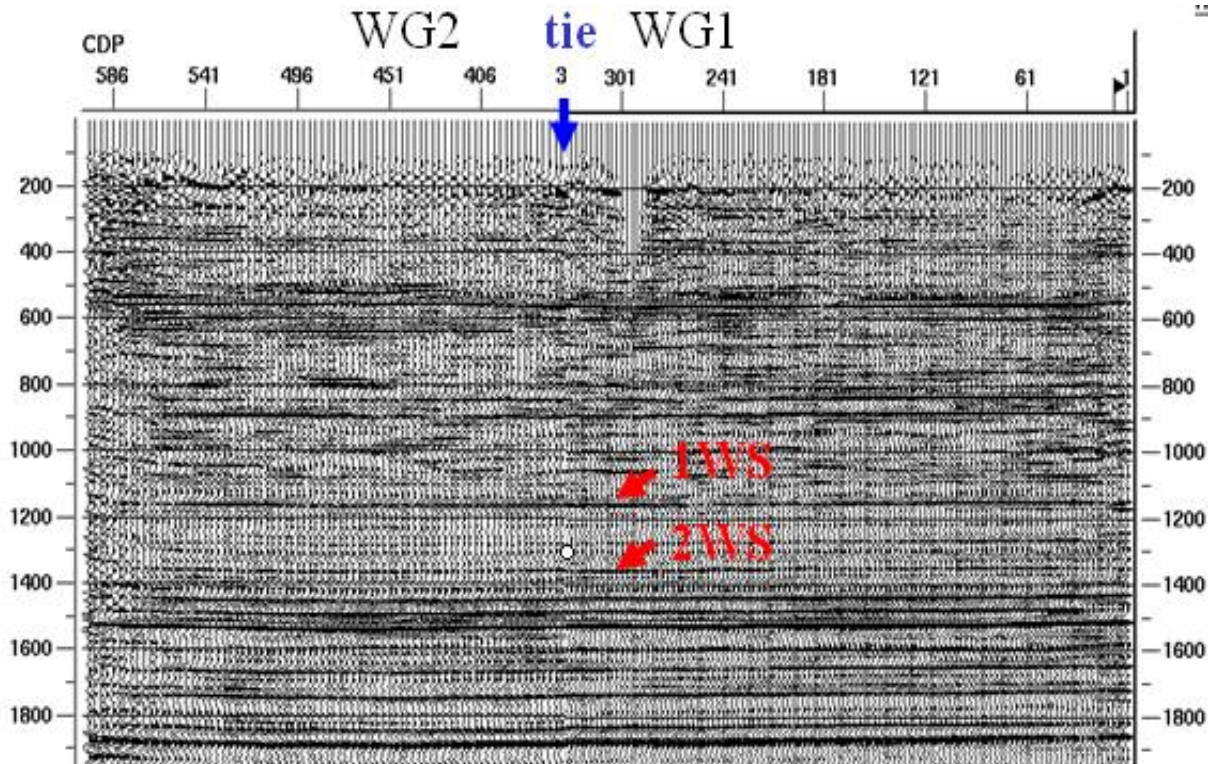


Figure 2.16: Tie line (blue arrow) between lines WG1 and WG2 on PP data. Red arrows indicate the 1WS and the 2WS markers (Seismic processed by Cary, 2004).

## 2.8 PP INVERSION

Inversion can be defined as a procedure for obtaining models which describe a dataset (Treitel and Lines, 1994). For our case, the migrated section constitutes the data to be inverted, and the acoustic impedance is the property to estimate. Well log data provide additional information to constrain the model and make the inversion result more accurate. The impedance is the product of density and velocity and is measured in  $m/s * g/cc$  (in this case).

To estimate the PP acoustic impedance, three post-stack seismic inversions were used in Strata: model-based, recursive and sparse-spike. Model-based inversion was chosen on both lines because of its more highly resolved appearance.

We assume that: the seismic trace and the wavelet are known, and the noise is uncorrelated and random. The program finds a reflectivity which convolves with the wavelet to get a good approximation of the seismic trace. The initial model uses an impedance log from the well, where the impedance is:

$$I = \rho * V \quad (2.1)$$

Then, the program iteratively updates an initial model (Figure 2.17).

The parameters for the model-based inversion are: inversion option-“constrained”, average block size 6 ms, number of iterations 15, processing sample rate 2, separate scaler for each trace, single trace inversion. This type of inversion is based on the convolutional model:

$$\text{Seismic trace} = \text{wavelet} * \text{reflectivity} + \text{noise}$$

The model is an initial low frequency P-impedance model, generated from well data and horizons. The seismic trace and the wavelet are assumed to be known, the noise is taken to be random. This method solves for the reflectivity iteratively, looking for differences between the real seismic trace and the synthetic formed from the model, and modifying the model to compensate (Hampson-Russell, 2008). The P-wave impedance model was constructed by blocking an impedance log from the wells and interpolating the values between the wells (Figure. 2.18). Note a general increase of impedance with depth. Using the blocked model and the wavelet, a synthetic trace is calculated, which is then matched to the actual seismic trace. The layers are modified in thickness and amplitude to improve the match. Then another trace is calculated, compared, and so on (Hampson-Russell, 2008). The statistical used wavelet was extracted from the PP seismic. For the PP

inversion, lower impedance values of 7000-9000 m/s\*g/cc correlate with the producing zones. After inversion, in Figure 2.19, note the low impedance (7800-8400 m/s\*g/cc) around the 2WS shale horizon. This confirms that well 8-26-41-6 is producing oil and gas

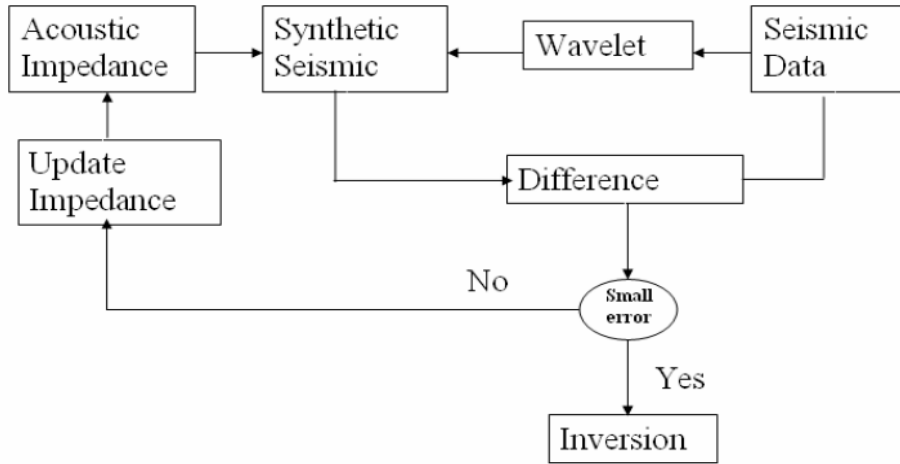


Figure 2.17: PP Model-based inversion-algorithm (after Russell, 1988)

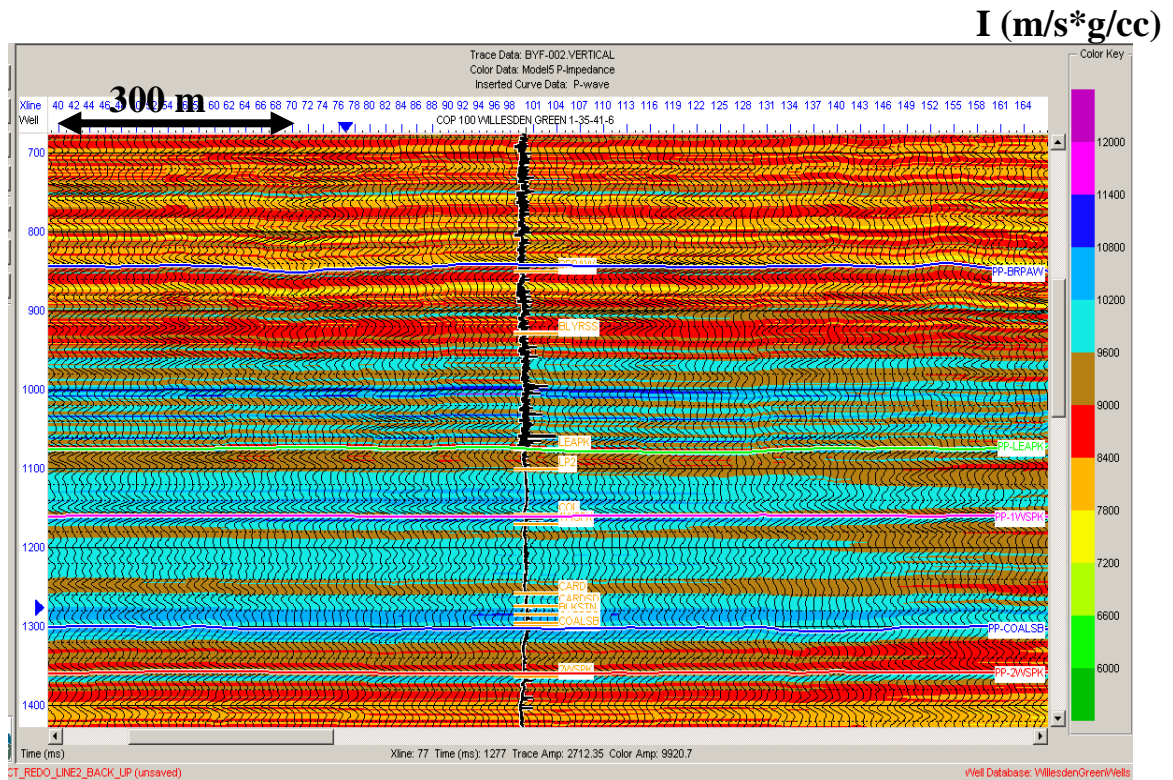


Figure 2.18: Model-P impedance used for inversion on line WG2.

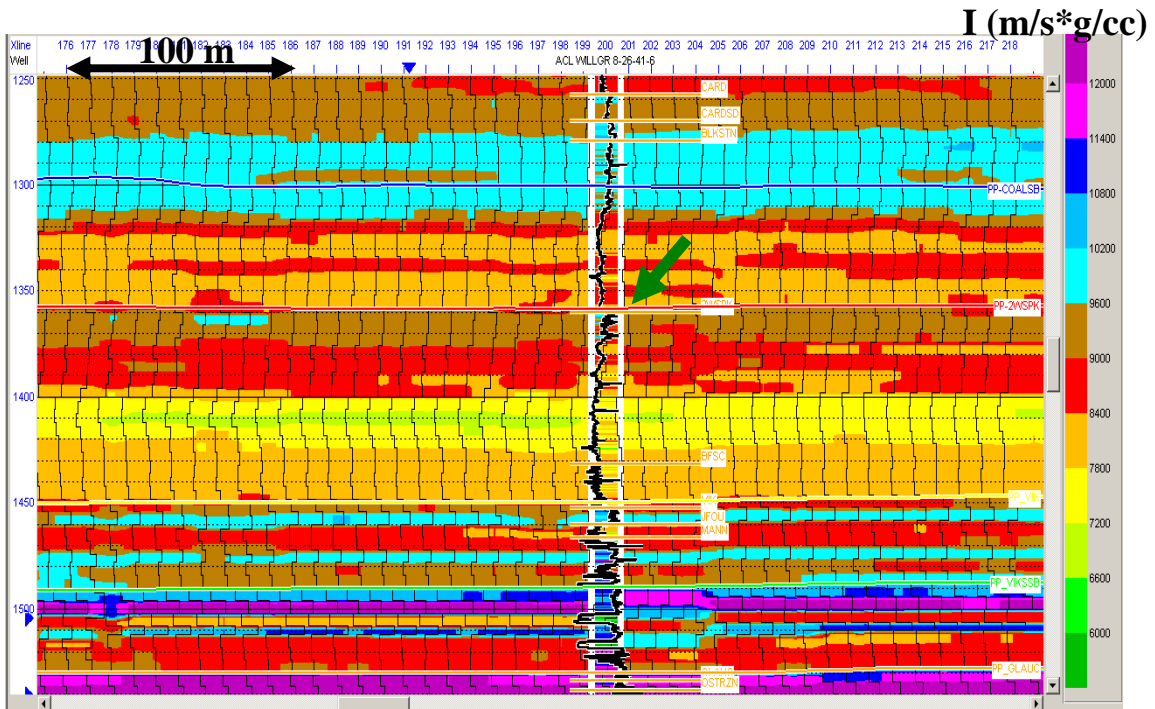


Figure 2.19: PP Model-based inversion (zoomed) on line WG2 at well 8-26-41-6W. The well is producing from the 2WS (green arrow). At the well location, the inserted black curve is the P-wave sonic and in colors the  $V_p/V_s$  ratio from the well data.

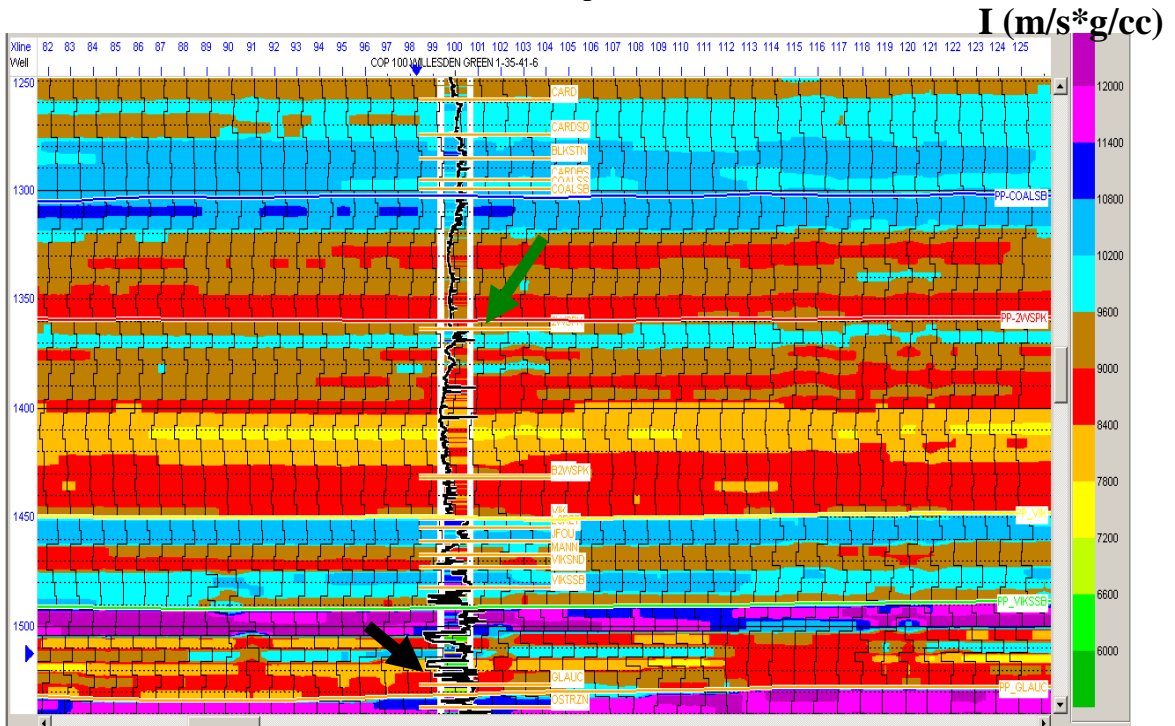


Figure 2.20: PP model based Inversion (zoomed) at well 1-35-41-6W5 on line WG2. This well is not producing from 2WS (green arrow). At the well location, the inserted black curve is the P-wave sonic and in colors the  $V_p/V_s$  ratio from the well data.

from the 2WS formation. On the same line WG2, one kilometer to the North, well 1-35-41-6 is not producing from the 2WS, see Figure 2.20. As expected, the 2WS horizon shows an impedance increase, of up to 10000 m/s\*g/cc.

From the inversion model derived from line WG2, the following observations can be made: well 1-35-41-6 is not producing from the 2WS horizon. This well is producing oil and gas from the Glauconitic horizon (black arrow on figure 2.20). Note the impedance drop around the Glauconitic between 7000-8000 m/s\*g/cc, and an increase in impedance (9000-10000 m/s\*g/cc) values at the 2WS shale. This suggests that zones of increasing porosity are associated with lower acoustic PP impedances. For well 8-26-41-6 (Figure 2.19), note lower impedance at the 2WS horizon; the well is producing from the 2WS formation.

For line WG1, after the model based-inversion was performed, the observations include: The P-Impedance model showed similar characteristics to the model created for line WG2. After inversion, a decrease in impedance (7000-9000 m/s\*g/cc) was observed at the 2WS shale formation in well 16-15-41-6; this well is producing oil and gas from this horizon.

## 2.9 PS INTERPRETATION

The correlation of the PS seismic data with a shear acoustic log was done in the same way as for PP seismic data. The S log was created in ProMC using Castagna's (1985) mudrock empirical regressions relating velocities with porosity and clay content under water-saturated conditions (equation 2.2), where  $V_p$  and  $V_s$  are the P- and S-wave velocities, in km/s:

$$V_p = 1.16V_s + 1.36 \quad (2.2)$$

These relations are empirical and apply only to the set of rocks studied. Since there is no PS response at zero offset, data for several offsets were stacked to obtain a synthetic PS response to compare with the seismic data. For line WG2, a 25 Hz Ricker wavelet was created. The radial seismic data was bandpass filtered at 5-10-40-50 Hz after processing. The wavelet parameters are: dominant frequency = 25 Hz, sample rate = 2 ms, wavelet length = 100 ms, phase type = constant phase, as in Figure 2.21. Figure 2.22 shows the correlation in PS time at well 8-26-41-6 on line WG2; the correlation coefficient was around 64%. On line WG1 the correlation in PS time with well 16-15 -41-6 is shown in Figure 2.23; the correlation coefficient was around 60%. For line WG1, a 20 Hz Ricker wavelet was created (the radial seismic data was bandpass filtered at 5-10-30-40 Hz after processing) to match the PS seismic data. The PS horizons were picked in PS time, as shown in Figure 2.23.

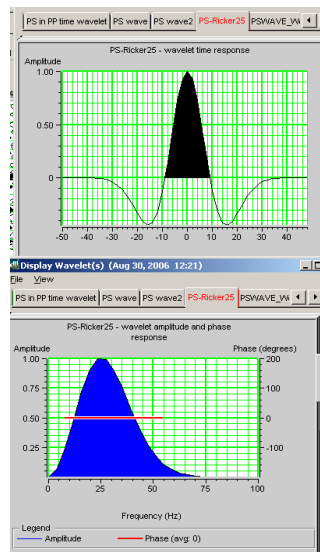


Figure 2.21: 25 Hz Ricker wavelet for the synthetic PS trace - with frequency band 8-45Hz. Red line indicate zero phase.



After the PS horizon picking, the next step was to match the PP and PS horizons in the ProMC package and register the data. The registration was done in PP time.

## **2.10 PP AND PS INTERPRETATION**

With traditional P-wave seismic data, geology is imaged with pressure waves (P-waves) reflecting from various rock interfaces. In the case of PS-wave seismic data, pressure waves are “mode converted” into shear waves at the same rock interfaces. The different velocities of seismic wave propagation between pressure and shear waves result in PS-wave seismic records typically being twice as long as P-wave seismic records. Consequently, the key to successful full-wave seismic interpretation lies in establishing a match between seismic data volumes through some form of “registration”. What makes this process particularly challenging is that the seismic character between full-wave seismic volumes can be very different, spanning amplitude, frequency and phase properties (Roth, 2007). An accurately registered PS volume appears to reduce the risk of correlations and reduce uncertainty in well targeting.

After the PP horizons were picked in PP time and the PS horizons in PS time, the registration was accomplished with the Horizons Matching tool in ProMC. This tool allows linking of the selected horizons (PP and PS data are viewed in a split mode) and then visualize them in PP or PS time. ProMC can calculate  $V_p/V_s$  value between the horizons, and can colour code its value along the entire line.

$V_p/V_s$  along the seismic lines were calculated using interval travel times with the following formula as derived in Stewart et al. (2000), Garotta, (2001):

$$\frac{V_p}{V_s} = \frac{2\Delta T_{ps}}{\Delta T_{pp}} - 1 \quad (2.3)$$

In equation (2.3),  $\Delta T_{pp}$  and  $\Delta T_{ps}$  are the time thicknesses between the interpolated horizons, on PP and PS data respectively. The equation is derived by expressing the thickness of a depth interval in terms of P-wave and S-wave travel time and its limitation is that it is an average over the time thickness interval.

The horizon match used the well logs as domain conversion: the active depth-time curves (from both, P and S-wave sonic) at the three selected well tie locations were used to create a velocity field for domain conversion.

For line WG2, after event matching, the 2WS shales can be delimited with higher  $V_p/V_s$  values of 2.16 to 3, on both, PP and PS data. Figure 2.24 bottom, indicates the 2WS formation with red arrows. The Cardium sandstones have lower values, from 1.5 to 2, as expected. The separation from shales to sands is clearly shown; the white arrows in Figure 2.24, bottom indicate this separation.

The 2WS horizon was picked as a peak on both, PP and PS data, as shown in figure 2.24 top. We note that in a gross perspective our PP and PS sections respond in a similar way to strong reflectors like coals, or thick sequences of sands or shales (Roth, 2006).

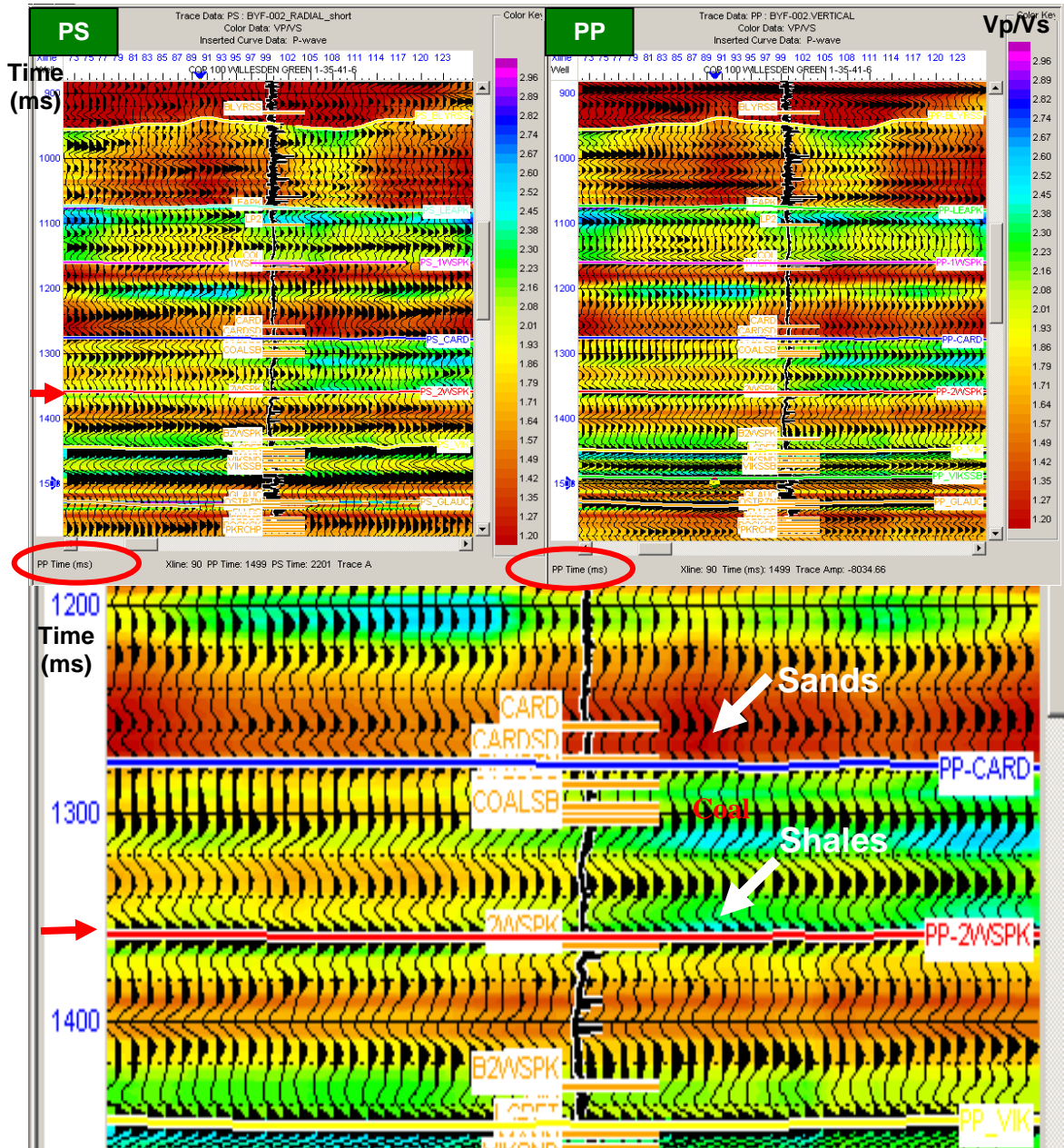
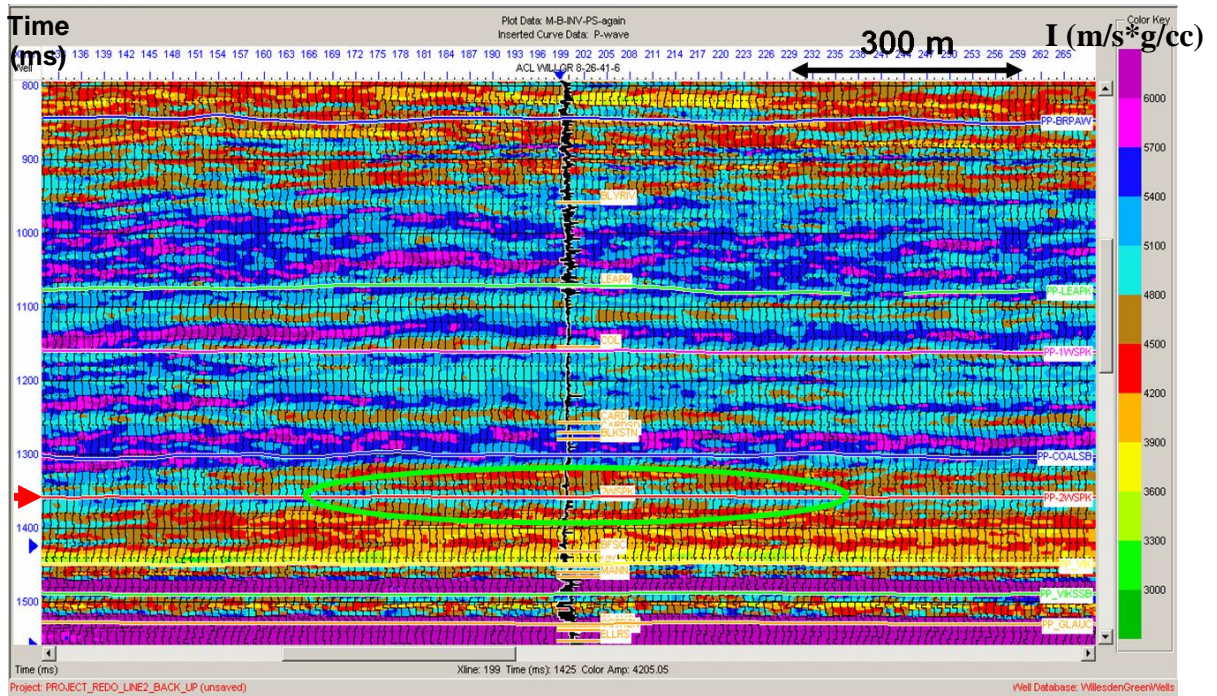


Figure 2.24: Top: PP and PS horizons in ProMC after registration (in PP time) and horizon match: line WG2, well 1-35-41-6; bottom: zoomed image on the cross-section of PP data registered in PP time at the 2WS interval. The used domain conversion is derived from the three well ties locations: 1-35-41-6, 8-26-41-6 and 8-13-41-6. The Vp/Vs ratio derived from horizon-based registration is shown in colors.



Figure 2.26 show the model-based PS inversion in PP time on line WG2 at well 8-26-41-6; note the increased impedance values 4800-5400 m/s\*g/cc at the 2WS shale, shown in the green ellipse. This well is producing from the 2WS formation.



Well 8-26-41-6W5 – producing from 2WSPK: note the increase  $\uparrow$

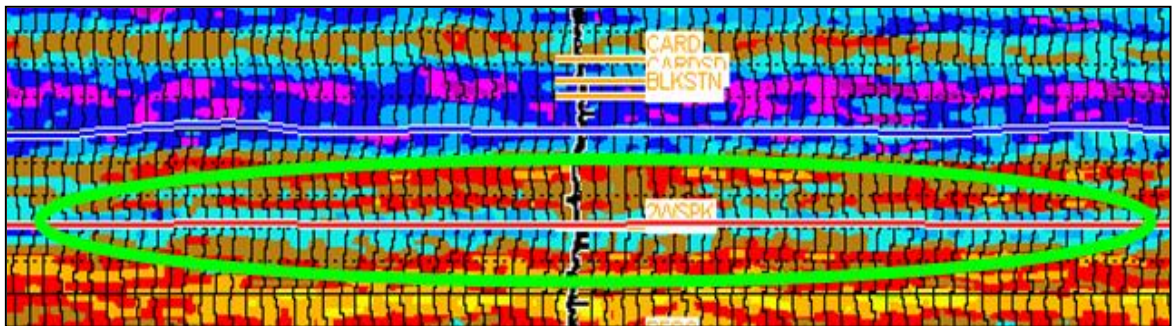


Figure 2.26: Top: model-based PS Inversion in PP time on line WG2 at well 8-26-41-6W5 location; bottom: zoomed image of producing well at the 2WS formation.

Figure 2.27 shows the model-based PS inversion in PP time on line WG1 at well location 8-13-41-6; observe the higher impedance values of 4800-5400 m/s\*g/cc at the

producing 2WS shale, marked by the black ellipse. The producing zones show an impedance increase, opposed to the impedance decrease in the PP case. The Cardium sandstones are delineated by a large increase in impedance (5400-6000 m/s\*g/cc). Producing wells on lines WG1 and WG2 show an S-impedance increase on the PS model-based inversion, while the non-producing wells show an S-impedance decrease, as expected.

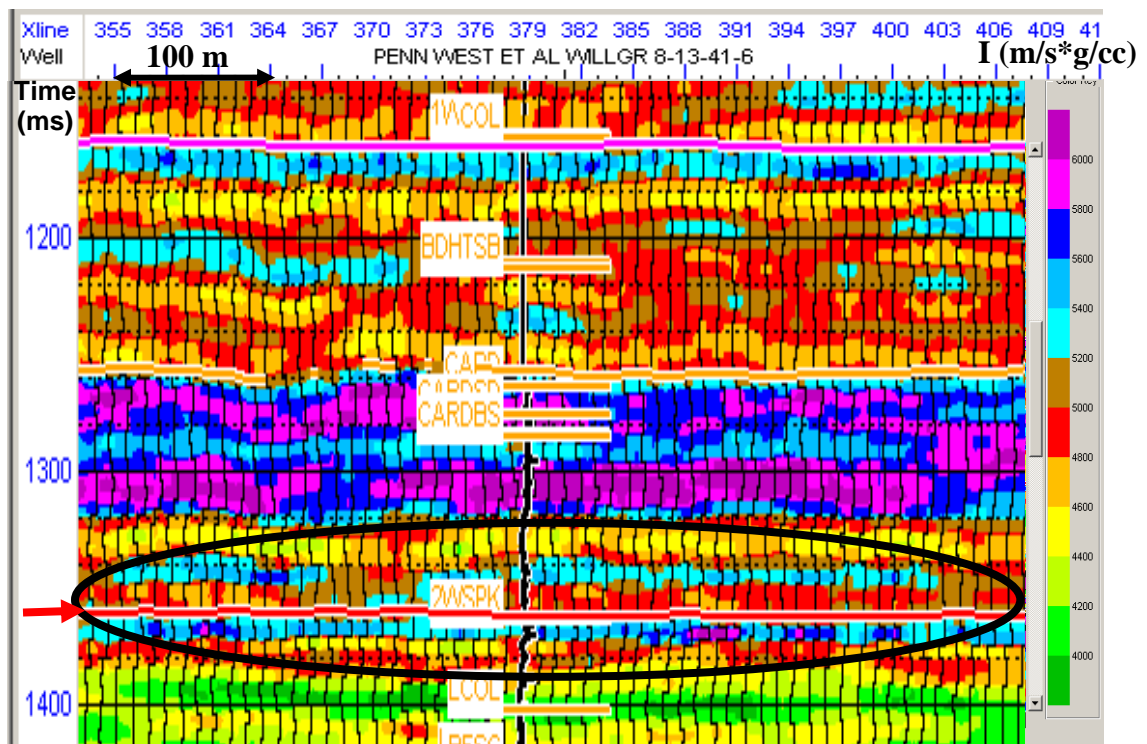


Figure 2.27: PS model-based inversion result for line WG1 at well location 8-13 at the 2WS formation, in the black ellipse.

After the inversion of both PP and PS datasets, impedance ratios were calculated (Figure 2.28). Low impedance ratios are interpreted as 1.44-1.79, indicating a potentially productive 2WS formation. Higher values of 1.8-2.2 above the anomalous zone could delineate the impermeable seals of this reservoir. The lower impedance ratios at the 2WS horizon correlate with the production from well 8-13-41-6. The anomaly on line WG2,

Figure 2.28, can be traced laterally for about 600 m towards the end of the line (South-East).

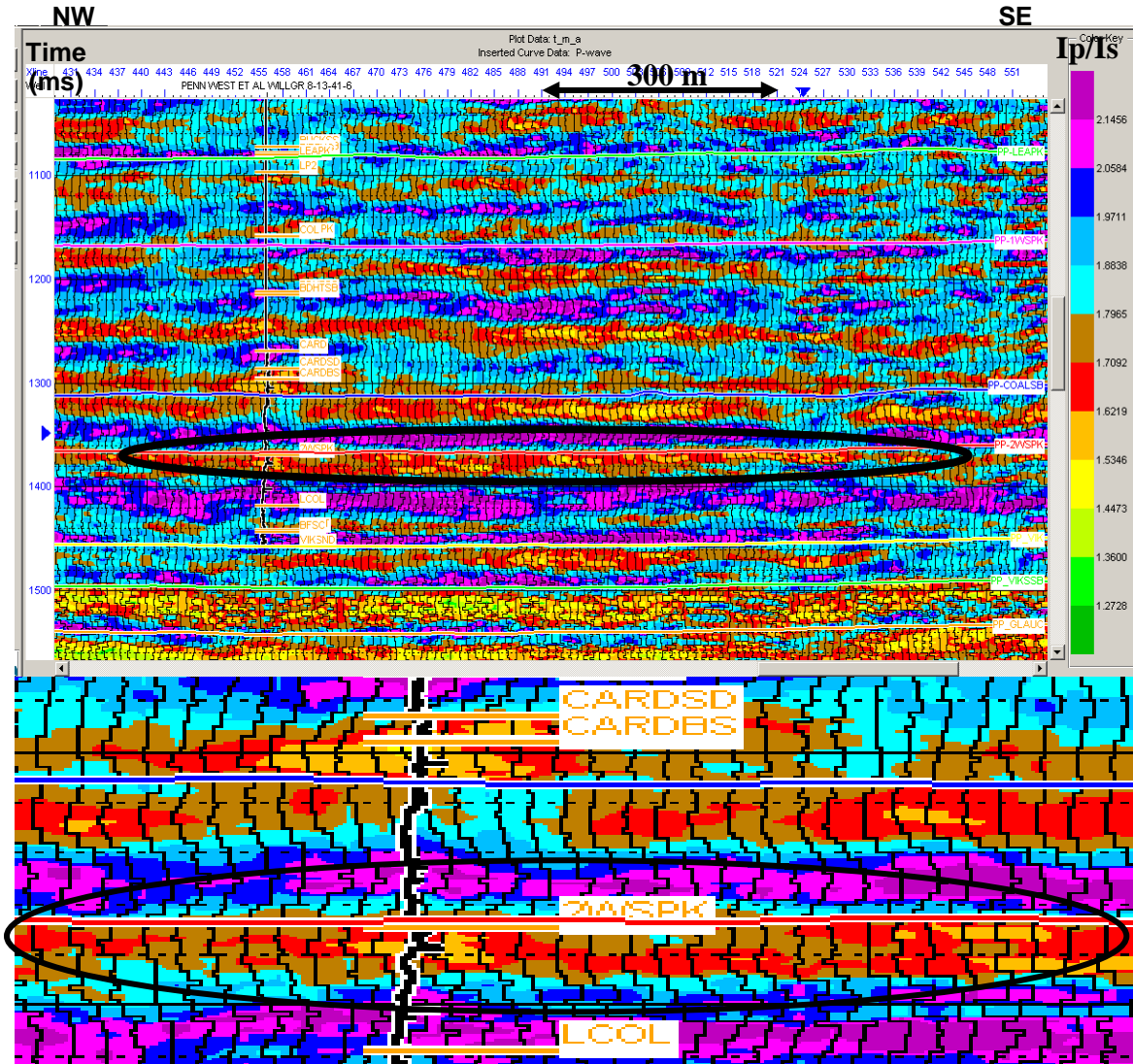


Figure 2.28: Top: The ratio of the PP to PS inversion in PP time on line WG2 at well 8-13-41-6 location. Bottom: Zoomed image at the 2WS horizon.

## 2.12 ANOMALOUS ZONES FOR LINE WG1

The ratio of the post-stack inversions of both PP and PS datasets correlates well with the production zones. Low values in the impedance ratios (1.6 -1.8) highlight potentially

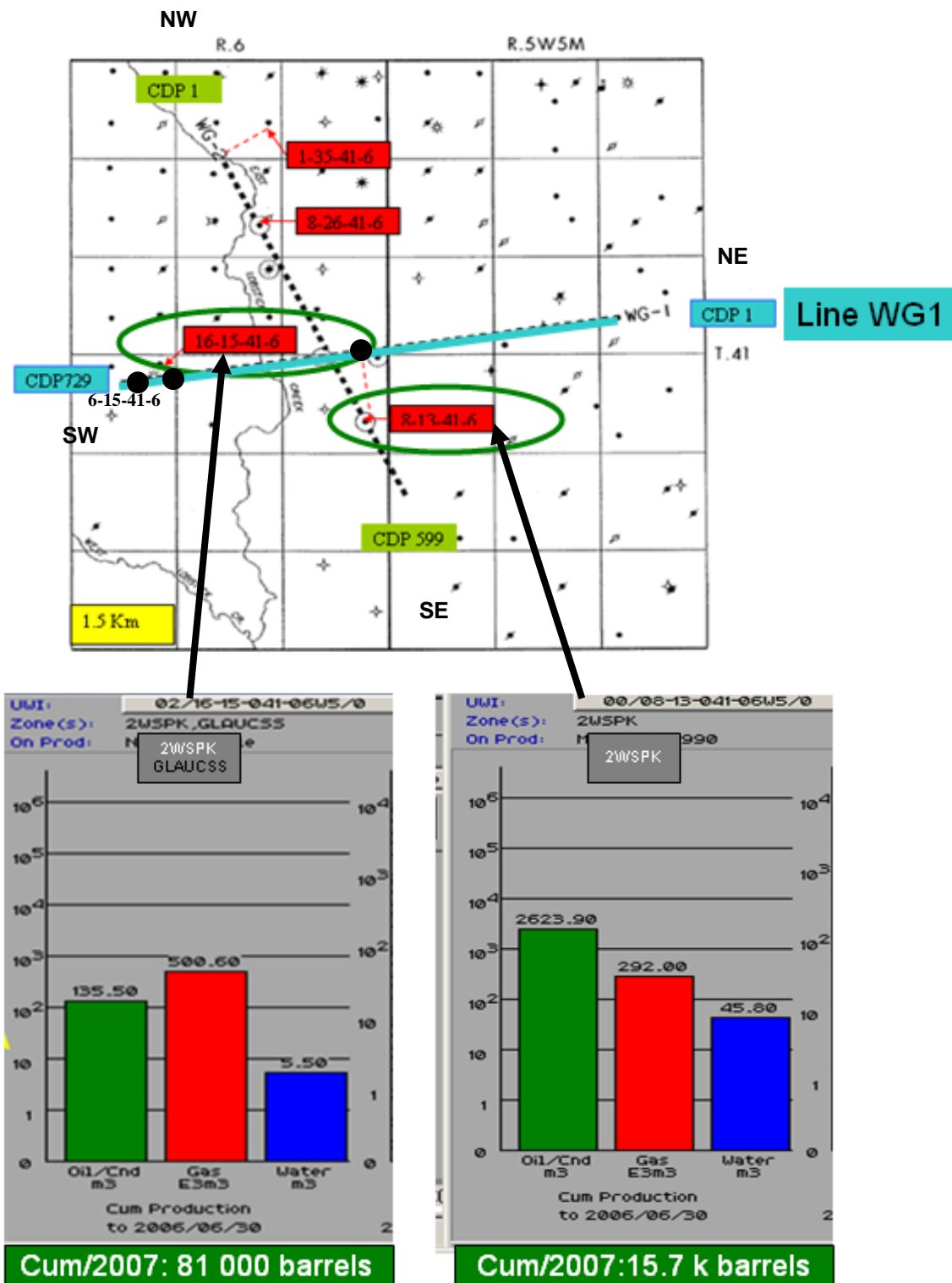
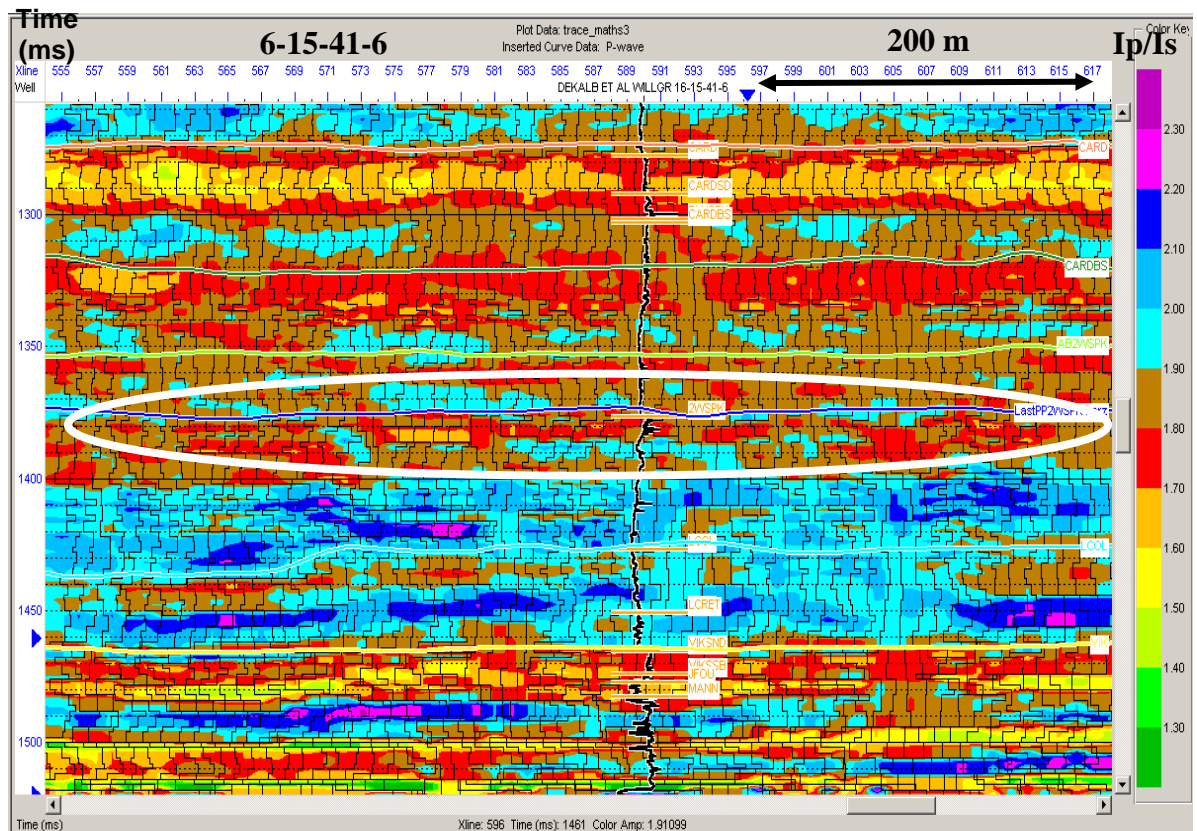


Figure 2.29: Wells (from Accumap) on Line WG1: cumulative oil and gas production of the 2WS horizon up to year 2007.

productive 2WS zones. Higher values than 1.9 are generally not associated with reservoir zones. Figure 2.29 shows the cumulative oil and gas production (up to 2007) of the 2WS horizon at the two well locations 16-15-41-6 and 8-13-41-6 (which is less than 1 km apart line 1 and was projected on line, Figure 2.29) for line WG1. Well 8-13-41-6 produced 15,700 barrels of oil up to year 2007, and well 16-15-41-6 81,000 barrels.

Figure 2.30 show the ratio of impedances for the two producing wells on this line: 8-13-41-6W5 and 16-15-41-6-W5. Lower values of the ratio (1.6-1.9) are associated with the productive zones and higher values as 1.9 - 2.2 (for well 6-15-41-6W5) with non production. Similar results have been derived for line WG2.



a)

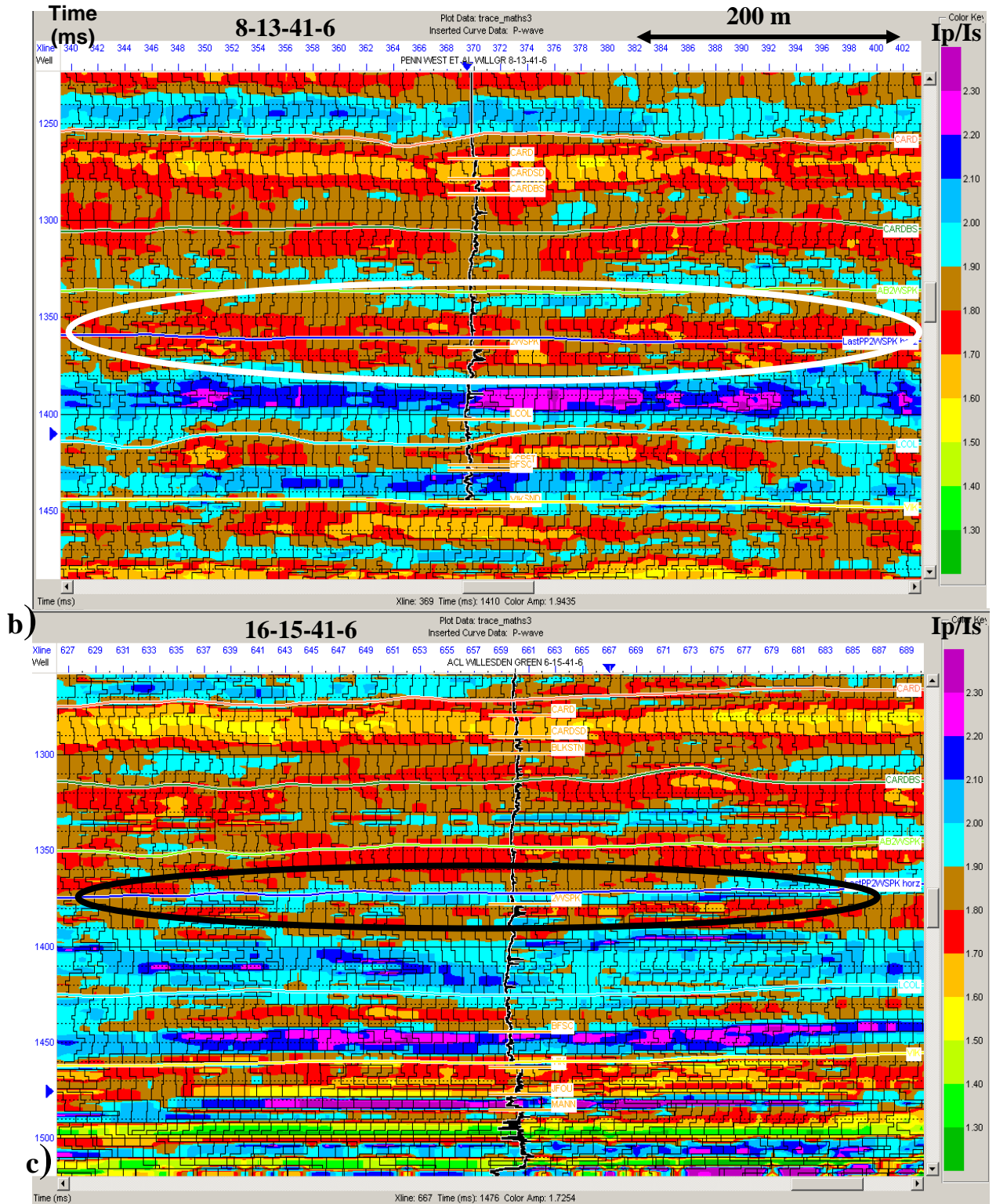
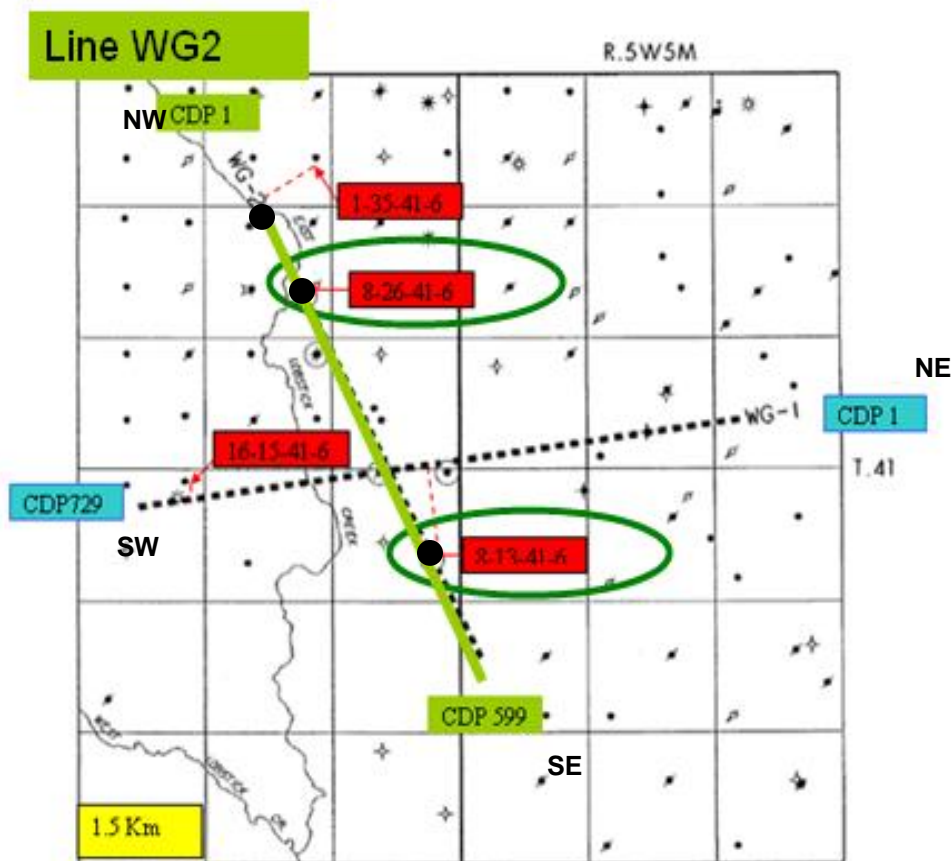


Figure 2.30: a) The ratio of PP to PS impedance inversion for line WG1; the two producing wells on this line: 8-13-41-6W5 (top) and b) 16-15-41-6-W5 (bottom) are delineated in white ellipses. Lower values of the ratio are associated with the productive zones; c) well 6-15-41-6W5 is not producing from the 2WS as shown in black ellipse.

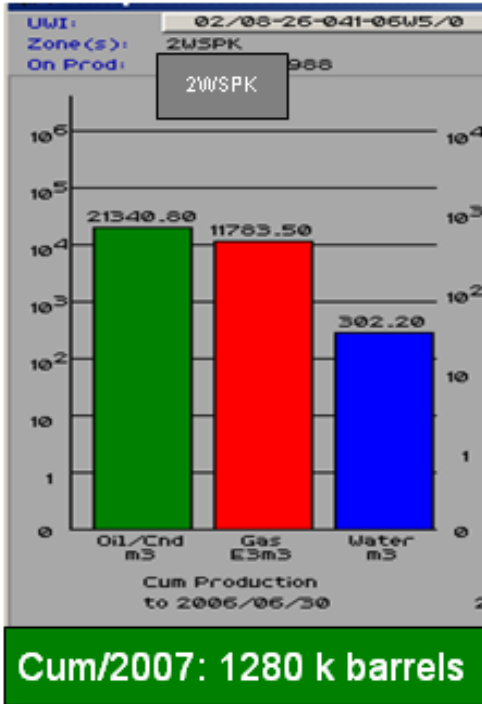
### 2.13 ANOMALOUS ZONES FOR LINE WG2

Lower  $V_p/V_s$  values at the 2WS horizon are seen in this example, from the wells: 8-13-41-6W5 and 8-26-41-6W5, as in figure 2.32. The lateral PS impedance increases on line WG2 at the productive wells locations correlates to the producing 2WS formation (Figure 2.31). Note similarities with the  $V_p/V_s$  value. Low values in the impedance ratios as 1.5-1.8 indicate the productive 2WS. Higher values 1.8 - 2.2 indicate the non productive areas, or could delineate the impermeable seal of the reservoir.

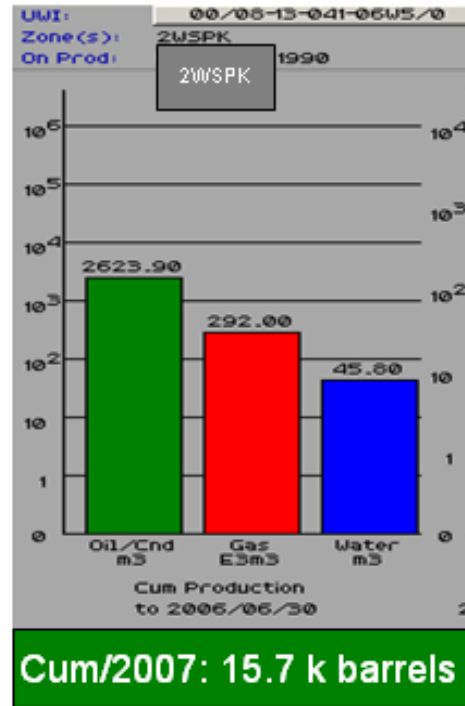


a)

8-26-41-6

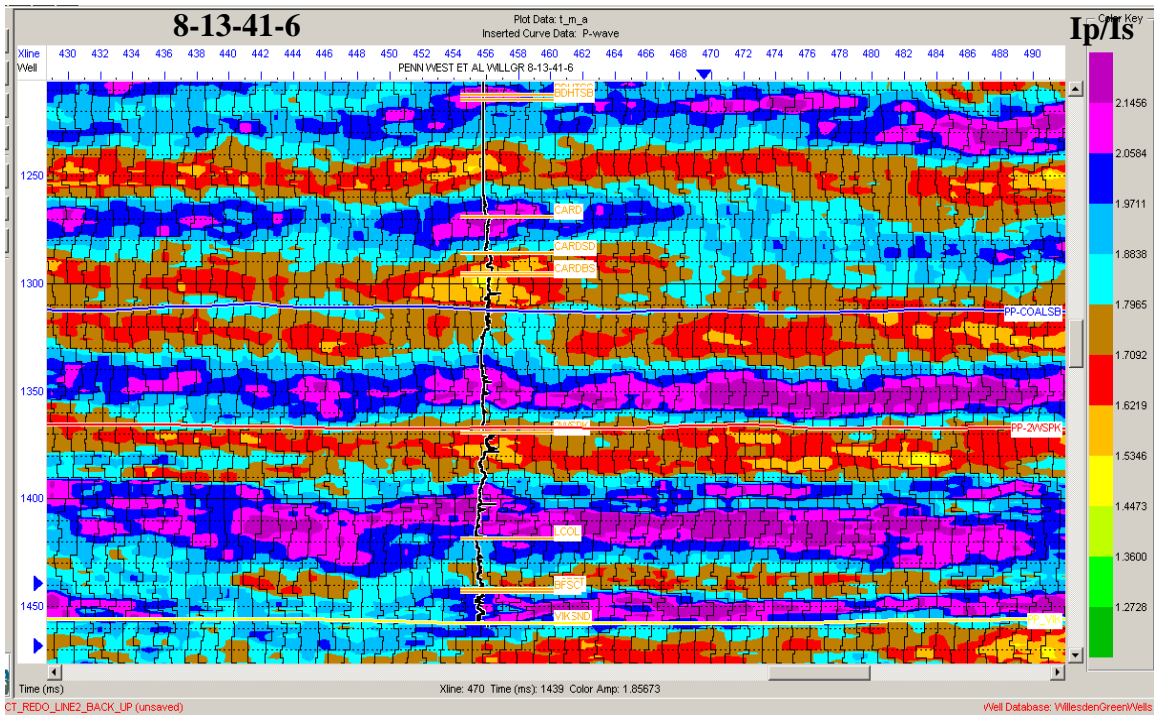


8-13-41-6



b)

Figure 2.31: a) and b) Wells (from Accumap) on Line WG2: cumulative oil and gas production of the 2WS up until 2007: well 8-26 produced 1,280,000 barrels and well 8-13 15,700 barrels.



a)



## 2.14 JOINT INVERSION OF WILLESDEN GREEN DATA

### 2.14A JOINT INVERSION OF LINE WG1

After separately inverting the PP and PS datasets in Strata, a joint inversion procedure was performed in the Hampson-Russell ProMC package using the post-stack, migrated multicomponent data. Event matching (Figure 2.33) between the PP and PS seismic has been done using the velocity (through “domain conversion”) from the model (Figure 2.34), created this time in the ProMC package (with the “Strata Model” option). The new velocity model builds simultaneously a P-wave model, an S-wave model, and a density model, as in Figure 2.34. The Vp/Vs ratio derived from horizon-based registration using the velocity from the “strata model” as “domain conversion” is shown in Figure 2.33.

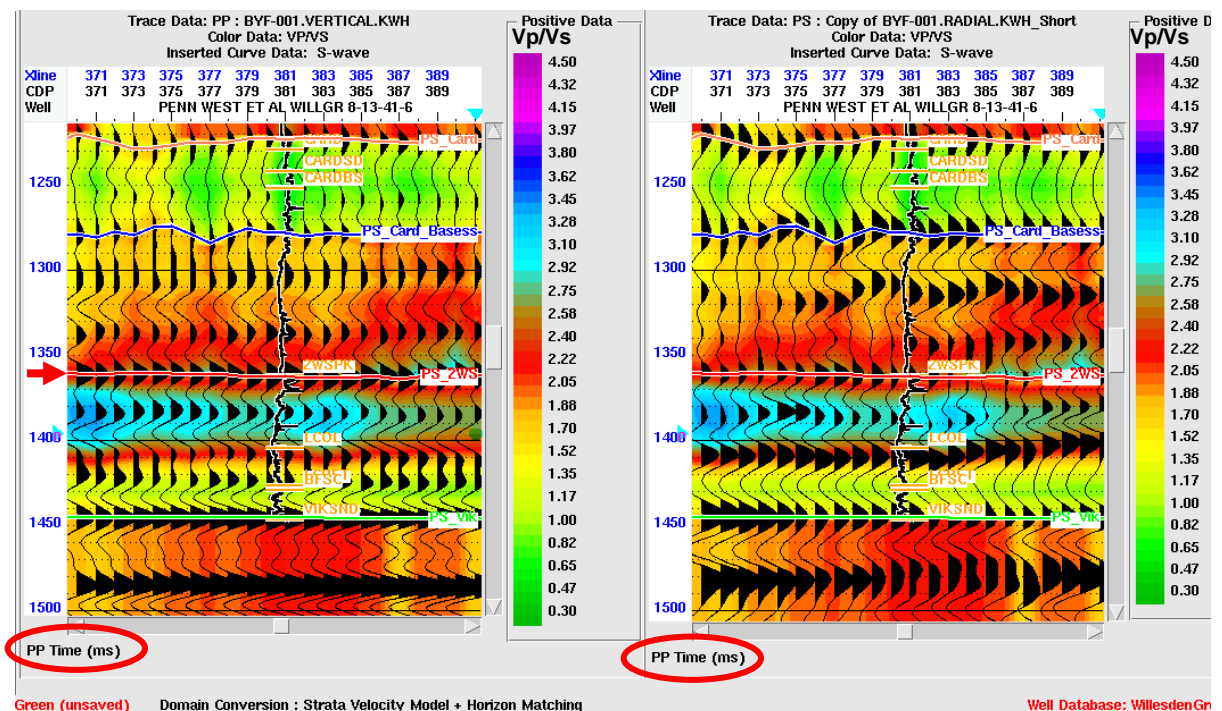


Figure 2.33: PP and PS data in ProMC after registration and horizon match: line WG1 at the well 8-13-41-6W5 location. Red arrows on the time scale (left) indicate the 2WS formation.

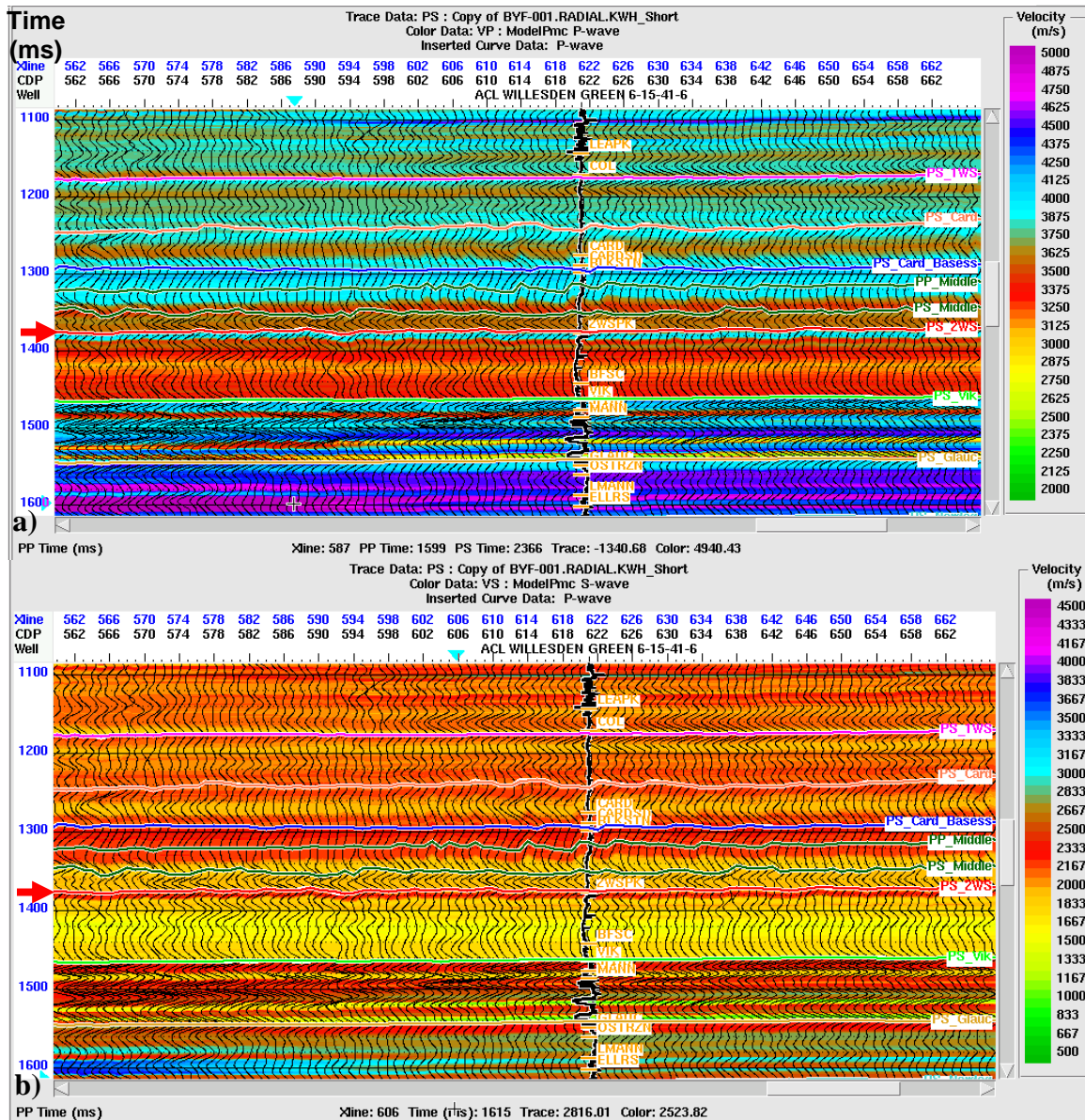


Figure 2.34: Models built in ProMC for line WG1 at well 6-15-41-6 location; a) P-wave model and b) S-wave model.

The PS statistical wavelet was created in the PP time domain in preparation for joint inversion. Figure 2.35 show the extracted wavelets from both, the PP and PS seismic (in PP time), used in the joint inversion. The joint PP-PS inversion of the PP and PS seismic volumes is a model-based inversion that estimates the acoustic properties that are consistent with the PP and PS amplitude volumes. This joint inversion uses an initial low

frequency model created from the extrapolated well logs, updated by the horizon matching performed in “domain conversion”. Then the model based inversion updates the initial model to create new models of P-impedance, S-impedance, Vp/Vs values, and densities that are consistent with the PP and PS seismic amplitude volumes.

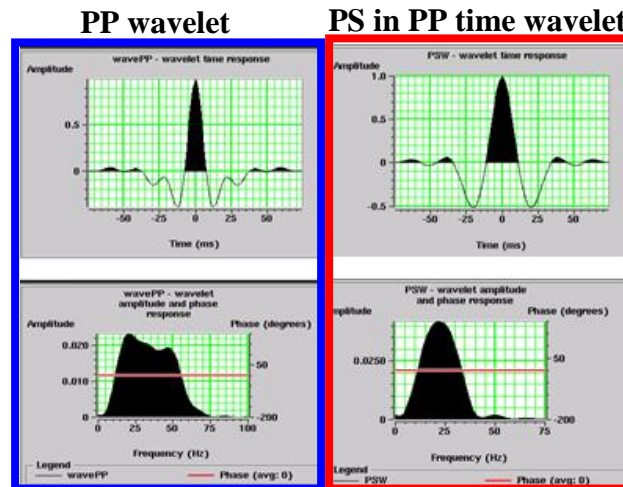


Figure 2.35: Statistically extracted wavelets for joint inversion on line WG1; left PP (blue rectangle) and right PS (red rectangle) in PP time; the top shows the wavelet in time domain and bottom in frequency domain.

The joint inversion results are shown on Figure 2.36. The best correlation with the production is given by the Vp/Vs values showing ratios of 1.3 - 2.2. The productive wells from the 2WS formation are 8-13-41-6 and 16-15-41-6. Well 6-15-41-6 is producing from the Glauconitic sandstones horizon. Black arrows are used to show 2WS interval on line WG1. On the P-wave inversion section the productive zones correlate with lower impedance values between 8000-9500 m/s\*g/cc. For the S-wave inversion, higher values such as 3500-6000 m/s\*g/cc were associated with the productive zones. Using both, the Vp/Vs values and P-impedance, future drilling locations can be considered from CDP 590, which is close to well 16-15-41-6 towards the NE (close to well 8-13-41-6). Well 16-15 is known to produce mostly from the 2WS formation: the anomalies shown in the joint inversion results confirm this, especially on a) and b) from figure 2.36.

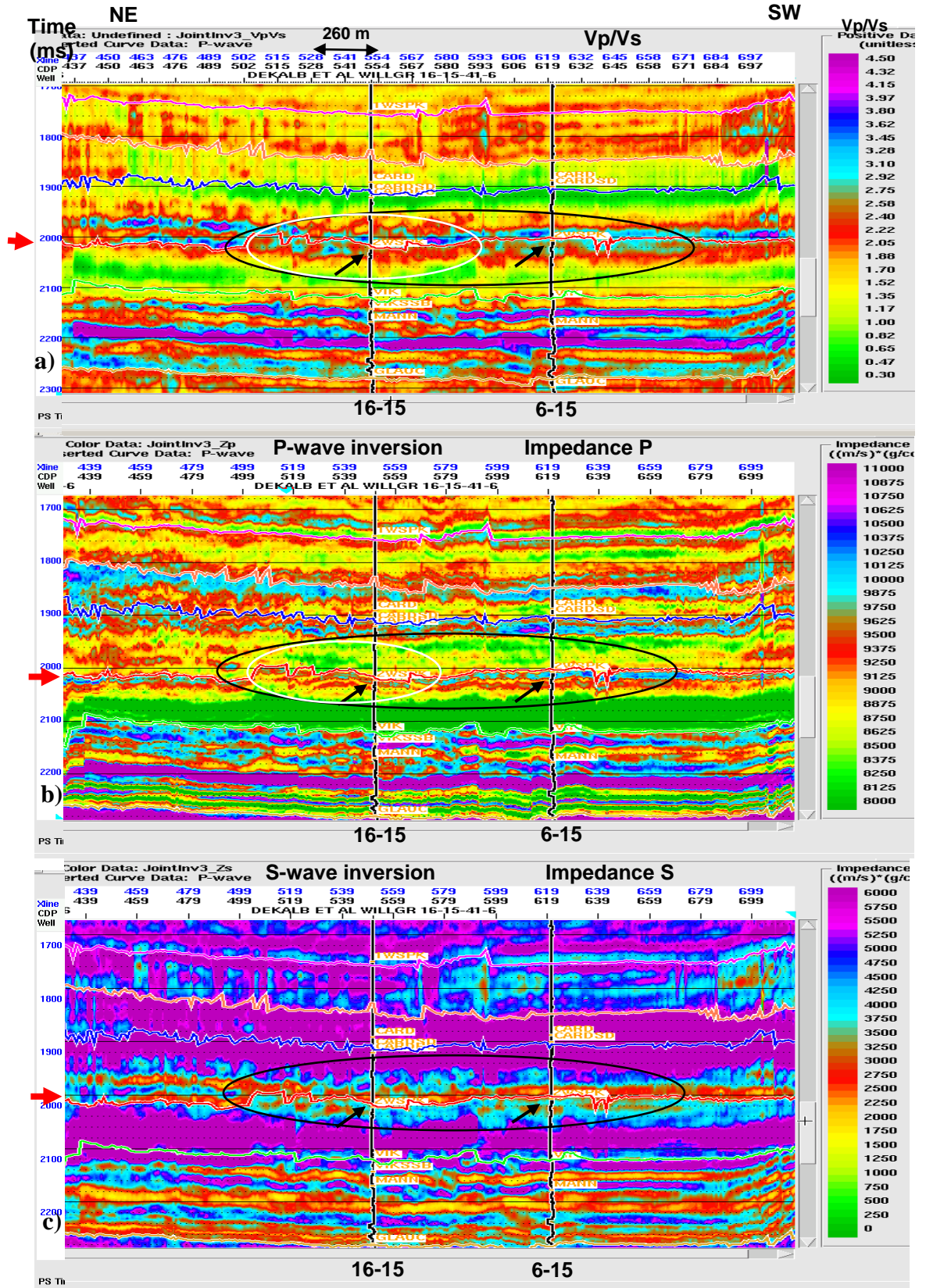


Figure 2.36: Joint inversion results for line WG1 in PS time: a) Vp/Vs values, b) Zp or P-wave inversion and c) Zs or S-wave inversion. Red arrow shows the 2WS horizon.

In conclusion, the recommended future drilling target is marked by white circled areas on Figure 2.36, from CDP's 490 to 590. High impedances values on the P-wave inversion and the high  $V_p/V_s$  values above the 2WS horizon may indicate a seal; below, the 2WS is possibly containing sand lenses and became a good reservoir. Well 8-13-41-6 is also producing some oil and gas from the 2WS, but the well was projected to tie line WG1 (the distance to the well is less than one kilometer) the seal conditions are not clearly shown above the reservoir, as in the circled area. The second recommended drilling area is the white circled area, CDP's 420-250 (around well 8-13-41-6), which contains probably less oil and gas: the S-wave inversion ( $Z_s$ ) result may indicate some possible oil/gas accumulations.

#### **2.14B JOINT INVERSION OF LINE WG2**

The same procedures have been used as for line WG2. Figure 2.38 show event matching between the PP and PS seismic; the  $V_p/V_s$  ratio derived from horizon-based registration using the velocity from "strata model" as "domain conversion" at well 8-26-41-6W5 is shown in colours. For the joint inversion preparation, the PS statistical wavelet was created in the PP time domain. Figure 2.37 shows the extracted wavelets from both, the PP and PS seismic (in PP time) on line WG2, used in the joint inversion. A P-wave model and an S-wave model were created in the ProMC package, as for line WG1; then the "domain conversion" was updated with a P and S-wave model; the result is shown in Figure 2.38.

The joint inversion result is shown in Figure 2.39. Black arrows indicate the production wells from line WG2. The  $V_p/V_s$  anomaly, shows in Figure 2.36 that high  $V_p/V_s$

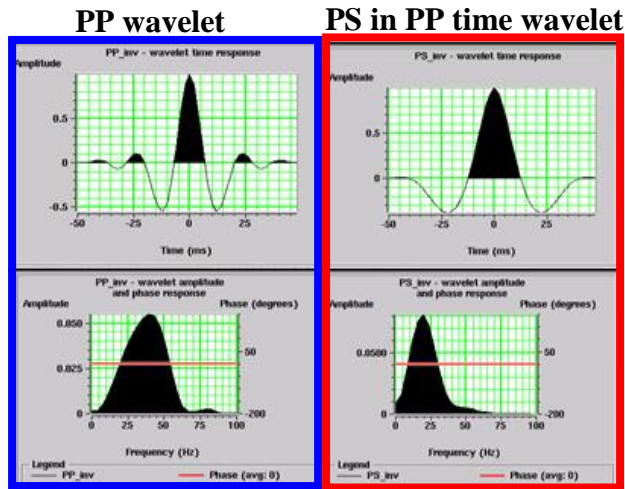


Figure 2.37: Statistically extracted wavelets for joint inversion on line WG2; left PP (blue rectangle) and right PS (red rectangle) in PP time; the top shows the wavelet in time domain and bottom in frequency domain.

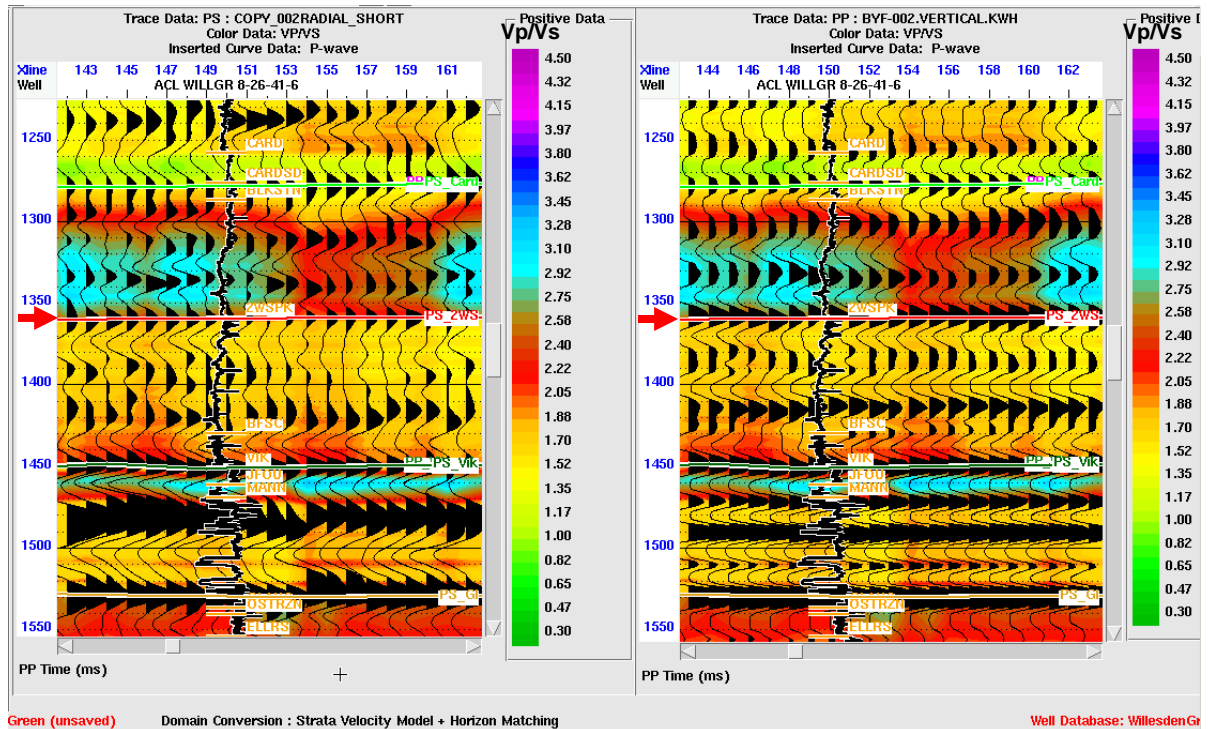


Figure 2.38: PP and PS data in ProMC after registration and horizon match: line WG2 at the well 8-26-41-6W5 location. Red arrows on the time scale (left) indicate the 2WS formation.

values (2.15 to 3) above the 2WS horizon can indicate a seal; below, the 2WS formation is possibly fractured and became a good reservoir, with values ranging from 1.3 to 2.15.

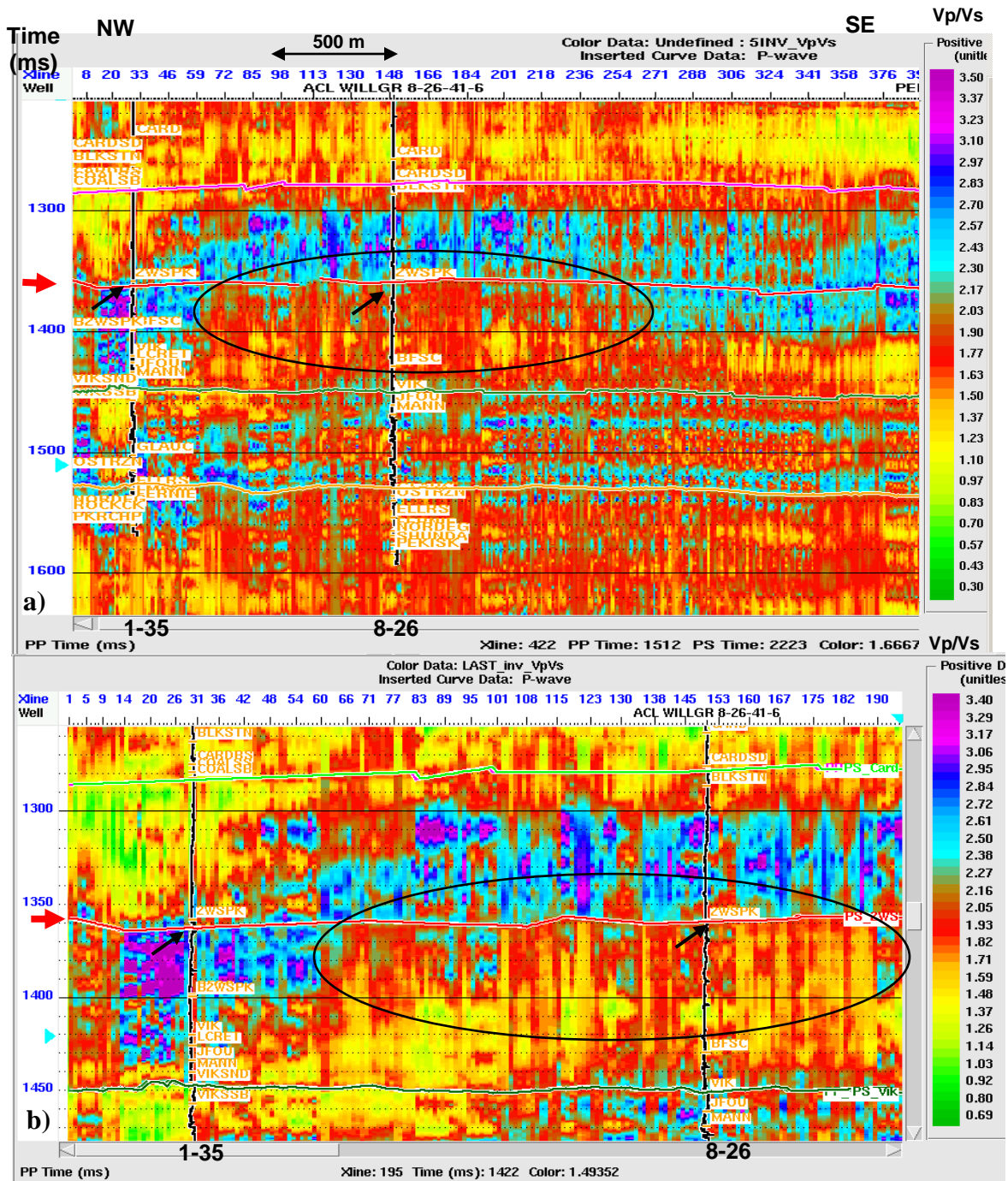


Figure 2.39: Joint inversion results for line WG2: a) Vp/Vs values on the line from CDP's 1-380 b) zoomed image around wells 1-35-41-6 and 8-26-41-6.

The producing wells on line WG2 are 8-26-41-6 and 8-13-41-6; see black arrows on Figure 2.39 a). Well 1-35-41-6 is not producing from the 2WS formation; our inversion result shows a thicker shale package at the 2WS horizon. Higher Vp/Vs values lead to the conclusion that there is no porosity or sand occurrence; there are no favorable conditions

for a good reservoir accumulation. Moving from NW to SE, towards well 8-26-41-6, note the low  $V_p/V_s$  values; this result shows a good reservoir, with a shale seal above. The recommended future drilling target is shown in the black circled areas in Figure 2.39, from CDP's 60 to 270. The second recommended drilling area is circled in white showing CDP's from 390-568 (around well 8-13-41-6), which contains less oil and gas. This area is probably more fractured, possibly containing sand lenses (lower values of  $V_p/V_s$  from 1.3 to 1.8). There are oil and gas accumulations in this area but migration has probably occurred; no obvious seal is seen above the formation.

#### **2.14C ANOMALOUS ZONES FOR WILLESDEN GREEN**

Figure 2.40 shows the cumulative oil and gas production for the Willesden Green area. The producing wells are 8-26, 16-15 and 8-13. The first recommended drilling area is according to chapters 2.14A and 2.14B located between the producing wells 8-36 and 16-15, towards 8-13, in the orange triangle area: The zone with less predicted production is surrounding well 8-13; it is shown by the yellow polygon around the orange triangle.

More investigations are recommended for the future in this area; polarization and splitting make shear waves a natural tool to investigate fracturing (Garotta, 2000). Future work in this project to better delineate the reservoir will need to investigate the 2WS fracture orientation and anisotropy.

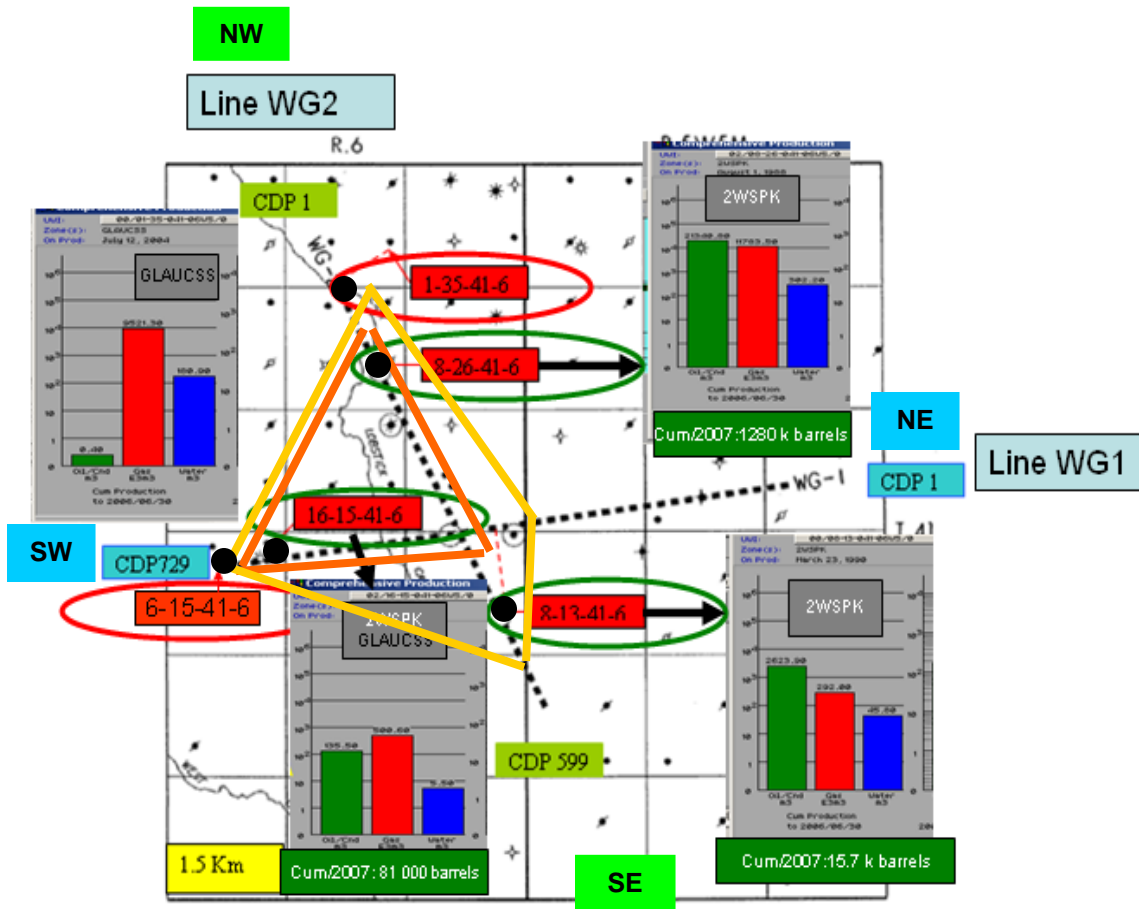


Figure 2.40: Wells from Accumap on Line WG1 and WG2: cumulative oil and gas production from 2WS, up until 2007: the three producing well are circled in green. The non producing wells are in red ellipses. Black circles indicate the well locations.

### 2.15 CONCLUSIONS

On Willesden Green data, the PP and PS separate post stack inversion method coupled with the joint inversion method were used to investigate the productive zones, based on the producing wells in this area: 8-13-41-6, 8-26-41-6 and 6-15-41-6. We find that:

- The main changes in the well logs roughly correspond to the lithology changes. P-wave sonic shows a lower increase than the S-wave sonic at the 2WS formation, hence the reservoir zone shows a low  $V_p/V_s$  value on the well logs.

- The model based inversion method using ProMC and Strata software has been used to predict reservoir properties along the seismic lines. PP and PS impedance sections were created and analyzed. The productive intervals are interpreted as a PP impedance drop and PS impedance increase. The calculated  $V_p/V_s$  values and the ratio of PP impedance and PS impedance were helpful for delineating the porosity zones and the sand/shale discrimination. The producing zones show values of  $I_p/I_s$  between 1.6-1.8 while the shales/seals have increased values, in between 1.9-3.5.
- Sands and shales were well separated in the  $V_p/V_s$  domain. There are benefits from using the velocity ratio;  $V_p/V_s$  less than 2.15 can give confidence in delineating the producing 2WS formation (possibly show an increase in porosity zones).
- This chapter indicates that the ratio of the PP inversion to the PS inversion in PP time can be useful for delineating the reservoirs.  $V_p/V_s$  values generated from joint inversion indicate anomalous areas similar to those found with impedance ratio values. Shear wave data use can bring useful information in future well positioning.
- According to Garotta (2000), shear waves have no conversion (at least in a one-dimensional environment) and are more sensitive to lithology, particularly because of higher and simpler axial isotropy. In this chapter, it has been shown that the main PP and PS impedance changes correspond to the major lithologic

boundaries. PS seismic data coupled with PP seismic data from multicomponent data can bring valuable information for future drilling location.

## CHAPTER 3 MANITOU LAKE, SASKATCHEWAN, 3D-3C PROJECT

### 3.1 INTRODUCTION

Lower Cretaceous fluvial sands channels with high porosity and permeability in the Manitou Lake area of Saskatchewan contain important oil and gas reserves. In this chapter, well logs and synthetic seismograms are used to correlate the PP and PS seismic sections, from a 3C-3D seismic survey which was undertaken to better delineate the Colony and Sparky reservoir sands. Mode-converted (PS) seismic amplitudes can complement traditional channel interpretation from PP data. PP and PS amplitude maps at the Colony sand level show different aspects of the channel's expression. Lithology and fluid discrimination based on  $V_p/V_s$  values are derived from the inverted PP and PS (registered in PP time) sections. Detailed registration of multicomponent seismic data aims to reduce the uncertainty of the channels interpretation and improve well targeting. An additional goal is to see if AVO attributes, LMR estimates, and elastic impedances values will highlight the drilled locations and possibly help identify new drilling locations.

Exploration targets of this survey include the Colony and Sparky sand channels, both members of the Cretaceous Mannville Group. These intervals are currently producing oil and gas in the area. Their thickness may be up to 10m. The oil at Manitou Lake is considered heavy oil; its gravity is around 12° API. This work investigates whether the interpretation of 3C-3D seismic data can help discriminate sand versus shale and find gas-charged porosity.

Greater porosity is expected in the channel deposits which contain thicker sand intervals. Log analysis indicates that the sand channels in the area have high porosities, up to 40%, and low water saturation (Quijada et al., 2007). Larger porosity values can lower the P-wave velocity. Thus, a good reservoir may have a lower  $V_p$  value. High resistivity values in the Colony and Sparky members indicate hydrocarbons, and the cross-over between the density and neutron porosity suggests gas. The presence of hydrocarbons might also lower the P-wave velocity. The S-wave velocity is seen to increase from shale to sand at the channel levels. Hence,  $V_p/V_s$  is often low in sandstones compared to shales. The interpretation of P-wave seismic reflection data alone can lead to ambiguous conclusions in certain exploration situations. Differentiation of prospective channel sands and non-productive shales can be problematic due to the similarity in P-wave impedance of these two lithologies. PS data are expected to be a direct measurement of the channel system, given that  $V_s$  should respond largely to the lithology and less to the fluid content.

### **3.2 LOCATION**

The location of the Manitou Lake area is shown in Figure 3.1. The red square shows the location of the 3D-3C survey in central Saskatchewan, close to Lloydminster, on the Alberta border. Figure 3.1 also shows a zoomed image of the red square: the map (T44, R27) shows the PP amplitude map at the Colony sand, from Calroc Energy Inc.

The red circles indicate the three wells available for this study. The data from these wells include spontaneous potential (SP), gamma-ray (GR), density (RHOZ), and resistivity

logs. Wells A11-17 and C07-16 both have a P-wave sonic log. A shear-wave sonic log is available only for well A11-17.

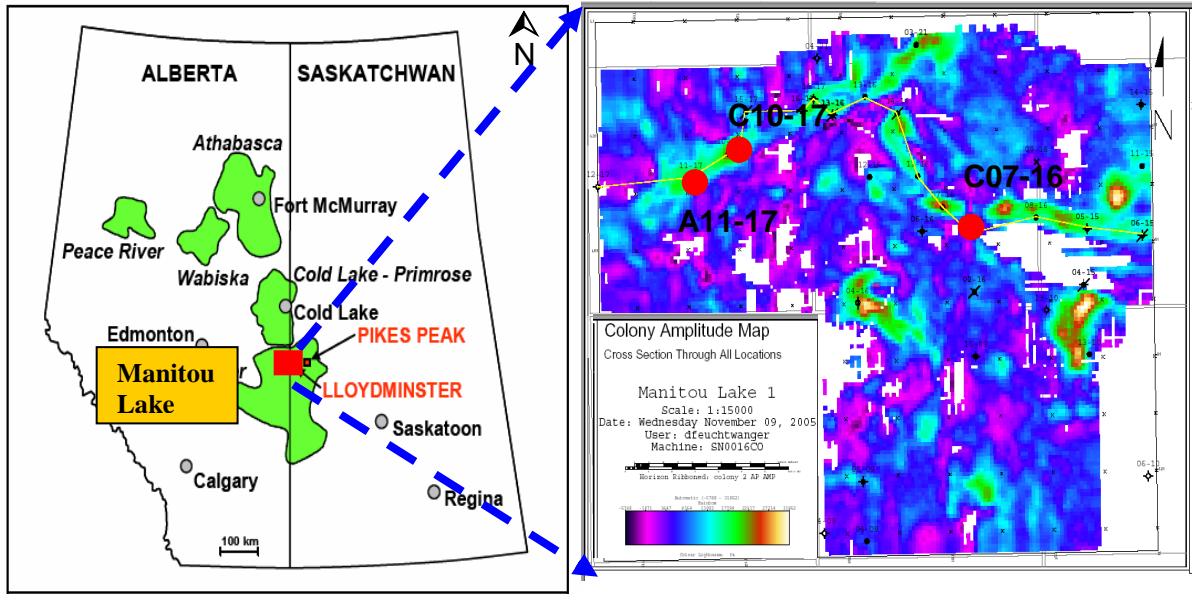


Figure 3.1. Left: Map of major heavy-oil deposits of Alberta and Saskatchewan, and location of the study area (after Watson, 2004); Right: Amplitude map for the Colony sand channel from Calroc Energy Inc.

### 3.3 GEOLOGY AND STRATIGRAPHY

Deposition in the Western Canada Sedimentary Basin (WCSB) can be divided into two successions, based on two different tectonic settings affecting sedimentation. The Paleozoic to Jurassic platformal succession, dominated by carbonate rocks, was deposited on the stable craton adjacent to the ancient western margin of North America. The overlying mid-Jurassic to Paleocene foreland basin succession, dominated by clastic rocks, formed during active margin orogenic evolution of the Canadian Cordillera, with

the emplacement of imbricate thrust slices progressively from east to west (Mossop and Shetsen, 1994).

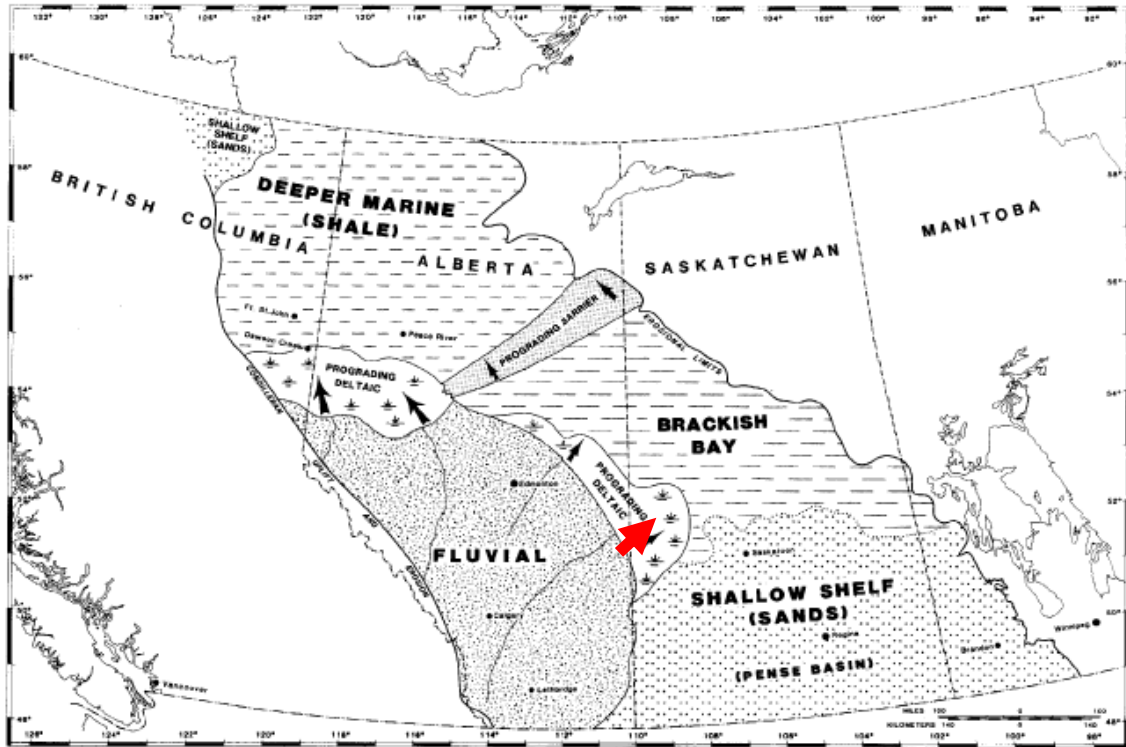


Figure 3.2: Paleogeographic reconstruction of the Upper Mannville deposition. Red arrow shows the location of the area (Modified from Leckie and Smith, 1992).

According to the stratigraphic column for west-central Saskatchewan (Figure 3.3), the Colony sand members of the Pense Formation, and the Sparky member of the Cantuar Formation, are both part of the Cretaceous Mannville Group. Most of the sediments in the area were deposited during the Cretaceous, and the top of the Mannville marks a clear separation between the predominant sands in Mannville and the overlying marine shales of the Colorado and Belly River Groups.

In the area, the Mannville Group lies unconformably on Paleozoic strata, and its sedimentary pattern consists of an interplay (interaction) of marine, estuarine and fluvial agents acting in a setting controlled by paleo-topographic relief and eustatic and

tectonic changes in relative sea-levels (Christopher, 1997). The Sparky member is informally grouped into the middle Mannville, which is dominated by sheet sandstone

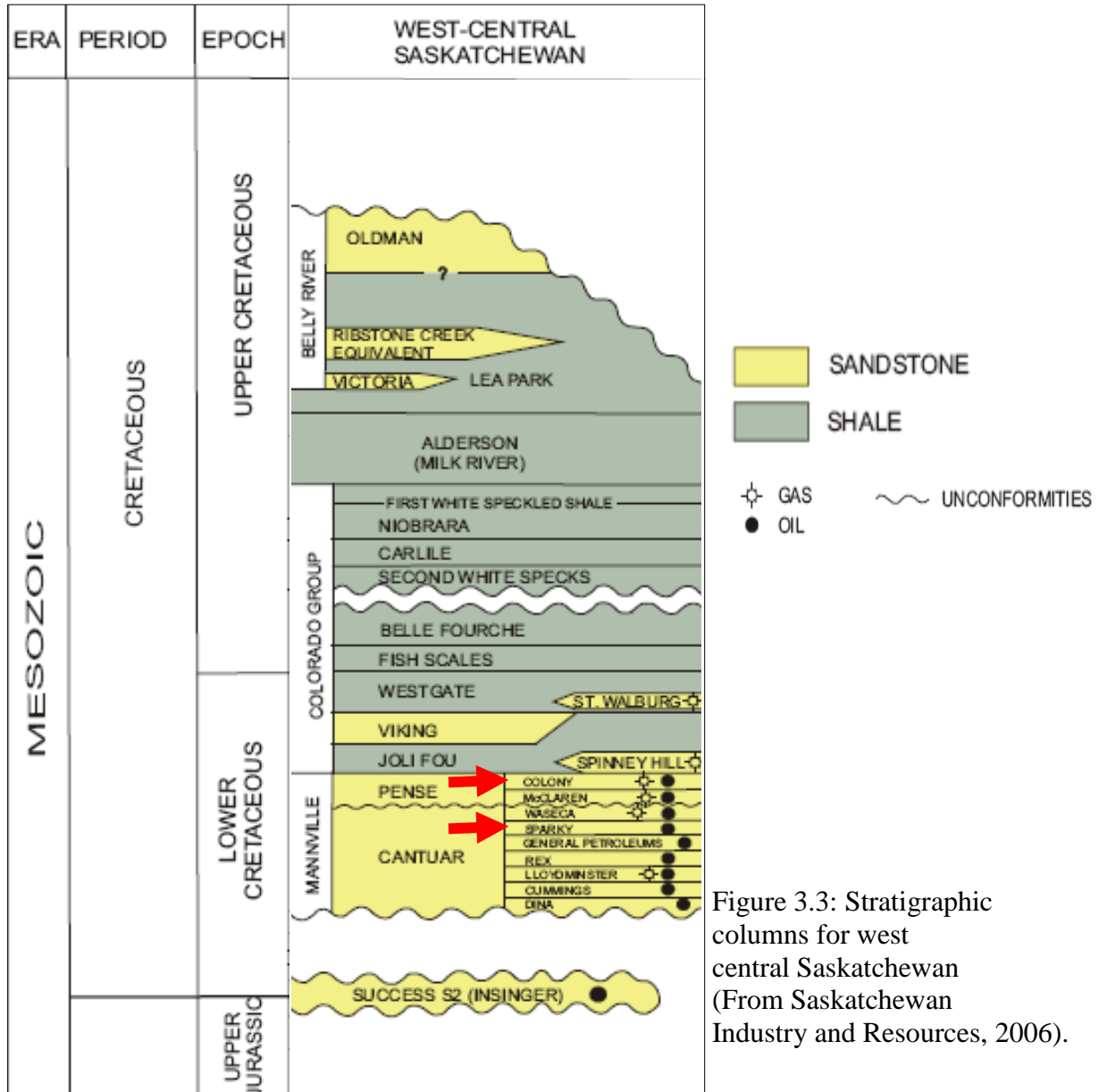


Figure 3.3: Stratigraphic columns for west central Saskatchewan (From Saskatchewan Industry and Resources, 2006).

development, with narrow channel sandstones and shales also present (Putnam, 1982). These units have been interpreted as delta-front facies with associated tidal-flat, tidal-channel, and beach environments (Vigrass, 1977). Several coal seams are found within

the Mannville Group in the Lloydminster area, mostly within the Cummings, Lloydminster, Rex and Sparky Formations. The distribution of coals in the basin is influenced by the tectonic events that created the foredeep.

The Colony sand member is unconformably overlain by the Joli Fou marine shale, representing the basal unit of the Colorado Group, which is dominated by marine shales encasing generally thin but extensive sandstones, such as the Viking and Cardium formations, as important petroleum reservoirs in other areas (Leckie et al., 1994). Within the Colorado Group, the First and Second White Speckled Shales, the Fish Scales Zone, and shale at the base of the Shaftesbury Formation are more radioactive than overlying and underlying shales, have high total organic carbon contents, and have considerable hydrocarbon generating potential. An interval such as the Second White Speckled Shale is potentially both a source and a reservoir rock for hydrocarbons (Mossop and Shetsen, 1994).

### **3.4 GEOLOGIC MODEL OF THE RESERVOIR**

Figure 3.4 shows a schematic depositional model for the Colony sands, including the three distinct facies units. They include (A) channel facies, (B) crevasse splay facies and (C) interchannel wetlands facies. Crevasse splay bodies are likely effective reservoirs in many thick tight-gas fluvial successions. They were formed usually during floods, in a wide crack or breach in the bank of a river. The sediments that spill out through the crevasse and fan out along the external margin of the river's bank form a crevasse splay deposit. A crevasse splay is defined (Allaby, 1999) as a small alluvial fan or other

outspread deposit formed where an overloaded stream breaks through a levee (artificial or natural) and deposits its material (often coarse-grained) on the floodplain. This is also known as channel splay. A floodplain is flat or nearly flat land adjacent to a stream or river that experiences occasional or periodic flooding. It includes the floodway, which consists of the stream channel and adjacent areas that carry flood flows.

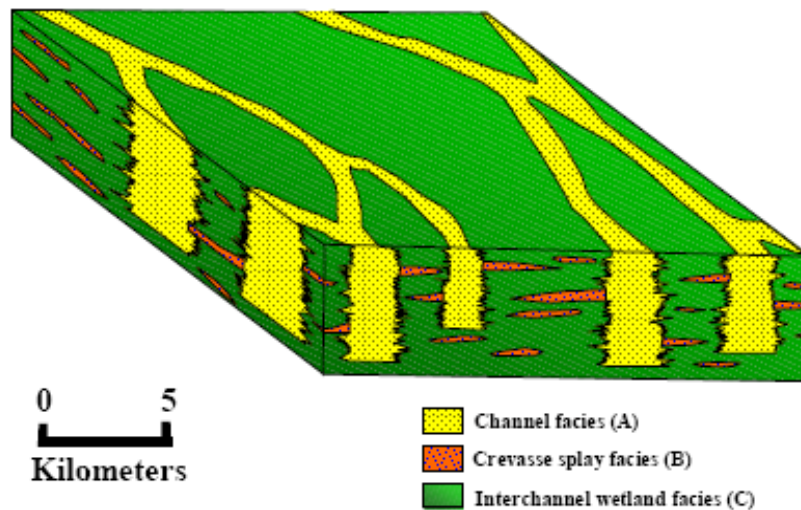


Figure 3.4: Depositional model for the Colony sand member after Putnam and Oliver (1980) from Royle (2002).

The **Colony** sand member is the uppermost unit of the nine member informal subdivision of the Mannville Group and consists of shales, siltstones, coals and sandstones. Deposition of this member occurred in an extensive complex of anastomosing (coming together or opening into each other, defined as the connection of separate parts of a branching system to form a network, as a river and its branches) channel sandstones, encased within siltstones, shales, coals and thin sheet sandstones (Putnam and Oliver, 1980). The Colony sand member is capped by the marine shales of the Joli Fou formation.

The **Sparky** member is informally grouped into the middle Mannville, which is dominated by sheet sandstone development, with narrow, channel sandstones and shales also present (Putnam, 1982). The sheet sandstones in the Sparky are commonly 6-9 m thick, and can be traced laterally for several tens of kilometers; however, they are commonly broken by thick, ribbon-shaped deposits or sandstone pinchouts (Putnam, 1982).

### **3.5 ACQUISITION AND PROCESSING FOR 3C-3D SURFACE SEISMIC**

The Manitou Lake 3C-3D survey was acquired for Calroc Energy Inc. near Manitou Lake, Saskatchewan (Figure 3.1), in February 2005 by Kinetex Inc. The survey covers an area of approximately 10 km<sup>2</sup> as in the base map (Figure 3.5), with twenty one south-north receiver lines and eighteen indicated west-east source lines, with 200 m line spacing and 50 m station spacing (Lu et al., 2006). The seismic data includes a suite of logs from three different wells in this area. Acquisition parameters are shown in Table 3.1.

The vertical (PP) and the radial (PS) component data were processed to a final migrated volume by Hanxing Lu and Kevin Hall of the CREWES project. Conventional processing flows for the PP data have been employed, as described by Lu and Margrave (1998). The processing flow for Manitou Lake migrated sections consists of deconvolution, time variant spectral whitening, and FD migration after CDP stack (Lu et al., 2007).

For the CDP gathers in the AVO analysis, the processing flow was done in the following order: SEG Y input, 3D geometry assignment, true amplitude recovery, elevation statics

and refraction statics, surface consistent deconvolution, front end muting, velocity analysis, residual surface-consistent statics, normal moveout, and trim statics.

For this survey, most of the coherent energy is in the 18-75 Hz range (Lu et al, 2006). The dominant frequency of the PP data is about 65 Hz, while that of the PS data is approximately 25 Hz. Because the PS data were much noisier than the vertical data, and the velocities were more difficult to pick, near offsets (0-400m) have been excluded in order to reduce the effects of source noise (Lu et al., 2006). PP shot and receiver statics were calculated using GLI3D. Due to large lateral variations in the near surface shear-velocity field, it was difficult to calculate PS receiver statics. Non-surface-consistent receiver statics were applied for the PS data.

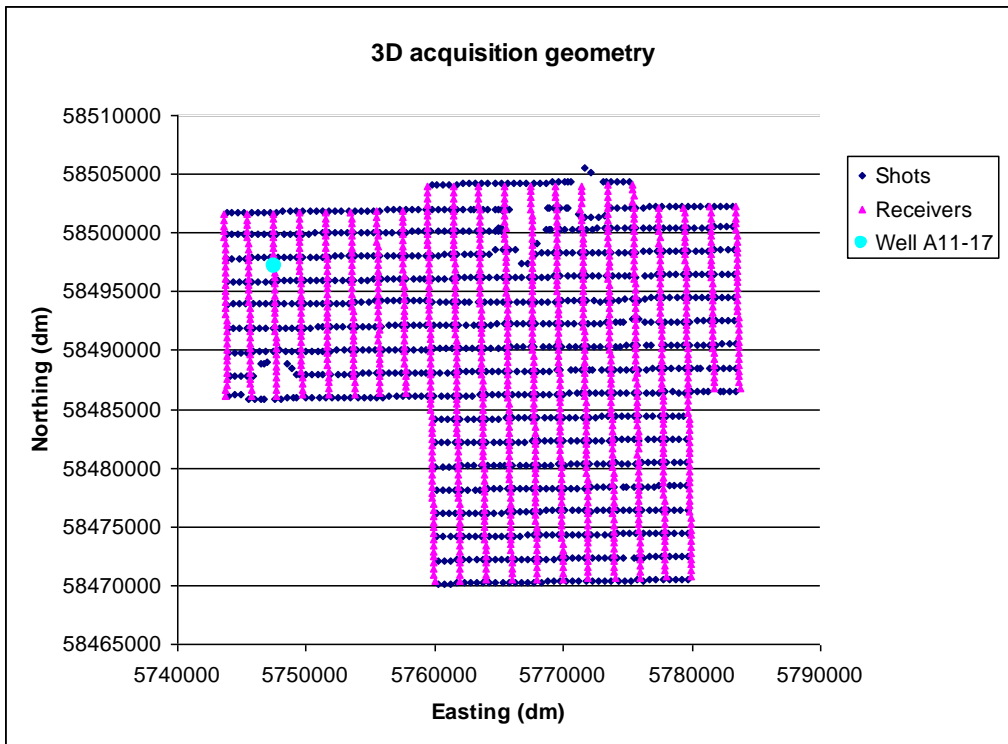


Figure 3.5: Acquisition geometry of the Manitou Lake survey from Lu et al., (2006): base map; Shots are in blue, receivers in purple, and well A11-17 is a cyan circle.

Table 3.1. Acquisition Parameters (Kinetex Inc.)

Recording System	I/O System 4
Source	Two vertical vibrators (IVI Y2400)
Source Array	16 m dragged array, 8 sweeps per VP, 1.14 m move-up per sweep. Diversity stacked in the field.
Sweep	8-144 Hz over 10 s with 5 s listen time
Receiver	I/O VectorSeis SVSM
Receiver Array	Single sensor per station
Station spacing	50 m source and receiver station spacing
Line spacing	200 m source and receiver line interval
Receiver lines	21 lines, total length 51.93 km
Source lines	18 lines, total length 53.89 km
Total area	~10 km <sup>2</sup>

For a preliminary interpretation, PP and PS synthetics were generated using the SYNGRAM package (CREWES) for the construction of synthetic seismograms at well A11-17 (Lu et al., 2006). Constant-phase bandpass wavelets were created in WAVELETED (Lu et al., 2006), with frequency bands matching the bandpass filter used for the seismic displays (PP=10-15-90-110, PS=15-20-30-45). Figure 3.6 shows the PS (right) and PP (left) migrated section at well A11-17, and the correlation with the synthetic seismograms (synthetics: the PP in blue and the PS in red). Red arrows on both, PP and PS data show the Colony sand member at the well location.

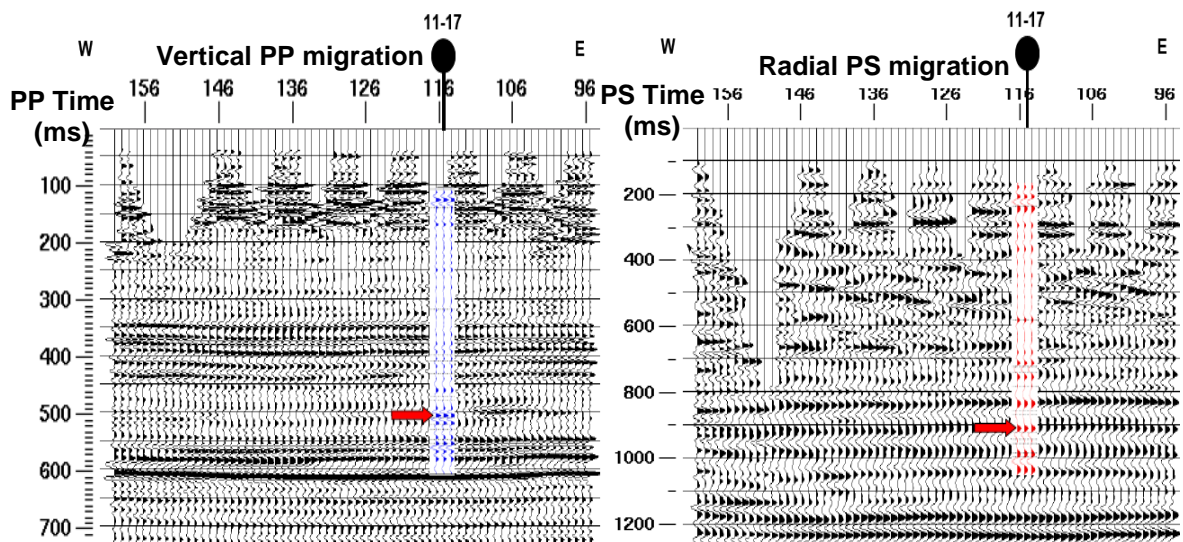


Figure 3.6: Well 11-17 location: Comparison of migrated PP (left) in PP time to migrated PS (right) in PS time. Red arrows shows top of Colony sand member. (after Lu et al, 2007).

### 3.6 LITHOLOGY DIFFERENTIATION

The first step in the interpretation is to differentiate, on the well logs, the clean sand zones and the shales. Figure 3.8 shows a suite of logs for well A11-17 and C7-17 (Quijada et al., 2007), where gas is highlighted in red, oil in green, and water in blue. The top of the Colony sand is clearly identified by a significant deviation to the right in the GR, SP and porosity logs. The P-wave shows almost no change while the S-wave velocity shows a significant increase. High resistivity values in the Colony and Sparky formations indicate hydrocarbons, while the cross-over between the density and neutron porosity logs at the Colony member suggest gas. The shear-wave velocity increases for water and gas, while it shows lower values where oil is present (Quijada et al, 2008). The best differentiation with regard to lithology was given by the  $V_p/V_s$  ratio: lower values than 2.15 corresponding to sands and higher values to shales( Quijada et al.,2008).

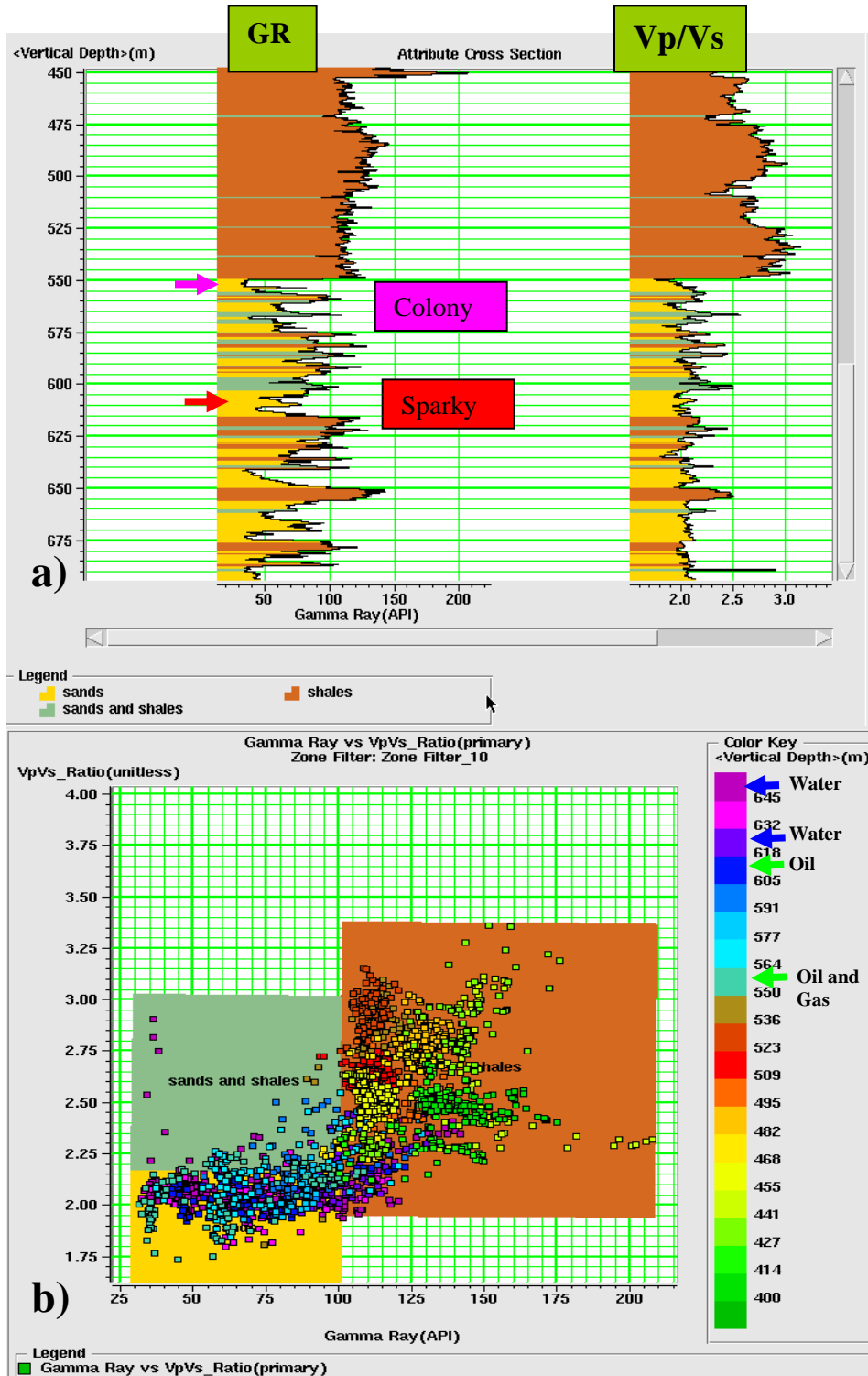
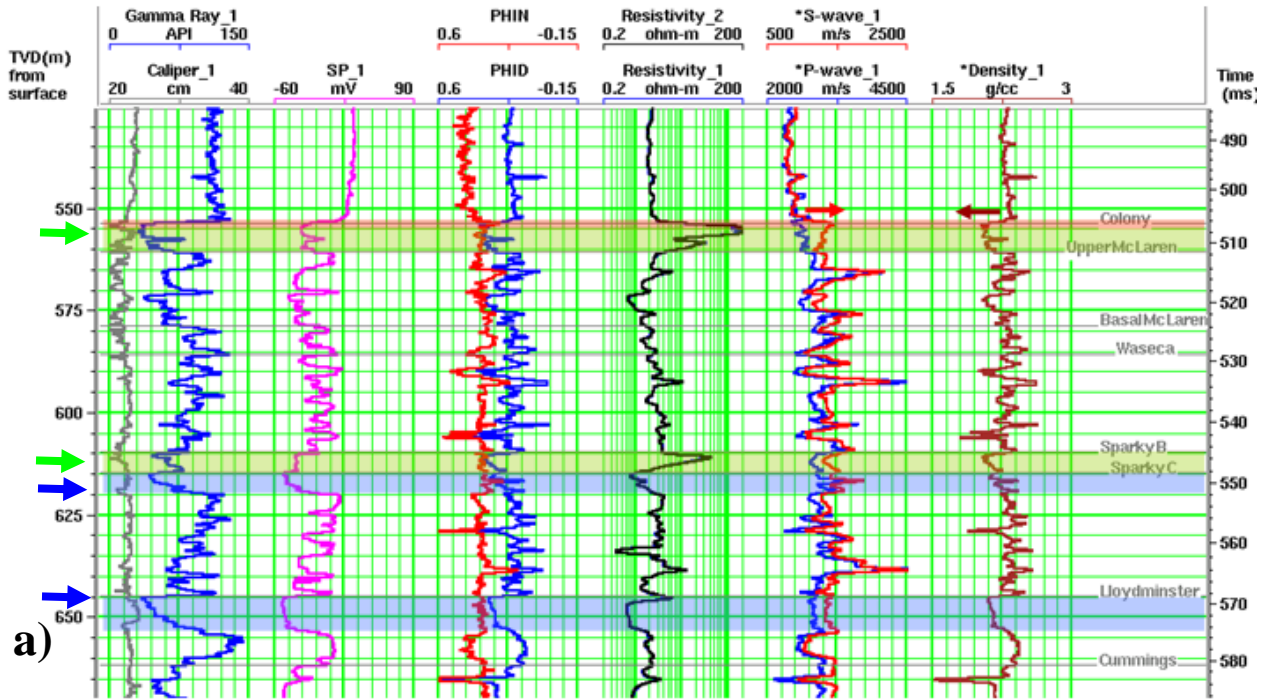


Figure 3.7: a) Log plots showing Gamma Ray and Vp/Vs ratio ray for the well A11-17; At 550m depth cyan arrow shows the Colony sand channel and around 610m the red arrow shows the Sparky level. b) Crossplot: Vp/Vs versus GR. The colour bar (left) shows the depth in m.

### Well A11-17



### Well C07-16

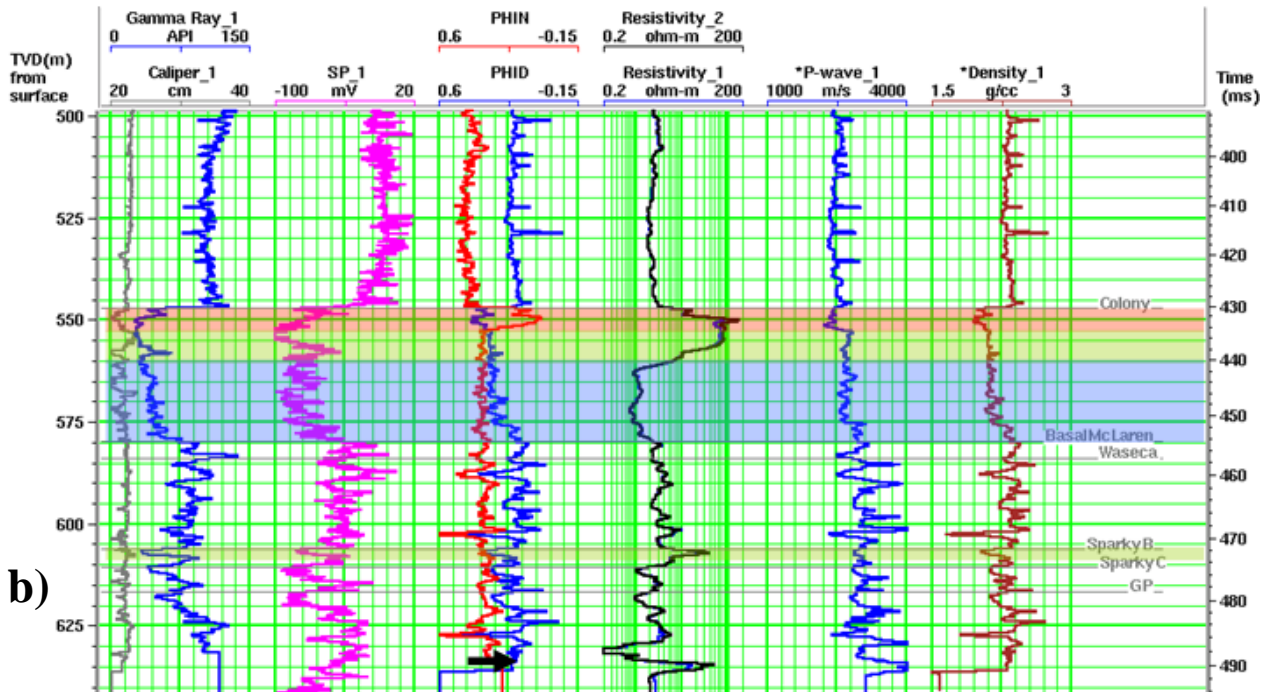


Figure 3.8: a) Suite of logs for well a) A11-17 and b) C07-16, gas is highlighted in red, oil in green and water in blue (after Quijada et al., 2007).

A lithology differentiation has been tried for well location A11-17, the single well with a shear (S) sonic log in this survey. Sand zones were considered to have values less than 100 API on the GR logs, and  $V_p/V_s$  values less than 2.15, as in figure 3.7: sands are shown in yellow, shales in brown and sand/shales in olive. The green arrows on the vertical depth scale (Figure 3.7 b) shows the hydrocarbon depth, while the blue arrows suggests the water depth, as in Figure 3.8 a.

The change of  $V_p/V_s$  values in the reservoir is not only due to the variation of porosity. It is also closely related to the shale content and water saturation variation. The shale variation may change the  $V_p/V_s$  value of the rock more drastically than the water saturation does. Water saturation increases the  $V_p/V_s$  value for both, sand and shale (Xu Y., 2002).

### **3.7 PP INTERPRETATION**

After the PP seismic data were processed, three sets of logs were chosen for correlations with seismic: A11-17, C10-17 and C07-16 (see Figure 3.1). The interpretation of the PP migrated volume was undertaken by correlating well logs to the seismic data and picking horizons based upon well control. Figure 3.9 shows the well log correlation with seismic at the A11-17 location. From left to right we can see the following curves a) Porosity (brown), Gamma Ray (blue), SP (red), Density (blue), Resistivity (black), S (blue) and P (red) sonic logs,  $V_p/V_s$  value (red) and the vertical component migration and b) the gamma-ray curve, sonic logs (P wave sonic in red and shear sonic in blue) and density. Note that the Colony sand channel was picked on a trough and shows an increase in

porosity, a sharp decrease on the gamma ray and SP logs, a density decrease, an increase in resistivity, an increase on the shear sonic log and almost no increase on the P-wave sonic, and a lower  $V_p/V_s$  value.  $V_p/V_s$  give the best differentiation regarding the lithology: values from 1.70 to 2.15 for sands and values from 2.15 to 3 for shales. Lower density values, less than  $1.7 \text{ g/cm}^3$  suggest coals. As shown by Quijada et al., 2007, in Figure 3.8, a) the S-wave velocity shows a very significant increase from 800 m/s in shales to 1300 m/s in sands. The high resistivity values in the Colony and Sparky members indicate hydrocarbons, while the cross-over between the density and neutron porosity logs in the Colony sands suggests the presence of gas. In the target zone, density is a good lithological indicator, with densities lower than  $2250 \text{ kg/m}^3$  indicating sands, and higher values corresponding to shaly sands and shales. Sparky B is picked on a zero crossing, showing similar characteristics to the Colony sand channel. Figure 3.9 a) shows for the Colony sand member an effective porosity up to 40%, and an average thickness of 10 m. The Sparky level has a similar porosity, showing a thickness of less than 10 m. As in Figure 3.8, high resistivity shows hydrocarbon saturation, and low values in  $V_p/V_s$  and gamma ray logs show decreased shale and more sandstone content. The oil gravity in this area is around  $12^\circ \text{ API}$ , which corresponds to a density of  $0.9861 \text{ g/cm}^3$ . The S-wave velocity increases for water and gas, showing lower values where water is replaced by oil. It is important to note (Quijada et al., 2007) that S-wave velocity appears to be the best lithological indicator, along with the  $V_p/V_s$  value, where sands have a ratio between 1.7 - 2.15, and shales between 2.15 - 4. Integration of seismic and well log information can lead to qualitative and often quantitative estimates of sand, shale, porosity, fluid saturation and other key reservoir attributes (Roth, 2007).

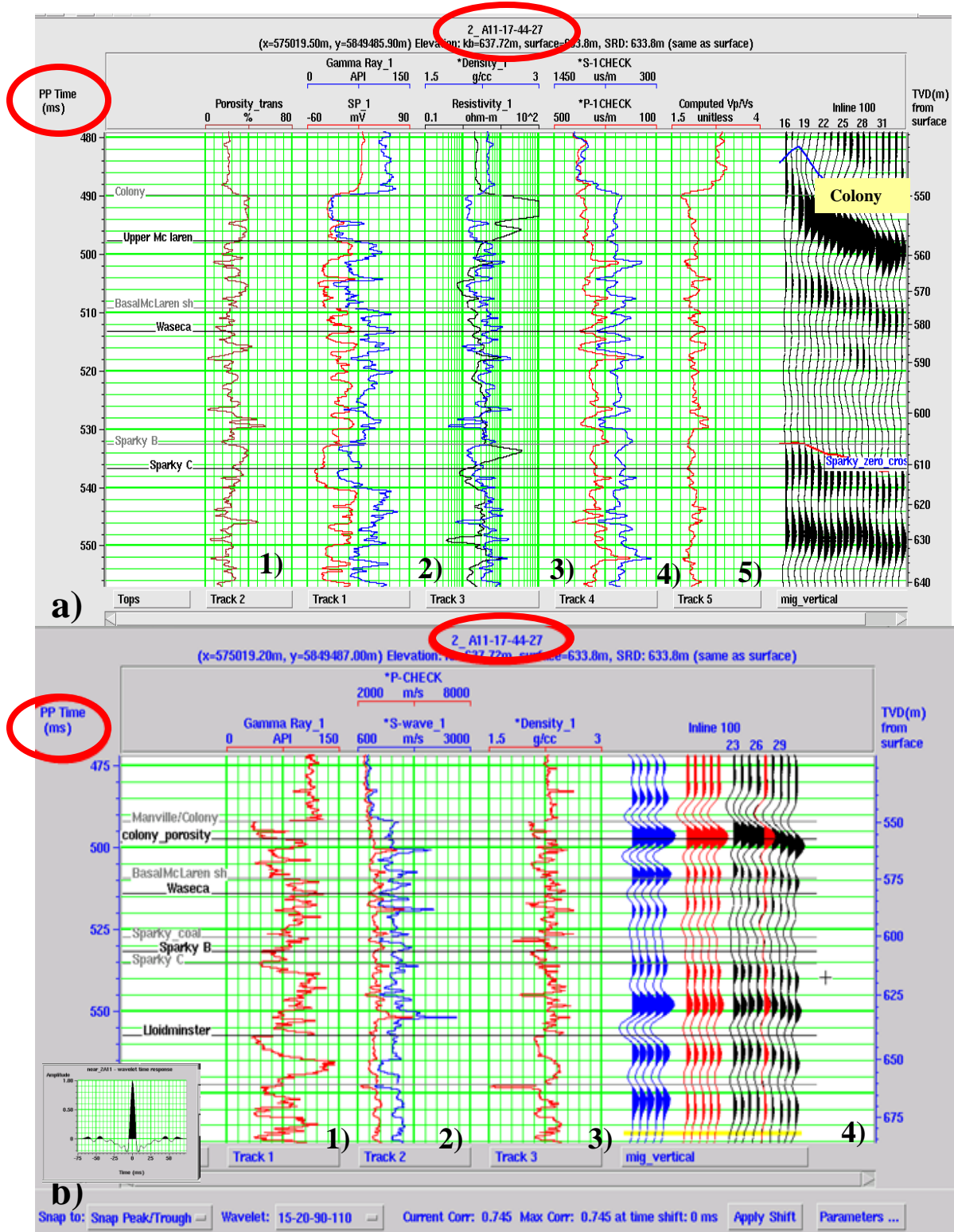


Figure 3.9: a) Well log correlation with seismic, well A11-17: Porosity (1), Gamma ray (2) in blue and SP in red, (3) density in blue and resistivity in black, (4) S (in blue) and P (in red) sonic logs, (5) Vp/Vs b) (4) Synthetic (blue), seismic (black) and well log correlation in PP time at well location A11-17 the GR(1), PP( in red) and PS( in blue) sonic(2) and density curves(3). Left b) the used wavelet in the synthetic calculation.

In Figure 3.10 we can identify the two sand channels (green arrows) on the PP migrated volume: Colony (above) and Sparky (below) at the well location C7-16. The inserted logs are GR in red and the S-wave sonic in blue. Note the lower values of GR at the sand channels. The Colony and Sparky tops were picked on troughs on the vertical section. At the Colony formation the amplitude clearly increases. The change in waveform on both, Colony and Sparky, suggest differential compaction of the sand channels. Figure 3.11 shows the log suites at the location of well C7-16. The oil/gas/water delineation on the seismic has been done by comparing the logs with Figure 3.8 b. The depth of the channels at this well location was found to be around 550m for the Colony and 605m for the Sparky member.

Amplitude maps were generated at the Colony and Sparky horizons, as in Figures 3.12 and 3.13. A comparison of the PP amplitude map (Figure 3.12) with the previous PP amplitude map processed by Calroc Energy (Figure 3.13) reveals a more continuous and sharper representation of the sand channel at the Colony level. Figure 3.14 top, shows our result for the PP amplitude map at the Sparky sand channel, compared with the previous amplitude map processed by Calroc Energy Inc. (below). Higher amplitudes (in blue-purple) in Figures 3.12 and 3.14 show a somewhat different image of the sand channel.

All wells are located on high amplitudes within the Colony sand channels, but only well A11-17 is producing from this interval. Wells C10-17 and C7-16 are producing from the Sparky formation. Black arrows on all amplitude maps indicate a possible reservoir based on PP data. In the next chapters, the response of PS volumes will be analyzed at the indicated location.

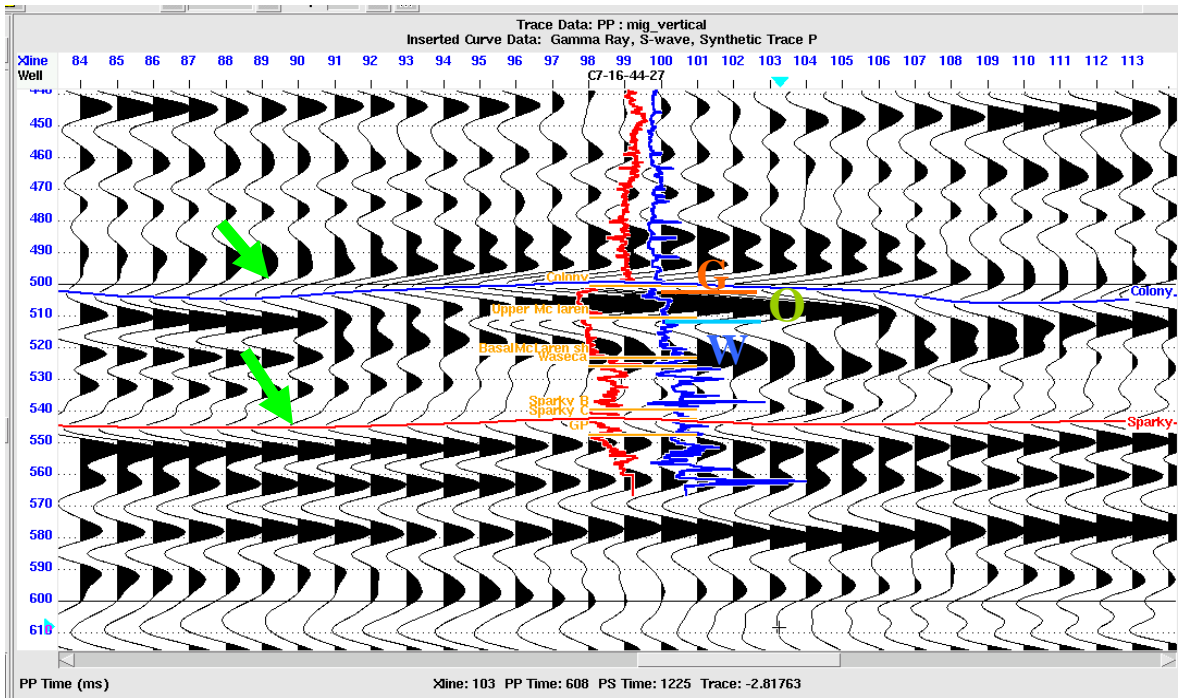


Figure 3.10: PP section showing the Colony (blue) and Sparky (red) horizons at the C7-16 well locations. Green arrows show the Colony (above) and Sparky (below) channels. The inserted logs are GR in red and the S-wave sonic in blue.

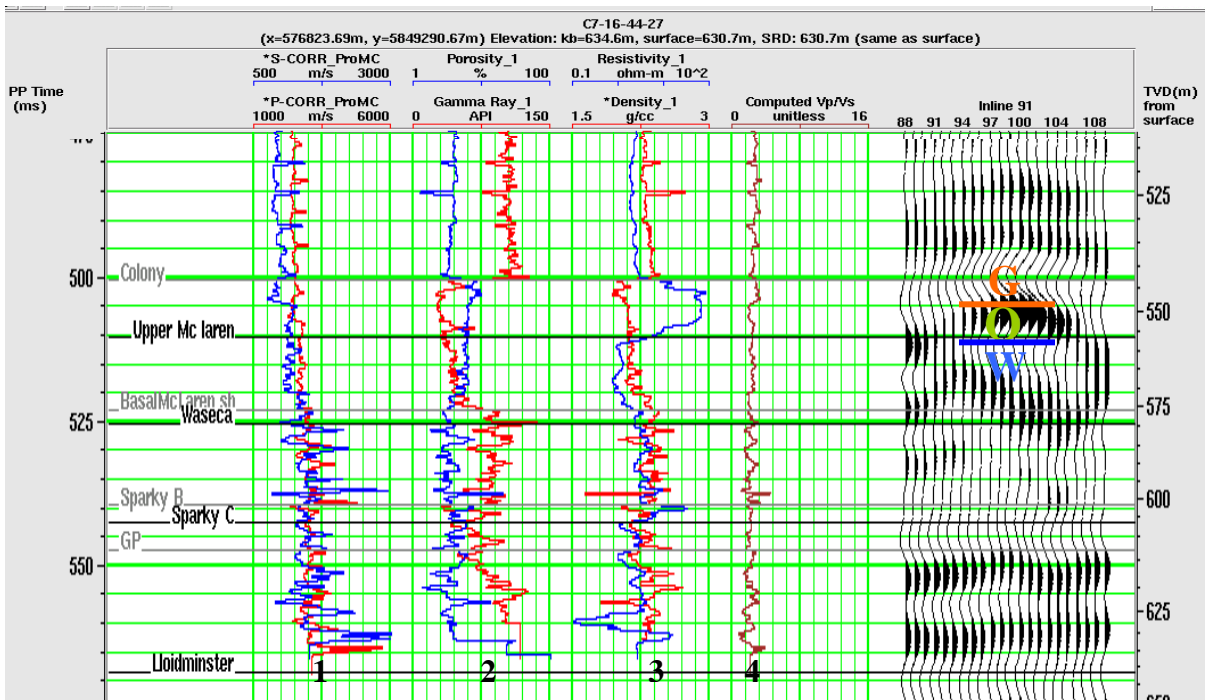


Figure 3.11: Well C7-16:(1) S (in blue) and P (in red) sonic logs; (2) porosity (blue) and Gamma ray;( 3) density (red) and resistivity (blue);(4)Vp/Vs and the migrated PP section showing an amplitude increase at the Colony sand channel. The depth of the channels is around 550 m for the Colony and around 605 m for the Sparky.

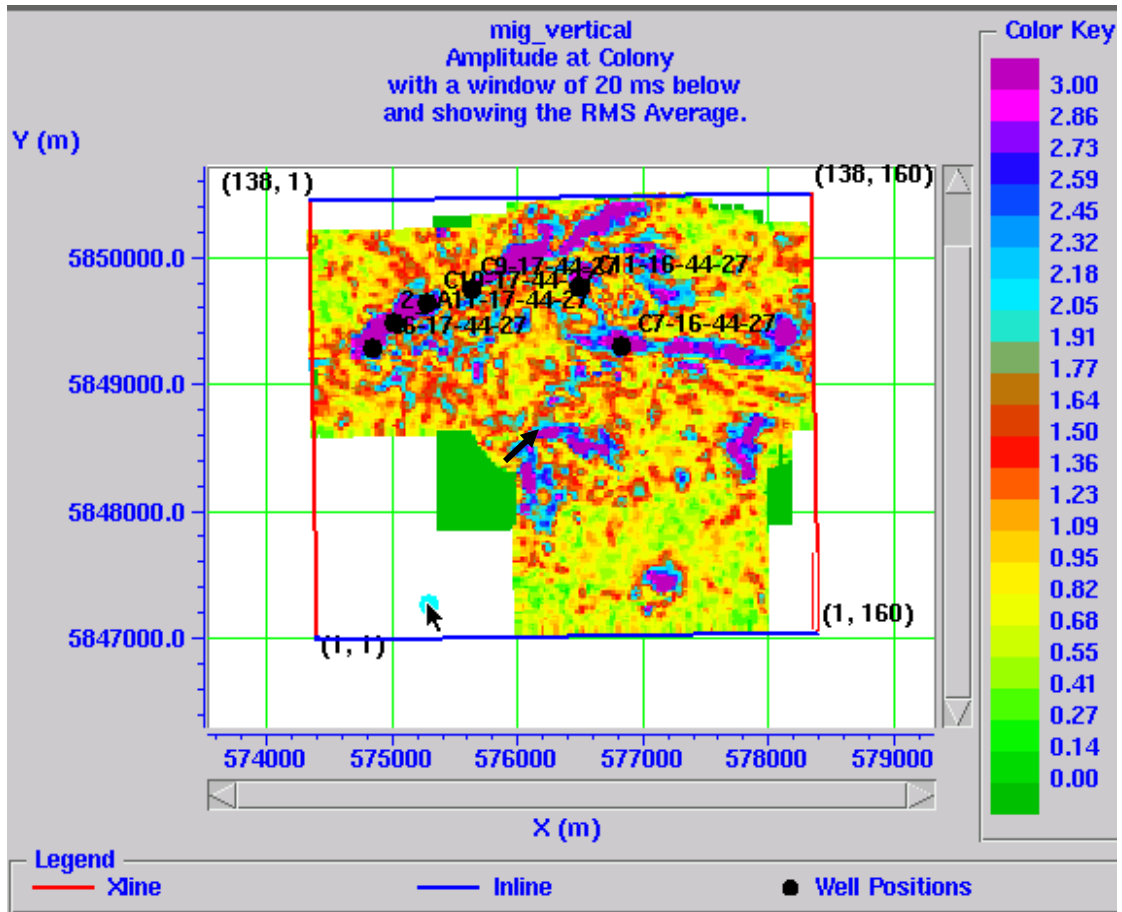


Figure 3.12: Amplitude map showing PP RMS amplitudes at the Colony horizon, with a 20 ms window below the horizon.

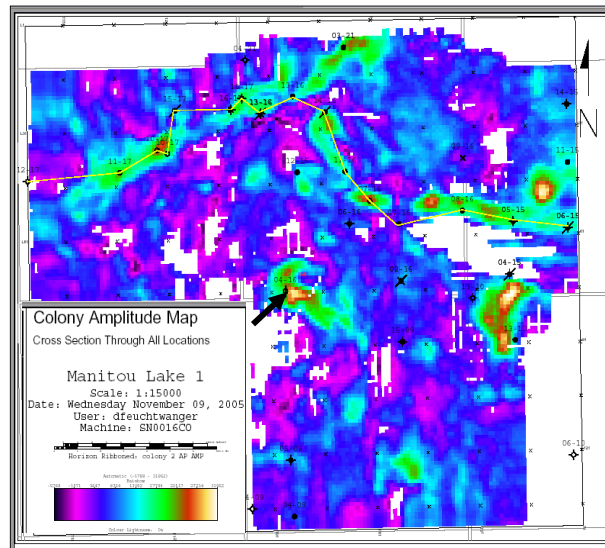


Figure 3.13: Amplitude map showing PP RMS amplitudes at the Colony sand channel, produced by Calroc Energy.

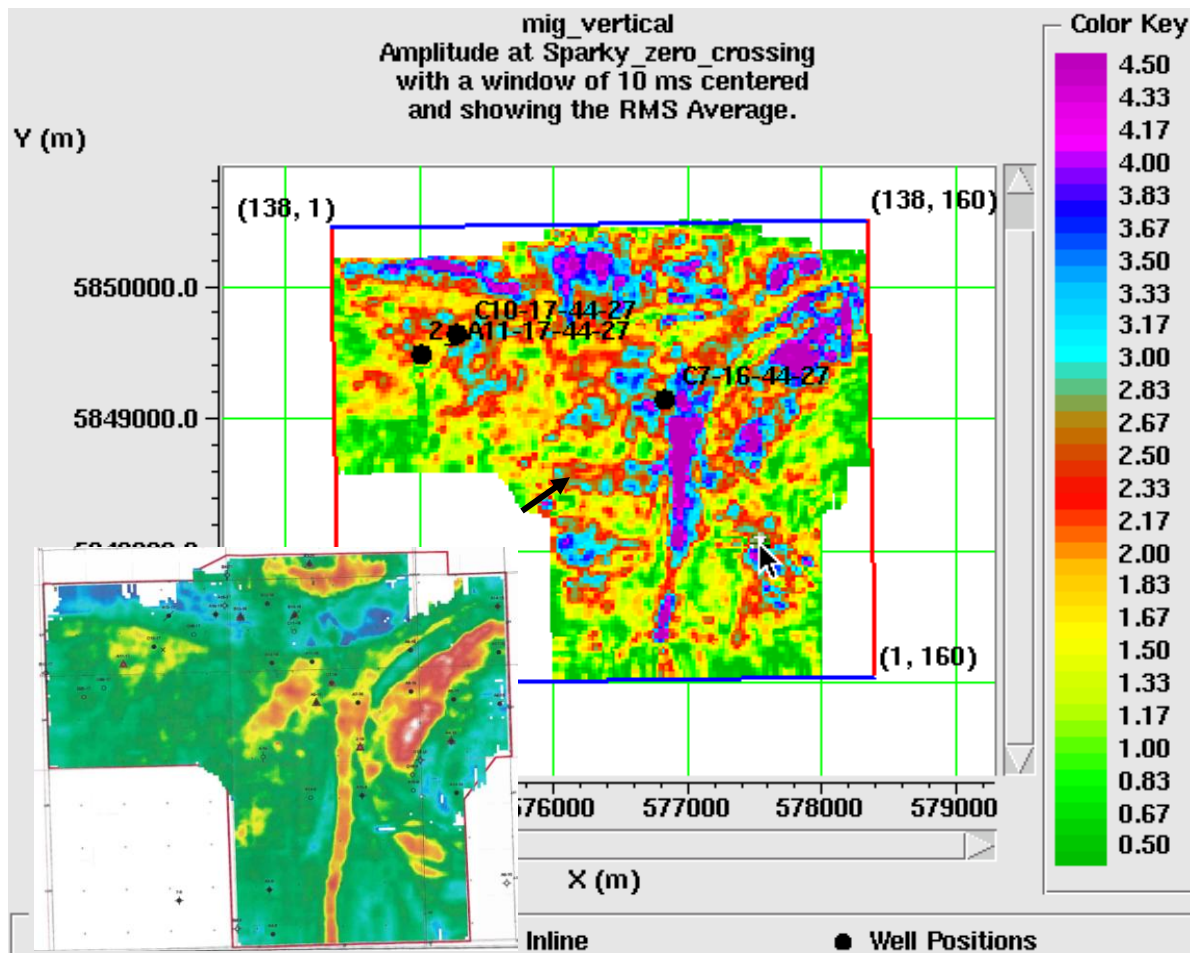


Figure 3.14: Amplitude map showing PP RMS amplitudes at the Sparky, with a centered 10 ms window. Below: comparing with the previous amplitude map processed by Calroc Energy Inc.

### 3.8 PP AND PS INTERPRETATION

Conventional PP seismic data acquired at the Manitou Lake project (as shown in Chapter 3.7) had limited value in detecting some targets. The PP amplitude maps show high amplitudes, originally suggesting a good drilling location. Black arrows from previous figures indicate a drilled location which did not encounter hydrocarbons. This work shows if combined PP and PS interpretation can distinguish between productive and dry locations.

Coupled PP and PS seismic analysis can increase confidence in interpretation, give rock property estimates, and provide additional information for imaging the subsurface detailed in the next chapters of this thesis.

When compressional P waves reach an interface at non-normal incidence, they are partitioned into transmitted and reflected P and shear (S) waves. Significant energy is converted to S waves which, in the absence of azimuthal anisotropy, will be recorded primarily on the radial (inline horizontal) component at the receiver. Due to the difference in travel path, wavelength and reflectivity, PS seismic sections can show significant changes in amplitude or character of events which are not apparent on conventional PP sections. Horizons can be better imaged on one or the other of the sections because of different multiple paths and wavelet interference effects such as tuning (constructive or destructive interference resulting from two or more reflectors spaced closer than a quarter of the dominant wavelength).

Garrotta et al., (2002) showed that shear waves are slower than compressional waves and cannot propagate through fluids, making converted wave exploration useful for fluid and lithology discrimination, imaging structure through gas clouds and fracture detection by analysis of shear wave splitting, among others.

The next step in this work is to create the PS synthetic seismograms, as in Chapter 2. In the wells without a dipole sonic, shear logs were created using Castagna's equation (Equation 2.2), where the velocities are in km/s:

$$V_p = 1.16V_s + 1.36 \quad (2.2)$$

This relation is generally defined as the mudrock line. A linear least- square fit of the P- and S-wave velocities logs from Manitou Lake results in a slope of 1.2 and an intercept

of 1.257 (Quijada, 2009) which are very similar to the parameters defined by Castagna et al. (1985) in equation 2.2.

The PS synthetic seismogram was correlated with the PS seismic volume in PS time. Figure 3.15 shows from left to right: the Gamma Ray log, the P-wave (blue) the S-wave (red) and the density. The well log is stretched in PS time with a correlation coefficient around 60%. The synthetic (in blue) was created using the wavelet shown below. The wavelet was extracted from the PS (radial) migrated stack. Figure 3.16 shows the PS seismic and well logs at well location A11-17. From left to right the following logs are: S-wave (blue), the P-wave (red), the SP (red), the Gamma Ray (blue), and the computed  $V_p/V_s$  values. Note the sharp increase in the S-wave value at the Colony level and the evident decrease in the  $V_p/V_s$  value.

Registration was done in PP time, thus shrinking the PS section to match the PP section, as in Figures 3.18 and 3.19. We consider PS data to be another indicator of the channel system, given that should respond largely to increased sand content.

There are some challenges when processing the mode-converted data: some issues include the separation of P wave arrivals, and the large magnitude of shear-wave statics. Shear statics have much larger variations at a much smaller distance scale than compressional statics. This originates from the higher variability of the shear velocity in near surface inhomogenous material (Garotta, 2000). Registration can be challenging. As seen in Figures 3.17 and 3.18, on the PS time correlated section, the Colony and Sparky horizons were picked on a peak. Only the horizon Sparky B was picked, due to the fact that it is the producing horizon for wells C7-16 and C10-17. The sand channels are

circled in colours. Note the lower frequency content of the PS data compared with the PP data and the amplitude and waveform changes in both cases. Hydrocarbon fluids can reduce the acoustic impedance of young unconsolidated reservoir rocks, producing a bright spot, as seen here.

Figure 3.18, shows the registration using the PP and PS picked horizons (Hampson – Russell software). The velocity derived from all three wells was used for domain conversion. On the left side is the PS migrated section, and on the right side is the PP

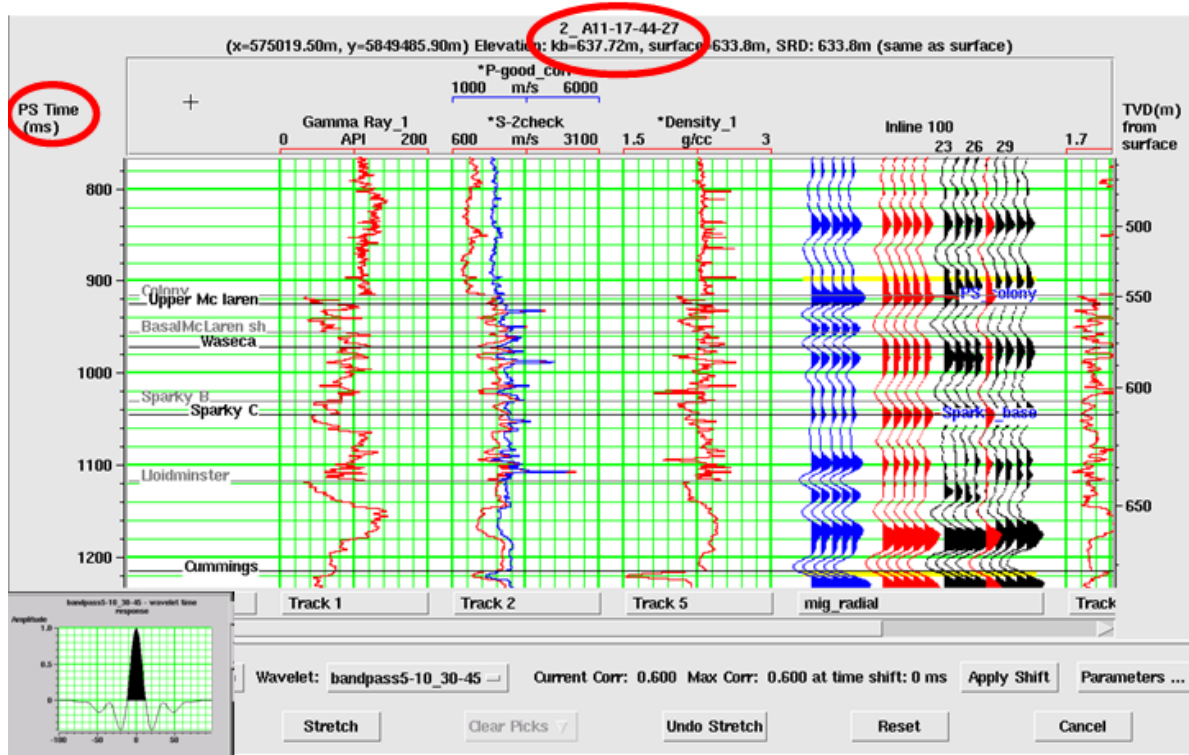


Figure 3.15: Synthetic, seismic and well log correlation in PS time at well location A11-17. The used wavelet (below) was extracted from the PS seismic data. From left to right: the Gamma ray log, the P-wave (blue), the S-wave (red) and the density.

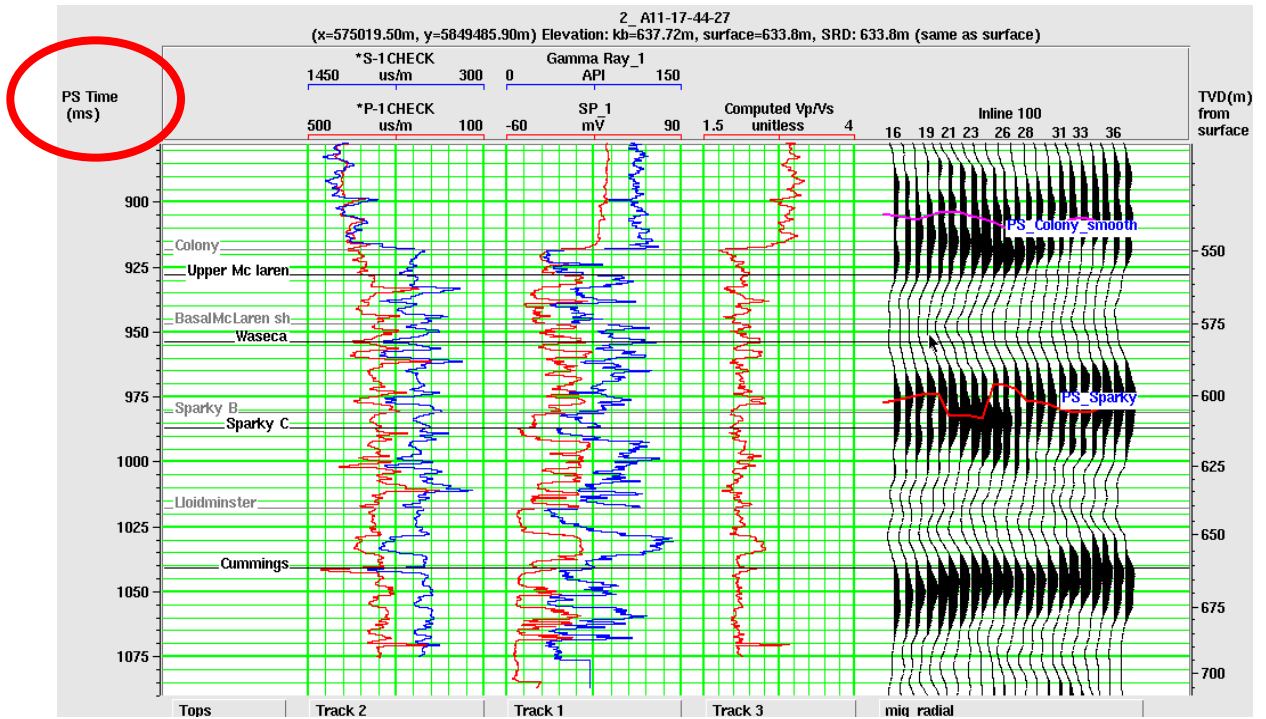


Figure 3.16: Seismic and well log correlation in PS time at well location A11-17. The PS Colony horizon is picked in purple and the Sparky in red.

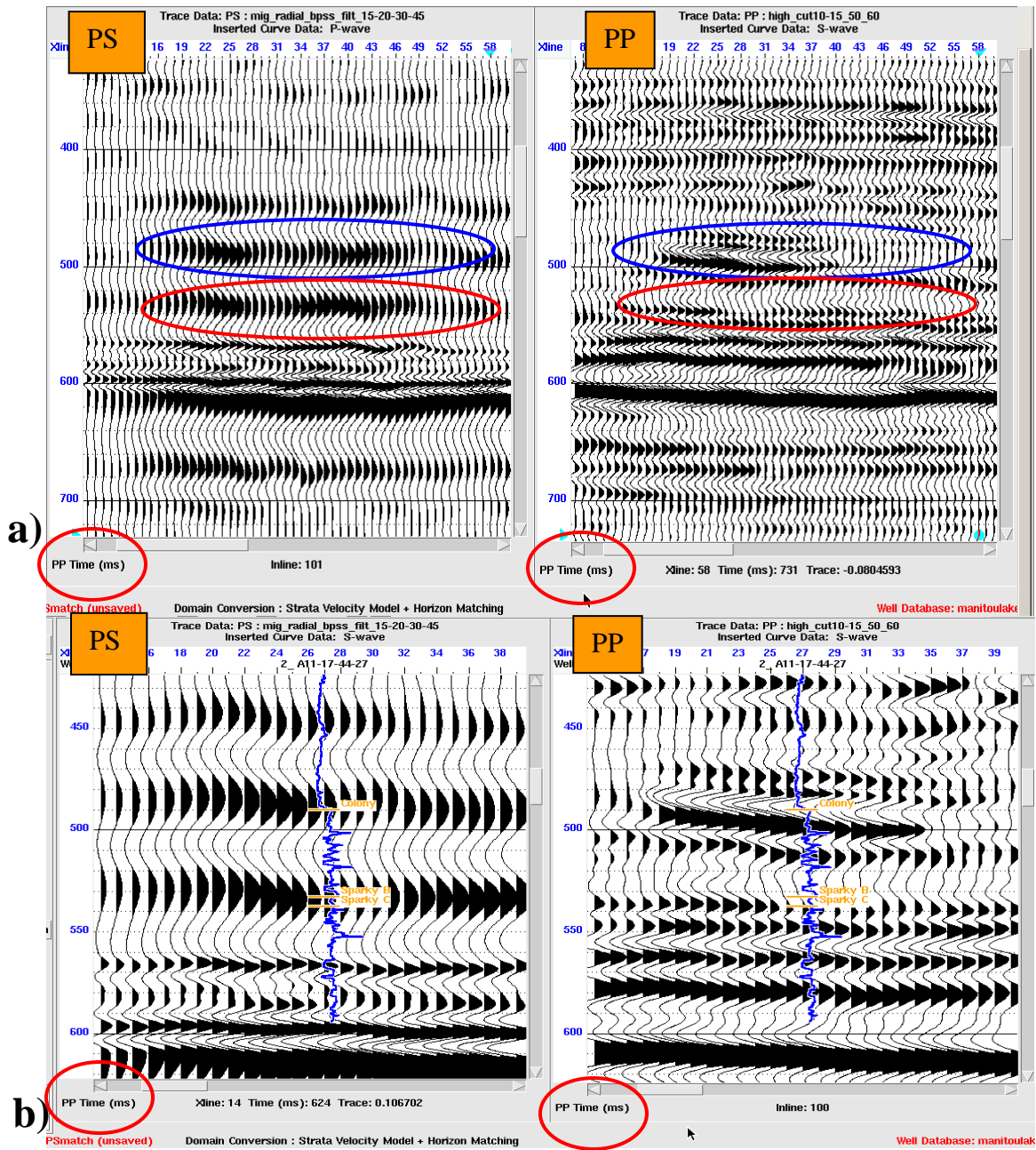


Figure 3.17: Inline 100: PS migrated and filtered 15-20-30-45 (left) and PP section high cut filtered 10-15-50-60 (right) stretched in PP time at well A11-17 location a) unzoomed (above) and b) zoomed (below) after registration (domain conversion – Strata velocity model, plus horizons matching applied). Circled in a) the sand channels on both, PP and PS datasets: Colony is in blue and Sparky in red colors.

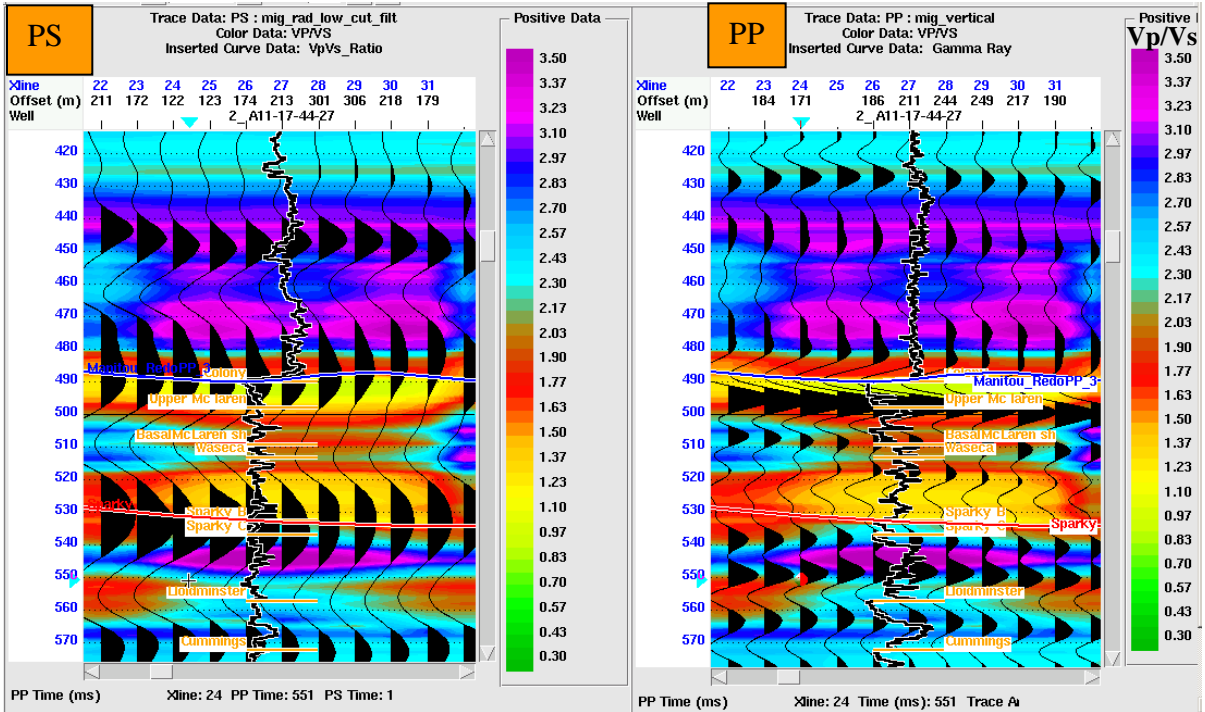


Figure 3.18: Well A11-17: Registration and horizon matching. On left we have the PS data and on right the PP data, both stretched in PP time. In colors, the sand channels are delineated by the  $V_p/V_s$  values calculated from time thickness (using wells for domain conversion).

migration, both stretched in PP time. The Colony PP-PS horizon after horizon matching is shown in blue, and the Sparky horizon in red. The sand channels are delineated by the  $V_p/V_s$  values calculated from time thickness. Closer inspection shows that values less than 2.15 delineate the sand channels.

Figure 3.19 shows the zoomed vertical migrated stack at the location of well A11-17. Gas, oil and water are shown in white arrows, and correspond to the marked zones, as in Figure 3.8 a): gas sands have  $V_p/V_s$  values up to 1.5; oil sands show values from 1.5 to 2.15, and brine filled sands have values higher than 2.15.

Figure 3.20 shows the zoomed vertical migrated stack at the C10-17 well location. Colour data shows  $V_p/V_s$  values. The inserted curve is the Gamma Ray log, indicating low values at the sand channel levels.

After registration, time structure maps were created at the Colony and Sparky horizons, as in Figure 3.21. Note the higher time trend from west to east and from south to north on

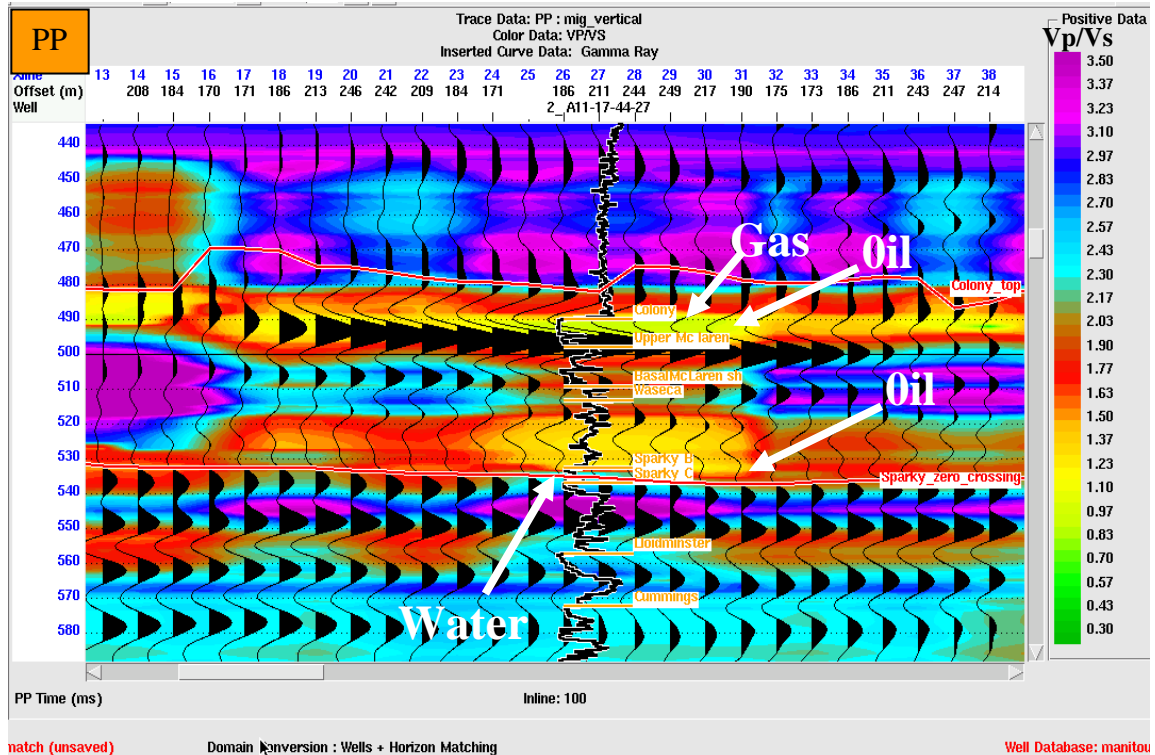


Figure 3.19: Well A11-17: Zoomed image of the PP migrated stack after the registration using horizon match (Hampson – Russell software). Colors show Vp/Vs from time thicknesses after horizon matching: oil is shown by a ratio value less than 2.15 and gas shows values less than 1.50. Inserted, is the GR in black colour.

both horizons, in blue. Lower time values in red to green, may suggest differential channel compaction. The channels may be delineated by different attributes, such as curvature.

An isochron map (calculate the time interval between two horizons) was created in Figure 3.22, showing the thicker time intervals in blue, up to 72 ms between the two horizons, compared with the red/yellow colors with values up to 50 ms. The larger values likely indicate lesser compaction of the sands in the channels. This leads to the idea that

under-compacted sand channels have a greater porosity and are possibly better performing reservoirs.

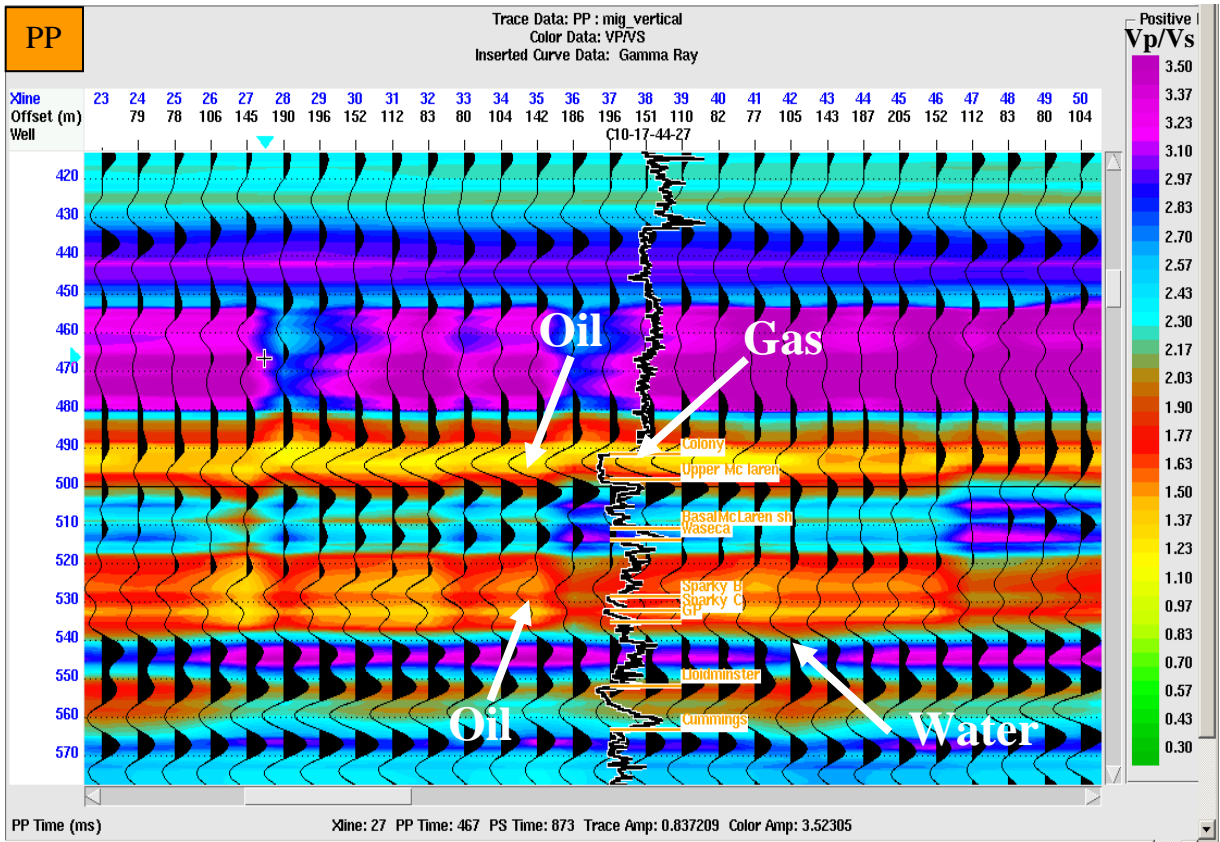


Figure 3.20: Well C10-17: Zoomed image of the PP migrated stack after the registration using horizon match in Hampson – Russell software.

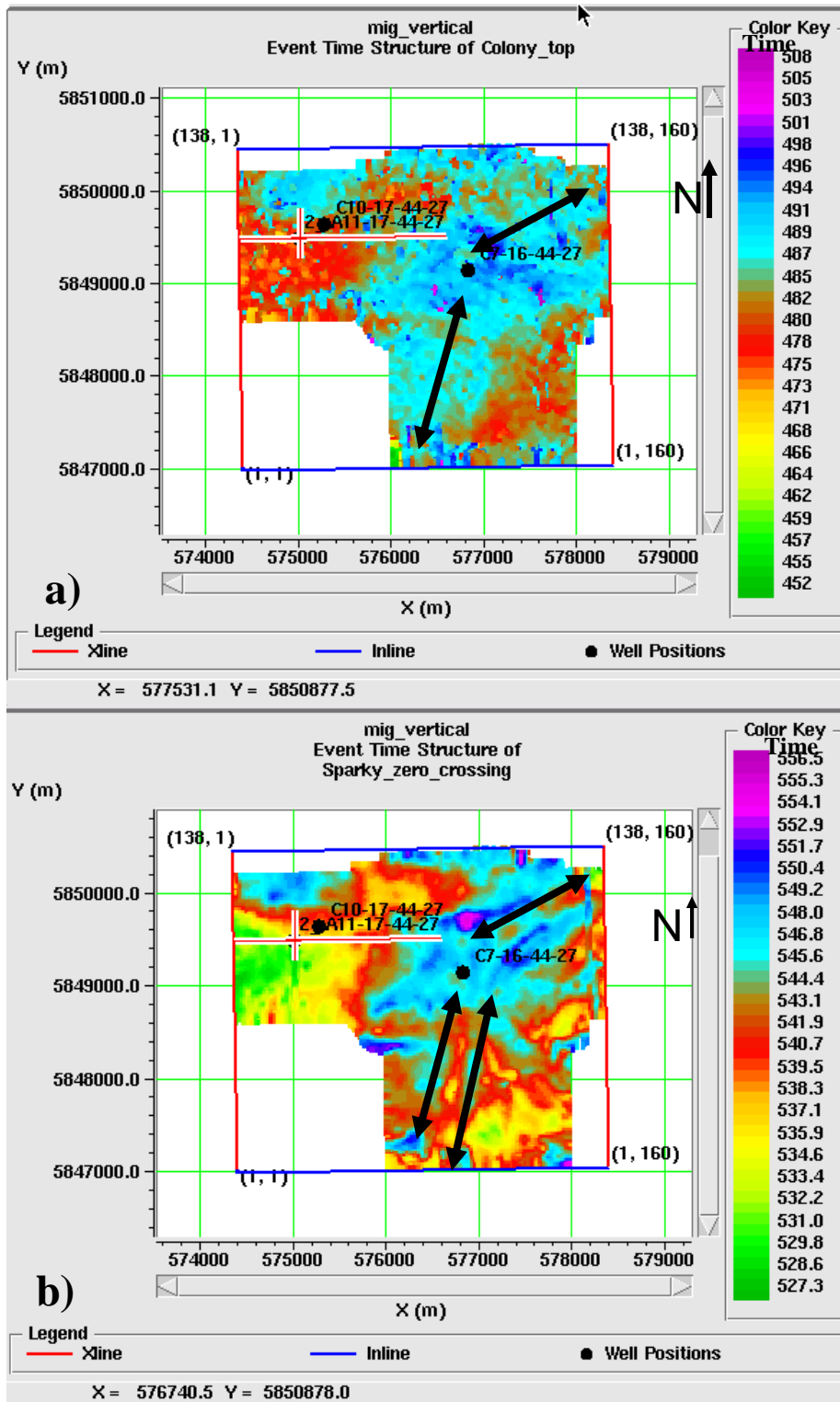


Figure 3.21: Time structure maps on the registered horizons in PP time: a) Colony and b) Sparky. Both sand channels show higher values towards NE-SW; the possibly uncompacted sand channels are in blue and cyan.

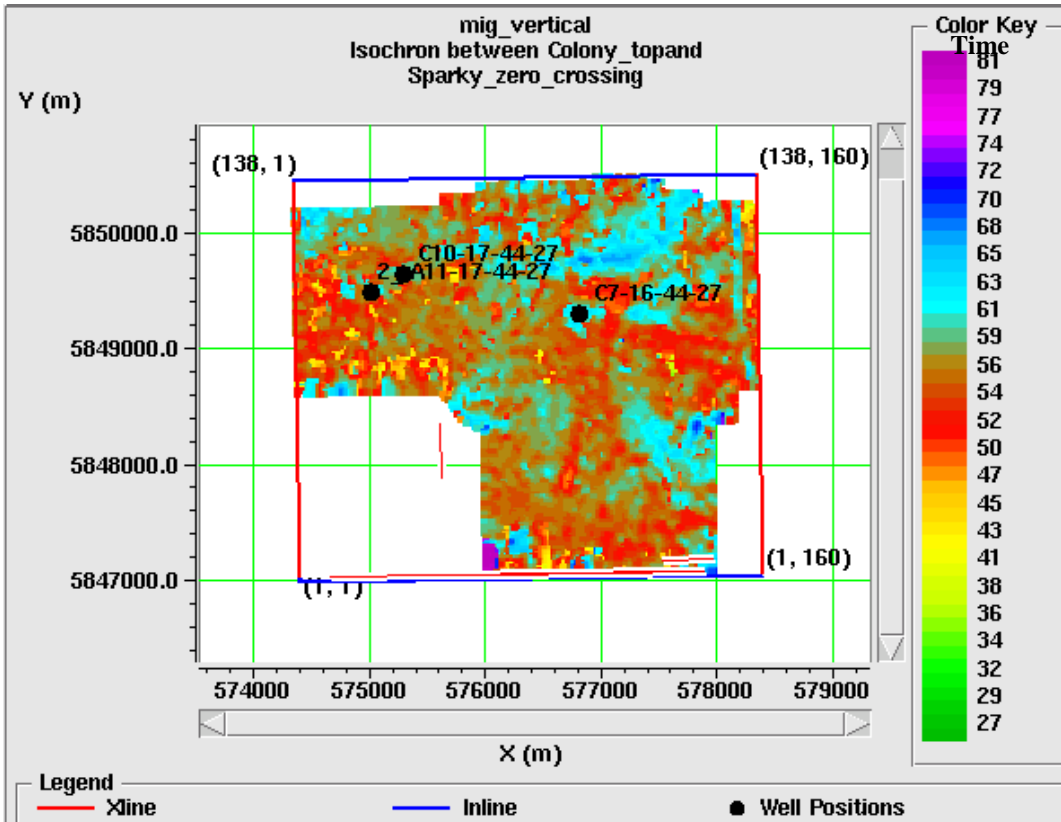


Figure 3.22: Isochron map between Colony and Sparky, on PP migration in PP time (after registration). Note thickness values in blue, up to 72 ms. A possibly higher compaction of the sand channels is shown in red/yellow colors, comparing with the blue colors who suggests less compaction.

The data were loaded in both Hampson – Russell and Transform software, where registration was again performed. Figure 3.23 shows the unregistered PP-PS display, and Figure 3.24 shows the registration using the amplitude envelope. The amplitude envelope is a useful seismic attribute for removing phase effects, reducing frequency effects, and highlighting high and low energy zones. Matching reflection energy “packets” provides a base methodology for multicomponent registration (Roth, 2006). Amplitude envelope can isolate amplitude information and discard the phase problem of correlating two datasets that have different phase properties. A time and spatially-variant registration (“gamma”) has been performed.

The energy packages are shown as in Figure 3.24; from left to right they are in order: the work space stretch, the QC with gamma function applied, and third, the QC plot for a sparse gamma grid. Colors show the co-rendering of different adjustments. Figure 3.25 shows the Vp/Vs (gamma) adjustment. Residual Gamma adjustment can be performed to take account of phase problems. In the present case, it was not necessary to perform a phase adjustment. The objective of registration preparation is to enhance the geology-driven features that will guide the registration process, such as boosting the frequency content in both PP and PS data. This can help amplify the event character, even as reflection continuity is reduced.

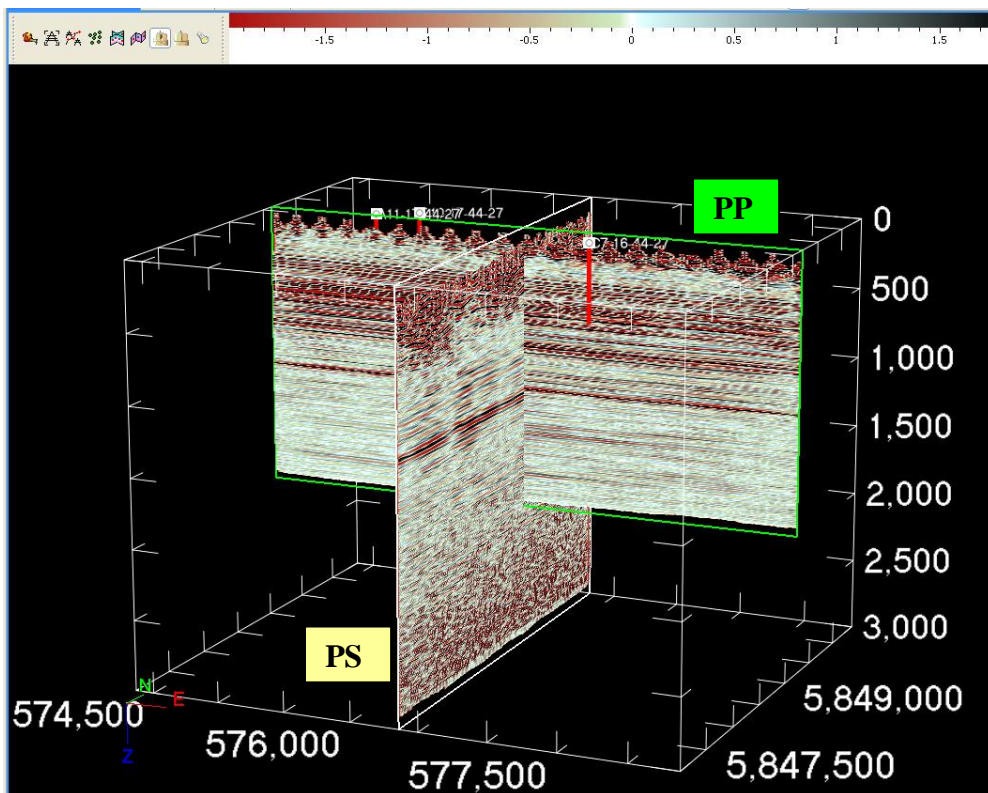


Figure 3.23: Unregistered PP-PS display in Transform software. The PP data is shorter than PS data and shows a higher frequency content.

After registration, new volumes were created for the PS data with the gamma function applied. PP and PS attributes such as amplitude envelope coherency, curvature and

inversions were created. The sand channels were better imaged as shown in the next two chapters.

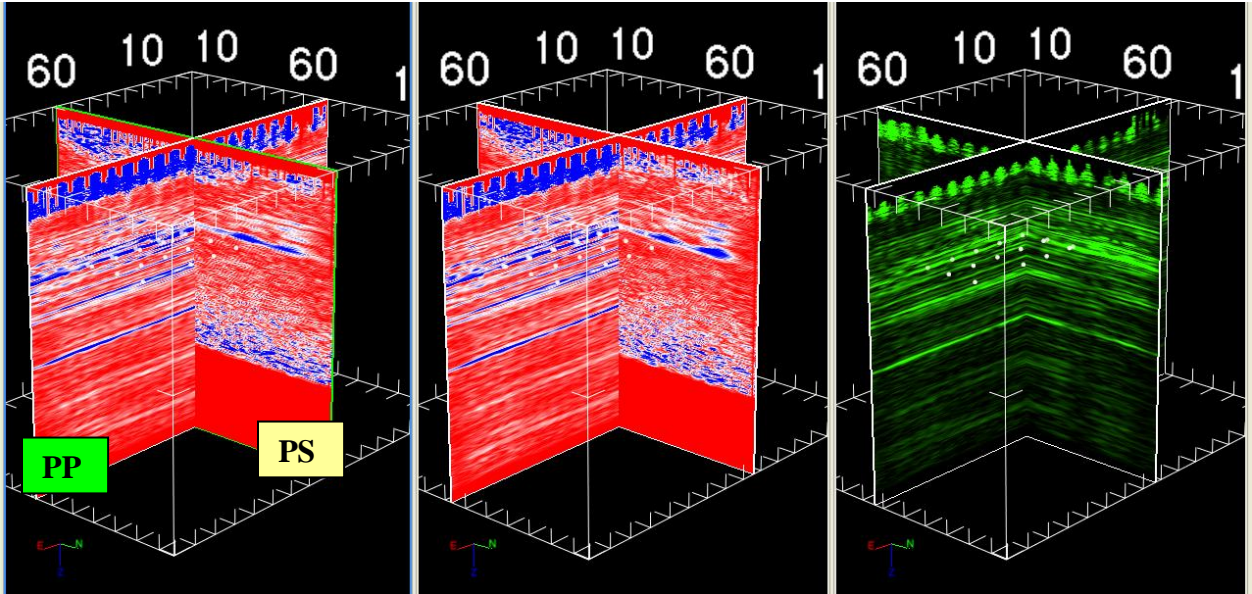


Figure 3.24: Registration using amplitude envelope in Transform software.

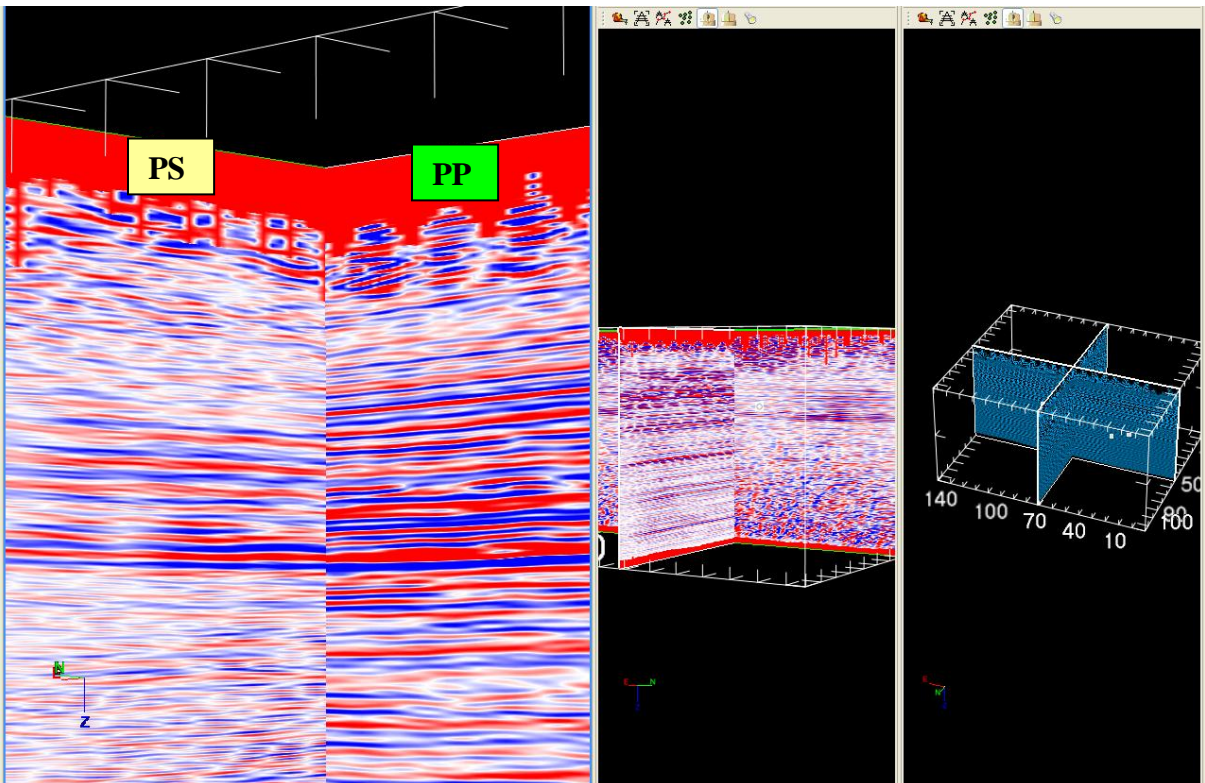


Figure 3.25: Registered PP and PS data showing the gamma adjustment (residual), in Transform software.

## CHAPTER 4 – ATTRIBUTES AT MANITOU LAKE

Seismic attributes are measurements derived from seismic data, usually based on measurements of time, amplitude, frequency and/or attenuation. Generally, time-based measurements relate to structure, amplitude-based ones to stratigraphy and reservoir characterization, and frequency-based ones to stratigraphy and reservoir characterization (Sheriff, 2006). Marfurt, 2008, states that a simple working definition for a seismic attribute is any measure of seismic data that helps to better visualize or quantify features of interest in interpretation.

### 4.1 PP AND PS AMPLITUDE MAPS

After the registration in Transform software, volumes with PP and PS data were created with a gamma function applied. Figure 4.1 shows PP time slices at the Sparky and Colony levels. Figure 4.2 shows the PS amplitude envelope on both horizons: this attribute does not help us in better delineating the channels due to the low frequency

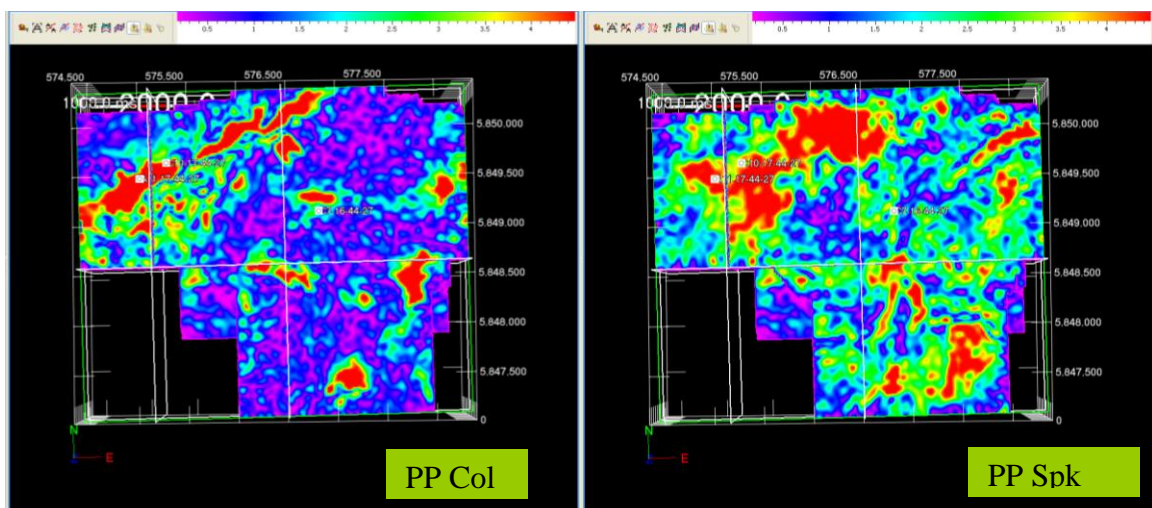


Figure 4.1: PP Colony (left) and Sparky (right) time slices. Red colors show high amplitudes.

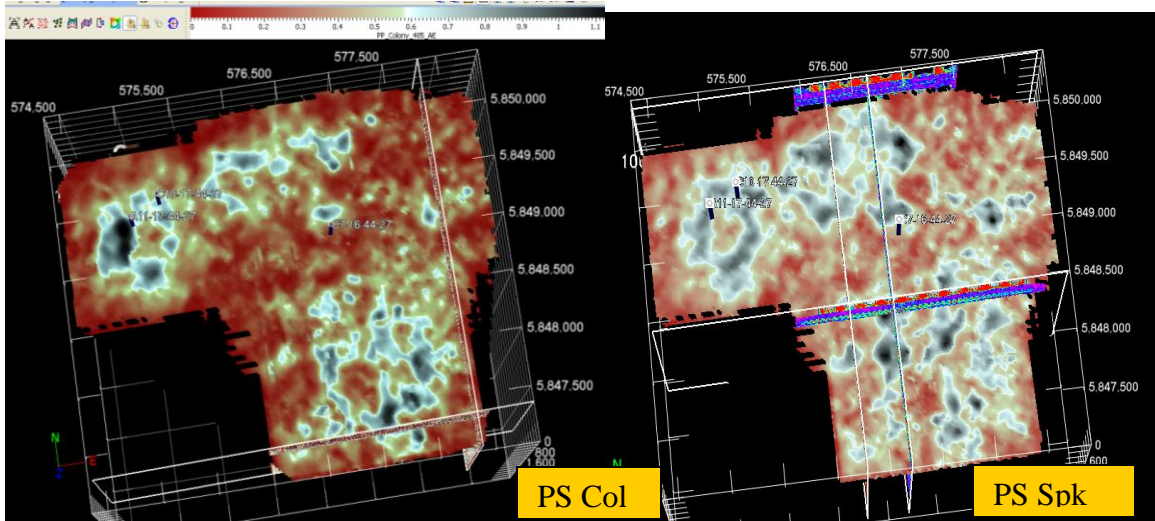


Figure 4.2: Left: PS Colony and right: Sparky amplitude envelope. Darker grey shows higher amplitudes.

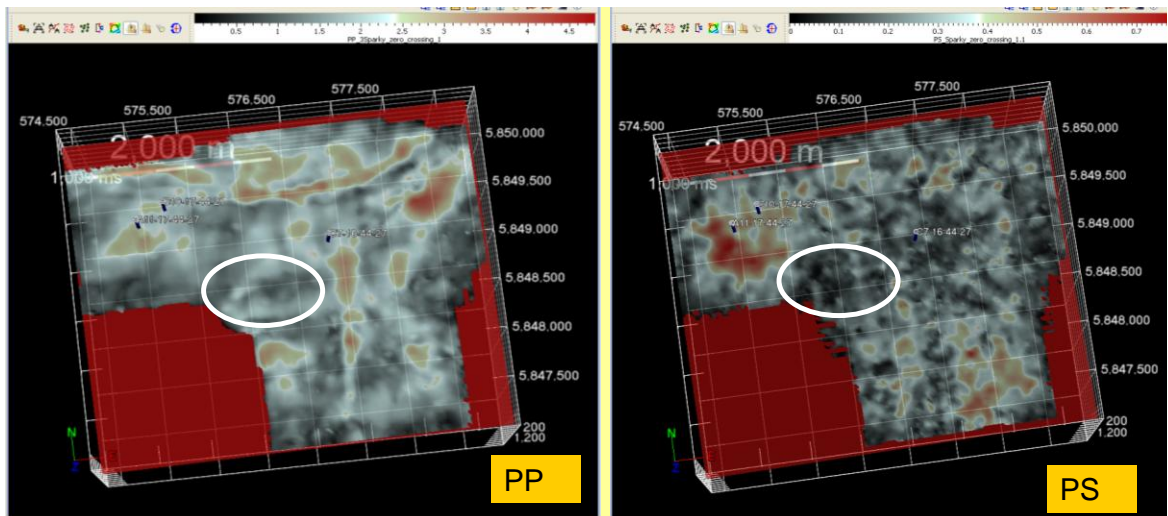


Figure 4.3: PP (left) and PS (right) amplitudes on the Sparky horizon. Red colours shows high amplitudes.

content of PS data. In Figure 4.3 compare the PP (left) and PS (right) amplitudes at the Sparky horizon. The useful information that PS data can provide at this stage is the fact that in the circled zone of interest, since high amplitudes do not show, drilling a new well is of questionable use. This leads to an investigation of whether the combination of amplitudes with other attributes will help in recognizing geologic features.

## 4.2 AMPLITUDE ENVELOPE AND CURVATURE

How can derived seismic attributes help in recognizing geologic features? According to Marfurt, 2008, coherence can help to localize lateral changes in waveform and amplitude, and curvature can help to see the localized, lateral changes in dip. Broader, lateral changes in amplitudes can be seen by RMS amplitudes, impedance inversion, or AVO analysis. Coherency can give more information about channel edge detection. Figure 4.4 shows how a sand channel can be detected with seismic attributes, according to its geologic features. The channel model in this case is considered as in Figure 4.5, showing differential compaction, plus dip and amplitude changes.

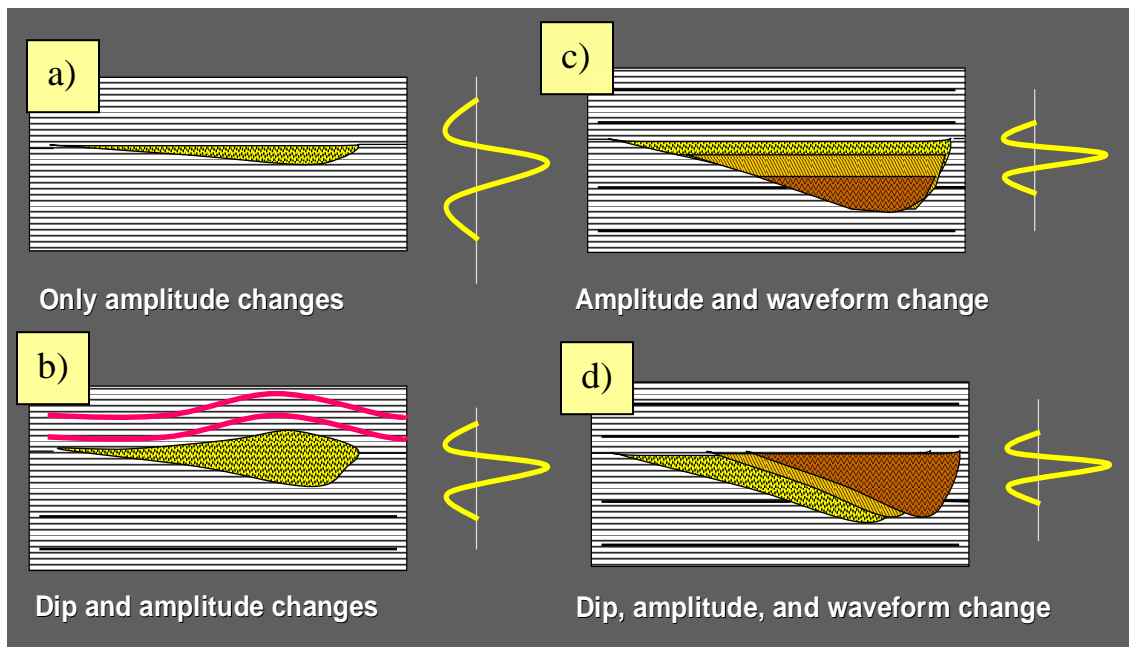


Figure 4.4: Detection of channels with seismic attributes. Attribute response to channel features preserved in the geologic record: (a) below thin-bed tuning, with homogeneous fill and no differential compaction; only the amplitude changes; (b) below thin-bed tuning, with homogeneous fill and differential compaction. Curvature and amplitude change; waveform does not change; (c) above thin-bed tuning, with heterogeneous horizontal fill and no differential compaction. Curvature does not change; amplitude and waveform do change; (d) above thin-bed tuning, with heterogeneous aggradational fill. Curvature, amplitude, and waveform all change (after K. Marfurt, 2008).

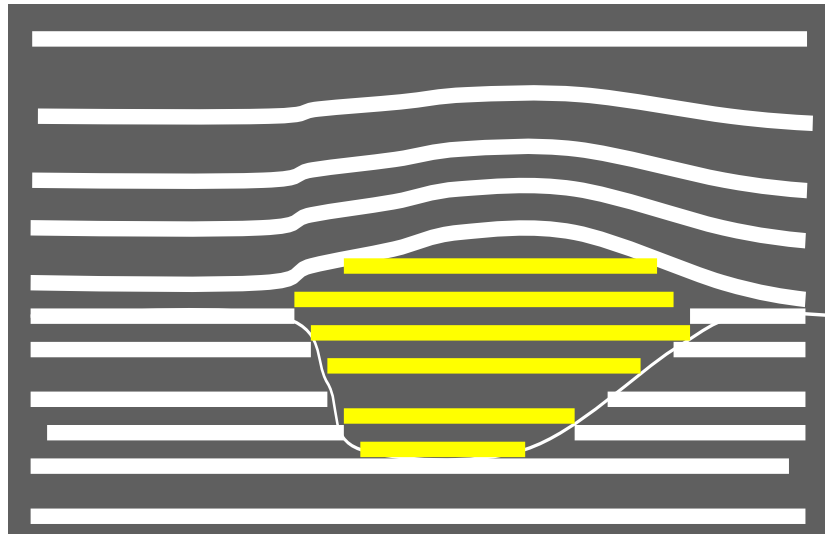


Figure 4.5: The sensitivity of curvature attributes to channels. Unless there is differential compaction, channels are not usually seen on curvature volumes (modified after K. Marfurt, 2008)

The channel features will be seen by the curvature attribute. However, since volumetric curvature calculations are performed on time slices rather than on picked horizons, channels that have little differential compaction or internal dip, experience no lateral change in dip, and thus will not be seen by curvature (Marfurt, 2008).

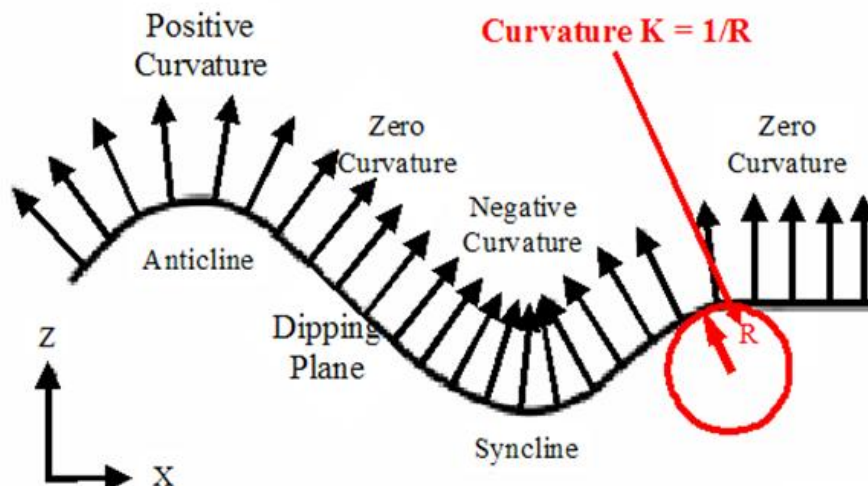


Figure 4.6: Sign convention for 3D curvature attributes: synclinal features have negative curvature, anticlinal features have positive curvature, and planar features have zero curvature (after Roberts, 2001).

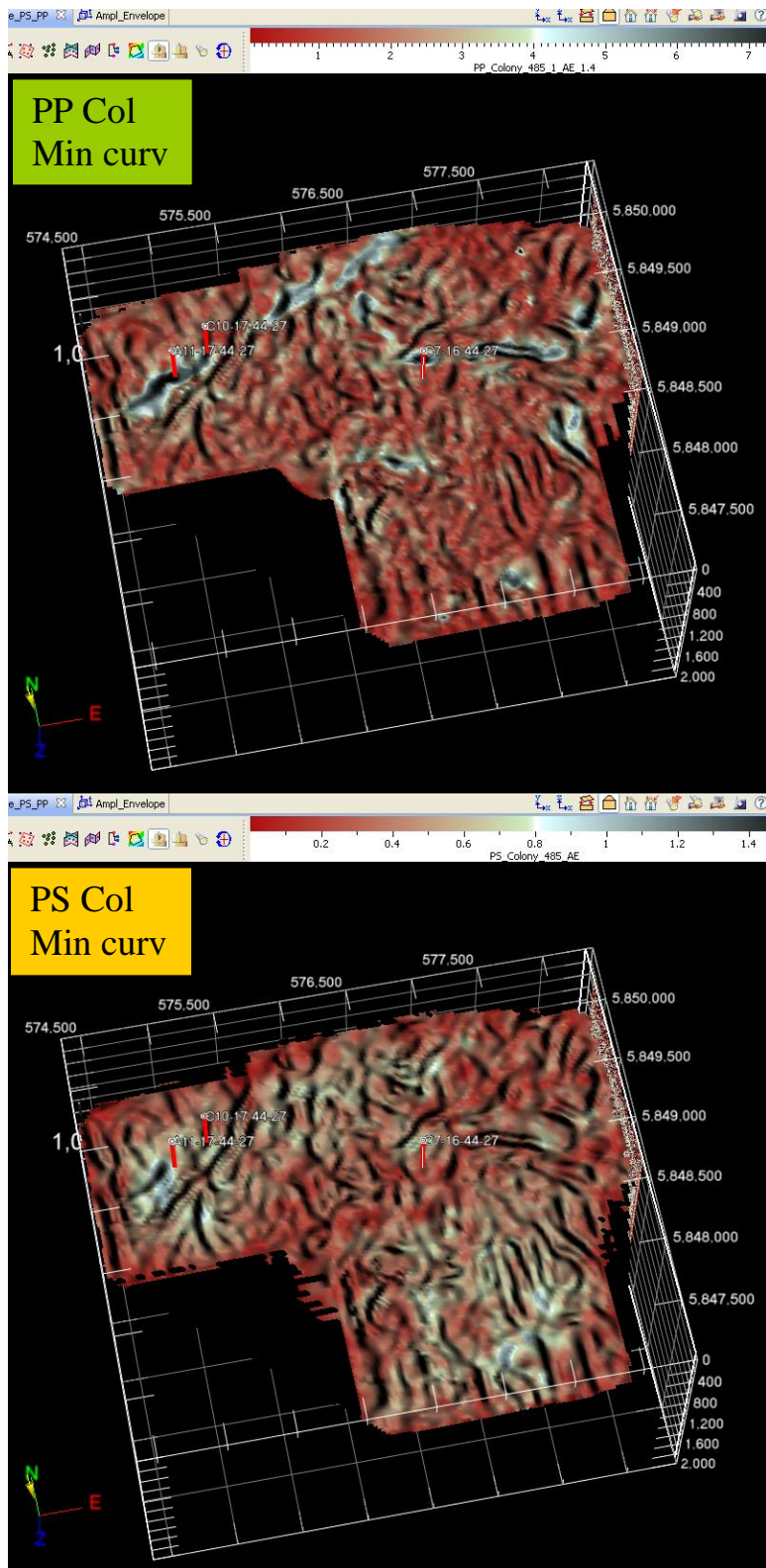


Figure 4.7: a) PP (top) and PS (bottom) amplitude envelope at the Colony co-rendered with the PP minimum negative curvature (bump-map). The darker channel features show the curvature, and the white-grey colour indicates higher amplitudes (Transform software).

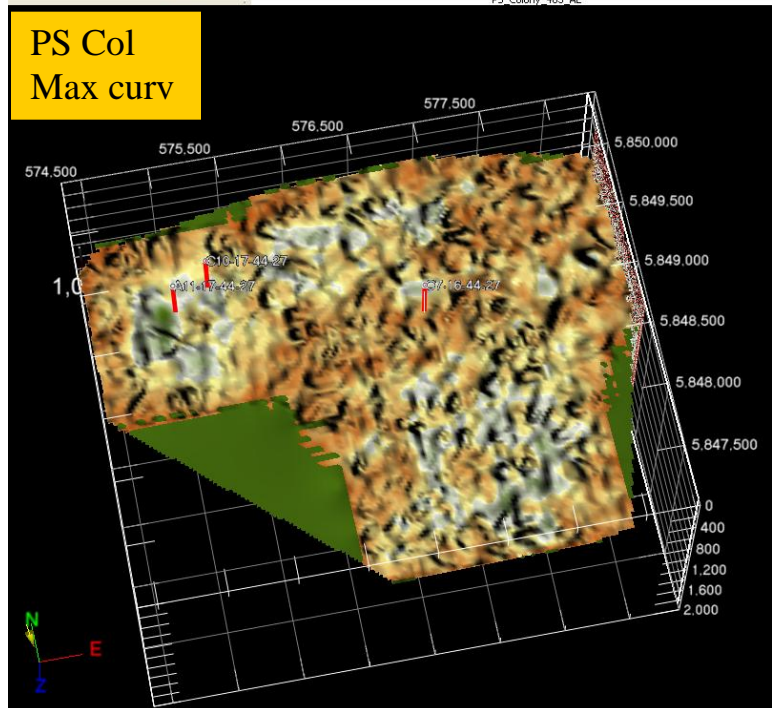
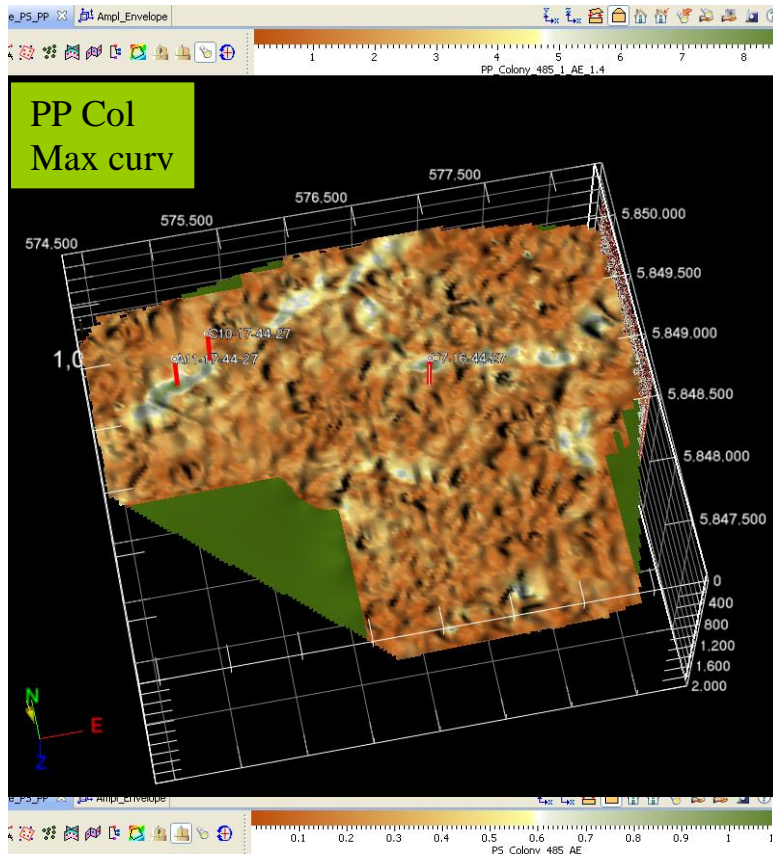


Figure 4.8: a) PP (top) and PS (bottom) amplitude envelope at the Colony co-rendered with the PP maximum positive curvature (bump-map). The darker channel features show the curvature, and the grey-green colour indicates higher amplitudes (Transform software).

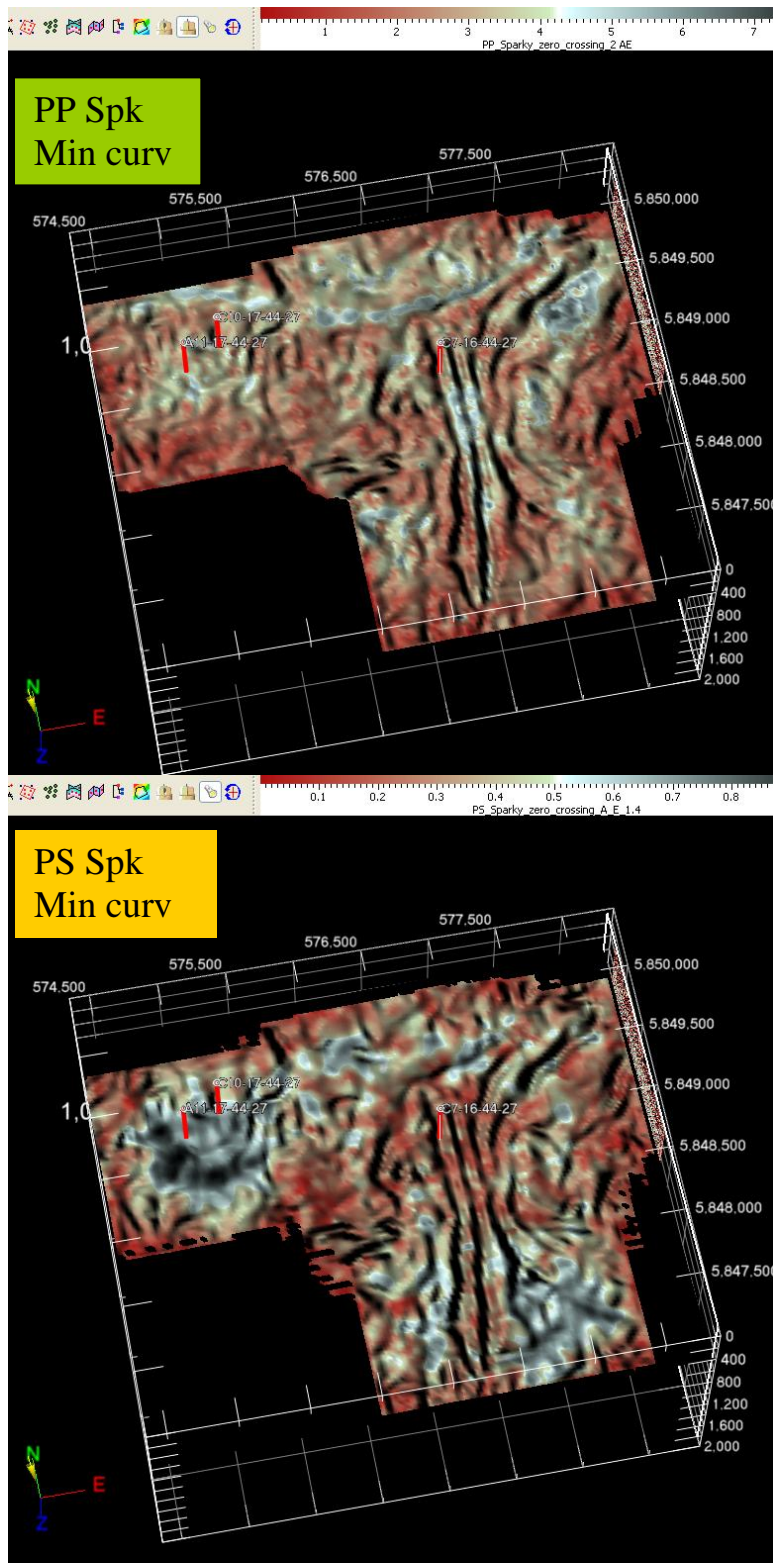


Figure 4.7: b) PP (top) and PS (bottom) amplitude envelope at the Sparky co-rendered with the PP minimum negative curvature (bump-map). The darker channel features show the curvature, and the white-grey colour indicates higher amplitudes (Transform software).

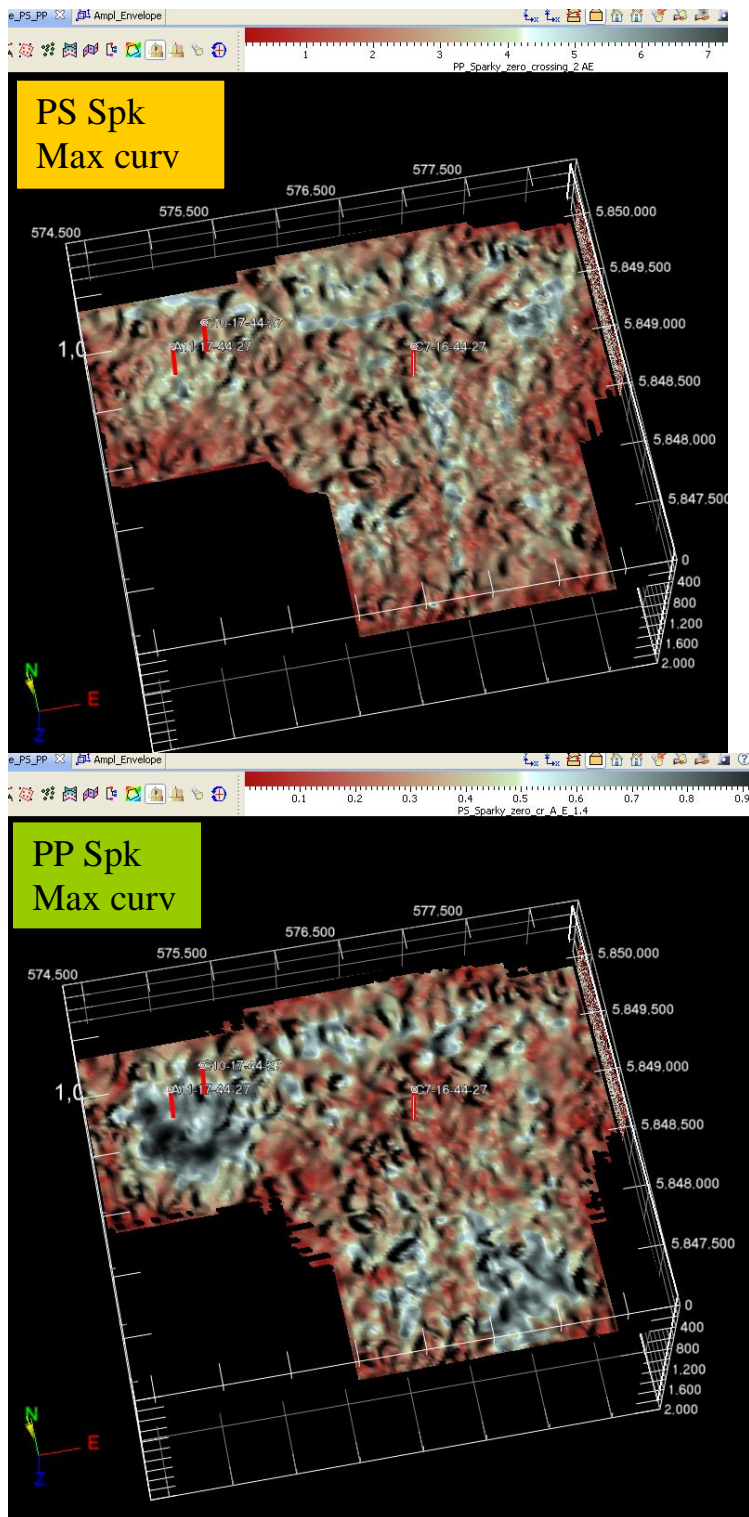


Figure 4.8: b) PP (top) and PS (bottom) amplitude envelope at the Sparky co-rendered with the PP maximum positive curvature (bump-map). The darker channel features show the curvature, and the grey-green colour indicates higher amplitudes (Transform software).

The amplitude envelope is used to calculate instantaneous amplitude characteristics, and is used to highlight the dominant energy pockets in the data. It is appropriate for identifying major amplitude anomalies. The combination of two attributes, performed with Transform software: the amplitude envelope and the most positive and negative curvature as in Figures 4.6 and 4.7 a) and b), show different aspects at the top and base of the channels. The “illumination” feature was used on both Figures, to add a third dimension to the view.

Figure 4.7 a) shows different aspects of the base of the Colony channel for PP and PS amplitudes respectively, whereas Figure 4.7 b) shows the top of the Colony sands. PS data show more information about the top and base of the channel, correlating nicely with the curvature features. The same clear result can be seen in Figure 4.7 and 4.8 b) at the Sparky level. The curvature attributes indicate a better focussing of the base (most negative) and the edges of the channels (most positive).

Sand-shale boundaries may produce poor P-wave velocity contrasts, and in the present case the PS converted mode enables the reservoir boundaries to be delineated. PS amplitude anomalies seen in Figures 4.7b) and 4.8b) show the top of the sands / reservoir, which could not be seen seismically on the PP amplitude map. This idea is based on the fact that Vs show an increase on logs, while Vp has almost no change at the top of the reservoir. This behavior is probably caused by the decreasing bulk density and bulk modulus in the hydrocarbon filled sands, while the rigidity remains basically the same when passing from shales to sands:

$$V_p = \sqrt{\frac{\lambda + 2\mu}{\rho}}, \quad V_s = \sqrt{\frac{\mu}{\rho}} \quad (5.0)$$

where  $\lambda$  is the incompressibility,  $\mu$  is the rigidity and  $\rho$  is the density;  $V_p$  and  $V_s$  are P-wave velocity and respectively S-wave velocity.

The PS-wave data indicated that the shape of the sand can be different than originally thought, and a new mapping of the reservoir was achieved.

Shear propagation is not disturbed by gas: if P-wave sections show amplitude anomalies (bright spot) as seen in Figures 3.17 and 3.19, then the S-wave section should not show those anomalies and are typically dim (Nahm, 2003, Garotta, 2005). If the amplitude anomalies appear in both P and S-wave modes, then this is caused by lithology, and not by gas saturation (Garotta, 2005). This is another important application of PS-waves for Class II and Class III, bright spot validation. Concluding, the created maps can show the prospective gas accumulation in this area: a bright spot on the P-wave and a respectively dimming observed on S-waves may be a criterion for distinguishing gas sand reflectors versus “false” bright spots.

### **4.3 CURVATURE, COHERENCE, AND RECURSIVE INVERSION**

An interactive registration based on the gamma function (related to P and S velocity ratios) was performed in Transform software after horizons were re-picked. The intention behind this registration was to focus on high and low energy zones using the amplitude envelope. Spectral enhancement was performed before applying the post stack recursive inversion, as in Figure 4.9 top: a zero phase deconvolution and a median filter were applied for spectral enhancement.

After registration, the Colony and Sparky PS and PP amplitude map were showing better results than the previous interpretation. Higher amplitudes indicate the sand channels as in figure 4.9. A better delineation of the sand channel at the Colony (left) and at the Sparky level (right) is available from the co-rendered curvature of the PP and PS picked horizons. The zone circled in white shows the place where the previous drilling location did not encounter the reservoir. The “dry hole” was drilled based only on conventional PP seismic data interpretation. Zero phase deconvolution helped to increase the high frequency data content.

Figure 4.10 shows a combination of attributes: curvature co-rendered with recursive inversion for the PP data (left), and the recursive inversion co-rendered with the amplitude envelope for the PS data (right) at the Colony channel. The recursive inversion performed in Transform software integrates the seismic data to approximate band-limited impedance and can be used as a gross porosity and fluid indicator. White ellipses indicate the same missed drilled location. The same warning arises from these attributes: no fluid indication or porosity is shown in this area. For increased confidence, one can look at the previous Figures, 4.7 and 4.8, and compare the results: the zone of interest does not show any indication of gas or fluid.

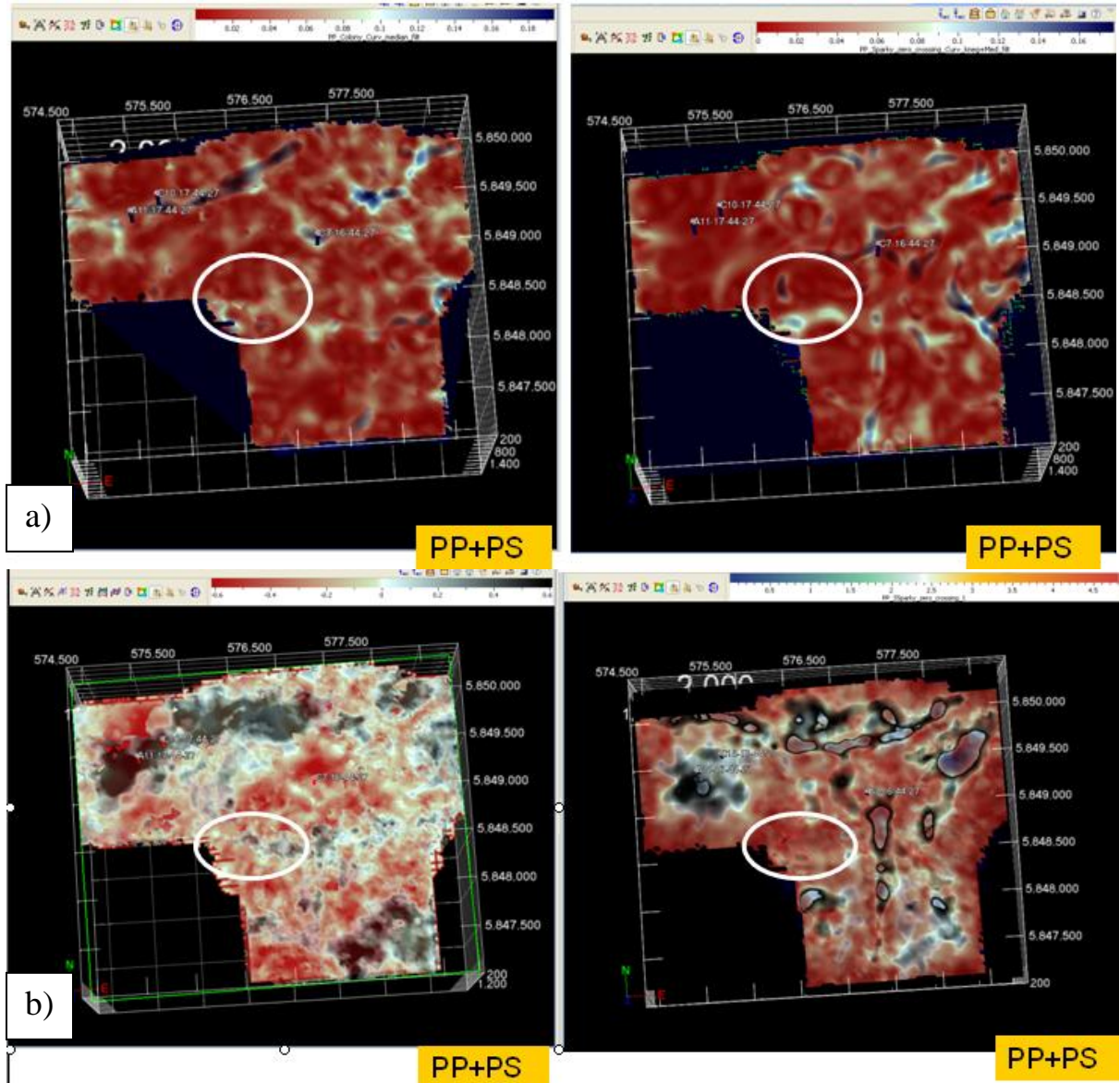


Figure 4.9: Left: the Colony and right: Sparky horizons in Transform software.  
 a) PP+ PS Curvature is co-rendered for PP and PS data at the Colony (left) and Sparky (right) interpreted horizons.  
 b) PP+PS recursive inversions co-rendered for PP and PS data in Transform software after applying a zero phase decon and a median filter for spectral enhancement: Colony is on the left side and Sparky on the right.

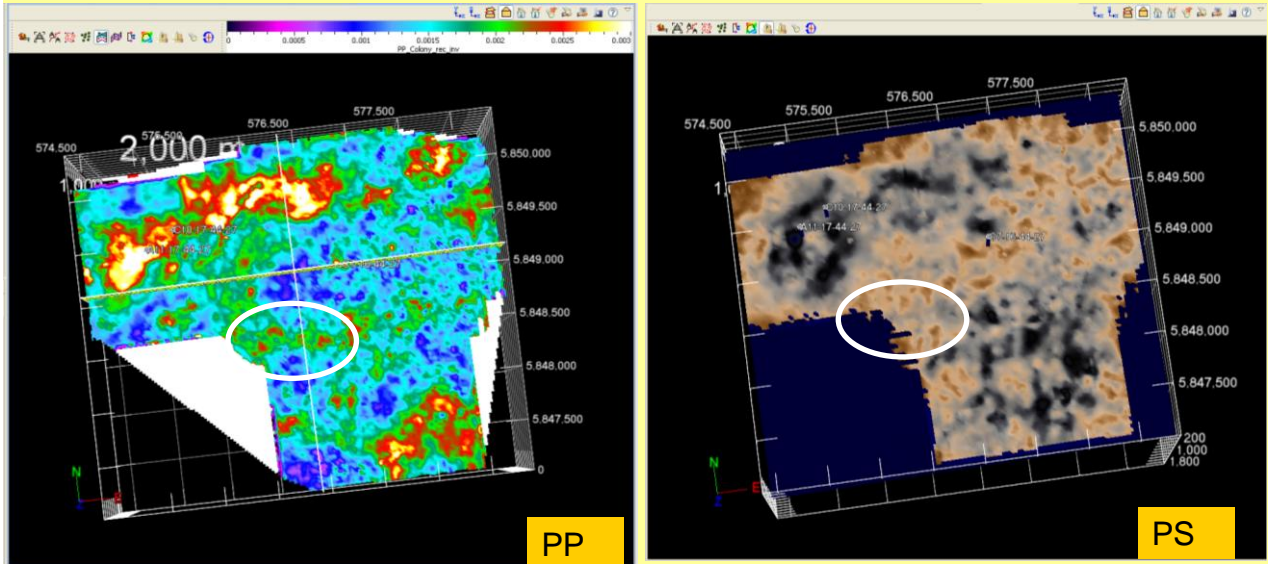


Figure 4.10: Left: PP, data and right: PS data at the Colony horizon showing the amplitude envelope co-rendered with the recursive inversion. Zero phase deconvolution was used to increase the high frequency content of the data.

The coherence attribute in Transform software creates a volume that highlights discontinuities and shows sensitivity to the lateral changes of the data. Coherence can be computed from both the original seismic data and from the relative acoustic impedance. Since impedance inversion acts as a filter, we can see less incoherent noise and a sharper delineation of edges (Suarez et al., 2008).

The maximum curvature co-rendered with incoherence on recursive inversion as in Figures 4.11 and 4.12 can show differential compaction of the channels, with a better edge delineation. Figure 4.13 shows the result of recursive inversions on PP data co-rendered with the curvature (above) and recursive inversions on PP co-rendered with PS data (below) at the Colony horizon. Yellow-brown (above) and blue-purple (below) colors indicate the fluid/porosity zones.

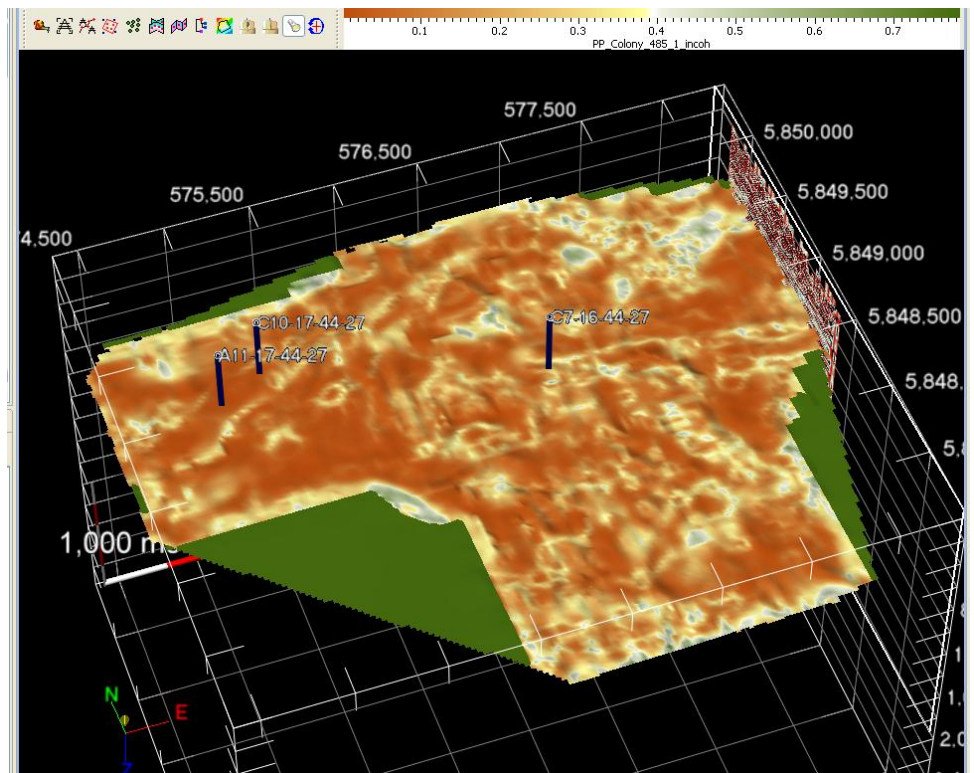
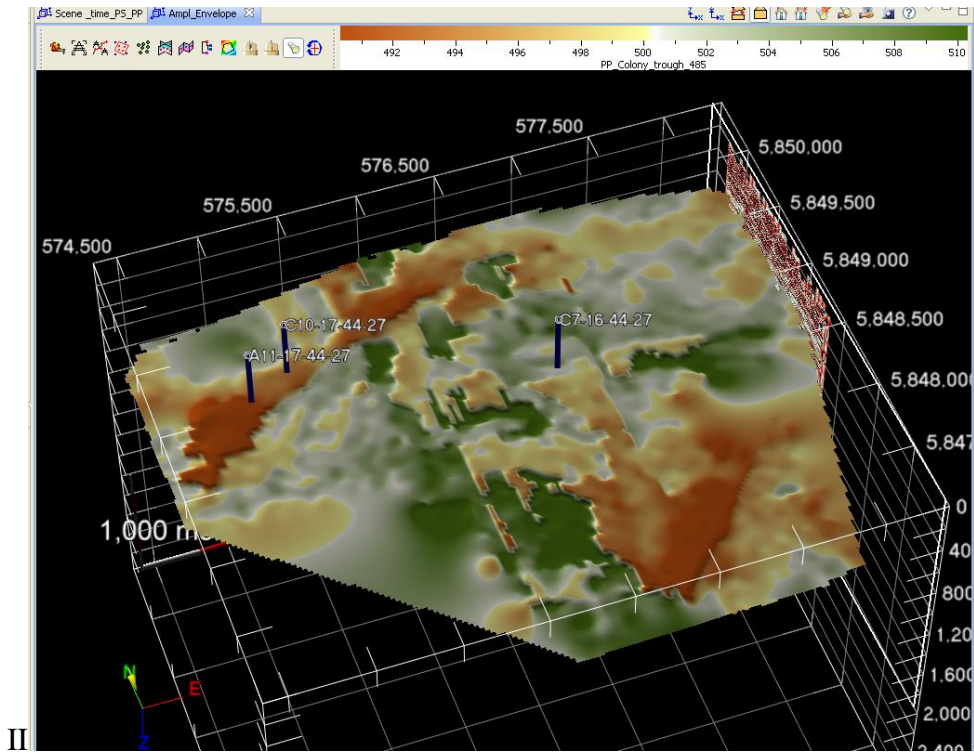


Figure 4.11: Top: Colony horizon on PP data (high brown, low green); bottom: incoherence on recursive inversion at the Colony horizon co-rendered with the maximum curvature (bump-map shadows) and illumination applied.

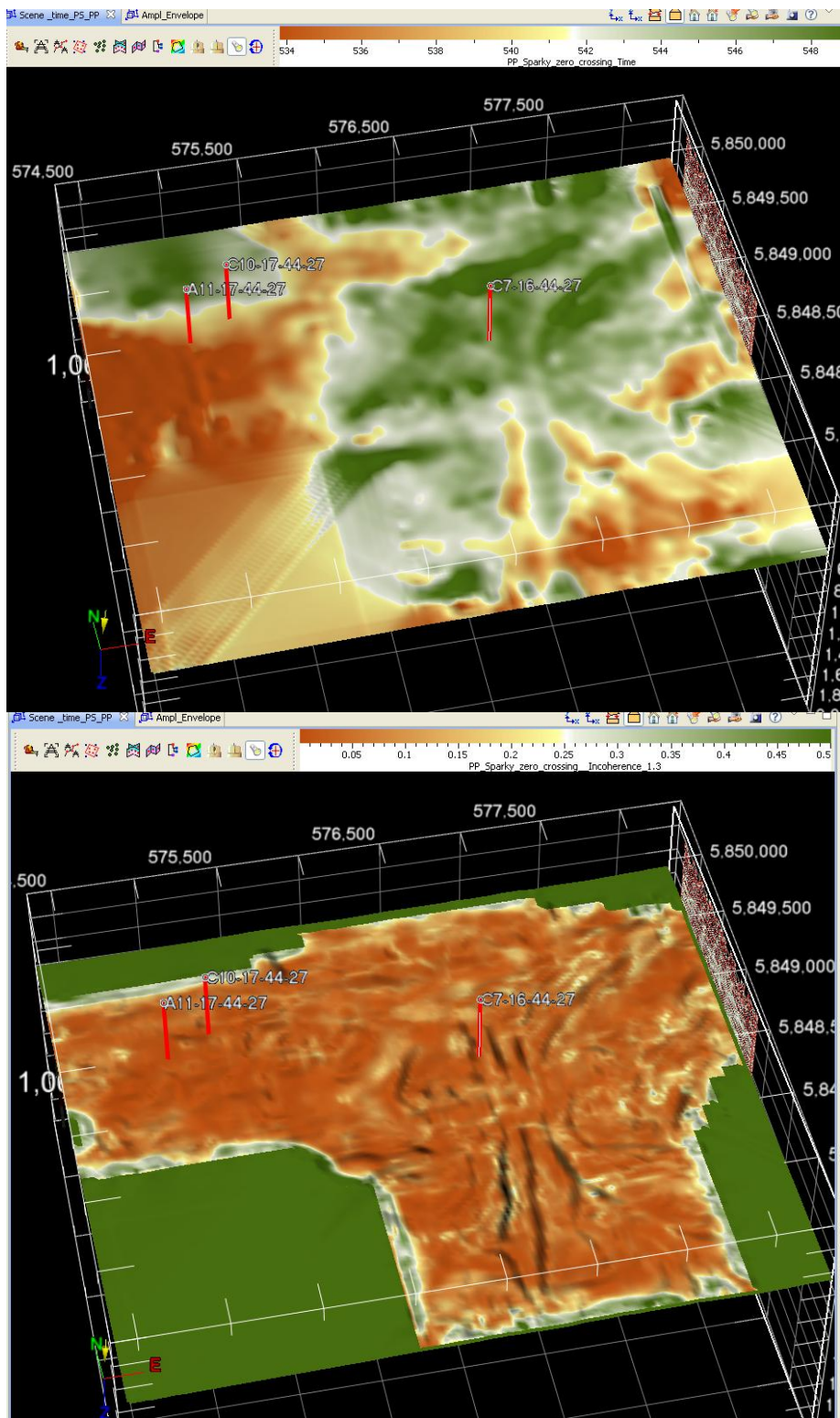


Figure 4.12: Top: Sparky horizon on PP data (high brown, low green); bottom: incoherence on recursive inversion at the Sparky horizon co-rendered with the maximum curvature (bump-map shadows) and illumination applied.

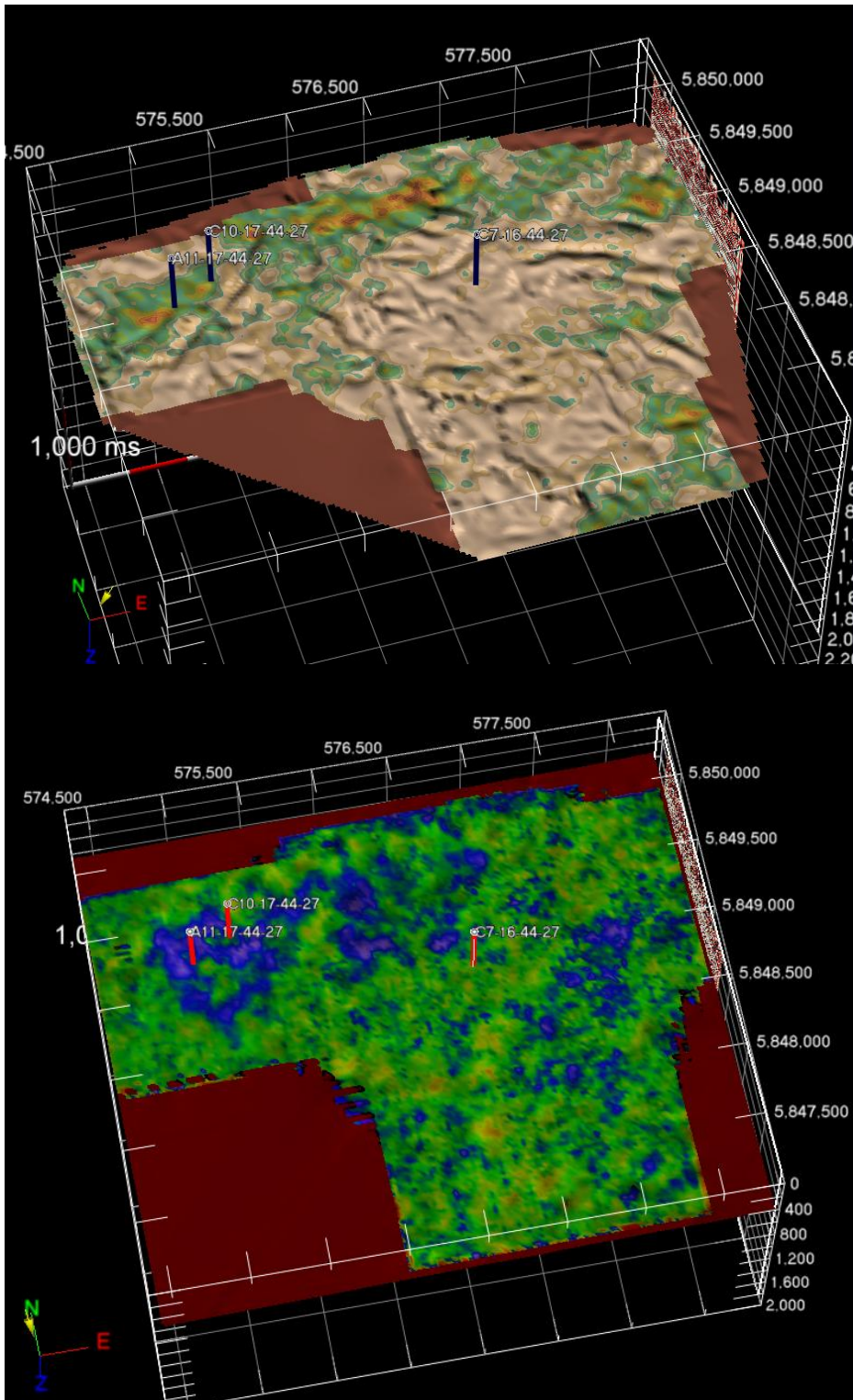


Figure 4.13: Top: Colony horizon on PP data: PP maximum positive curvature co-rendered with PP recursive inversion; bottom: PP and PS recursive inversions co-rendered at the Colony horizon.

The result is consistent with the previous attributes, giving confidence in the improved interpretation of the drilled location. PS data add more confidence showing that only well A11-17 should be mainly producing from the Colony horizon, as has been seen in the production chapter of this thesis; the zone of interest shows a light-yellow colour and gives a indication that there is no reservoir at that specific location.

#### 4.4 PP AND PS AMPLITUDE MAPS AND VP/Vs MAPS

In Figures 4.14 and 4.15, PS amplitude maps (Hampson - Russell) help to better understand the lack of success at the drilling location. PP amplitude maps can be compared with the maps generated from the PS amplitude. The black arrows show the unsuccessful drilling location, based previously only on PP amplitude maps.

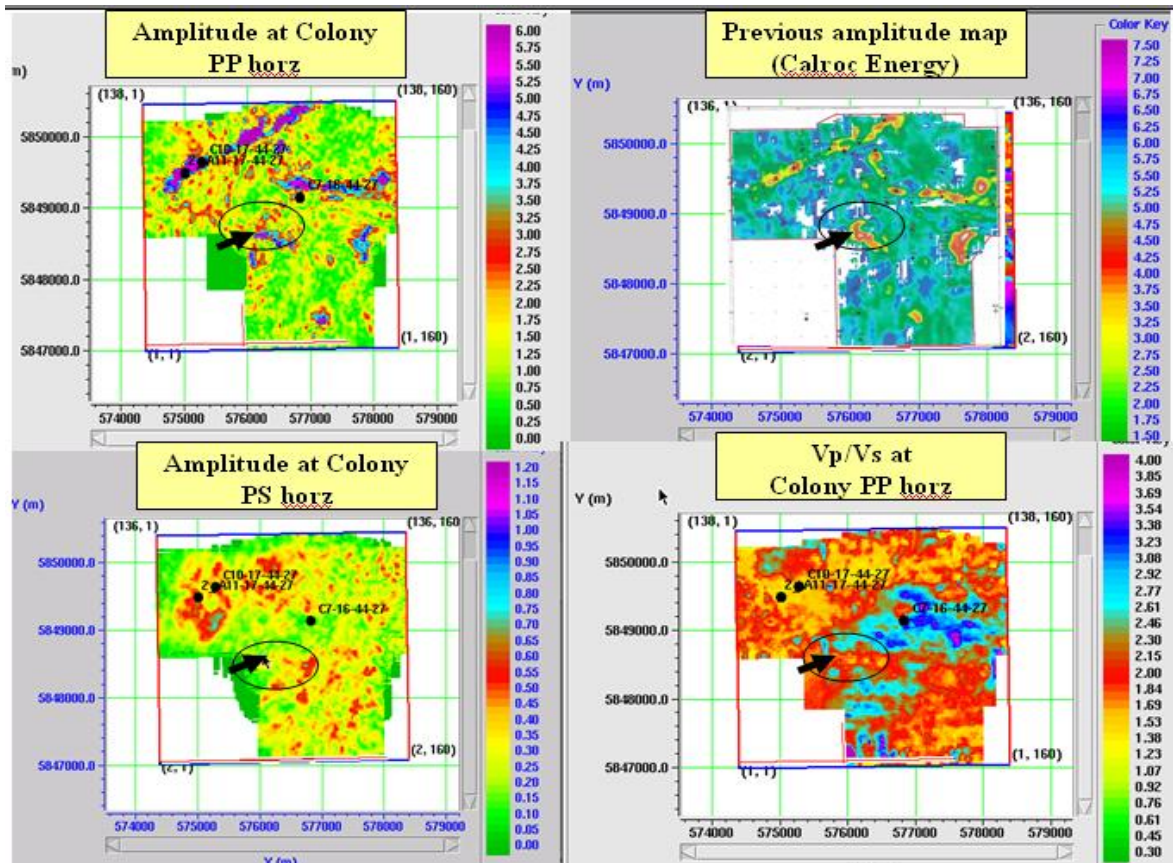


Figure 4.14: PP and PS amplitude maps (left) for the Colony channels are compared with the previous (right above) PP interpretation. Vp/Vs map of the registered PP data is on the right (below) side of the picture. Black arrows and black ellipses show a previous unsuccessfully drilled location.

The PS amplitude show low values in green at the drilling location. The PP Vp/Vs map after the registration shows low values (less than 2.2) at the location; high ratios indicate (Figure 4.14) a low probability to encounter the reservoir. Due to the low frequency

content of PS data, the channel delineation is poor compared with delineation afforded by PP data, but the frequency content is sufficient to provide useful information about rock properties and the reservoir.

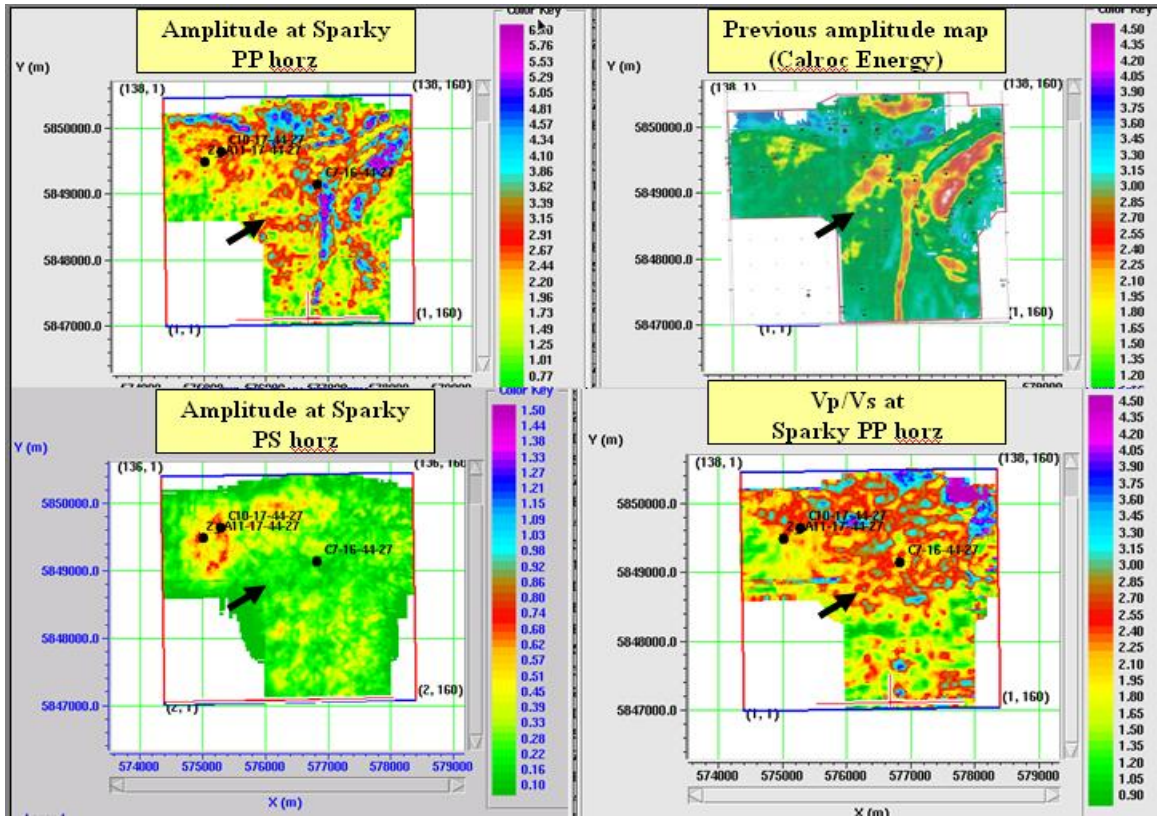


Figure 4.15: PP and PS amplitude maps (left) for the Sparky sand channels are compared with the previous (right above) PP interpretation. Vp/Vs map of the registered PP and PS data is on the right (below) side of the picture. Black arrows show a previously unsuccessfully drilled location.

As seen in Figures 4.7 a) and b), PS data correlates better with the top and bottom of the reservoirs. PS amplitude maps combined with Vp/Vs maps are useful in reservoir delineation.

## **CHAPTER 5 - AVO ANALYSIS AT MANITOU LAKE**

AVO or “Amplitude Variation with Offset” and refers to the changes of amplitudes with an increasing offset. Pre-stack seismic data will be analyzed (PP gathers) to identify anomalies, and to try to determine the fluid content of the rocks. The processing flow for CDP gathers included true amplitude recovery, elevation statics and refraction statics, surface consistent deconvolution, front end muting, velocity analysis, residual surface consistent statics, normal moveout, and trim statics. Then PP-AVO analysis was performed on the processed gathers of PP-seismic data, using Hampson - Russell’s AVO software. The PP-AVO attributes were inverted to derive information on rock properties, such as reservoir rigidity and incompressibility (LMR).

### **5.1 AVO SIMULTANEOUS INVERSION**

Upon completion of the PS processing, well log correlations were performed in PS-time in the PS-migrated stack in order to pick geologic events corresponding to those picked on the PP-migrated stack. This is a critical phase in the process as this can reveal the AVO expression of key events; for example, a peak on the PP-section does not necessarily correspond to a peak on the converted wave section. These horizons were used to register the post-stack PS data against PP-time. The horizons were used along with the PP-velocity model in the use of PP-AVO to perform PS-AVO extraction. PP gathers were used for this step, as shown in Figure 5.1. Attributes resulting from this analysis include P-impedance reflectivity ( $Z_p$ ), S-impedance reflectivity ( $Z_s$ ), and density reflectivity (Hampson et al., 2006). The purpose of simultaneous inversion is to invert

pre-stack CDP gathers (PP and optionally PS angle gathers) to determine the compression impedance, shear impedance, and density. Post-stack inversion ignores the fact that, in wet clastic rocks,  $Z_p$  and  $Z_s$  should be related.  $V_p$  and  $V_s$  should be linearly related (as shown from Castagna's equation) when there are no complicating factors, such as the presence of hydrocarbons. Also, density should relate to  $V_p$  through some form of Gardner's equation. Therefore, simultaneous or joint inversion would include some form of coupling between the variables. This should add stability to a problem that is sensitive to noise and usually produces non-unique solutions. It is called simultaneous inversion because two or more lithologic volumes are created simultaneously (Hampson et al., 2006).

The fully NMO-corrected CDP gathers should be brought into super-gathers to enhance the S/N ratio. Residual NMO or Trim statics are helpful to align the events, with amplitude balancing. Since pre-stack inversion operates in the incident angle domain a conversion from offset to angle is required, creating angle-gathers (Figure 5.2). A sonic log from the database was used to create a velocity field. The useful angles range up to  $30^\circ$ . A near angle gather ( $0-15^\circ$ ) and a far angle gather ( $15^\circ-30^\circ$ ) were extracted from seismic. An angle gather model P-impedance is created. The complete model consists of three volumes, including the S-impedance and density. First, the seismic data is trained at well locations to derive log properties. Then, the training results are validated before being applied to the full seismic volume (Hampson et al. 2006).

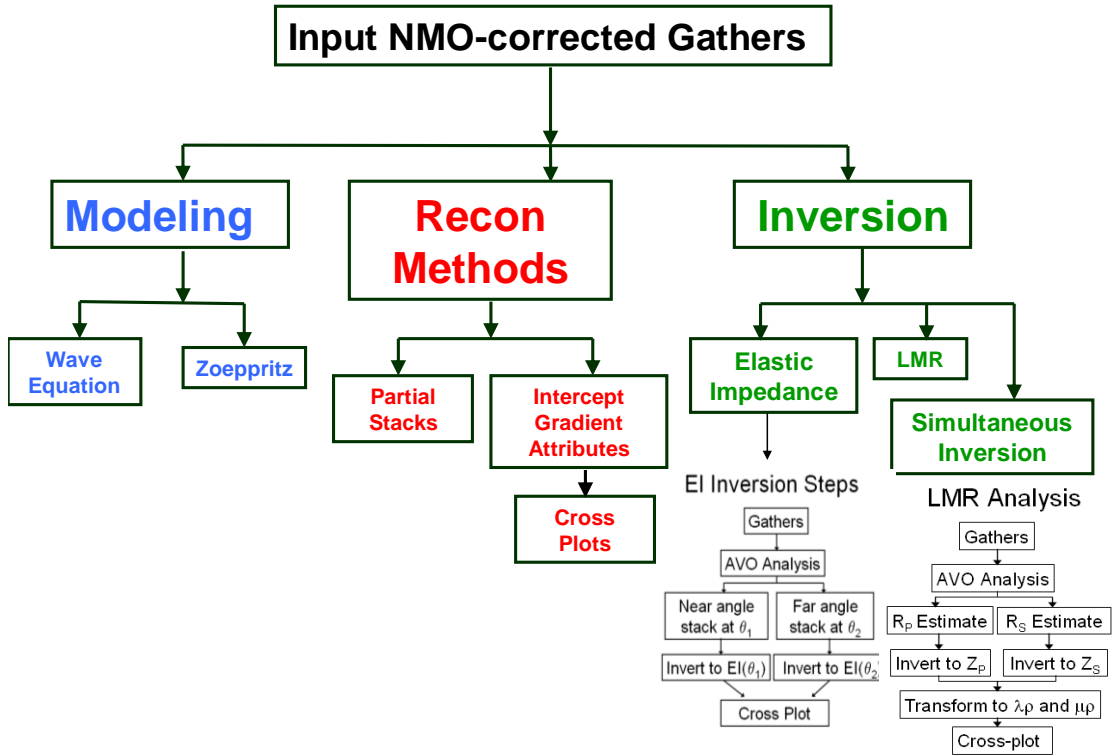


Figure 5.1: Summary of AVO Methodology, (Modified after Hampson-Russell, 2007)

After the reflectivity estimates,  $R_p$  and  $R_s$ ,  $Z_p$  volumes (P-impedance) and  $Z_s$  volumes (S-impedance) were created. Figure 5.3 shows the ratio of  $Z_p$  to  $Z_s$  on the Sparky (right) and Colony (left) sand channels. Both pictures show high  $Z_p/Z_s$  values, around 2.5 and up at the missed drilled location (black arrows). This suggested it might be worthwhile to see if the post-stack joint inversion (ProMC package) can give a better result.

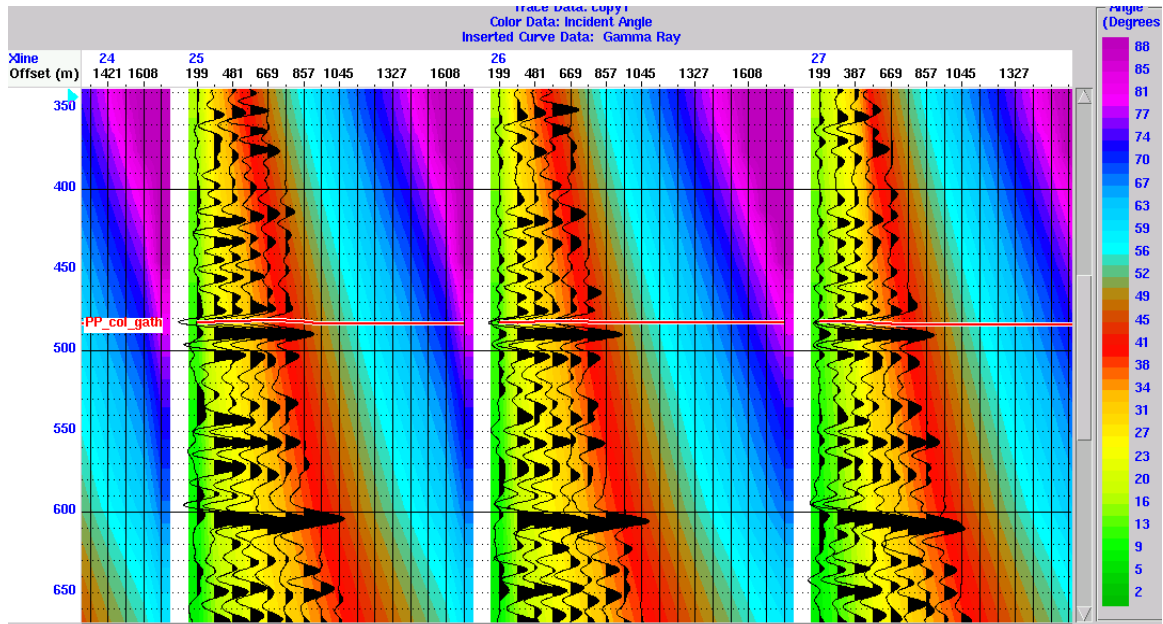


Figure 5.2: PP- gathers used in the prestack AVO inversion. Incident angles are shown in colours: maximum angle is up to 45°.

Figure 5.4 shows that a  $Z_p$  (P impedance) versus  $V_p/V_s$  crossplot at the Colony sand channel can be a good gas indicator. The crossplot shows a strong separation between the background trend and the hydrocarbon zone. The circled zone (in blue) cannot give sufficient information about the missed drilling location. Figure 5.5 shows a lithology differentiation at well C7-16. The sand channels (in yellow) are clearly differentiated: this well is producing mainly from the Sparky horizon.

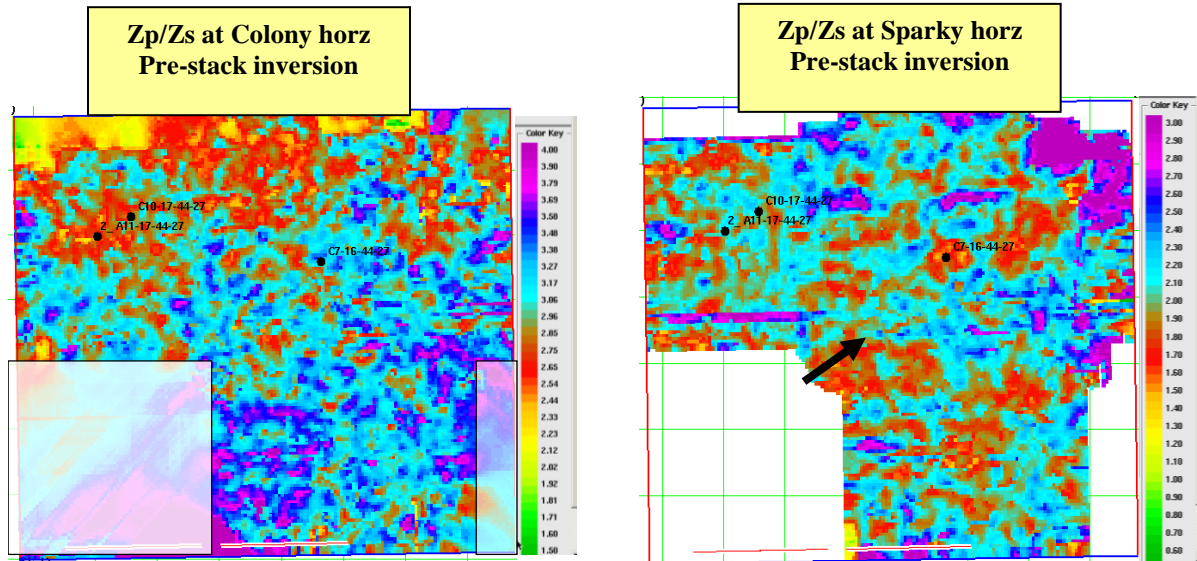


Figure 5.3: The ratio of  $Z_p/Z_s$  at the Colony sand channel (left) and Sparky (right) after AVO prestack inversion. High values of the ratio are in blue. Red and yellow colors show low values of the ratio.

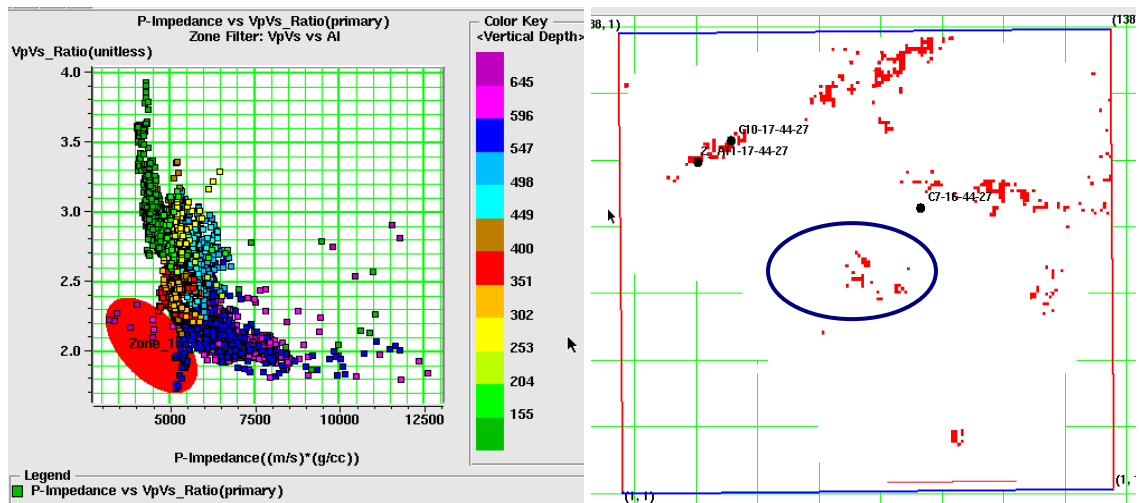


Figure 5.4: After the simultaneous inversion:  $Z_p$  (P impedance) versus  $V_p/V_s$  crossplot at the Colony sand channel (left) and the Colony map (left). The strong separation between the background trend and the hydrocarbon zone is shown in red. This result can be an indicator for porosity/gas. The right map shows RMS amplitudes for zone 1 (probably gas indicator).

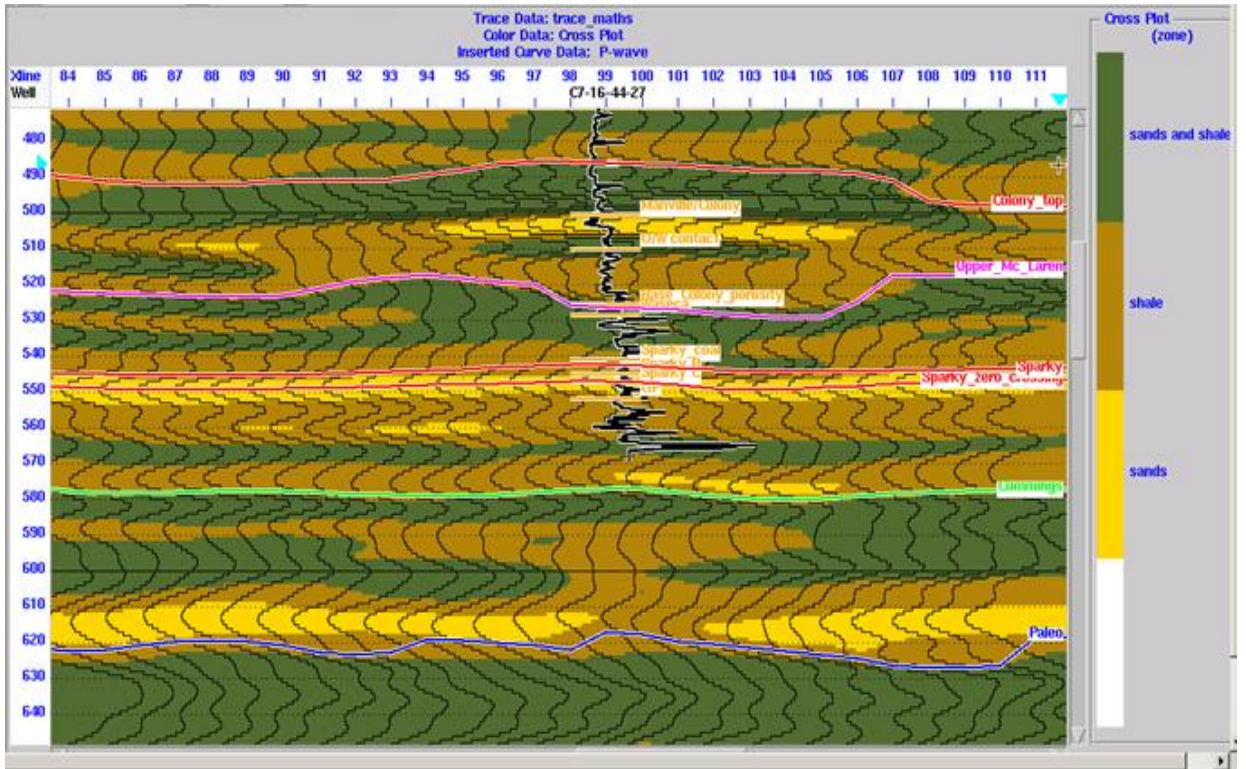


Figure 5.5: Lithology differentiation for  $Z_p/Z_s$  after the simultaneous inversion at the well C7-16 location; inserted is the P-wave, olive= sands + shales, brown = shale, yellow = sands.

## 5.2 AVO ATTRIBUTES

Attribute analysis may often reveal subtle features. It measures and plots specific seismic attributes to see what they show, often revealing AVO anomalies. Using AVO attributes, either the zero-offset and gradient component of the amplitude or the zero-offset P-wave and S-wave reflection coefficients can be determined at each time sample. These results are derived from two formulations of the Aki-Richards approximation to the Zoeppritz equations. Formula (5.1) shows Fatti's version for the Aki-Richards equation (5.2):

$$R_{pp}(\theta) = c_1 R_p + c_2 R_s + c_3 R_D \quad (5.1)$$

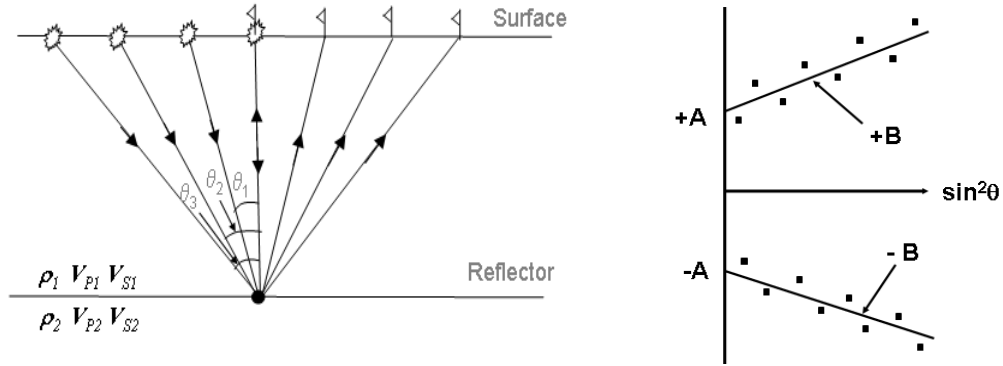


Figure 5.6: Left: traces in a seismic gather reflect from the subsurface at increasing angles of incidence  $\theta$ ; right: plot of two terms of the Aki-Richards equation (Hampson-Russell, 2007).

$$R(\theta) = A + B \sin^2 \theta \quad (5.2)$$

The Aki-Richards equation (5.2) predicts a linear relationship between the amplitudes (Figure 5.6) and  $\sin^2\theta$ . Regressions are thus calculated to give A and B values for each time sample. A is the intercept, and B is the gradient term which produces the AVO effect. It is dependent on changes in density  $\rho$ , P-wave velocity  $V_p$ , and S-wave velocity  $V_s$ . The most popular AVO intercept and gradient derived attributes are: AVO Product:  $A*B$ ; Scaled Poisson's Ratio Change:  $A+B$ ; Shear Reflectivity:  $A-B$ ; Fluid Factor. A number of other possibilities of AVO attributes are: Offset or angle limited stacks, elastic impedance inversion, extraction of  $R_p$  and  $R_s$  reflectivity, inversion of  $R_p$  and  $R_s$  to give  $Z_p$  and  $Z_s$  impedances and a Lambda-Mu-Rho(LMR) analysis of  $Z_p$  and  $Z_s$ .

### 5.21 AVO PRODUCT $A*B$

Figures 5.7 to 5.9 show that the synthetics and the crossplot with the Gradient versus Intercept have mainly class III and II AVO. Figure 5.7 shows (in red) a class III anomaly

at the Colony level, and at the Sparky level (in pink) a class II anomaly. Figure 5.8 shows the gradient versus intercept crossplot with class III (low impedance contrast) or class II

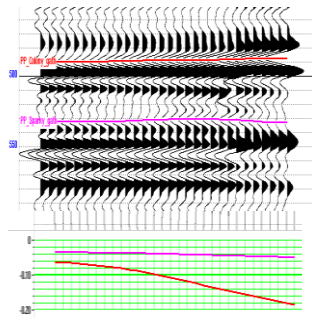


Figure 5.7: The offset synthetic at well A11-17: the Colony horizon (red) and Sparky horizon (pink). The Colony shows a class III AVO anomaly and the Sparky class II.

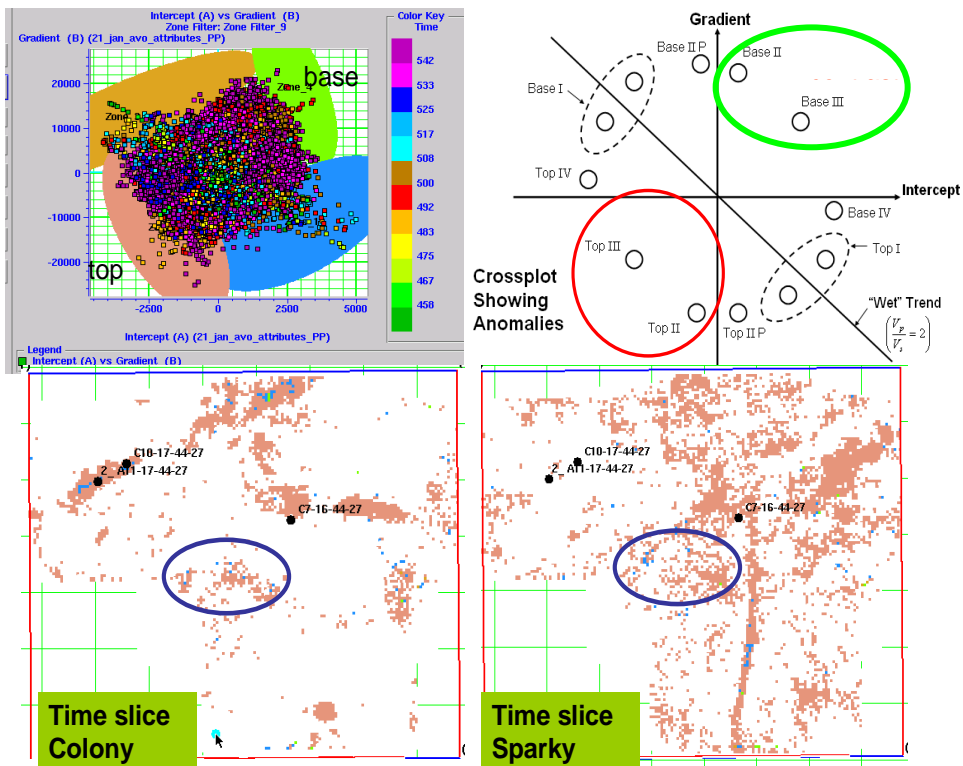


Figure 5.8: Gradient versus intercept crossplot (upper left) shows class II and III anomaly at the top of the reservoirs, circled in red (upper right).

anomaly (near zero impedance contrast as in Figure 5.10). The top of the reservoir is shown in pink-salmon colour (Figure 5.8), and the base in light-green (Figure 5.9).

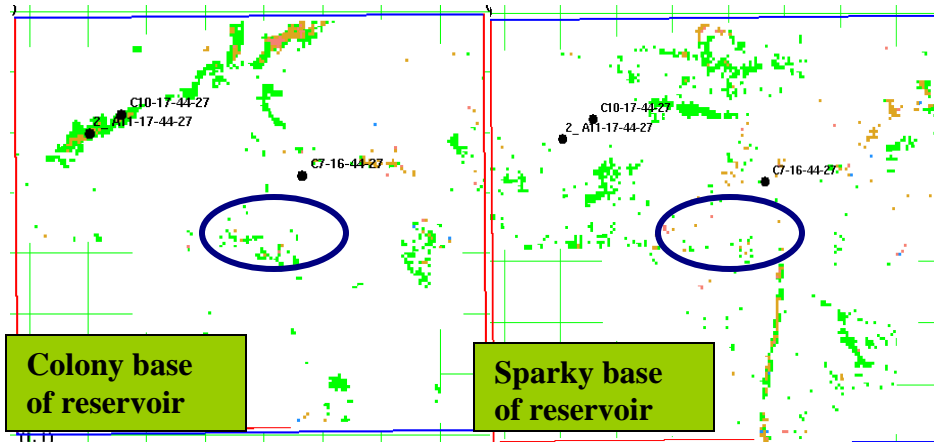


Figure 5.9: Gradient versus intercept shows class II and III anomaly at the base of the reservoirs, according to the gradient versus intercept chart (upper Figure 5.7).

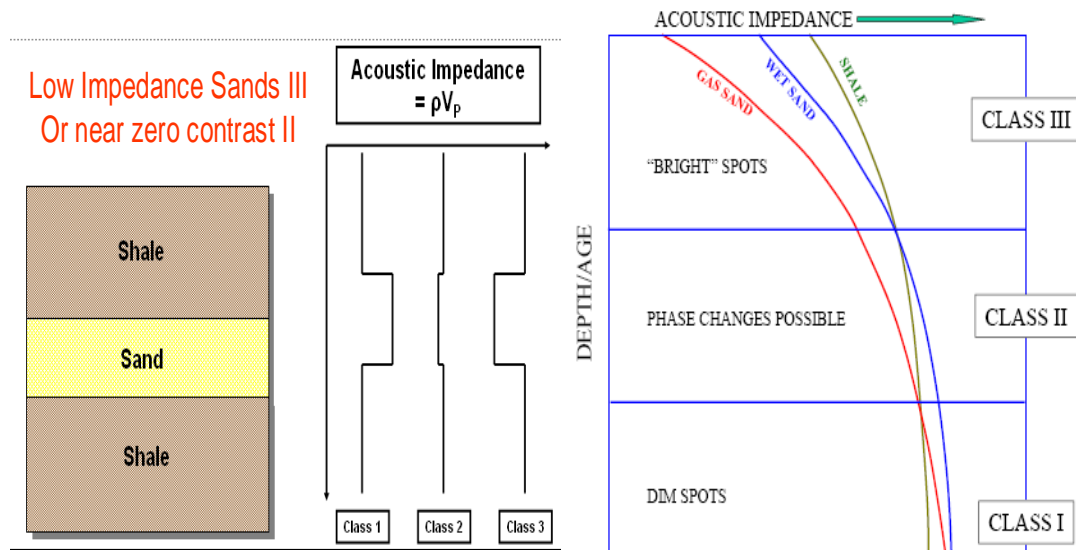


Figure 5.10: The AVO classification (left) after Rutherford/Williams and (right) AVO classification after A. Brown, 2006.

A low impedance contrast between shale and sand shows a class III AVO, and a near zero impedance contrast shows a class II AVO (Figure 5.10). There is a better acoustic impedance contrast between gas sand, wet sand and shale at smaller depths (for class III) as seen in Brown's classification (2004).

## 5.22 AVO SCALED POISSON'S RATIO A+B

The sum  $A+B$  is proportional to the change in Poisson's Ratio, as in formula 5.3. Poisson's ratio is directly related to the  $V_p/V_s$  values. Interestingly, well 2A-11 (left, red arrow) is producing from the Colony and C7-16 (right, green arrow) is producing from the Sparky horizon. The delineation of the channels in the interest zone (black ellipse) looks better for the Sparky level, but not satisfactory for the Colony sand channel. The scaled Poisson's ratio is proportional to the change in  $\Delta\sigma$  as in the formula:

$$A + B = \frac{9}{4} \Delta\sigma \quad (5.3)$$

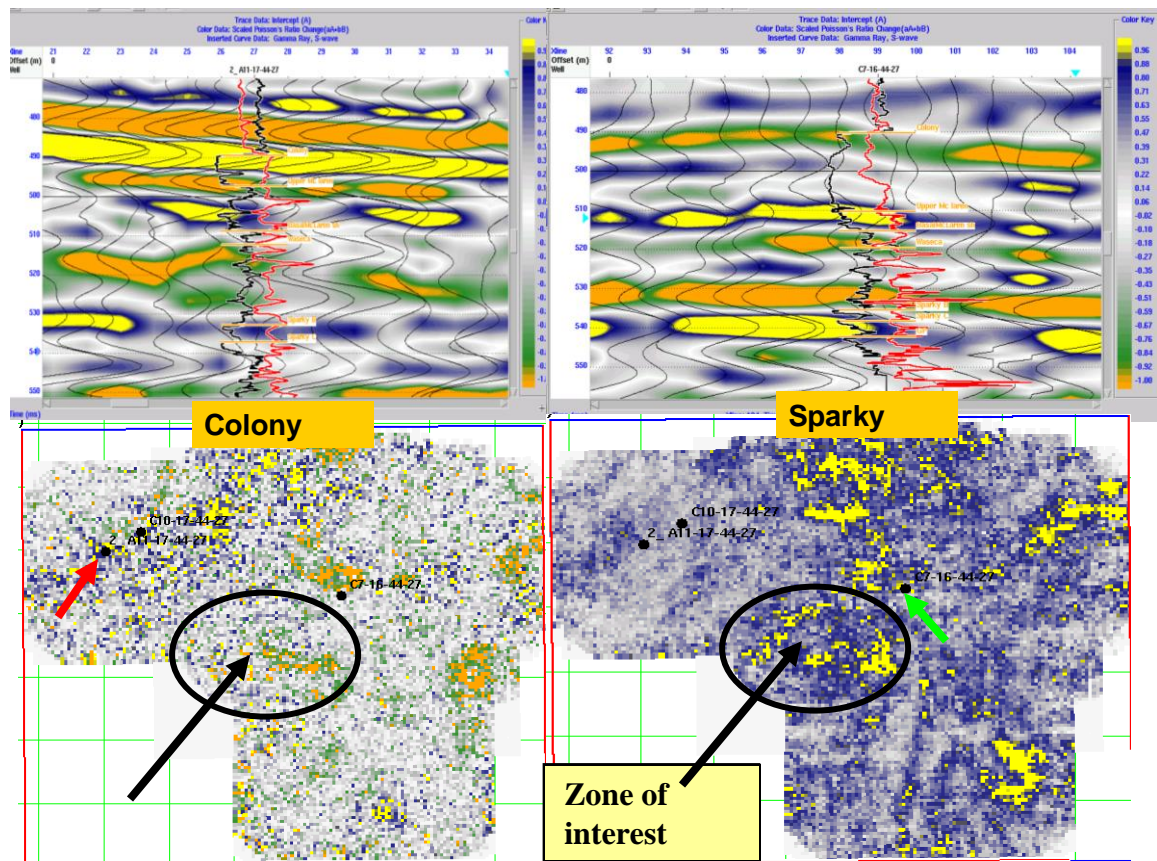


Figure 5.11: The sum  $A+B$  is proportional to the change in Poisson's Ratio. Top: the scaled Poisson's ratio at the well 2A-11 (left) and C7-16 (right). Bottom: the Colony and Sparky horizons showing Poisson's ratio.

### 5.23 AVO – ELASTIC CONSTANTS

Elastic contrasts are derived from the three term AVO (Aki-Richards) equation:

$$R(\theta) = A + B \sin^2 \theta + C \tan^2 \theta \sin^2 \theta \quad (5.4)$$

Where

$$A = R_{P0} = \frac{1}{2} \left[ \frac{\Delta V_P}{V_P} + \frac{\Delta \rho}{\rho} \right] \quad (5.41)$$

$$B = \frac{\Delta V_P}{2V_P} - 4\gamma \frac{\Delta V_S}{V_S} - 2\gamma \frac{\Delta \rho}{\rho} \quad (5.42)$$

$$C = \frac{\Delta V_P}{2V_P}, \text{ and } \gamma = \left[ \frac{V_S}{V_P} \right]^2. \quad (5.43)$$

Equation (5.41) shows that the zero offset P mode section exhibits density and compressibility contrasts while in (5.42) the PS converted mode section exhibits mainly density and rigidity contrasts. The reflectivity of compressional waves depends on the shear wave velocity contrast, provided that the recording offset is long enough (Garotta , 2000).

Three maps were generated for both Colony (top) and Sparky (bottom), Figure 5.12.

There are several things to highlight:

- Density is a direct measure of the hydrocarbon saturation.
- The density map highlights the same areas as  $\Delta V_P$ .
- The hydrocarbon anomaly is associated with the change in  $\Delta V_P$ , probably the best in the presented data.

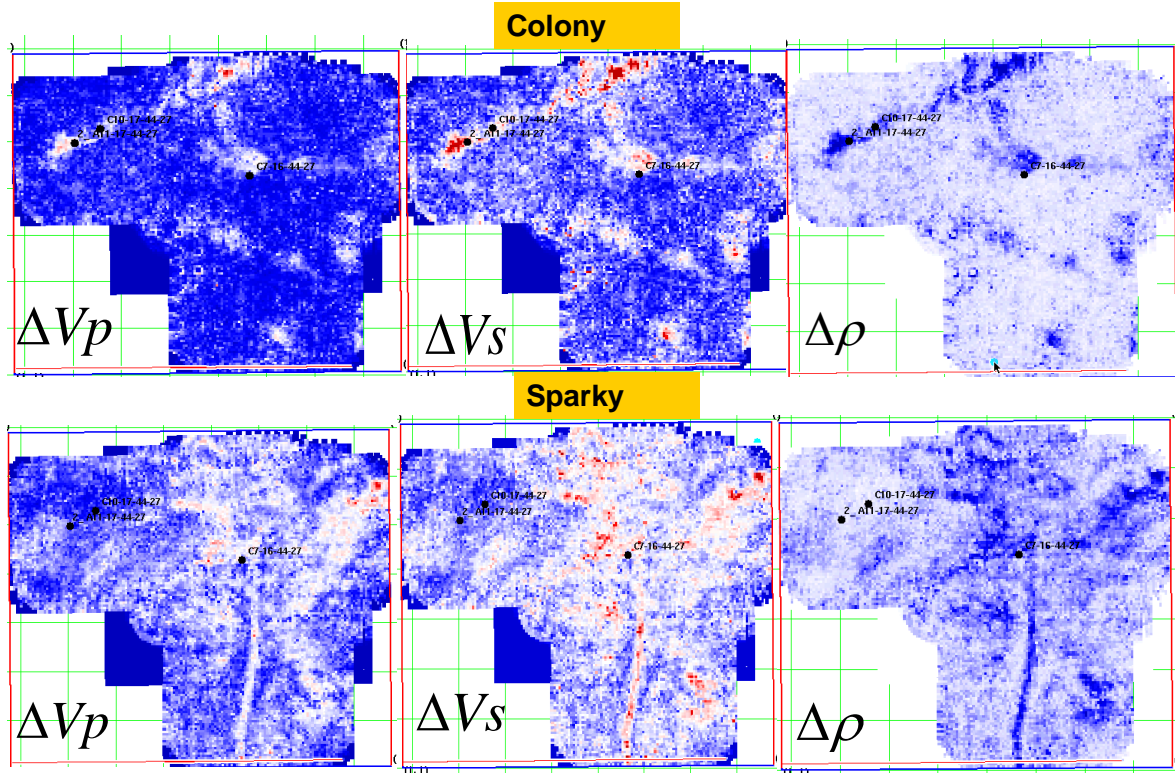


Figure 5.12: The elastic contrasts derived from the three terms AVO. Top: Colony and bottom: Sparky time slices.

## 5.24 AVO – FLUID FACTOR

The Fluid Factor attribute (Smith and Gidlow, 1987; Fatti et al., 1994) is based on Castagna's mudrock equation (2.2), which is assumed to be true for non-hydrocarbon filled layers:

$$V_p = 1.16 V_s + 1.36 m/s \quad (5.5)$$

The Fluid Factor is defined to highlight layers where there is a deviation from Castagna's equation, such as potential hydrocarbon (gas) zones:

$$\Delta F = R_p - 1.16 \frac{V_s}{V_p} R_s \quad (5.6)$$

The top picture in Figure 5.13, shows well A-11 which is producing mainly from the

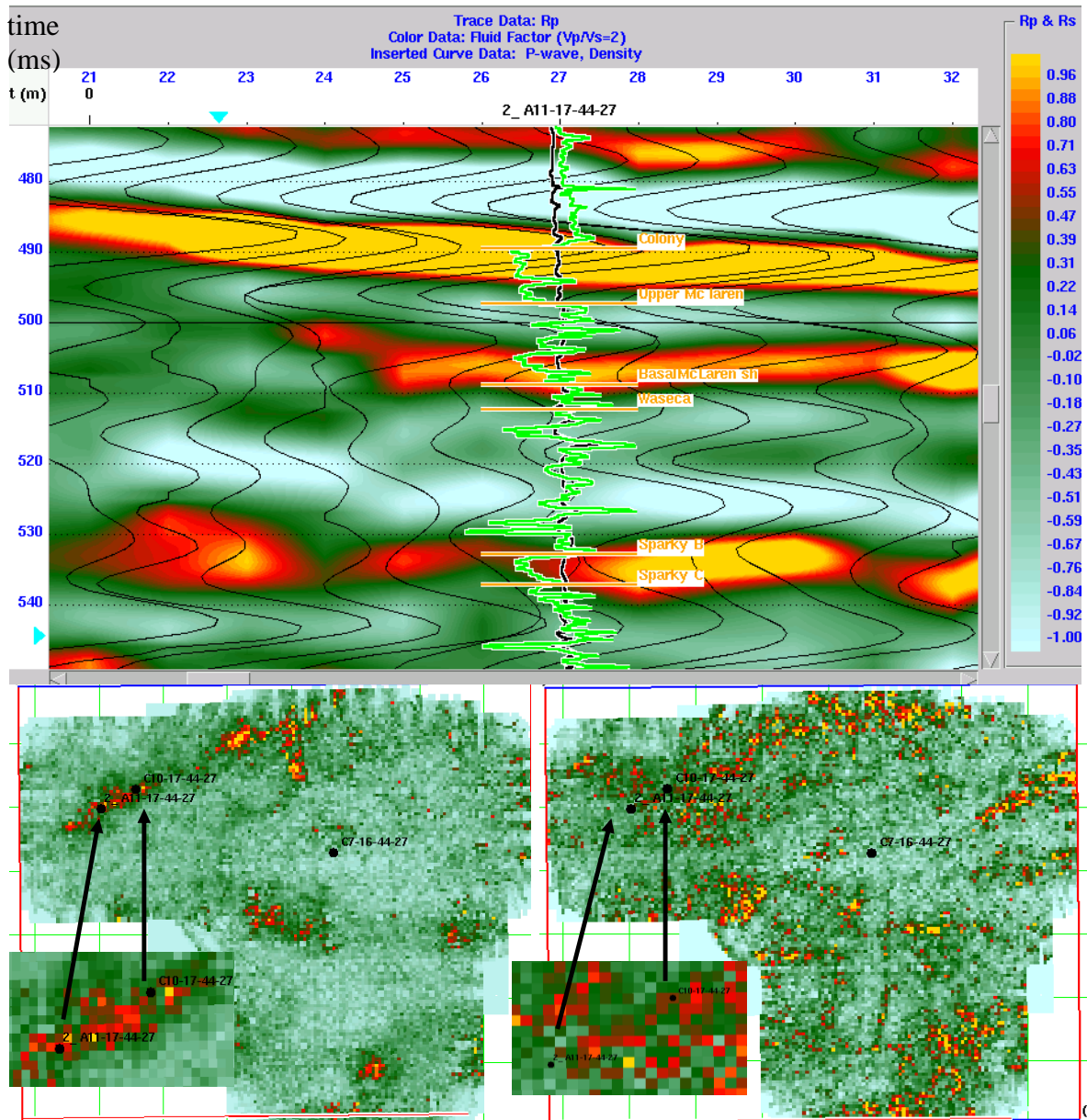


Figure 5.13: Fluid factor at well A-11-17(Top); bottom the fluid factor at Colony time slice (left) and Sparky (right). Inserted curves are P-wave (black) and density (light green).

Colony formation. The fluid factor zoomed section correlates with the well production, for wells A-11 and C-10. We can conclude:

- The fluid factor worked better in delineating the sand channels than the pseudo-Poisson's ratio.

- A11-17 Colony shows clean sand with gas saturation. This well is not producing from Sparky.
- Well C-7-16 at the Sparky sand channel shows no gas saturation.
- Well 10-17 shows production from the Sparky gas sand horizon.

### 5.25 AVO - LMR

The incompressibility attribute,  $\lambda$ , is sensitive to pore fluids and is known to be a good indicator of gas content from shale to gas sands as seen in Table 5.1 (Goodway, 1997).

The rigidity  $\mu$  is sensitive to the rock matrix and density. It is impossible to de-couple the effects of density from  $\lambda$  and  $\rho$  when extracting the information from the seismic data. It is therefore beneficial to cross-plot  $\lambda\rho$  versus  $\mu\rho$  to minimize the effects of density. Goodway et al. (1997) proposed a new approach to AVO inversion based on the Lamé parameters  $\lambda$  and  $\mu$ , and density  $\rho$ , or Lambda-Mu-Rho (LMR). The theory shows that:

$$V_p = \sqrt{\frac{\lambda + 2\mu}{\rho}} \quad \text{and} \quad V_s = \sqrt{\frac{\mu}{\rho}} \quad (5.7)$$

$$Z_s^2 = (\rho V_s)^2 = \mu\rho \quad (5.8)$$

$$Z_p^2 = (\rho V_p)^2 = (\lambda + 2\mu)\rho \quad (5.9)$$

$$Z_p^2 - 2Z_s^2 = \lambda\rho \quad (5.10)$$

Table 5.1 indicates that  $\lambda/\mu$  is most sensitive to variations in rock properties going from shale to gas sand.

Table 5.1. Petrophysical analysis for LMR (Goodway et al., 1997)

	$V_p/V_s$	$(V_p/V_s)^2$	$\sigma$	$\lambda+2\mu$	$\mu$	$\lambda$	$\lambda/\mu$
<b>Shale</b>	<b>2.25</b>	<b>5.1</b>	<b>0.38</b>	<b>20.37</b>	<b>4.035</b>	<b>12.3</b>	<b>3.1</b>
<b>Gas Sand</b>	<b>1.71</b>	<b>2.9</b>	<b>0.24</b>	<b>18.53</b>	<b>6.314</b>	<b>5.9</b>	<b>0.9</b>
<b>Change / Average</b>	<b>-27</b>	<b>-55</b>	<b>-45</b>	<b>-9.5</b>	<b>44</b>	<b>-70</b>	<b>-110</b>

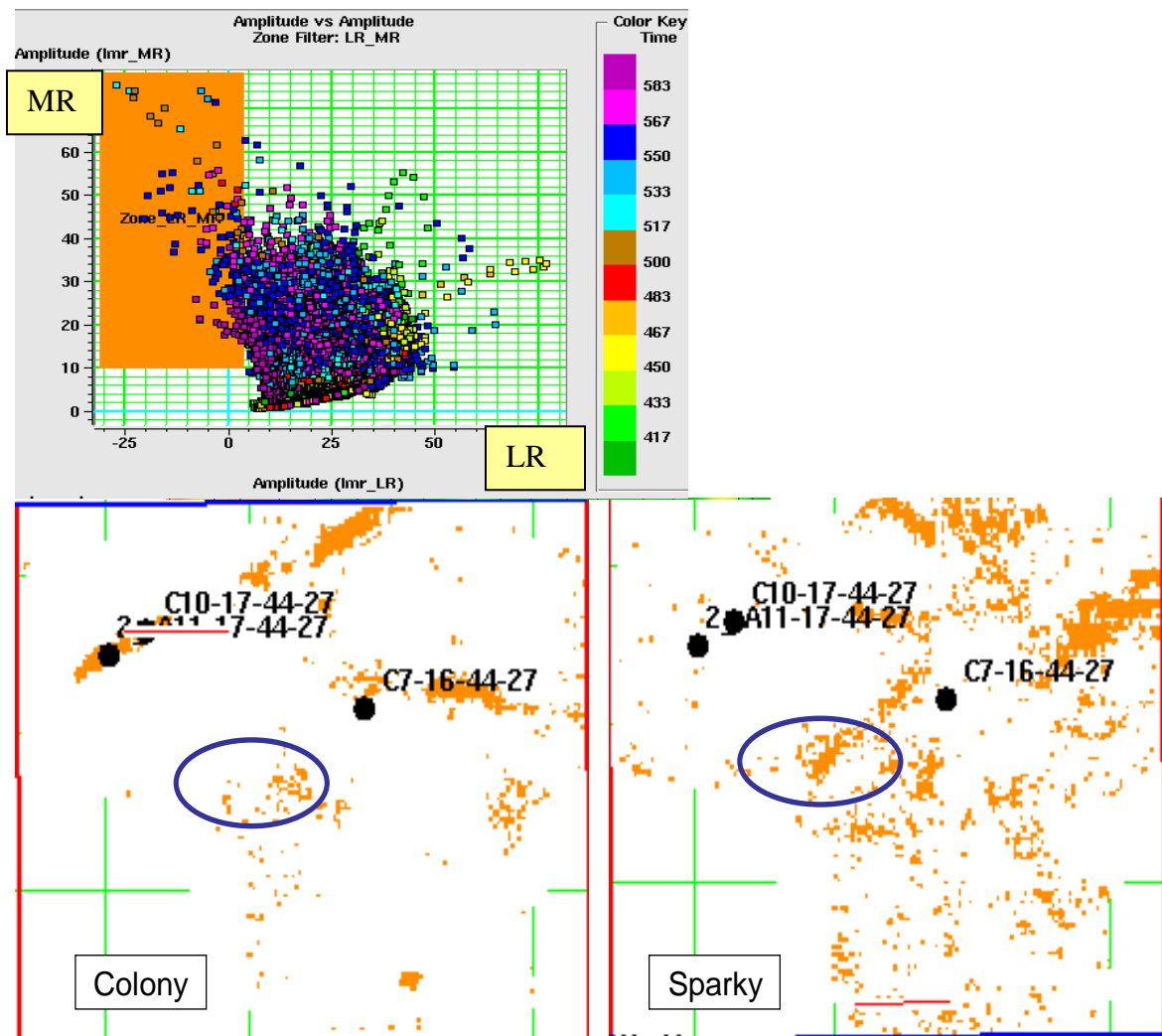


Figure 5.14: Above: MR versus LR from the LMR crossplot:  $\lambda\rho$  versus  $\mu\rho$  shows the anomalous gas sand in orange. Below, are the results at the Sparky (right) and Colony (left) time slices.

The potential anomalous gas sand locations are shown in Figure 5.14 for the Sparky and Colony time slices. This result can be compared with the gas sands delineations from Chapter 4.2 but is not too helpful in understanding the missed drilled location, circled in blue.

## CHAPTER 6 – JOINT INVERSION AT MANITOU LAKE

### 6.1 JOINT INVERSION METHOD

A joint inversion analysis was undertaken (as in Chapter 2) in ProMC (Hampson-Russell package), using post-stack, migrated, 3D multi-component data. The steps in this work were, in order (Figure 6.2): modeling of PP and PS synthetic seismograms, wavelet extraction from both, well log correlation to the seismic data, horizon picking on both, PP and PS data, horizon matching to update the Vp/Vs data using wells on this stage (for P and S wave conversion in domain conversion), building a Strata velocity model using the typical set-up of ProMC model, updating the domain conversion using the Strata model, Vp/Vs mapping through the entire volume, extracting statistical (Figure 6.1) wavelets for

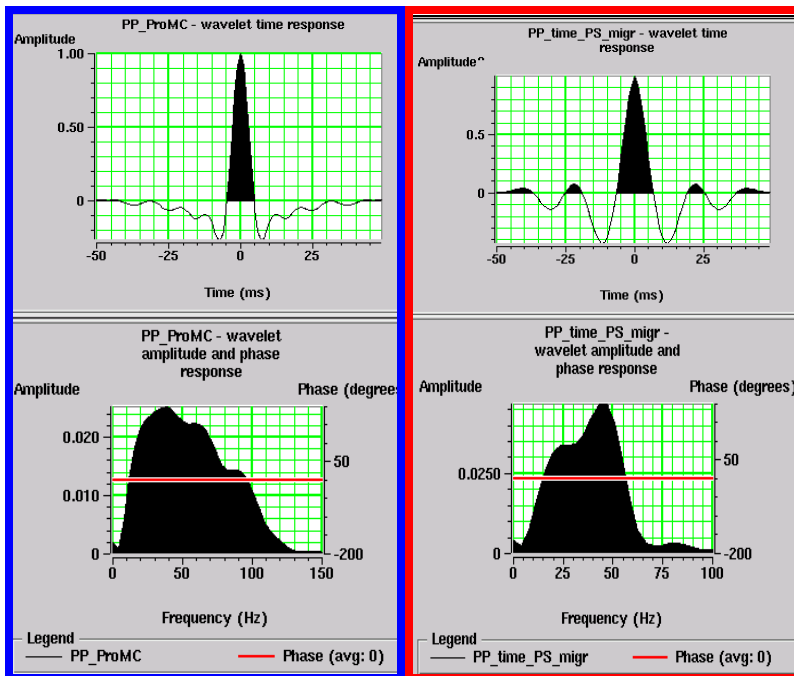


Figure 6.1: The extracted statistical wavelets (in time above and phase below) from the PP data (left) and from the PS data transformed in PP time (right) used for the joint inversion in ProMC. Red line indicate zero degrees phase.

PP and PS (in PP time) and jointly inverting (model based) the PP and PS data to create 3D volumes of either P impedance or S impedance, the  $V_p/V_s$  ratio and density.

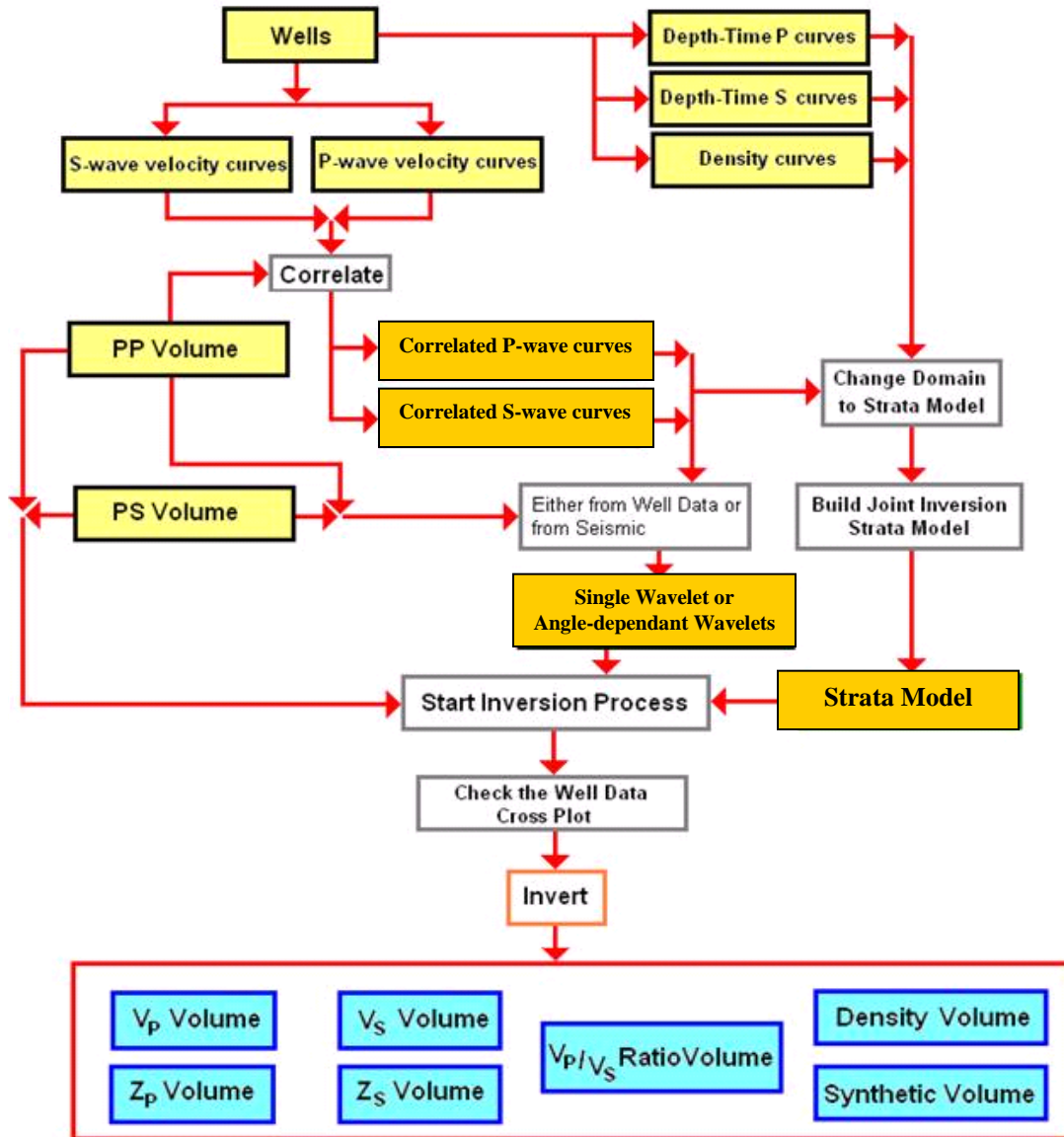


Figure 6.2: Joint PP-PS inversion procedures (after Hampson-Russell, 2008).

The model based joint inversion will update an initial model to create new models of P-impedance, S-impedance,  $V_p/V_s$ , and density, that are consistent with both, the PP and PS seismic amplitude volumes (Figure 6.2).

## 6.2 JOINT INVERSION RESULTS

Figure 6.3 shows the inverted density at well location A11-17. Sands are indicated by values of density lower than 2.25g/cc at both Colony and Sparky horizons.

Figures 6.4 and 6.5 shows a comparison between the previous amplitude maps and the  $V_p/V_s$  maps obtained after joint inversion at the Colony and Sparky horizons respectively. The white arrows show the previously drilled dry hole (white ellipse).

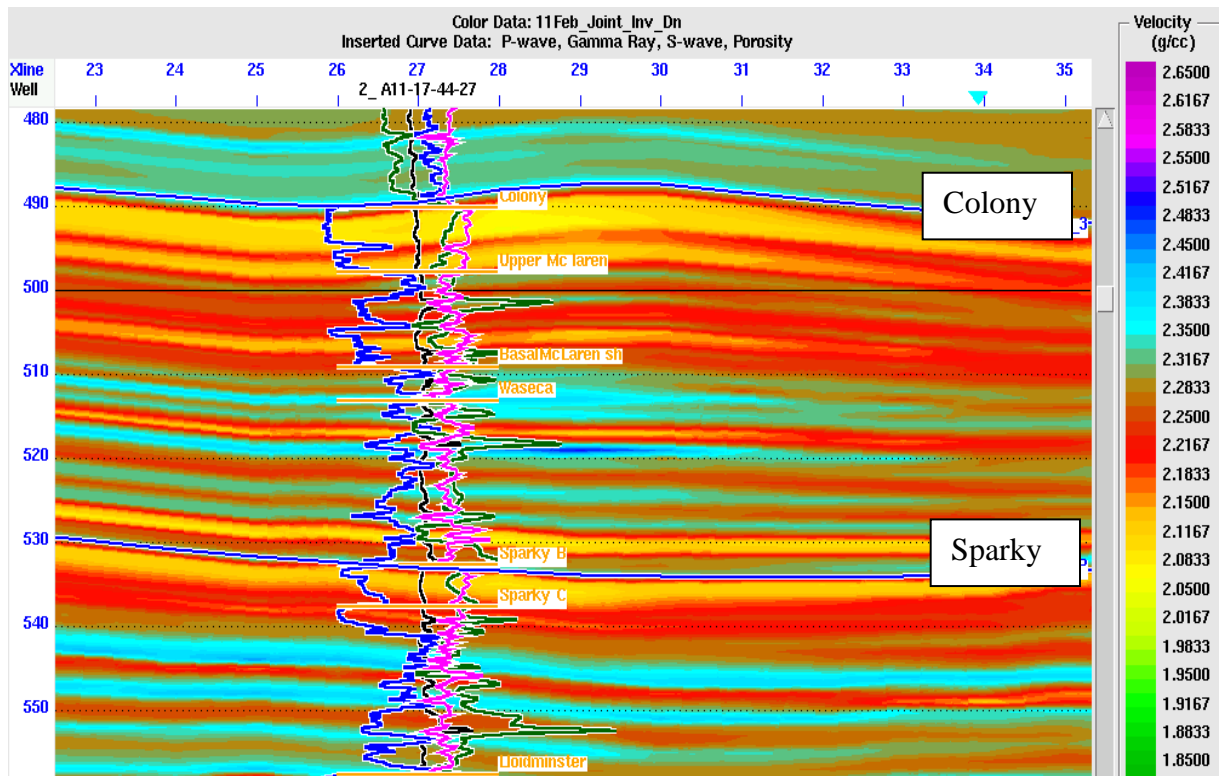


Figure 6.3: Joint PP-PS inversion: density at the well A11-17: inserted curves: Gamma ray (in blue), P-wave (black) S-wave (green) and porosity (pink).

The  $V_p/V_s$  maps give a warning about this location, showing  $V_p/V_s$  values higher than 2.15, so drilling is not recommended. Figure 6.6 shows the cumulative oil production up to 2008 from Accumap. Comparing these results with results obtained from Accumap (Figure 6.6) our confidence increases due to the following observations:

- only well A11-17 is mainly producing from the Colony formation, with 80,659 bbl cumulative production up to 2008;
- at well C10-17 the Sparky formation is mainly producing, with 114,404 bbl cumulative production up to 2008;
- well C7-16 cumulative production is less than for C10-17: 18,307 bbl up to 2008, producing mainly from Sparky.
- all three wells are producing since 2006.
- Well results obtained from the  $V_p/V_s$  maps after the joint inversion are comparable with Accumap results.

The two small red arrows on the amplitude maps (bottom) from Figures 6.4 and 6.5 show two potential future drilling locations. Brown long arrows show the same locations on the  $V_p/V_s$  map, circled with black ellipses: the Colony  $V_p/V_s$  values are clearly higher than 2.15, and at the Sparky level we are close to the channel edges, also on higher values. According to our result, we strongly recommend caution with respect to those prospective locations.

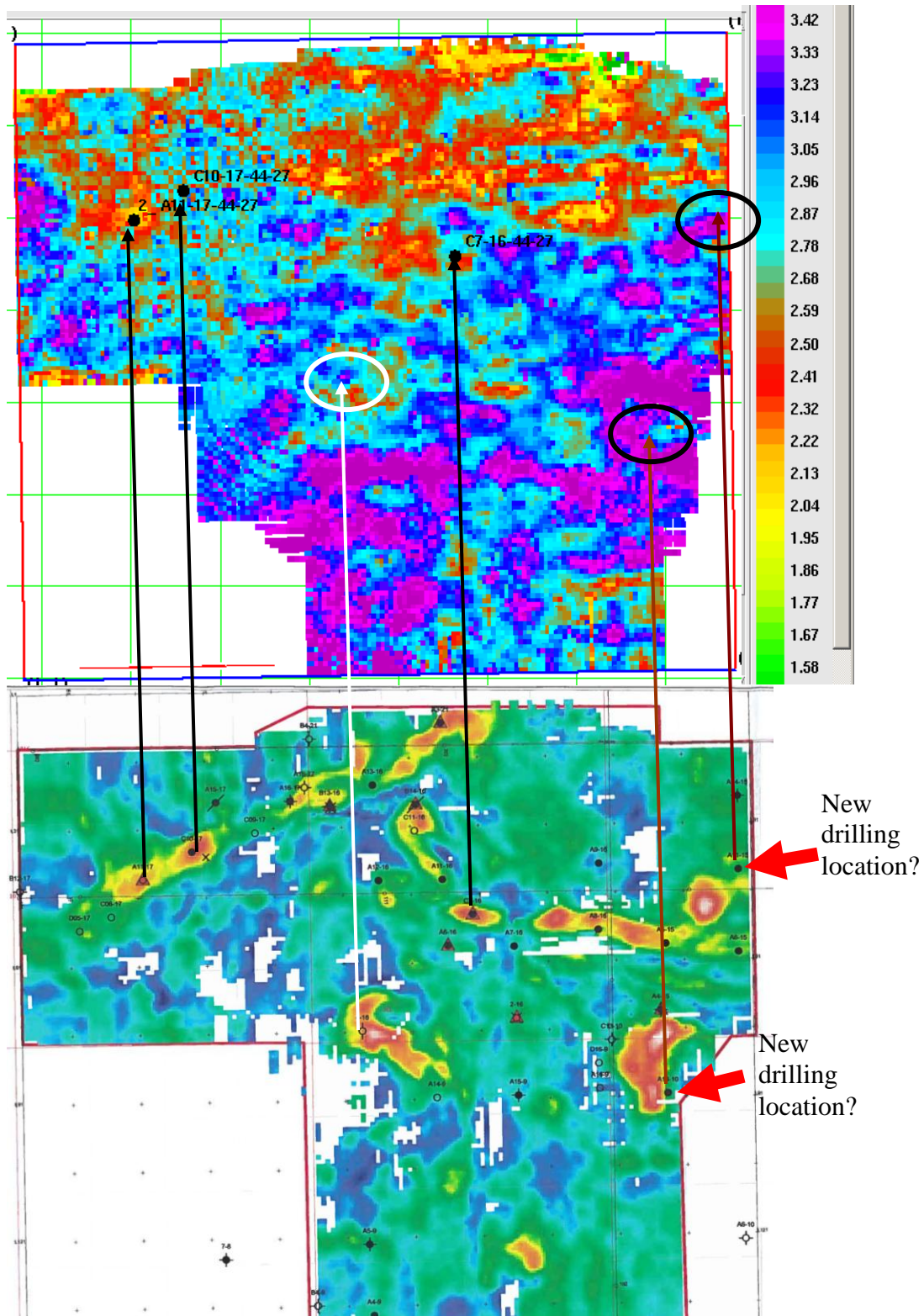


Figure 6.4: Top:  $V_p/V_s$  values after joint inversion at the Colony horizon. Values less than 2.15 show the productive sands, in yellow. Bottom: previous Colony PP amplitude map from Calroc Energy.

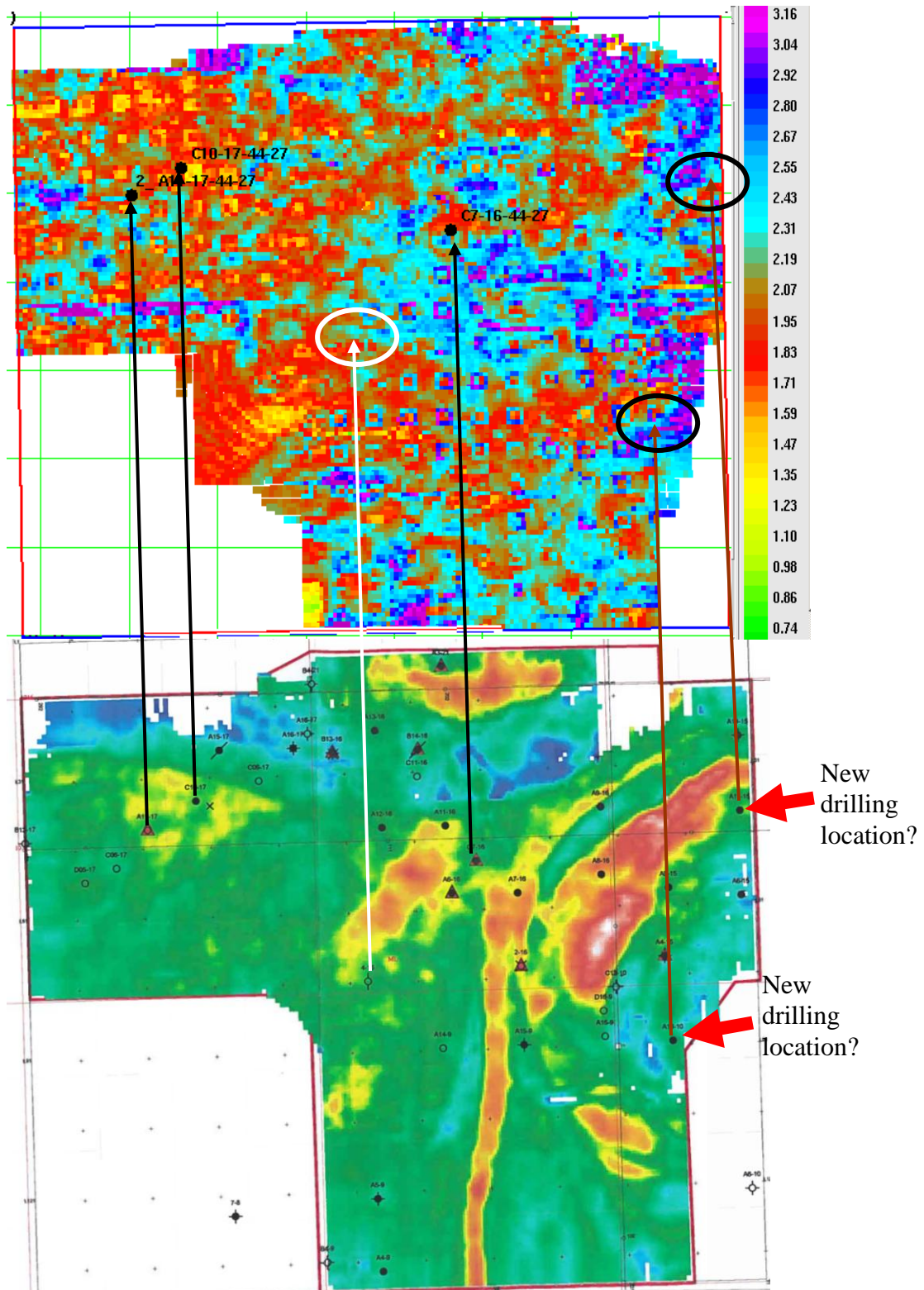
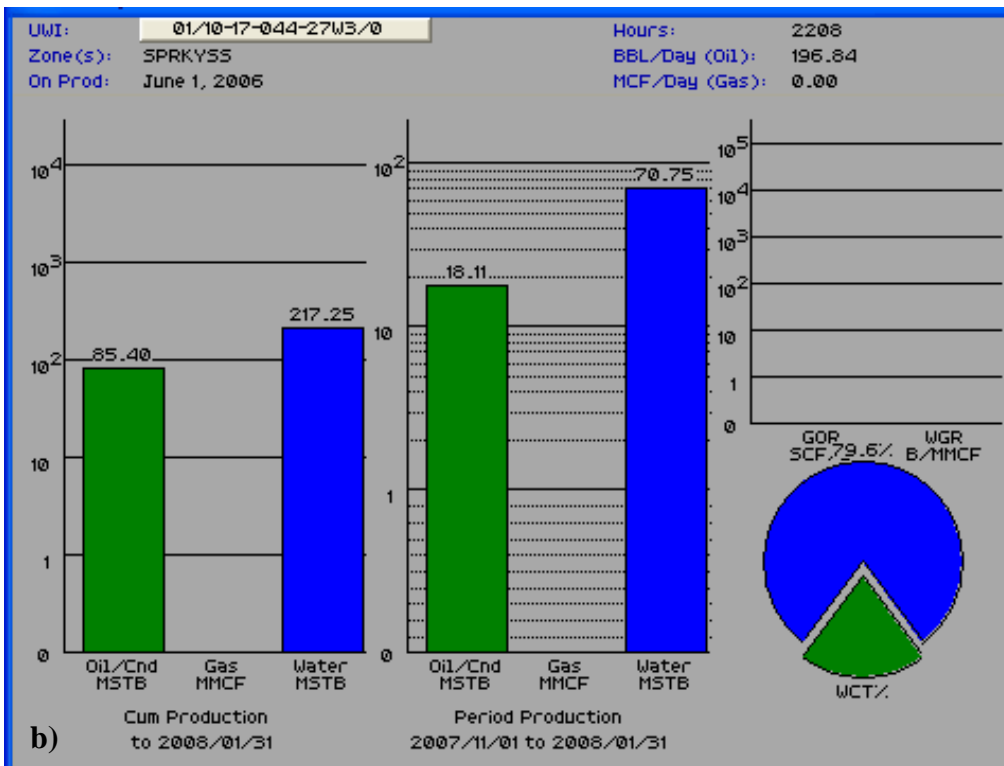
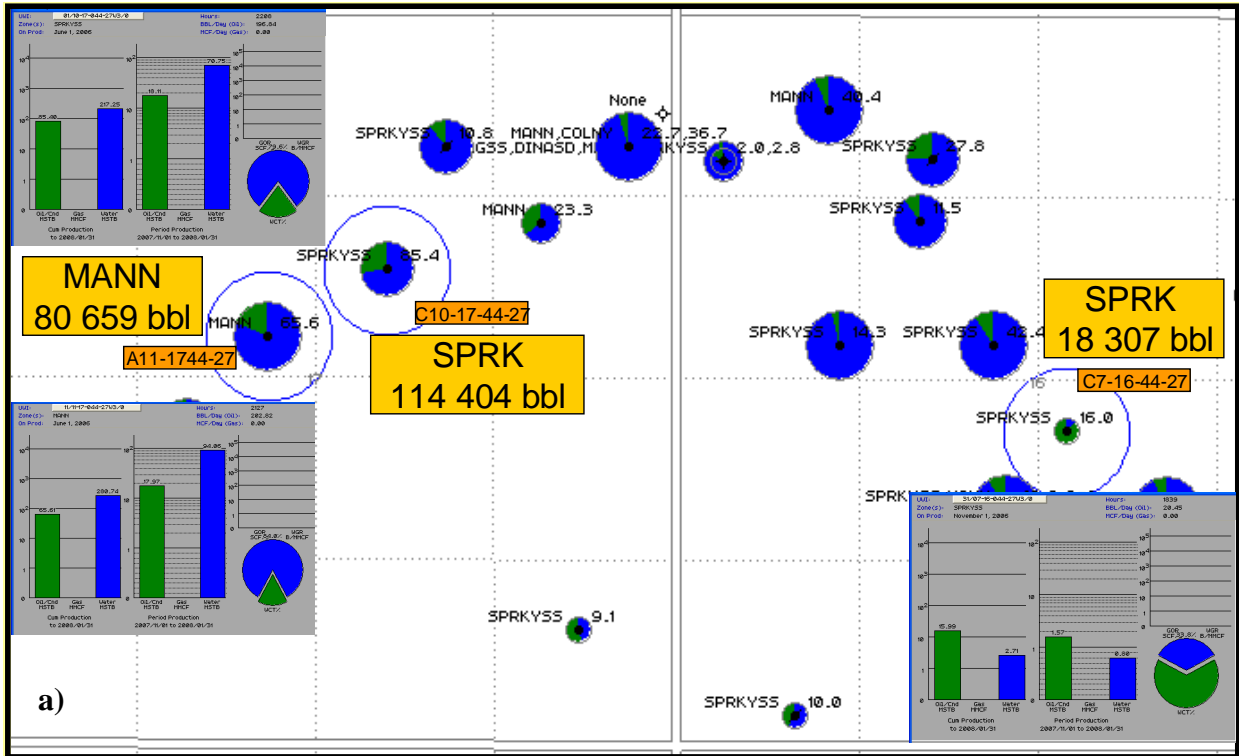


Figure 6.5: Top:  $V_p/V_s$  values after joint inversion at the Sparky horizon. Values less than 2.15 show the productive sands, in yellow. Bottom: previous Sparky PP amplitude map from Calroc Energy.



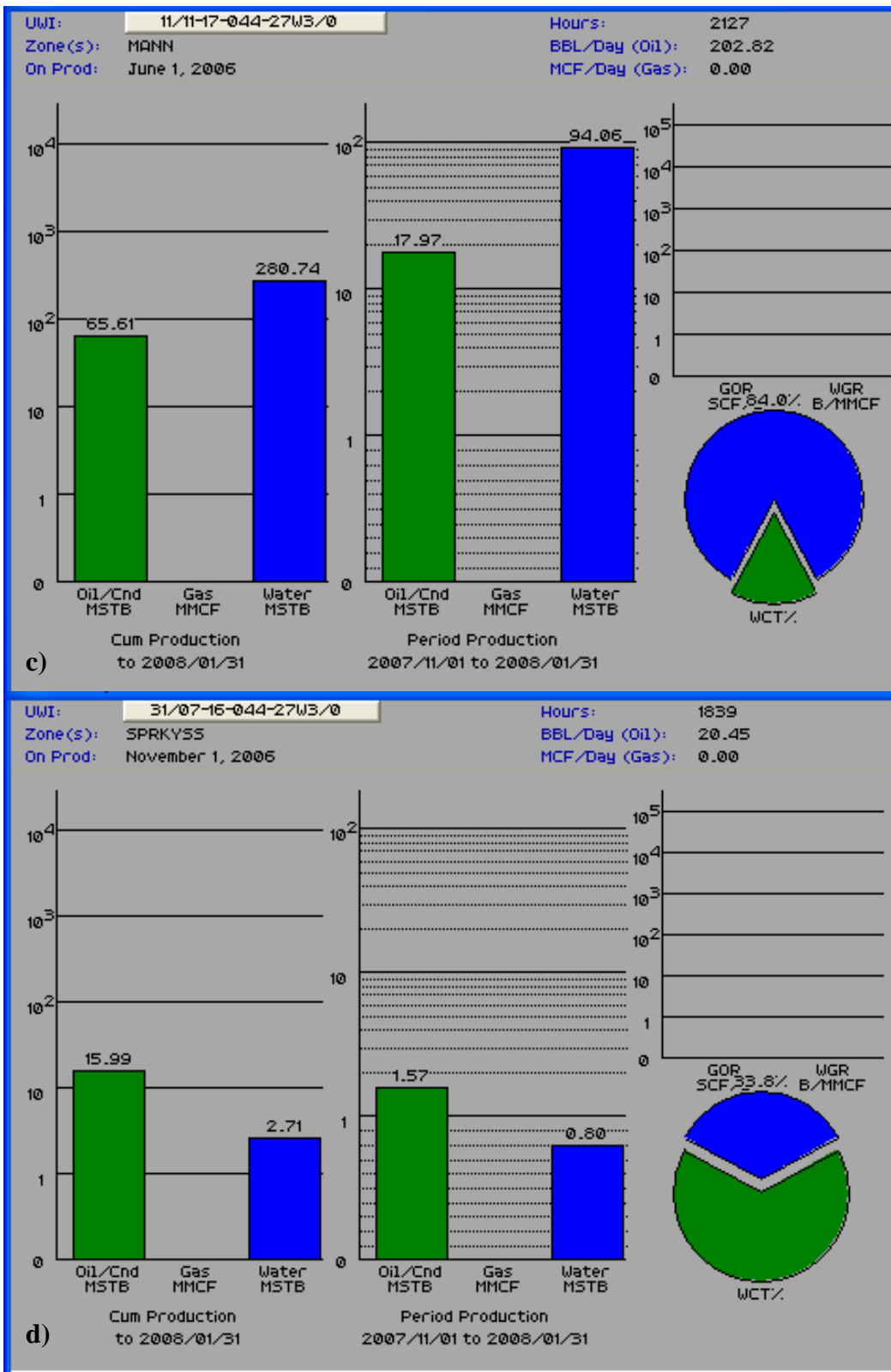


Figure 6.6: a) Cumulative oil production up to 2008 from Accumap, at the Manitou Lake area. All three wells are on production after June, 2006. In green is shown the oil production and in blue is the water. The production numbers are shown in the yellow rectangles. b), c) and d) zoomed images of wells production.

### 6.3 CONCLUSIONS

This work shows that converted-mode acquisition provides information on shear reflectivity and shear propagation (compared with the shear wave velocity information obtained from PP gathers) in a more robust way. PS data is helpful in the planning and risk assessment of new drilling locations. Differences in PP and PS amplitude maps can assist with drilling positioning, due to the direct response of PS data largely to lithology. Oil and gas saturated sand channels should give relatively low  $V_p/V_s$  values, a P impedance decrease, and an S impedance increase. The channels can be filled with sands and/or shales, with similar P-wave impedances. The dipole sonic log showed S-wave impedance to be higher in the sands than in shales, and the top of the reservoir could be delineated. Since PP and PS reflectivities are different, attributes computed from PP and PS volumes show different geologic features. The ratio of the joint PP inversion to the PS inversion ( $V_p/V_s$  from amplitudes) in PP time is very useful in delineating the reservoir. These points allow the conclusion that:

- The combination of PP and PS attributes helps in analyzing channel morphology.
- PP and PS amplitude maps are different: PS amplitude maps can increase our confidence in choosing future drilling locations. High RMS amplitudes are interpreted to be a PS seismic response to the presence of channel sands.
- Sand-shale boundaries may produce poor P-wave velocity contrasts, and in the present case the PS converted mode data enable the reservoir boundaries to be

delineated. PS amplitude anomalies show the top of the reservoir, which could not be seen on the PP amplitude map.

- The productive sand channel is interpreted as a PP impedance drop, a PS increase and a low  $V_p/V_s$  ratio, less than 2.15. It was shown that the main impedance changes correspond to the major lithologic boundaries.
- The density map shows a direct measure of hydrocarbon saturation. The hydrocarbon anomaly is associated with the change in the delta  $V_p$  map.
- The fluid factor did a better job in identifying the channels at the missed drilling location than the pseudo-Poisson's ratio.
- AVO, fluid factor, and simultaneous inversions can give important information in delineating sand channels. Post stack inversion, which allows only the estimation of acoustic impedance, is sometimes not sufficient for inferring fluid content.
- The combination of PP and PS data can validate the "bright spots": gas accumulations are not supposed to show on PS amplitude maps.
- The channel edge has been delineated by a combination of attributes like coherence, curvature, inversion and illumination. Amplitude envelope co-rendered with the most positive and negative curvature on both PP and PS data, can show the prospective gas accumulation in area.

- The Joint inversion shows the best result on the Vp/Vs maps. Our confidence increased when the results were compared with well production information from Accumap.

## CHAPTER 7 – SUMMARY AND RECOMMENDATIONS

The Upper Cretaceous Second White Specks (2WS) formation from Willesden Green (2D project) and the Lower Cretaceous fluvial sand channels from Manitou Lake (3D project) are attractive prospects for oil and gas production. The future potential values on both surveys were demonstrated with the use of interpretation strategies on multicomponent (full wave) seismic data.

In Chapter 2, the calculated  $V_p/V_s$  values and the ratio of PP inversion to PS inversion indicated comparative results with joint inversion, being helpful for sand/shale discrimination. A drop in  $V_p/V_s$  can show the producing horizons (increase in porosity/fractures) between the well locations. Other shown anomalies between the well locations indicate possible future drilling targets.

In Chapters 3 to 6, the differences in PP and PS attributes have shown that they can assist with interpreting sand development, due to the direct response of PS data primarily to lithology. Amplitudes from the PP and PS volumes show different geologic features when combined with curvature. As bright spots were supposed to originate from gas, they do not show in the PS amplitude map; hence this information can lead to a better understanding of channel “sweet spots” (favorable locations to drill a well) for future well placements. The fluid factor shows high anomalous values within the channel boundaries.  $V_p/V_s$  values from joint inversion, combined with  $V_p/V_s$  derived from AVO simultaneous inversions, can help in delineating the reservoir. Hydrocarbon filled sandstones have higher S-wave velocities; hence oil- and gas- saturated sand channels manifest with relatively low  $V_p/V_s$  values (less than 2.15). The channels may be filled

with sands and/or shales, with similar P-wave impedances. The lithology predictions from inverted rock properties show good correlation to the wells. Joint inversion minimizes the uncertainty in sand and shale identification, contributing to optimal well placement.

While PS seismic data can provide new insights into reservoir lithology and fluid characteristics, interpretation results are dependent upon the quality of the registration between PP and PS seismic times. Full-wave seismic data hold tremendous potential value for reservoir understanding, leading to better well placement and field development (Roth, 2007). As interpretation of multicomponent seismic data is in its beginnings, more successful case studies are essential for wider acceptance.

Knowing that shear sensitivity to azimuthal anisotropy is higher than for compressional waves, further study is required. The unique travel time and polarization properties of S-wave splitting are useful for fracture characterization (Garotta, 2005).

## REFERENCES

- Anderson, P.F., 2007, Multicomponent case study - Continued Multicomponent Experience in Eastern Alberta, SEG, 2007 Annual Meeting, p.1878-1882.
- Anderson, P.F., Chabot, L., and Gray, D., 2005, A proposed workflow for reservoir characterization using multicomponent seismic data: 75<sup>th</sup> Annual International Meeting, SEG, Expanded abstracts, 991-994.
- Anstey, N. .A., 1991, Velocity in thin section: First Break, 9, 449-457.
- Bancroft, J.C., 2005, A practical understanding of pre- and poststack migration: Society of Exploration Geophysicists, Tulsa, OK.
- Bloch, J. D.,1994, The Methods and Results of Geochemical Analyses of Cretaceous Colorado Group Shales From the Western Canada Sedimentary Basin, Open File Report, 2810: Institute of Sedimentary and Petroleum Geology, Geological Survey of Canada, Calgary, Alberta, p. 87.
- Bloch, J. D., Schroeder-Adams, C.L., Leckie, D.A., Craig, J., and McIntyre, D.J., 1999, Sedimentology, Micropaleontology, Geochemistry, and Hydrocarbon Potential of Shale from the Cretaceous lower Colorado group in Western Canada: Geological survey of Canada, Bulletin 531, p.185.
- Brown, A. R., 2004, Interpretation of three-dimensional seismic data, sixth edition, AAPG memoir 42, SSE Investigations in Geophysics, No. 9.
- Castagna, J.P., M.L. Batzle, and T. K. Kan, 1993, Rock physics – The link between rock properties and AVO response in Castagna, J.P., and M. Backus, Offset dependent reflectivity, Theory and Practice of AVO analysis: SEG, 135-171.
- Creaney, S., Allen, J., Cole, K.S., Fowler, M.G., Brooks, P.W., Osadetz, K.G., Macqueen, R.W., Snowdon, L.R. and Riediger, C.L. 1994, Petroleum Generation and Migration in the Western Canada Sedimentary Basin, p 455-468., In: Geological Atlas of the Western Canada Sedimentary basin. G.D. Mossop and I. Shetsen (compilers). Canadian Society of Petroleum Geologists and Alberta Research Council, Chapter 31.
- Creaney, S., Allen, J., 1992, Petroleum systems in the foreland basin of Western Canada. In: Foreland Basins and Fold Belts. Macqueen, R.W. and Leckie, D. A., (eds), American Association of Petroleum Geologists, Memoir 55, p.279-308.
- Cristopher, J.E., 1997, Evolution of the Lower Cretaceous Mannville Sedimentary Basin in Saskatchewan in Pemberton, S.G. and James, D.P.(eds.), Petroleum Geology of the Cretaceous Manville Group, Western Canada, Can. Soc. Petrol. Geol. Memoir, **18**, 191-210.

- Domenico, S.N., 1984, Rock lithology and porosity determination from shear and compressional wave velocity; *Geophysics*, 49, 1188-1195.
- Downton, J., 2005, seismic parameter estimation from AVO inversion: Ph.D. Thesis, University of Calgary.
- Dumitrescu C., 2007, Practical Interpretation of Multi-Component seismic data: CSEG CSPG Annual Convention, Expanded Abstracts, 465.
- Garotta, R., Marwchal, P., and Megesan, M., 1985, Two-component acquisition as a routine procedure for recording P-waves and converted waves: *Journal of the Canadian Society of Exploration Geophysicists*, 21, 40-53.
- Garotta, R., 2000, Shear waves from acquisition to interpretation: 2000 Distinguished Instructor short course, Society of Exploration Geophysicists, 3, 1.1-3.20.
- Garotta, R., 2005, Acquisition and application of multicomponent vector wavefields: are they practical? ,EAGE, First Break volume **23**, June, 61-66
- Goodway, B., Chen, T. and Downton, J., 1997, Improved AVO fluid detection and lithology discrimination using Lamé parameters, 67<sup>th</sup> Ann. Internat. Mtg: SEG, 183-186.
- Hampson, D. Russell,B.and Cardamone, M.,2004, Uncertainty in AVO-How can we measure it?: *Recorder*, **29**, 3, 5-11.
- Hampson, D. Russell,B., 1990, AVO inversion: theory and practice: 60<sup>th</sup> Ann.Internat.Mtg., Soc. Expl. Geophys., Expanded Abstracts, 1456-1458.
- Hampson-Russell package, 2008, Geoview, on-line software guide.
- Hill D., 2000, Overview of Gas shale potential, Internal presentation, GTI E&P Services Canada, Calgary, Alberta.
- Hill D. and Nelson C., 2000, Gas Productive Fractured Shales: An Overview and Update. GasTIPS, summer 2000.
- Hilterman F., 2001, Seismic amplitude interpretation, SEG, EAGE, Distinguished instructor series, 2.1 - 2.22.
- Keith, D. A., 1985, Sedimentology of the Cardium Formation (Upper Cretaceous) Willesden Green Field, Alberta: M.Sc. Thesis, University of Calgary, Department of Geology and Geophysics.

- Kohrs, B.M. and Norman, D.K., 1988, Stratigraphic Correlation Chart, in Hills, L.V. and Cederwall, D.A., Eds., The CSEG/CSPG Western Canadian Atlas of Hydrocarbon Pools, VIII.
- Kuster, G.T. and Toksoz, M.N., 1974, Velocity and attenuation of seismic waves in two phase media: Part 1. Theoretical formulations: *Geophysics*, 39, 587-606.
- Larson, G.A., 1996, Acquisition, processing and interpretation of PP and PS 3-D Seismic data: M.Sc Thesis, University of Calgary, Department of Geology and Geophysics.
- Leckie, D.A., and D.G.Smith, 1992, Regional setting, evolution, and depositional cycles of the Western Canada Foreland Basin in Foreland Basins and Fold Belts, Macqueen, R. W., Leckie, D.A.(Eds), AAPG Memoir, **55**, 9-46.
- Leckie, D.A., Bhattacharya, J.P., Bloch, J., Gilboy, C.F., and Norris, B., 1994, Cretaceous Colorado/Alberta Group of the Western Canada sedimentary Basin: in Geological Atlas of the Western Canada sedimentary Basin. G.D. Mossop and I. Shetsen (Comps.), Calgary, Canadian Society of Petroleum Geologists and Alberta Research Council, chpt.20.
- Lexicon of Canadian Stratigraphy , 1997, Volume 4, Western Canada, Including Eastern British Columbia, Alberta, Saskatchewan and Southern Manitoba, D.J., Glass, Canadian Society of Petroleum Geologists, Calgary, Alberta.
- Lines, L.R., Newrick, R.T., 2004, Fundamentals of geophysical interpretation: Society of Exploration Geophysicists.
- Lu H., Hall K., Stewart R., Feuchtwanger D., Szatkowski B., 2006, Searching for sand reservoirs: Processing 3C-3D seismic data from Manitou Lake, Saskatchewan, CREWES Research Report, **18**.
- Margrave, G.F, Lawton D. C., and Stewart R.R., 1998, Interpreting channel sands with 3C-3D seismic data: *The Leading Edge*, **17**, 509-513.
- Marfurt K. J. and Chopra S., 2008, 3D Seismic attributes for prospect identification and reservoir characterization, Doodle train course.
- Miller, S.L.M., and Stewart R.R., 1990, Effects of lithology, porosity and shalliness on P- and S-wave velocities from sonic logs: *Can. J. Expl. Geophys.*, 26, 94-103.
- Miller, S.L.M., 1996, Multicomponent seismic data interpretation: M.Sc Thesis, University of Calgary, Department of Geology and Geophysics.
- Minear, J.V., 1982, Clay models and acoustic velocities: Soc. Petr. Eng. Of AIME 57<sup>th</sup> Annual Tech.Conf. and Exhib.

- McCormack, M.D., Dunbar, J.A. and Sharp, W.W, 1985, A stratigraphic interpretation of shear and compressional wave seismic data for the Pennsylvanian Morrow formation of southeastern New Mexico, in *Seismic Stratigraphy II: AAPG Memoir 39*, 225-239.
- McGeary D., Plummer C., Carlson D., 2006, *Physical Geology: Earth revealed*, McGraw-Hill science.
- McKinstry, B., 2001, *Tight Shale Gas Plays: Lewis Shale, San Juan Basin: Internal Presentation*, GTI E&P Services Canada, Calgary, Alberta.
- Mossop, G.D. and Shetsen, I.,(comp), 1994, *Geological Atlas of the Western Canada Sedimentary Basin: Canadian Society of Petroleum Geologists and Alberta Research Council*, Calgary, Alberta, URL.
- Nahm, J. W and Duhon, M. P, 2003, Interpretation and practical applications of 4C-3D seismic data. East Cameron gas fields, Gulf of Mexico. *The Leading Edge*, 300-309.
- Pendrel, J., Stewart R.R., and Van Reel P., 1999, Interpreting sand channels from 3C-3D seismic inversions: *CSEG Recorder*, **24**, 3, 24-35.
- Pickett, G.R., 1963, Acoustic character logs and their applications in formation evaluation: *J. Petr. Tech.*, June, 659-667.
- Putnam, P.E. and Oliver, T.A., 1980, Stratigraphic traps in channel sandstones in the Upper Mannville (Albian) and east-central Alberta, *Bulletin of Canadian Petroleum Geology*, **28**, 489-508
- Putnam, P.E., 1982, Aspects of the petroleum geology of the Lloydminster heavy oil fields, Alberta and Saskatchewan: *Bulletin of Canadian Petroleum Geology*, **30**, 81-111.
- Quijada, M.F. and Stewart R.R., 2008, Characterizing the elastic properties and seismic signature of a heavy oil sand reservoir: Manitou Lake, Saskatchewan: 78<sup>th</sup> Annual International Meeting, SEG, Expanded Abstract, **25**.
- Quijada, M.F. and Stewart R.R., 2007, Density estimations using density-velocity relations and seismic inversion: *CREWES Research Report*, volume 19.
- Quijada, M.F. and Stewart R.R., 2007, Petrophysical analysis of well logs from Manitou Lake, Saskatchewan: *CREWES Research Report*, volume 19.

- Russell, B., 1988, Introduction to seismic Inversion Methods: Society of Exploration Geophysicist, Course Notes, Series, 2.
- Russell, B., 2007, AVO Workshop, part I and II, seismic course.
- Roth, M., 2006, Practical Interpretation of Multi-Component seismic data: CSEG Recorder, **31**, 5, 23-26.
- Roth, M., 2007, Identifying gas channel sweet spots through multi-component seismic interpretation, CSPG CSEG Convention, 469-472.
- Roth, M., and Davis T., 2007, Demystifying tight-gas reservoirs using multi-scale seismic data, CSPG CSEG Convention, 355-359.
- Royle A., 2002, Exploitation of an oil field using AVO and post-stack rock property analysis methods: 72<sup>nd</sup> Annual International Meeting SEG, Expanded Abstracts, **21**, 289-292.
- Rutherford, S. R., and Williams, R.H., 1989, Amplitude-versus-offset in gas sands: Geophysics, 54, 680-688.
- Sheriff, R.E., 2006, Encyclopedic dictionary of applied geophysics: Society of Exploration Geophysicists., 13.
- Sheriff, R.E., 1999, Reservoir Geophysics, Investigations in Geophysics: Society of Exploration Geophysicists, 7, 37-63.
- Shuey, R.T, 1985, A simplification of the Zoeppritz equations: Geophysics, 50, 609-614.
- Stewart, R.R., 1990, Joint P and P-SV seismic inversion, CREWES Research Report, **2**.
- Stewart, R.R., Pie, G., Cary, P., and Miller S., 1993, Interpretation of P-SV seismic data: Willesden Green, Alberta, CREWES Research Report, **5**.
- Stewart, R.R., Gaiser, J, Brown R., Lawton, D.C., and 2002, Converted-wave seismic exploration: Methods: Geophysics, **67**, 1348-1363.
- Stewart, R.R., Gaiser, J, Brown R., Lawton, D.C., 2003, Converted-wave seismic exploration: Applications: Geophysics, **68**, 40-57.
- Stewart, R.R., 2007, Interpreting multicomponent seismic data: Clastic and carbonate case histories: CREWES Research Report, volume 19.
- Soubotcheva, N, 2006, Reservoir property prediction from well-logs, VSP and multicomponent seismic data: Pikes Peak heavy oilfield, Saskatchewan: M.Sc Thesis, University of Calgary, Department of Geology and Geophysics.

- Soubotcheva, N, and R.R Stewart, 2006, Estimating lithology and porosity from 3C seismic data and well logs: Pikes Peak heavy oilfield, Saskatchewan: CSEG Recorder, 31.
- Travis, S.,2002, Organic Geochemical Analysis of the Second White Speckled Shale Formation, Upper Cretaceous Colorado Group, West Central Alberta, Implications for Shale Gas Production: M.Sc. Thesis, University of Calgary, Department of Geology and Geophysics.
- Treitel, S and Lines, L.R, 1994, Geophysical inversion and application: Memorial University of Newfoundland.
- Varga, R. M., Stewart R.R., and Bancroft.J. C.,2006, Inversion and interpretation of multicomponent seismic data: Willesden Green, Alberta: CREWES Research Report volume **18**.
- Varga, R. M., and Stewart R.R., 2008, Searching for sand in Saskatchewan: Manitou Lake 3C-3D Seismic Project: CSEG Annual Convention, Calgary, AB., Expanded Abstracts.
- Varga, R. M., and Stewart R.R., 2008, Delineation of a sand reservoir at Manitou Lake Saskatchewan: Interpretation of 3D-3C seismic data: CREWES Research Report.
- Vigrass, L.W., 1977, Trapping of oil at intra-Manville (Lower Cretaceous) disconformity in Lloydminster area, Alberta and Saskatchewan: American Association Petroleum Geologists Bulletin, **61**, 1010-1028.
- Watson, I.A., 2004, Integrated geological and geophysical analysis of heavy-oil reservoir at Pikes Peak, Saskatchewan: M.Sc. Thesis, University of Calgary, Department of Geology and Geophysics.
- Xu R. C., and Stewart R.R, 2006, Delineating a sand channel using 3C-3D seismic data: Ross Lake heavy oilfield, Saskatchewan: CSEG Recorder, Special edition, 87-89.
- Yilmaz, O., 2001, Seismic data analysis, Processing, Inversion and Interpretation of seismic data, Volume II, Investigations in geophysics No, 10, p.1794.
- Yong Xu, 2002, Rock physics and AVO sensitivity in Mackenzie Delta, Canada, SEG 72<sup>nd</sup> Annual Meeting, Expanded abstracts **21**, 285.